Marine and Coastal Morphology: medium term and long-term area modelling

Kristensen, Sten Esbjørn; Deigaard, Rolf; Fredsøe, Jørgen; Hjelmager Jensen, Jacob

Publication date:
2013

Document Version
Publisher's PDF, also known as Version of record

Marine and Coastal Morphology: medium term and long-term area modelling

Sten Esbjørn Kristensen

TECHNICAL UNIVERSITY OF DENMARK
DEPARTMENT OF MECHANICAL ENGINEERING
SECTION OF FLUID MECHANICS, COASTAL AND MARITIME ENGINEERING
SEPTEMBER 2012

Published in Denmark by
Technical University of Denmark

Section of Fluid Mechanics, Coastal and Maritime Engineering
Department of Mechanical Engineering
Technical University of Denmark
Nils Koppels Alle, Building 403, DK-2800 Kgs. Lyngby, Denmark
Phone +45 4525 1384
E-mail: jf@mek.dtu.dk
Homepage: http://www.fvm.mek.dtu.dk/

Publication Reference Data
Kristensen, S.E.
Marine and Coastal Morphology: medium term and long-term area modelling
PhD Thesis
Technical University of Denmark, Section of Fluid Mechanics, Coastal and Maritime Engineering.
September, 2012
ISBN XX-XXXXX-XX-X
Keywords: Hybrid Morphological modelling, Shoreline evolution, Coastal structures, Groyne, Breakwater, Seawall, Nourishment, MIKE21 FM

Preface

The present Ph.D. thesis is submitted as part of the requirement to obtain a Ph.D. degree at the Technical University of Denmark (DTU). The Ph.D. study has been conducted in collaboration between the Department of Mechanical Engineering, DTU and the Department of Coastal and Estuarine Dynamics, DHI. The study has been supervised by prof. Jørgen Fredsøe (DTU), Rolf Deigaard (DHI) and Nils Drønen (DHI).

I would like to thank my supervisors for their invaluable assistance during the last 3-4 years. With their guidance; I have explored many different methods for moving around virtual sediment grains, and they have always accepted the challenge of making these ideas/methods more consistent.

October 1st 2012

Sten Esbjørn Kristensen

Abstract

This thesis documents development and application of a modelling concept developed in collaboration between DTU and DHI. The modelling concept is used in morphological modelling in coastal areas where the governing sediment transport processes are due to wave action. The modelling concept is defined: *Hybrid morphological modelling* and it is based on coupling calculated sediment transport fields from a traditional process based coastal area model with a parametrised morphological evolution model. The focus of this study is to explore possible parametric formulations of the morphological evolution model and apply them to problems concerning coastal protection strategies (both hard and soft measures). The applied coastal protection strategies involve morphological impact of detached shore parallel segmented breakwaters and shore normal impermeable groynes in groyne fields, and morphological evolution around seawalls and response to beach and shoreface nourishment.
The hybrid morphological modelling concept is introduced and is put into context with existing models used for medium term and long-term morphological simulation. The modelling concept is intended to improve the long-term predictive capabilities of process based area models thereby bridging the gap between short term models and long-term models.

A number of different implementations within the hybrid morphological modelling concept have been developed and tested in order to ascertain the usefulness of the concept. The implementations are grouped into shoreline models and models used to develop local features on the coastal profile such as alongshore migration of a bar front or redistribution of a shoreface nourishment. The implementations are tested on a variety of problems (idealised cases and case studies at specific locations). Applications of the modelling concept have been collected into 5 papers (1 accepted journal paper, 3 published conference papers and 1 unpublished journal manuscript) which each contain an introduction to the implementation, the motivation for the implementation and the overall results from the application. The 5 papers are enclosed as separate chapters of this thesis.

The overall conclusions to each of the model implementations are given as follows.

1D shoreline model

Implementing the hybrid morphological modelling concept with a 1D morphological model is a strong engineering tool. The model is robust and computationally efficient and it may be adapted to real engineering problems. The results of the 1D shoreline model are however greatly affected by the imposed freedom of the model, and exaggerated alongshore smoothing of the calculated shoreline may occur if the 1D model is applied to problems in which the true solution has a two dimensional nature.

1.5D shoreline model

A so-called "1.5D" implementation which introduces redistribution of sediment within a coastal profile in response to horizontal 2D currents makes it possible to simulate the morphological development in areas where 2D evolution occurs. The coastal profiles tend however to drift due to the fact that the response of an entire profile is coupled thereby in some cases leading to morphological activity in inactive areas. Diffusion of the coastal profile is therefore introduced in order to weakly force the profile towards an equilibrium form. The 1.5D model is seen to produce reasonable results when subject to cases with detached breakwaters and groynes. The computational efficiency of the model is however reduced compared to the 1D model, because the increased freedom of the model reduces the maximum stable morphological time step.

Bar models

The models for redistributing sediment on the shoreface have been applied with limited success. The models can only be applied to cases where cross-shore transport processes are of minor importance, due to inaccuracies in the calculated cross-shore transport in the applied 2D coastal model. Stabilisation of the bar parameters using behaviour-oriented methods may be possible but will require a strong forcing which according to the author reduces the significance of the modelling concept.

Synopsis

Denne afhandling dokumenterer udvikling og anvendelse af et morfologisk modelleringsprincip. Arbejdet er udført i et samarbejde mellem Danmarks Tekniske Universitet(DTU) og Dansk Hydraulisk Institut (DHI). Modelleringsprincippet anvendes på kystrelaterede opgaver, hvor de dominerende morfologiske processer skyldes tilstedeværelse af brydende bølger. Modelleringsprincippet kaldes populært: *Hybrid modellering* og er baseret på en kobling mellem eksisterende processbaserede areal modeller, til beregning af sediment transport, med en parametrisk model for morfologisk udvikling. Formålet med studiet er at udforske forskellige parameteriseringer og anvende dem på problemstillinger omhandlende kystbeskyttelse. De undersøgte problemstillinger indeholder morfologisk udvikling omkring bølgebrydere, impermeable høfder og strandmure samt morfologisk udvikling som følge af strand- og revlefodring.

Hybrid modelleringsprincippet bliver i afhandlingen introduceret og relateret til eksisterende morfologiske modeller der anvendes på problemstillinger af mellemlange og lange tidsskalaer. Undersøgelsen indeholder en række forskellige implementeringer indenfor hybrid modelleringsprincippet, hvis anvendelse på kystrelaterede problemer er blevet vurderet. Implementeringerne inddeles i kystliniemodeller og modeller til simulering af revleudvikling og omfordeling af sand fra en sandfodring. Modellerne er anvendt på idealiserede problemstillinger og på eksisterende kyster og resultaterne er samlet i 5 artikler (1 accepteret artikel i et videnskabeligt tidsskrift, 3 konference artikler samt 1 ikke-publiceret manuskript til et videnskabeligt tidsskrift). Artiklerne indeholder en introduktion af modellerne, motivation for anvendelse af modellerne samt resultaterne af anvendelsen. Artiklerne er vedlagt denne afhandling som separate kapitler.

De overordnede konklusioner af ph.d. studiet er som følger:

1D kystliniemodel

Anvendelse af en 1D kystliniemodel i hybrid modelleringsprincippet er et stærkt ingeniør værktøj. Modellen er robust og tidseffektiv og den kan anvendes på generelle kystlinier. Resultater fra 1D kystliniemodellen er dog påvirket af den begrænsede frihed som modellen har og dette medfører overdreven udjævning af den beregnede kystlinie hvis modellen anvendes på problemstillinger der ikke kan beskrives af en 1D model.

1.5D kystliniemodel

1.5D kystliniemodellen tillader omfordeling af sediment inden for kystprofilet som følge af horisontale 2D cirkulationsstrømme. 1.5D modellen kan derfor anvendes på 2D morfologiske problemstillinger. Modellen er dog påvirket af, at den morfologiske respons er sammenkoblet over et

helt kystprofil. Dette resulterer i nogle tilfælde i en overdreven aktivitet i områder hvor der ikke burde være nogen aktivitet. En svag diffus omfordeling af sand påtrykkes derfor kystprofilet, så det tenderer mod et forventet ligevægtsprofil. Med denne tilføjelse har modellen været anvendt med rimelig succes på tilfælde med bølgebrydere og høfder. Modellen er dog ikke ligeså tidseffektiv som 1D kystliniemodellen da den øgede frihed af kystprofilet nedsætter det størst tilladelige stabile morfologiske tidsskridt.

Revlemodeller

Revlemodellerne har været anvendt med begrænset succes. Modellerne kan kun anvendes på problemstillinger, hvor tværtransporten er begrænset pga. usikkerheden i beregning af disse. Revlemodellerne kan stabiliseres og styres af adfærdsregulerende modeller, men forceringen af disse skal være betydelig hvilket ifølge forfatteren vil være i modstrid med formålet for hybrid modellering.

Contents

Preface i

Abstract iii

Synopsis (in Danish) v

Contents vii

Symbols xi

1 Coastal morphology 1
1.1 Processes causing coastal sediment transport . . . 1
1.1.1 Longshore transport . . . 1
1.1.2 Cross-shore sediment transport . . . 2
1.1.3 Sediment budget . . . 3
1.2 Coastal protection . . . 3
1.2.1 Detached shore parallel breakwaters . . . 4
1.2.2 Groynes . . . 5
1.2.3 Seawalls . . . 7
1.2.4 Shoreface and beach nourishment . . . 8
1.2.5 Shoreline management in Denmark . . . 9

2 Medium term and long-term morphological modelling 11
2.1 Changing level of abstraction in the model type . . . 11
2.1.1 1D shoreline models . . . 11
2.1.2 Behaviour-oriented models . . . 12
2.2 Changing level of abstraction in the input type . . . 14
2.3 Improving computational efficiency . . . 14
2.4 Hybrid morphological modelling . . . 15

3 Scope of the thesis 17
3.1 Structure of the thesis . . . 17

4 Model documentation 19
4.1 Hybrid morphological modelling concept . . . 19
4.2 Calculating evolution in profile volume . . . 22
4.3 Boundary conditions on littoral drift . . . 24
4.4 Morphological shoreline evolution models . . . 26
4.4.1 1D shoreline models . . . 26

4.4.2 1.5D morphological model . . . 29
4.5 Morphological models for local features . . . 37
4.5.1 Profile definition . . . 37
4.5.2 Updating bar parameters using streamlines . . . 38
4.5.3 Updating bar parameters using optimisation . . . 39
4.5.4 Updating bar parameters using moments . . . 41
4.5.5 Simulation of bypass of a bar around a groyne . . . 43

Paper I : ICCE 2010, citation Kristensen et al. (2010)

5 Longterm Morphological Modelling 49
5.1 Introduction . . . 49
5.1.1 Simple one-line models . . . 50
5.1.2 N-line models . . . 51
5.1.3 2D area models . . . 51
5.2 Introduction of the model concept . . . 52
5.2.1 Implementation of the model concept . . . 53
5.3 Application of the model - shoreline evolution . . . 53
5.3.1 Coastline evolution around a groyne field . . . 53
5.3.2 Coastline evolution behind a breakwater . . . 55
5.4 Simulations with profile evolution . . . 56
5.4.1 Morphological evolution of a shoreline nourishment . . . 56
5.4.2 Alongshore migration of a bar . . . 59
5.4.3 Bypass of bar at a harbour . . . 62
5.5 Discussion and conclusions . . . 64

Paper II : ICCE 2012, citation: Kristensen et al. (2012)

6 Morphological Modelling of the Response to a Shipwreck 67
6.1 Introduction . . . 67
6.1.1 Previous application of the hybrid model concept . . . 69
6.2 Numerical model . . . 69
6.3 Case study - SELI 1, Cape Town . . . 70
6.3.1 A brief history of the shipwreck . . . 70
6.3.2 The site - Table Bay . . . 70
6.3.3 The beach at Table View . . . 71
6.4 Model setup . . . 71
6.4.1 Wave climate . . . 71
6.4.2 Domain for morphological simulations . . . 74
6.5 Morphological simulations . . . 75
6.5.1 Baseline - conditions prior to grounding of Seli 1 . . . 75
6.5.2 Morphological response to shipwreck . . . 76
6.5.3 Morphological response to removal of shipwreck . . . 77
6.6 Conclusion . . . 77

Paper III : Coastal Engineering 2013, citation: Kristensen et al. (2013a)

7 Hybrid Morphological Modelling of Response to a Detached Breakwater 79

7.1 Introduction . . . 80
7.2 Numerical Model . . . 82
7.2.1 Coastal area model for the sediment transport field . . . 82
7.2.2 Parametrised morphological update of bed . . . 83
7.3 Offshore breakwater - 1D morphological model . . . 83
7.3.1 Model formulation . . . 83
7.3.2 Simulations of the morphological response to offshore breakwaters . . . 84
7.3.3 Case study: Salient formation behind a shipwreck . . . 87
7.3.4 Planform sensitivity analysis, mean wave direction normal to the shoreline . . . 89
7.3.5 Planform sensitivity analysis, mean wave direction oblique to the shoreline . . . 91
7.3.6 Prospects for the 1D hybrid morphological model . . . 92
7.4 Coastal breakwater - 1.5D morphological model . . . 92
7.4.1 Numerical model . . . 92
7.4.2 Morphological response to a coastal breakwater . . . 96
7.5 Discussion . . . 100
7.6 Conclusion . . . 101
7.A Optimisation of coastal parameters in the 1.5D morphological model . . . 102
7.B Adding a cross-shore diffusion towards the equilibrium profile . . . 103

Paper IV : Unpublished, citation: Kristensen et al. (2013b)

8 Hybrid Morphological Modelling of Response to a Groyne Field 107
8.1 Introduction . . . 107
8.1.1 Present study . . . 108
8.1.2 Hybrid morphological modelling concept . . . 109
8.2 Numerical model . . . 109
8.2.1 2D coastal model for sediment transport . . . 109
8.2.2 Hybrid morphological model . . . 110
8.3 Model setup . . . 112
8.3.1 Coastal profile and sediment properties . . . 112
8.3.2 Wave forcing . . . 112
8.3.3 Periodic boundary conditions . . . 112
8.3.4 Definition of morphological model . . . 113
8.3.5 Wave reflection . . . 116
8.4 Morphological response to groyne fields . . . 118
8.4.1 Groyne length . . . 118
8.4.2 Wave height . . . 119
8.4.3 Wave direction . . . 122
8.4.4 Wave period . . . 123
8.4.5 Groyne spacing . . . 125
8.4.6 Varying groyne design . . . 125
8.5 Reduction in littoral drift . . . 129
8.5.1 Conceptual function of groyne fields . . . 129
8.5.2 Simulated reduction in littoral drift . . . 130
8.6 Discussion . . . 132
8.7 Conclusion . . . 133
8.A 1D curved baseline model . . . 134

8.A.1 Model description . . . 134
8.A.2 Avoiding crossing profiles . . . 135
8.A.3 Examples of morphological evolution around a groyne . . . 136

Paper V : ICCE 2012, citation: Grunnet et al. (2012)

9 Evaluation of Nourishment Schemes Based on Morphological Modeling 139
9.1 Introduction . . . 139
9.2 Study area . . . 140
9.2.1 Environmental setting . . . 140
9.2.2 Complex morphodynamic setting . . . 140
9.3 Baseline study on a fixed bed . . . 142
9.3.1 Process-based 2DH modelling . . . 142
9.3.2 Schematisation of forcing conditions . . . 143
9.3.3 Model set-up . . . 143
9.3.4 Calibration of the area model . . . 143
9.4 Set-up of morphological model . . . 145
9.4.1 Hybrid modelling concept . . . 145
9.4.2 Definition of shoreline model . . . 145
9.4.3 Model for evolution of shoreface nourishment . . . 146
9.4.4 Definition of nourishment scenarios . . . 147
9.5 Simulation of morphological response . . . 148
9.5.1 Beach nourishment alone . . . 148
9.5.2 Beach and shoreface nourishment coupled . . . 148
9.5.3 Comparison of nourishment scenarios . . . 149
9.6 Conclusions . . . 151

10 Conclusion 153

Bibliography 155

A Integration of flux over a line 163
A.1 Extraction and integration using discrete points . . . 163
A.2 Extraction and integration using coordinate transformation . . . 164

B Creating a periodic mesh with conforming elements 167
B.1 Definition of a periodic mesh . . . 167
B.2 Creating a periodic mesh . . . 167
B.2.1 Generalisation of periodic mesh generation . . . 170

C Derivation of the bar moment method 173
C.1 Reduced moments . . . 176
C.2 Temporal derivatives of reduced moments . . . 177
C.2.1 Derivatives in terms of bar parameters . . . 177
C.2.2 Derivatives in terms of erosion/deposition distribution . . . 179

Symbols

Sub-indices

$\square_0$	Berm/shoreline
$\square_0$	Deep water wave characteristic
$\square_{\mathrm{act}}$	Active profile
$\square_{\mathrm{b}}$	Bar
$\square_{\mathrm{bc}}$	Given at offshore boundary of domain
$\square_{\mathrm{BW}}$	Breakwater
$\square_{\mathrm{c}}$	Bar crest
$\square_{\mathrm{cl}}$	Closure depth
$\square_{\mathrm{crs}}$	Cross-shore
$\square_{\mathrm{dom}}$	Domain
$\square_{\mathrm{eq}}$	Equilibrium
$\square_{\mathrm{gap}}$	Gap (alongshore spacing)
$\square_{\mathrm{geo}}$	Geometric
$\square_{\mathrm{gross}}$	Gross, absolute sum of positive and negative contributions
$\square_{\mathrm{g}}$	Groyne
$\square_{\mathrm{l}}$	Longshore
$\square_{\mathrm{net}}$	Net, vector sum of positive and negative contributions
$\square_{\mathrm{space}}$	Alongshore spacing
$\square_{\mathrm{SW}}$	Seawall

Super indices

$\square^*$	Dimensionless quantity
$\square^k$	Time step number

Greek letters

α	Bed level gradient
β	Angle of re-orientation of shoreline normal
δ	Centroid location of bar

Δt	Morphological time step increment
ϵ_0	Intermediate shoreline (used in curved baseline implementation)
ε	Area weighted rms-difference between parametric and discrete coastal profile
ζ	Bar skewness
η	Local axes, normal to line of extraction of littoral drift
θ	Angle of wave incidence; angle between incident waves and shoreline normal
λ	Dimensionless breakwater configuration: ratio Breakwater length to breakwater distance from shoreline
ξ	Dummy variable of integration
σ_{w}	Directional spreading of wave energy spectrum
τ	Local axes, tangential to line of extraction of littoral drift
ϕ	Argument to periodic functions (radian)
ψ_j^k	Vector containing profile parameters of the jth coastal profile at time step k
$\hat{\psi}$	Profile parameter, bound by continuity
Ω	Selection of elements

Latin letters

A	Parameter which controls slope of coastal profile
A	Horizontal area of integration
A_{b}	Bar amplitude
A_j	Area of of the jth computational element
$d_{16/84}$	Geometric spreading of sediment grain size distribution
d_{50}	Mean sediment grain size
$\mathcal{F}_i$	ith known integral function (used in the bar-moment method)
h	Height
H_{s}	Significant wave height, typically given on deep water
$H_{\mathrm{s,b}}$	Significant wave height at breaking
K	Cross-shore diffusion coefficient
L	Length
m	Parameter which controls slope of the coastal profile
M_i	ith moment of bar amplitude
$\mathcal{M}_i$	ith reduced moment of bar amplitude
n	Porosity, taken as $n = 0.4$ in this study
$\bar{n}$	Normal vector
r	Alongshore coordinate
$\tilde{r}$	Polynomial function which defines curved coastal profile
s	Cross-shore coordinate
t	Time
T_{p}	Peak wave period

V	Profile volume (m^3/m)
$\tilde{V}$	Profile volume (m^3)
W	Width
W_{shadow}	Geometric shadow from breakwater on shoreline
q	Sediment transport rate ($m^3/yr/m$)
Q	Sediment transport rate (m^3/yr)
z	Vertical coordinate

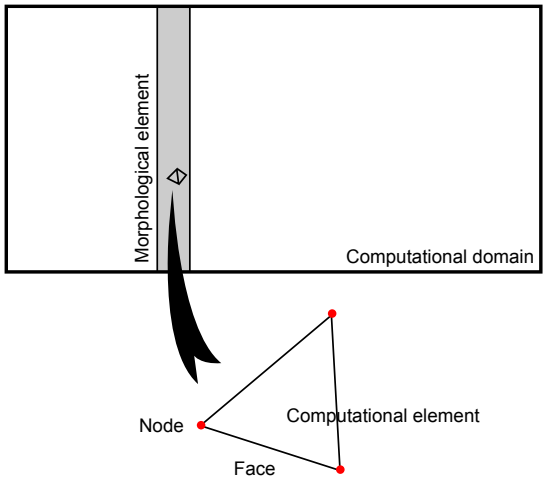

Figure 1: *Definition of the components of a computational domain.*

Definition of concepts

Baseline Present conditions. Used to compare against future shoreline management scenarios

CD Chart datum; level relative to lowest astronomical tide

Coastal area model 2D process based coupled model which is composed of a module for transformation of waves, a module for calculation of a depth integrated wave generated current field and finally a module for calculation of a 2D sediment transport field in a 2D *computational domain*. The term *2D coastal model* may also be used.

Computational element The coastal area model is solved on a 2D computational mesh which is composed of a number of computational elements

Edge see *Node*

Face see *Node*

Far-field Area located at some distance from a coastal structure. The area is indirectly affected by the structure due to morphological changes

LHS Left hand side of an equation

Morphological element Control volumes used in the morphological model. The morphological elements are generally larger than the computational elements in the hybrid morphological modelling concept, while they are identical in traditional 2D models

Morphological modelling "What happens if you run the model a little longer"

MSL Mean sea level

Node Computational elements are defined by 3 or more points called nodes. The nodes are connected with linear segments called *faces* or *edges*

RHS Right hand side of an equation

Chapter 1

Coastal morphology

1.1 Processes causing coastal sediment transport

Understanding the morphological effect of coastal structures requires a basic understanding of the most important hydrodynamic processes inside and outside the surf zone. This chapter gives a brief review of the most important processes for coastal sediment transport according to the tradition of the coastal group of the Department of Mechanical Engineering at DTU.

Figure 1.1: *Surf zone at the West Coast of Jutland during medium wave conditions. Coastal morphology is a result of hydrodynamic process occurring in the surf zone. Photo by author, June 2010.*

1.1.1 Longshore transport

Longshore transport in the surf zone

Longshore transport inside the surf zone is a result of advection of sediment along the longshore current, which is generated by gradients in the wave radiation stress field due to wave breaking, see e.g. Fredsoe and Deigaard (1992). The magnitude of the longshore transport depends therefore on the wave height, angle of wave incidence, sediment characteristics and bed shear stress. The wave height affects both the driving force of the longshore current but is also important for the

bed shear stress in the combined wave-current boundary layer which governs stirring of sediment into the water column. The mechanics of the longshore transport are fairly well known and many models for describing it exists, covering bulk transport models such as the CERC formula for the integrated longshore transport (the littoral drift) and process resolving models in which models for suspension of sediment and models for it's subsequent advection are coupled to calculate longshore transport, see e.g. Deigaard et al. (1986a).

Longshore transport in the swash zone

Transport in the swash zone occurs at the interface between water and land and is often treated separately due to the large difference in important processes compared to those known from the surf zone (see Elfrink and Baldock (2002) for a comprehensive review and discussion). Existing models which include swash zone transport tend to use semi empirical models and focus on the longshore transport component assuming that the asymmetric flow motion which forms a zig-zag pattern may give a reasonable estimate of the transport in this area, Nam et al. (2011). It is often speculated that the swash zone transport is a significant contribution to the total littoral drift. As an example Kamphuis (1991a,b) propose that swash transport is up to 50% of the total littoral drift.

1.1.2 Cross-shore sediment transport

Cross-shore sediment transport is the result of many different first order and higher order processes. Accurate prediction of the cross-shore transport is linked to the fact that large amounts of sediment may be moved back and forth during each wave cycle, while the long term effect on the morphology is linked to the net sediment transport over a wave period (or wave group). This is further complicated by the large number of different cross-shore processes and their interaction or as described in Fredsoe and Deigaard (1992): "The main difficulty lies in the many different contributions that are all small compared to the gross sediment motion due to the wave-orbital motion".

Cross-shore transport inside the surf zone

Cross-shore transport inside the surf zone is generally dominated by a vertically segregated return current (the undertow) which causes offshore sediment transport. Deigaard et al. (1991) show that the undertow is generated due to an imbalance in the vertical force distribution of the radiation stress gradient due to breaking of waves and pressure gradients (wave setup) and a zero net flux of water in the cross-shore direction. For beaches with breaker bars and rip channels the undertow may however completely vanish in certain profiles due to horizontal 2D circulation currents caused by alongshore differences in wave breaking intensity, Drønen and Deigaard (2007).

Cross-shore transport outside the surf zone

The cross-shore transport is here generally onshore due to higher order effects such as wave asymmetry (velocity skewness) from non-linear waves, boundary layer streaming caused by systematic build-up of boundary layer thickness) and wave drift due to an oscillatory particle trajectory, Fredsoe and Deigaard (1992).

Offshore transport may however occur in this area due to presence of bed forms which introduce lag between near-bed flow velocities and suspended sediment concentration that reverse the transport direction Nielsen (1992) or by infragravity advection in which high waves in a wave group stir up sediment to be advected by the bound infragravity flow component, Aagaard and Greenwood (2008); O'Hare and Huntley (1994); Villard et al. (2000). Finally streaming effect due to reflected

infragravity waves represents also a mechanism for cross-shore transport towards the node or anti-nodes of the standing wave depending on whether the transport is predominantly bed load or suspended load, Carter et al. (1973).

While identification and modelling of the most important cross-shore processes may be possible; application in engineering models will require an equally detailed representation of the local site specific forcing conditions on a scale which makes long-term simulation of the cross-shore processes questionable.

1.1.3 Sediment budget

Setting up a sediment budget (as seen in figure 1.2) illustrates the relationship between the longshore and cross-shore transport processes and the resulting shoreline change. The figure contains a large range of different contributions to the total sediment budget, some of which are often not included in morphological simulations. Progressing from offshore to towards land we find cross-shore processes which supply/remove sediment from the coastal area. These processes may be associated with wave action as mentioned in the previous section, but they may also be a result of other effects such as up-welling/down-welling due to action of wind or residual effects due to tidal flow. Outside the surf zone longshore transport may occur due to steady currents caused by tidal flow or action of wind.

Inside the surf zone we find that a significant contribution to the sediment budget is that of gradients in the littoral drift, and longshore swash zone transport. The contribution from these processes to the sediment budget are traditionally taken as very significant to shoreline evolution, and much effort has over the last five decades been given to describe the relation between waves and sediment transport.

The beach and backshore are also subject to transport of sediment. Typically during storm events sediment is eroded from the beach and the aeolian dunes while supply of sediment to the beach occurs during calm periods where cross-shore swash zone transport feeds sediment from the surf zone onto the beach. Aeolian processes redistribute the sediment alongshore and further inland. Contributions to the sediment budget from aeolian processes is difficult to model due to the fact that the sediment transport depends not only on sediment size and wind but also other effects such as beach width and water content play an important role. As a result, aeolian transport is often neglected in morphological modelling or comments as to the effect of these processes are merely indicated or discussed qualitatively.

From this discussion it should be clear that a large range of different processes contribute to the complete sediment budget. In this study however, only gradients in the littoral drift are modelled, and used to impose coastal morphological changes. It is assumed that the morphological effect on the coastal profile from other processes may be prescribed rather than modelled.

1.2 Coastal protection

The importance of successful design of coastal protection increases because an increasing number of the Worlds population tends to live at or near the coast. The coastal structures may be constructed for different reasons; some are used to protect a local area from waves and flooding (detached breakwaters, harbours, dikes, seawalls) while others are used to reduce erosion or enhance the recreational value of a nearby beach (detached breakwaters, groynes, seawalls). The structures used to reduce erosion may also be used to widen the beach locally in order to improve the protection

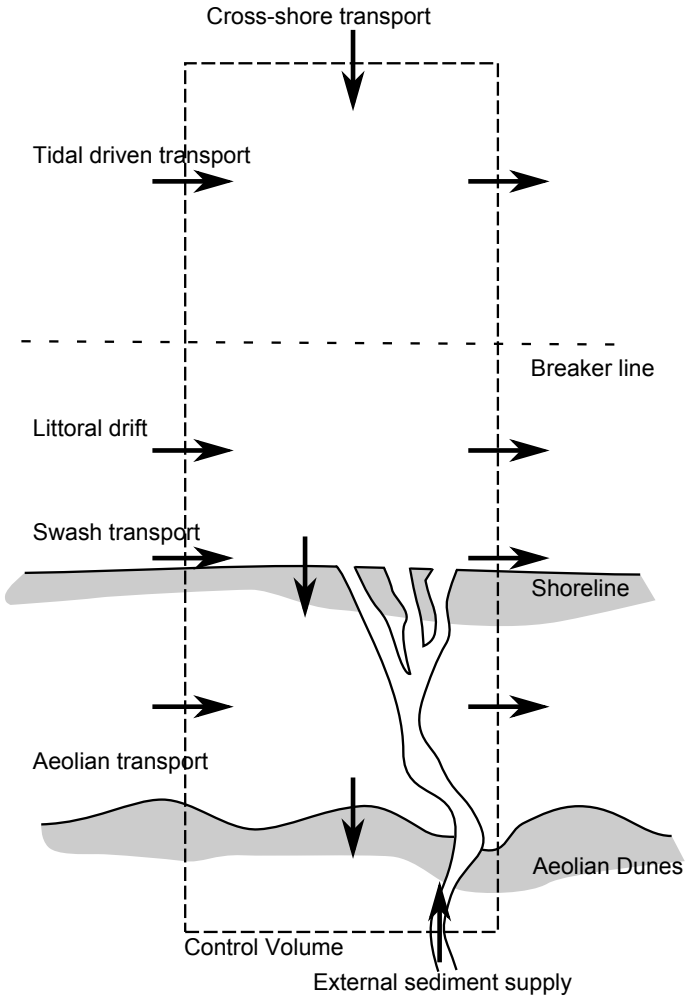

Figure 1.2: *A sediment budget for a coastal area illustrates the relation between various sediment transport processes.*

level of the beach against storm impact, thereby reducing the risk of flooding the hinterland. In practice several different types of coastal structures are often combined into a larger shoreline management scheme, Mangor (2004).

1.2.1 Detached shore parallel breakwaters

Detached shore parallel breakwaters force waves to break or be reflected at their seaward side depending on the inclination of the seaward facing side of the structure, the construction material and permeability. The breakwater causes thereby sheltering from wave energy in it's lee and reduces the alongshore forcing of the breaking waves. The size of the sheltered area and the impact on the alongshore forcing depends greatly on the length of the breakwater and on the distance from the shoreline to the breakwater as discussed in Kristensen et al. (2013a) (enclosed in this thesis as chapter 7). Constructing a series of breakwaters (a segmented breakwater) allows the reduction in forcing of the longshore current to be distributed over a longer stretch of coastline.

Breakwaters may efficiently increase the width of the sheltered beach or stabilise a nourishment. A common criteria for success is therefore the resulting planform (salient/tombolo) which develops

Figure 1.3: *Salient in the lee of a shore parallel detached breakwater at the North coast of Sealand, Denmark. Photo by Jens Kirkegaard, August 2011.*

in the lee of the breakwater. A salient will generally impose a weak effect on the littoral drift and allows bypass of sediment landward of the structure, while a tombolo extends all the way out to the structure thereby blocking the transport or forcing bypass to occur only on the seaward side of the structure. The downdrift erosion is therefore stronger if a tombolo develops. A tombolo is however considered more stable planform compared to that of a salient, although in many cases the planform type may change depending on the recent forcing history.

1.2.2 Groynes

Groynes are traditionally shore normal structures which are designed to block the littoral drift thereby trapping sediment on the upstream side and causing erosion on the downstream side. Groynes are considered the oldest type of shoreline defence and are also subject to a great deal of controversy as to whether this type of structure in fact is advantageous, CEM (2002a). Adverse effects of groynes are commonly associated with an offshore directed rip current which develops updrift of impermeable groynes. The rip current causes offshore transport which particularly for long groynes (relative to the surf zone width) may result in loss of sediment. Design guidelines from the Coastal Engineering Manual suggest therefore that groynes should be constructed as permeable groyne, which act as a template for the subaerial beach while providing full bypass in order to minimize downstream erosion.

Impermeable groynes which have a significant impact on the shoreline may however be preferred over the permeable groynes in some shoreline management schemes. Single long groynes may function as headlands that divide a beach into several smaller sediment cells in a manner which allows the beach to turn up against the local prevailing waves as described in Mangor et al. (2008) or as terminal structures which limit the amount of sediment deposited in a downstream tidal inlet

Figure 1.4: *Aerial photo of Amager Beach Park, Denmark. Single long groynes may be used to divide a beach into smaller sections. The photo from Mangor et al. (2008).*

or navigation channel, Basco and Pope (2004); Grunnet et al. (2009). The first type of groynes should only be applied on shorelines where the net transport is small (as in the design of Amager Beach Park, Denmark in figure 1.4), while the latter type often will be applied to beaches with a significant net transport. Construction of the terminal structures should be accompanied with a dredging plan in order to avoid eventual bypass of sediment.

Figure 1.5: *Groyne field at Fjaltring, West Coast of Denmark. A shore normal groyne field with a significant upstream and downstream shoreline response. Photo by author, June 2010.*

Use of impermeable groynes in groyne field may be applicable for schemes, where the groyne field is designed to reduce the littoral transport by a certain amount. The groyne field will reduce the

littoral drift by re-orientation of the bed contours. Short groynes (relative to the surf zone width) will primarily affect the bed contours landward of the groyne tip, while long groynes (groyne length comparable with surf zone width) may also affect bed contours seaward of the groyne tip as shown in Kristensen et al. (2013b) (reproduced as chapter 8 in this thesis). The amount of reduction depends on the groyne length relative to the surf zone and to some degree on the groyne spacing.

1.2.3 Seawalls

Seawalls are shore parallel structures which separate the sea from dry areas. Seawalls are passive structures which protect the coast against erosion and flooding. The structures do not directly affect erosion/deposition but reduce rather the amount of sediment released from the coastal profile. Construction of seawalls may therefore also result in downstream erosion. Figure 1.6 shows an example of a seawall along a protected shoreline at the east coast of Sealand, Denmark. Seawalls are often constructed in urban areas where space is scarce.

Figure 1.6: *Seawall fronted by a revetment at Charlottenlund, Denmark. Seawalls force the water depth at the structure to increase in response to erosion. Photo by author, September 2012.*

Seawalls may affect the magnitude of the littoral drift for cases where erosion has removed the beach in front of the seawall. The reflection coefficient of seawalls may generally be taken as larger than that of an open coast thereby increasing transport magnitude. However when sufficient erosion has increased the water depth to some value, the transport magnitude may decrease because the seawall effectively reduces the amount of wave breaking and thereby the driving forces of the longshore current.

Revetments function similar to seawalls, although they are are not intended to protect the hinterland against flooding. Instead revetments are built at the foot of dunes, dikes or seawalls as a measure of protecting these structures against erosion. As shown in figure 1.7 revetments may

Figure 1.7: *A buried revetment at the West Coast of Denmark, which is intended as armouring of the dune during storm conditions. Photo by author, June 2010.*

be buried into the dune thereby functioning only during storm conditions as a last line of defence. The figure shows a buried revetment which has been exposed during a storm.

1.2.4 Shoreface and beach nourishment

Nourishment is often referred to as a soft management strategy in contrast to hard solutions such as breakwaters and groynes. Nourishment is an artificial supply of sediment to the sediment budget. Nourishment will not reduce erosion but is rather used to strengthen the coastal profile. For this reason, nourishment in general requires a long-term maintenance effort - a fact which has traditionally caused politicians to avoid this type of management scheme, Laustrup and Madsen (1998).

Nourishment may either be performed as shoreface nourishment where sediment is supplied somewhere inside the surf zone (typically on the seaward side of a breaker bar), as beach nourishment or as backshore nourishment. Beach nourishment increases initially the beach width thereby improving both the recreational value of the beach and the level of protection against dune erosion and flooding of the hinterland during storm events. Based on analysis of a 2 year field campaign (NOURTEC) Laustrup et al. (1996) argue however that beach nourishment after a year only improves coastline stability and the coastal protection level, whereas the beach width is not improved.

A shoreface nourishment acts indirectly as shore protection by decreasing wave exposure. The cost of shoreface nourishment is significantly lower compared to beach nourishment (approximately 30% cheaper, Laustrup et al. (1996)) because it may be performed much faster. Field surveys suggest furthermore that the nourishment volume within the project site is maintained for a longer period of time in a shoreface nourishment. Laustrup et al. (1996) argue that nourished sand placed on the breaker bars is more quickly integrated into the existing bar system because the imposed perturbation is more natural than that of a beach nourishment thereby increasing the lifetime of the shoreface nourishment.

Use of nourishment is becoming increasingly popular in both Denmark and the Netherlands. The increasing volumes and experience coupled with increasing application of shoreface nourishment has resulted in a lowering of the unit price of nourishment over the last couple of decades.

Figure 1.8: *Nourishment near the shoreline at Thyborøn on the West Coast of Denmark by use of rainbowing. Photo by Hunderup Luftfoto, reproduced with permission from the Danish Coastal Authorities, June 2007.*

1.2.5 Shoreline management in Denmark

The following discussion on shoreline management in Denmark focuses on the efforts on the West Coast of Denmark. Maintenance and protection of the coast is performed by DCA and it is therefore well documented. This stands in contrast to the efforts along the inner coastlines which are more chaotic and characterised by the fact that protection measures are not integrated into larger management schemes. They are typically designed by local landowners and municipalities without regard to the downstream landowners, although DCA do attempt to guide the local stakeholders.

West Coast of Denmark - history

Integrated shoreline management along the West Coast of Denmark[1] dates back to 1862 in connection with a breach in the Limfjord barrier at Thyborøn (figure 1.9 shows an overview of the coastline). At that time it was decided that the opening should be maintained in order to allow free passage of ship traffic between the North Sea and the Limfjord.

In the following years shoreline retreat around the breach increased because the breach acted as a sediment drain. A commission decided therefore in 1874 that groynes should be constructed along the surrounding shorelines in order to mitigate erosion. The groynes were built in the period 1875 to 1907 and covered the shorelines between Ferring and Agger. Over the next half a century (from 1909 to 1962) additional groynes have been constructed between Ferring and Fjaltring. As a result; the West Coast displays today 83 impermeable rubble mound groynes and the channel at Thyborøn has 11 smaller channel groynes.

Since 1983 a general agreement between DCA and the coastal municipalities in the area has formed the economic basis for coastal management. The agreement was formed because it had become

[1] The history of the shoreline management is detailed in DCA (2008) (in danish)

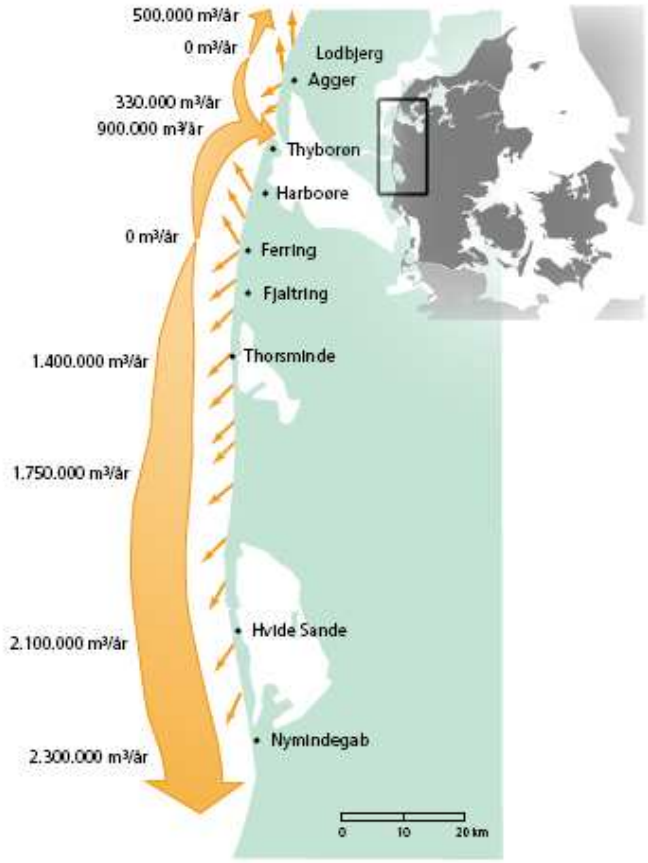

Figure 1.9: *Overview of part of the West Coast of Denmark. Estimated littoral drift is given in m^3/yr. The figure is reproduced from DCA (2008) with permission from DCA.*

evident that large parts of the shoreline could not be maintained by structures and dune stabilisation alone, Laustrup and Madsen (1998). The general agreement added financial support to the shoreline protection and was during the first years used to construct detached low-crested impermeable rubble mound breakwaters and revetments. Nourishment was only used on a small scale due to the politicians trust in hard structures.

Growing awareness of environmental issues among the public and politicians has however according to Laustrup and Madsen (1998) resulted in an increasing use of nourishment. In the middle 1990's nourishment volumes had risen to roughly $3 \cdot 10^6$ m^3/yr and is today more or less unchanged, DCA (2008). Construction of new hard structures has been limited since the middle 1990's. This is by Laustrup and Madsen (1998) attributed to the fact that exposed areas have already been protected by structures and due to the previously mentioned growing public awareness of environmental issues.

Annual field surveys are used to monitor the entire West Coast and analysis performed by DCA suggests that the combination of structures and nourishment effectively reduce retreat of bed contours above -6 m CD, whereas the contours further seaward continue to retreat, thereby causing profile steepening.

Chapter 2

Medium term and long-term morphological modelling

As pointed out previously in reviews of long-term modelling approaches in Cowell et al. (2003b); Hanson et al. (2003); de Vriend et al. (1993) one of the key-points in morphological modelling is to: Resolve processes of time scales and spatial scales which are relevant to the addressed problem. It is generally argued that short term processes affect only medium term and long-term processes through their residual effects, while long-term and medium term processes may act as external forcing conditions for small scale processes. At some point if the difference in time scale between the short term and the long-term processes is too large, the short term processes may in reality be regarded as noise. Applying morphological models to increasing time scales requires therefore an increasing level of abstraction. The increasing level of abstraction may basically be implemented in the model type (see section 2.1) or in the input type (see section 2.2). Furthermore application of long-term models may also require increased computational efficiency - a matter which will be addressed in section 2.3.

2.1 Changing level of abstraction in the model type

For the purpose of illustrating changes to the level of abstraction in the model type, the models developed for long-term modelling will be compared to 2D process based morphological models, which are generally recognised as models which can be applied to short term or medium term problems. The process based 2D models will not be introduced here, but models such as DHI's MIKE21 FM or Delft3D from Deltares may be taken as representative of 2D process based morphological models. These models solve governing equations for wave field and flow field in order to calculate the sediment transport. The model variables; wave height, wave period, wave direction, water depth and flow velocity are therefore solved in a time resolving 2D or 3D spatial domain. Kristensen et al. (2010) gives a description of the short terms models with details on the challenges associated with long-term modelling, see page 51.

2.1.1 1D shoreline models

Morphological evolution in 1D shoreline models is simplified by the fact that it is assumed that the evolution of the shoreline contour may characterise the evolution of the entire profile. The level

of abstraction is therefore increased in 1D shoreline models by not modelling cross-shore processes which will otherwise redistribute sediment in the coastal profile. The justification for neglecting to resolve cross-shore processes is that cross-shore transport may be taken as a seasonal process and that the coastal profile, when averaged over a year does not change significantly. A 1D shoreline model is therefore applicable to simulation of shoreline evolution over several years (decades or centuries), while it may not be used to describe short term changes to the shoreline e.g. when the coastal profile is eroded during a storm and rebuilt during a subsequent calm period.

Applicability of 1D shoreline models is furthermore improved by the fact that many shoreline models use a bulk longshore transport formulation (e.g. CERC formula), which are empirical models in which the longshore transport is a function of a few parameters, typically the wave height and the angle of wave incidence at breaking, bed slope of the coastal profile and sediment grain size. The bulk sediment transport formulas improve the computational efficiency compared to process based models. Process based longshore transport formulations such the one in Deigaard et al. (1986a) allow however application of the model to specific coastal profiles which include bar-trough features and they give also a detailed description of the cross-shore distribution of the sediment transport field in contrast to the bulk sediment transport formulations.

As pointed out in Hanson et al. (2003); 1D shoreline models are only applicable to problems where the littoral drift (the transport due to wave breaking) is dominant. For problems where tidal process govern the morphological evolution, other types of models must be used.

2.1.2 Behaviour-oriented models

A large range of different levels of abstraction may be included in the model type: Behaviour-oriented models. Common to all models in this group is however that evolution of the model parameters is rule based and the model variable is often forced towards equilibrium values by use of a diffusive formulation. A selection of different behaviour-oriented models is discussed in the following sections.

Bar position model

The breakpoint hypothesis describes that the cross-shore position of breaker bars coincides with the point of wave breaking due to convergence of cross-shore transport from undertow and wave asymmetry. Based on 16 years of field observations Plant et al. (1999) formulated a behaviour-oriented model in which the model variable: the bar position, is modelled as a function of the incident wave height.

$$\frac{\mathrm{d}X_\mathrm{c}}{\mathrm{d}t} = -\alpha(H(t))\left(X_\mathrm{c} - X_\mathrm{eq}(H(t))\right) \tag{2.1}$$

The cross-shore migration rate of the bar position, X_c is defined to be some function of the difference between the existing cross-shore position of the bar and the equilibrium position X_eq which according to the breakpoint hypothesis is a function of the incident wave height. By defining the coefficient α as a function of the wave height to some power, Plant et al. (1999) showed that even for a intra-annual (seasonal) variation in wave height, the model will predict continual inter-annual offshore bar migration - a behaviour which is reported in many field studies e.g. Grunnet and Hoekstra (2004).

Profile diffusion

Profile diffusion models mimic an observed diffusive behaviour of coastal profiles to perturbations from e.g. beach or shoreface nourishments. It is observed that perturbations are "smoothed" out over the equilibrium profile, Stive et al. (1992). Furthermore, it seems that the smoothing is greater near the shoreline and weak on large water depths. In Capobianco et al. (1994) cross-shore diffusion of a discrete coastal profile is therefore formulated, where the model variable, x, is the cross-shore displacement of points along the coastal profile with respect to an assumed equilibrium profile.

$$\frac{\partial x}{\partial t} = \frac{\partial}{\partial z}\left(D(z)\frac{\partial x}{\partial z}\right) + S(z,t) \tag{2.2}$$

$D(z)$ is a depth-dependent diffusion coefficient which needs to be calibrated and $S(z,t)$ is a depth varying and time varying source function used to simulate sediment sources due to nourishment.

Using this diffusion type profile model, Capobianco et al. (1994) show that they can describe the temporal evolution of the profile volume in the trunk section of a beach nourishment at Delray Beach where three nourishments were applied over a 17 year period.

N-line models

Multi-line models are an extension of 1D shoreline models. Multi-line models represent not only the shoreline as a model variable, but introduce additional contours, and evolve each line by solving 1D sediment continuity equations. Multi-line models are in this study regarded as behaviour-oriented models because most often exchange of sediment between the different layers is handled by source terms, which assume that the coastal profile should evolve such that a certain cross-shore distance between the layers is maintained.

The first application of multi-line models is given in Bakker (1969) in which morphological development is simulated around a groyne system. In this study Bakker (1969) showed that increasing the morphological freedom of the 1D shoreline model makes it possible to represent accretion and erosion around groynes in a more reasonable manner, compared to existing 1D shoreline models.

Aggregated models

Simulation of very long time scales (centuries and millennia) requires and entirely different level of abstraction compared to the models described previously. Basically this type of model aggregates coastal processes and features into sub-systems. The sub-systems share sediment and interact therefore dynamically on time scales of change related to the size of the sub-system, Cowell et al. (2003a). A thorough introduction and review of various aggregated models is given in the two companion papers Cowell et al. (2003a,b). In the following we will describe one of the models, namely the ASMITA (Aggregated Scale Morphological Interaction between a Tidal inlet system and Adjacent coast).

The model was developed for classic tidal inlet systems. The model variable is the volume of certain elements in the tidal area which as an example can be: Tidal channel, tidal flats and the ebb-tidal delta, see figure 2.1. Each of the model elements contains an equilibrium volume, and exchange of sediment between the three systems is based on differences in sediment availability (related to the equilibrium volume). The model is calibrated against historical data and may be used to simulate development of sediment volume in each model element, taking into account effects of sea level rise.

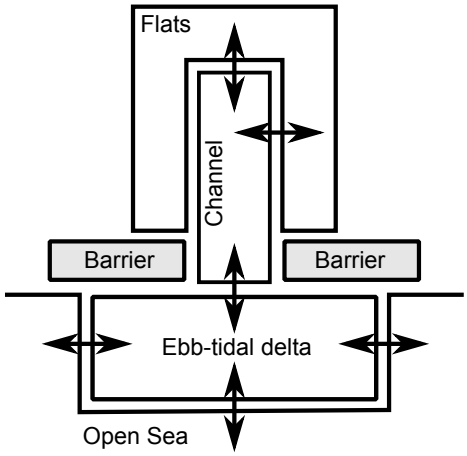

Figure 2.1: *Schematic representation of the ASMITA model. The tidal system is divided into aggregated model elements which exchange sediment according to differences in sediment availability. The sketch is adopted from Rossington et al. (2011).*

2.2 Changing level of abstraction in the input type

Input reduction techniques may be used to shorten the time required to simulate morphological evolution.

For problems where the tidal range is significant, Latteux (1995) showed that a single representative tide (*morphological tide*) may be defined such that the cumulated effect is similar to that obtained if morphological evolution is performed on the full spring-neap tidal cycle. Latteux (1995) found that the tidal range of the morphological tide should be 7-20% of the average tidal range, although this is based on sediment transport in a tide-only domain. Grunnet et al. (2004) found that for the coast at Terschelling, The Netherlands where both waves and tide are present, the morphological tide may be taken as 10% larger than the average tidal range.

Morphological modelling of problems which are governed by gradients in the littoral drift are often subject to *schematic representations of the wave climate*. The schematic representation requires that a certain number of sea-states are defined and weighted according to their occurrence during a year. The schematic wave representation reduces computational effort compared to using a full time series of the wave climate. Alternatively, a *reduced wave climate* which contains only time series of storm events is sometimes used since these events contain most of the annual littoral drift. Care should however be taken when applying the condensed wave climates because the cross-shore distribution of the littoral drift may not be well represented.

2.3 Improving computational efficiency

Application of short and medium term models (coastal area models) to increasingly large time scales has over the last couple of decades been possible due to efforts of increasing the computational efficiency of the models. Roelvink (2006) gives a review of these methods and the most relevant are briefly mentioned here.

One of the computationally most expensive calculations in coastal area modelling is solution of the flow. A *continuity correction* may therefore be used to limit the number of calls to the flow

model because it is assumed that small changes to the bed level (due to deposition/erosion) may be quantified using the continuity equation.

Another commonly applied method is use of *morphological speed-up* in which it is exploited that flow and waves react at a much shorter time scale compared to the morphology. It is therefore possible to speed-up the calculated erosion/deposition without affecting the end result, thereby reducing the simulation time within the flow model.

Finally, *parallel computation* where the computational work is split out on several CPU's or PC's has greatly changed the size (both spatial and temporal) of the morphological problems that we solve today.

2.4 Hybrid morphological modelling

The hybrid morphological modelling concept which is used in this study represents an attempt at combining traditional 2D coastal models with behaviour-oriented models for the morphological evolution. The concept builds on many of the existing principles of medium term and long-term morphological models which have been described in the previous sections. The concept differs by the fact that the existing principles are used in the hybrid morphological modelling concept to guide/correct the solution calculated by a 2D coastal model whereas they in the existing models are used as the primary forcing term.

Examples of this is the general application of coastal parameters which describe and evolve a 2D bathymetry. Furthermore direct adoption of the profile diffusion model introduced in Capobianco et al. (1994) to correct coastal profiles evolved by the 2D coastal model is shown in Kristensen et al. (2013a,b) (sections 7 and 8). Finally examples where the 2D coastal model is used to calculate alongshore migration of a bar front is shown in Kristensen et al. (2010) (section 5).

The key motivation of hybrid morphological modelling is that it is possible to exploit that 2D coastal models may be used to calculate the detailed distribution of littoral drift and use this to evolve the coastal morphology on time scales of decades. Concurrently it is possible to prescribe the effect of cross-shore processes (which are ill-described by the 2D models) by use of behaviour-oriented concepts.

Chapter 3

Scope of the thesis

The study presented in this thesis has focussed on developing different implementations within the principles of the hybrid morphological modelling concept. The implementations should ideally address problems concerned with coastal protection. The exact form of the implementations was not given beforehand and the problems addressed in this study span therefore over a wide range of problems and methods. Consequently this thesis does not describe all implementations and some of the implementations may be rather questionable but have been included for the purpose of discussion.

We acknowledge the fact that validation against field experiments and physical experiments is an important part of morphological modelling but our efforts within this field have been kept at a minimum. We feel that adequate validation would limit our possibilities to explore different implementations within the principles of hybrid morphological modelling. For the same reasons we have spent no effort on implementing the methods directly into a coastal area model but have rather worked in a layer outside the coastal area model within a Matlab framework. Function prototyping and debugging is substantially easier and faster within Matlab.

A number of articles and conference proceedings have been published during this study. They generally present examples with a number of different hybrid morphological model implementations to certain engineering problems. Some include validation against field measurements on a very basic level and in other papers, application of the hybrid morphological model is used to gather insight into important morphological processes.

3.1 Structure of the thesis

After the introductory part of the thesis (chapters 1 and 2), the remaining part is structured as follows:

Chapter 4 gives a detailed description of the hybrid morphological model implementations developed in this study with reference to the papers in which each implementation is applied. First, section 4.1 presents an illustration of the hybrid morphological modelling concept and a brief summary of the components required for the implementation is given. Further details into the implemented components are then given in the following sections. Sections 4.2 to 4.4 are concerned with the 1D

and 1.5D shoreline models while section 4.5 describes three different implementations of models used for morphological evolution of alongshore migrating bars.

Chapters 5 to 9 contain 5 papers which have been prepared during this study. The first paper in chapter 5 is a conference proceedings paper from 2010 where the hybrid modelling concept is introduced for different coastal problems (groynes, breakwaters, nourishment and alongshore migrating bars).

Chapter 6 is a conference proceedings paper from 2012 which contains a validation of a 1D shoreline model to a salient evolution behind a shipwreck located in Table Bay, South Africa. The paper shows also that the hybrid morphological modelling concept can be applied to general cases.

Chapter 7 is an accepted journal paper in which 1D and 1.5D shoreline models are used to simulate morphological evolution around segmented breakwaters. The 1D model is applied to cases where the breakwaters are located seaward of the surf zone while the 1.5D model is applied to coastal breakwaters. The paper discusses salient response to breakwaters and changing wave forcing. The paper shows furthermore that the 1.5D model may be used to predict the type of equilibrium planform behind coastal breakwaters for a given forcing condition.

Chapter 8 is an unpublished manuscript in which morphological response to groyne fields is examined using both 1D and 1.5D shoreline models. The paper describes important processes around groynes in groyne fields and it is concluded with a discussion on how length scales of groynes impact the average littoral drift.

Chapter 9 is a conference proceedings paper from 2012, which describes a case at the East harbour of Dunkerque, France where the hybrid morphological modelling concept is applied as a decision support tool for 5 different nourishment scenarios. In the work presented in the paper, morphological evolution of beach nourishment and shoreface nourishment over 10 years are treated and discussed.

Finally, discussions and conclusions of the study are given in chapter 10 with recommendations for future work.

Chapter 4

Model documentation

The different model implementations of the hybrid morphological concept which have been developed in the course of this study are documented in detail in this chapter. A general definition of the hybrid modelling concept is given in section 4.1 in order to illustrate the tools required to implement the concept.

Some of the concepts given here are repeated in the 5 papers. This chapter is included to give a more comprehensive description, including details which are not possible to include in journal papers or in conference papers.

4.1 Hybrid morphological modelling concept

The hybrid morphological modelling concept combines the 2D information obtained from a *coastal area model* for waves, flow and sediment transport with a simplified scheme for the *morphological evolution* of the coastal area. The coastal area model and the morphological evolution model are coupled by defining the 2D bathymetry parametrically and by allowing morphological evolution in terms of evolution of the coastal parameters. Changes to the coastal parameters are based on gradients in the 2D sediment transport field. The steps of a morphological cycle are illustrated in figure 4.1 and listed here:

1. Define shoreline and a parametric description of the coastal profile
2. Construct a 2D bathymetry from the parametric description
3. Calculate the 2D sediment transport using a coastal area model
4. Integrate longshore transport, to form the alongshore variation of the littoral drift
5. Calculate changes in profile volume (or shoreline position) due to gradients in littoral drift
6. Update coastal parameters according to changes in profile volume

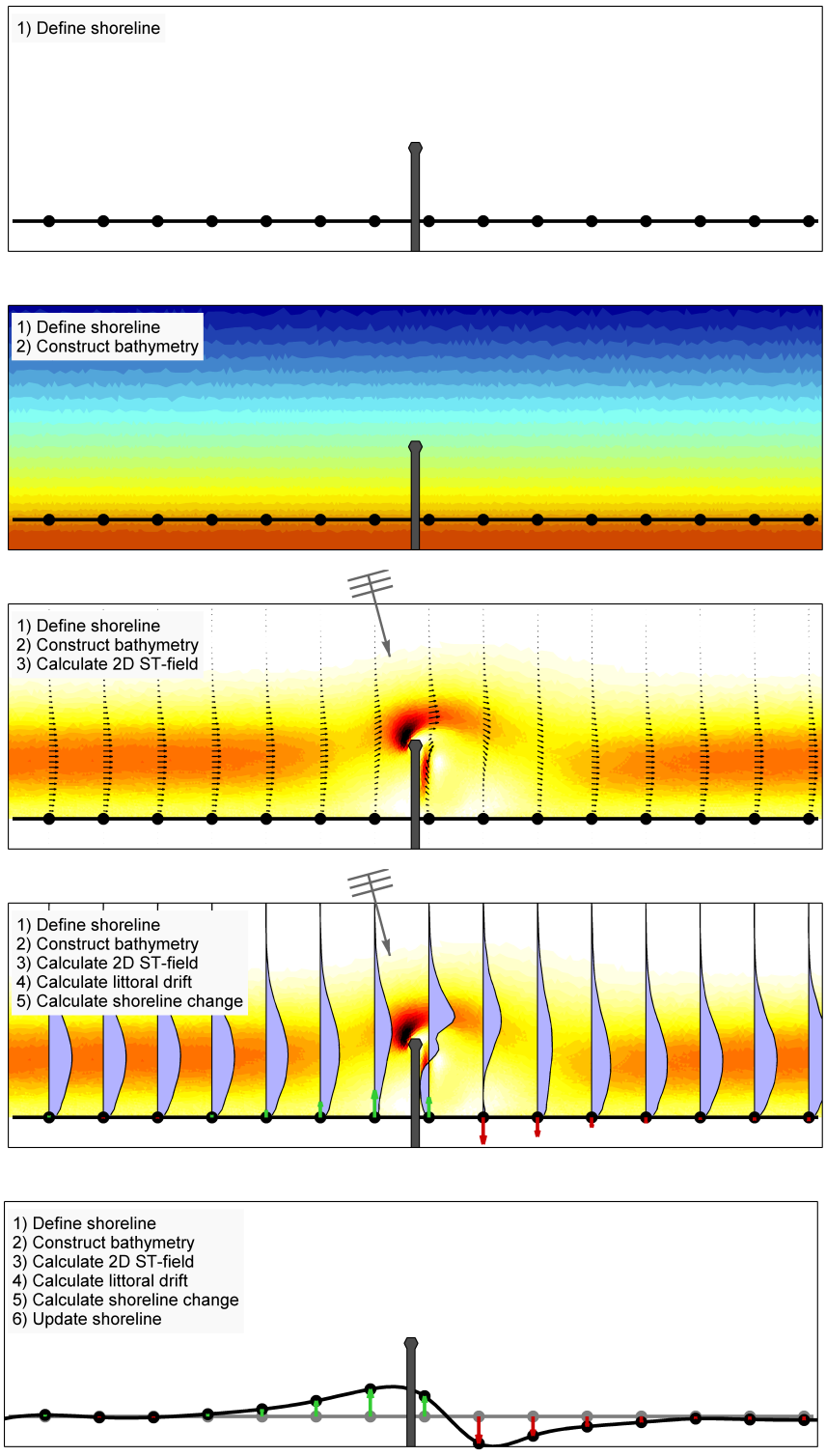

Figure 4.1: *Illustration of the hybrid morphological modelling concept applied to a groyne.*

The particular definition of the parametric coastal profile varies depending on the model implementation (1D,1.5D,Bar) and the different definitions treated in this study are therefore described together with definitions of the morphological models in section 4.4. Common to all implementations is however that the implementations use a local Cartesian coordinate system where the first coordinate r is oriented in the general longshore direction and the second coordinate s is oriented in the cross-shore direction, positive in the seaward direction. The local coordinate system simplifies greatly all discussions and has been introduced in order to make the model implementations as general as possible. Figure 7.2 in Kristensen et al. (2013a) shows an example of the local coordinate system for the case of a detached breakwater.

Writing the parametric profile to the 2D bathymetry is done irrespective of the individual model implementations because the coastal parameters are defined as functions of the alongshore coordinate r. The 2D bathymetry can therefore be calculated by evaluation of the cross-shore coordinate and by evaluation of each of the coastal parameters (e.g. shoreline position and profile slope) at a particular longshore coordinate, i.e.:

$$z(r,s) = s_0(r) + A(r)\,(s - s_0(r)) \tag{4.1}$$

The above expression illustrates that by defining a shoreline position $s_0(r)$ and a profile slope $A(r)$, calculation of a 2D bathymetry (in (r,s)-space) is possible. The coastal parameters are however in practice discrete values, and linear interpolation of the coastal parameters is therefore employed when the 2D bathymetry is constructed.

The 2D sediment transport field is calculated by use of a 2D coastal model. In this study the coupled model by DHI, MIKE21 FM is used. The model is composed of a spectral wave module for transformation of waves over a 2D bathymetry, a depth integrated flow model based and an intra-wave sediment transport model. The coastal model solves wave field, flow field and sediment transport field on an unstructured mesh which can include triangular and quadrilateral elements using a finite volume method. MIKE21 FM has not been modified in this study, and no further documentation of the coastal model is given. Some additional details of the setup of the model may be found in the enclosed articles where the hybrid modelling concept is applied to various cases (see sections 7.2.1, 8.2.1).

Two different methods have been used for cross-shore integration of the calculated 2D sediment transport field. The first method distributes a number of discrete points along the coastal profile which are then used to calculate the littoral drift using numerical integration. The second method applies coordinate transformation to identify elements intersecting the coastal profile. The littoral drift in the second method is then determined as a weighted sum of each intersecting element. The second method was developed late in the study in order to remove the discrete representation of the littoral drift. Both methods are presented in appendix A.

The evolution of the profile volume follows the well known 1D continuity equation:

$$\frac{\partial V}{\partial t} = \frac{-1}{1-n}\frac{\mathrm{d}Q_\mathrm{l}}{\mathrm{d}r} \tag{4.2}$$

Details are as given in section 4.2. Basically gradients in the littoral drift are evaluated using an upwind finite volume method and the temporal derivative of the profile volume, V is evaluated using a first order explicit Euler scheme. This combination of spatial and temporal scheme is often in

the literature also referred to as Forward in Time Backwards in Space (FTBS), and is considered a simple scheme which has some amount of inherent diffusion (for small time steps). FTBS is therefore within other disciplines often viewed as inaccurate and inappropriate, while it within morphological schemes is widely used. Higher order temporal schemes may in some morphological application be used because they are fairly simple to implement. They are however not used within the hybrid modelling framework because the wave forcing in some applications, changes significantly between each successive morphological time step (due to simulation of sea-states), thereby rendering the assumptions in the higher order temporal schemes meaningless.

Finally, update of the coastal parameters depends on the particular definition of coastal profile and it's freedom. Update of the coastal parameters is therefore treated separately in sections 4.4 and 4.5 where each of the morphological models are treated.

4.2 Calculating evolution in profile volume

The evolution of profile volume is determined using the 1D continuity equation which is derived from the general 2D continuity equation:

$$\frac{\partial \tilde{V}}{\partial t} = \frac{-1}{1-n} \int_A \left(\frac{\partial q_\mathrm{r}}{\partial r} + \frac{\partial q_\mathrm{s}}{\partial s} \right) \mathrm{d}A \tag{4.3}$$

where $\tilde{V}$ is the volume of sediment within a 2D control volume spanned by the area A, $q_\mathrm{r}, q_\mathrm{s}$ are the alongshore transport and cross-shore transport (solid volume) respectively, and n is the volumetric porosity of the deposited sand. The control volume is sketched in figure 4.2. The 1D continuity equation is obtained by evaluating the cross-shore component of the area integral in equation 4.3:

$$\frac{\partial \tilde{V}}{\partial t} = \frac{-1}{1-n} \int_R \frac{\mathrm{d}Q_\mathrm{l}}{\mathrm{d}r} + q_\mathrm{crs,off} \, \mathrm{d}r \tag{4.4}$$

where Q_l is the littoral drift. By use of the divergence theorem and by defining a zero cross-shore transport over the landward edge of the control volume, the second term in the 2D continuity equation reduces to the cross-shore transport component over the offshore edge of the control volume.

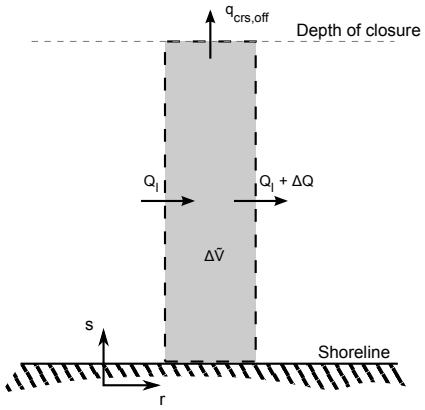

Figure 4.2: *Control volume used for derivation of 1D continuity equation.*

A special case of the 1D continuity equation forms when the control volume is rectangular in which case the alongshore width of the control volume is constant in the cross-shore direction. The profile volume may in this case be defined in terms of the cross-sectional area of the profile, V where $\tilde{V} = \int_R V \, \mathrm{d}r = V \Delta r$. Furthermore assuming that the contribution from the cross-shore transport is zero, the 1D continuity equation reduces to the well known form:

$$\frac{\partial V}{\partial t} = \frac{-1}{1-n} \frac{\mathrm{d}Q_\mathrm{l}}{\mathrm{d}r} \tag{4.5}$$

Using the 1D continuity equation it is clear that deposition of sediment within the control volume occurs when the gradient in the littoral drift is negative. The magnitude of the littoral drift is of no importance for the sediment balance.

Numerical scheme

Equation 4.5 is used in a finite volume form, where the alongshore integral of the divergence of the littoral drift is evaluated as the difference in littoral drift between the east and the west edge of the control volume as indicated in figure 4.2. Extraction of littoral drift as described in appendix A is however performed along the centreline of the control volume. First order upwind reconstruction of the littoral drift is therefore performed, in order to apply the extracted transport rates on the edges of the control volume. For example, reconstruction of the littoral drift on the west edge of the control volume shown in figure 4.3 is performed using the definition:

$$Q_{\mathrm{l,w}} = \begin{cases} Q_{\mathrm{l,P}} & , (Q_{\mathrm{l,W}} + Q_{\mathrm{l,P}}) \leq 0 \\ Q_{\mathrm{l,W}} & , (Q_{\mathrm{l,W}} + Q_{\mathrm{l,P}}) > 0 \end{cases} \tag{4.6}$$

This is a standard Finite Volume flux reconstruction scheme, in which the upwind "direction" is based on the direction of the average transport between the two neighbouring control volumes. It is assumed that a positive transport occurs to the right.

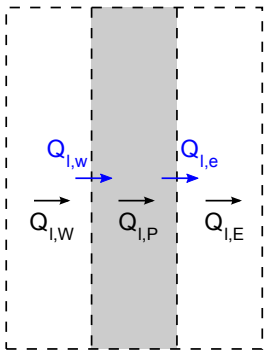

Figure 4.3: *First order upwind flux reconstruction in the Finite Volume method. Positive transport towards right.*

The upwind flux reconstruction has in this study proven to give stable schemes. Other implementations where the littoral drift is extracted directly at the edge of two control volumes results in an unstable numerical scheme. This is not unexpected, since the spatial derivative in this case corresponds to a central difference scheme, which when combined with an Explicit Euler scheme for the temporal derivative is known to be unconditionally unstable for hyperbolic differential equations, which equation 4.5 is a member of.

4.3 Boundary conditions on littoral drift

Evaluating the spatial derivative of the 1D continuity equation (equation 4.5) requires also definition of boundary conditions at the lateral boundaries[1] of the model domain. Four different boundary conditions to the littoral drift have been used in this study, namely:

- Periodic flux
- Zero gradient on flux
- Constant gradient on flux
- Zero flux

The periodic boundary conditions have been used extensively in this study. The zero gradient on flux and constant gradient on flux have in practice served more as definitions for extrapolating the coastal parameters rather than actual boundary conditions, as will be evident from the following sections where each of the first three boundary conditions are treated separately.

Periodic boundary conditions

Periodic boundary conditions can only be defined in pairs, because quantities which exit the model domain at one boundary, enters the domain through the other boundary and vice versa. The principle of periodic boundaries is illustrated in figure 4.4, in which the model domain is wrapped into a cylinder. The line where the two edges connect is the periodic boundary. Periodic boundary condition do not require the solution to be uniform perpendicular to the periodic boundaries just a perturbations are allowed to travel around the cylinder in the figure with no regard to the location of the periodic boundary.

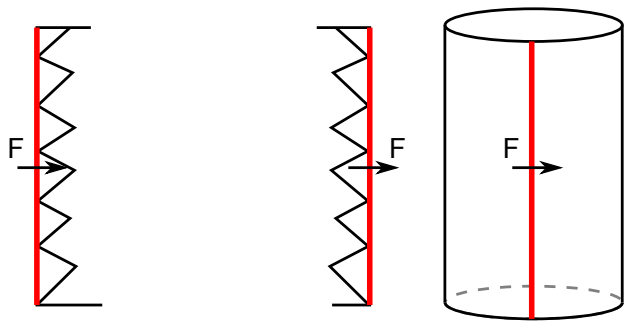

Figure 4.4: *Principle in periodic boundary conditions. The domain is conceptually wrapped into a cylinder.*

Periodic boundary conditions are easily implemented in 1D schemes since it requires simply that the extracted transport rates at the western most profile and at the eastern most profile are padded onto the existing vector of extracted littoral drift, i.e. if the littoral drift is extracted along N profiles:

$$Q_l = \left[\begin{array}{ccccc} Q_1 & Q_2 & \dots & Q_{N-1} & Q_N \end{array} \right]$$

[1] The boundaries which are normal to the shoreline

then, a periodic calculation of gradients in the littoral drift may be obtained by defining a periodic transport vector:

$$Q_{\mathrm{l,p}} = \left[\begin{array}{ccccccc} Q_N & Q_1 & Q_2 & \dots & Q_{N-1} & Q_N & Q_1 \end{array} \right]$$

and performing the usual upwinding on $Q_{\mathrm{l,p}}$ as discussed previously.

Periodic boundary conditions need also to be implemented in the 2D coastal model in order for the extracted littoral drift near the lateral boundaries to be consistent. The 2D coastal model used in this study supports periodic boundary conditions assuming that the mesh is constructed such that the mesh elements along two periodic boundaries conform to each other. Example of periodic boundaries with conforming and non-conforming computational elements are shown in figure 4.5. Construction of a periodic mesh with conforming elements is however not available within the DHI software, and two alternative methods have therefore been developed during this study. The methods are documented in appendix B.

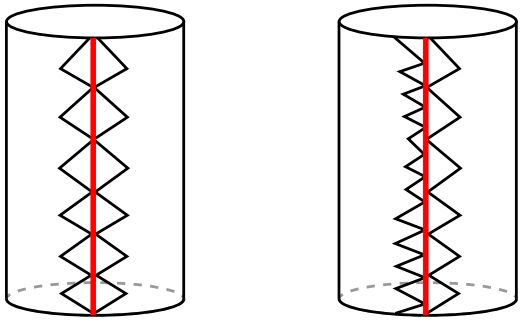

Figure 4.5: *Definition of a periodic mesh with conforming (left) and non-conforming (right) computational elements*

Zero gradient boundary condition

The zero gradient boundary condition on the littoral drift implies that the change in profile volume at the lateral boundaries should be zero. This type of boundary condition is therefore implemented by defining the LHS of equation 4.5 as zero at the outermost profiles.

The condition is in most cases applied to a number of profiles and is also combined with a blending function which ensures a gradual transition from the reduced morphological evolution to full freedom. The boundary condition is illustrated in the left panel of figure 4.6 which shows a conceptual shoreline evolution around a groyne.

Constant gradient boundary condition

The constant gradient boundary condition on the littoral drift implies that the shoreline orientation is fixed at the boundary. The boundary condition is therefore implemented by constant value extrapolation of the LHS of equation 4.5 to the outermost profiles.

The constant gradient boundary condition is in most cases applied over a number of coastal profile which ensures that the shoreline orientation is maintained at a certain distance from the model domain. The boundary condition is illustrated in the right panel of figure 4.6.

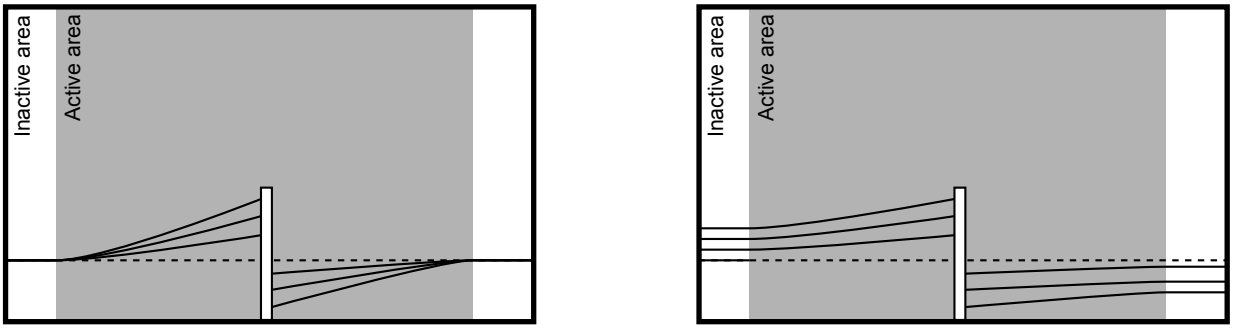

Figure 4.6: *Conceptual illustration of zero gradient boundary condition (left) and constant gradient boundary condition (right) applied in a 1D shoreline model.*

4.4 Morphological shoreline evolution models

This section focusses on coupling the evolution of the coastal parameters with the evolution in profile volume. The section is divided according to the model type (1D and 1.5D) since each model type contains a separate definition of the coastal profile and degree of freedom of the profile. The section is structured as follow: Details on 1D shoreline models are given in section 4.4.1. Details on the 1.5D shoreline model are given in section 4.4.2 with an emphasis on the implementation of the cross-shore redistribution used by this model type.

Each of the sections include a short description on where application of the individual models may be found.

4.4.1 1D shoreline models

All the shoreline models used in this study make use of a Dean type power profile, which is defined as:

$$z(s) = \begin{cases} z_0 & , \quad s \leq s_0 \\ z_0 - A\,(s - s_0)^m & , \quad s_0 < s \leq s_{\mathrm{cl}} \\ z_{\mathrm{cl}} & , \quad s_{\mathrm{cl}} < s \end{cases} \tag{4.7}$$

where (s_0, z_0) is the berm position, A and m control the average and local slope of the profile and z_{cl} is the level of closure depth beyond which no morphological activity exists. The power profile is shown in figure 4.7.

The freedom of the coastal profile may vary. For this study the degrees of freedom examined are:

- Translation of the coastal profile
- Hinged response: profile is hinged to the depth of closure
- Translation of the coastal profile, but deposition is restricted by seawall and/or offshore breakwaters

Each of the model implementations are treated in the following sections.

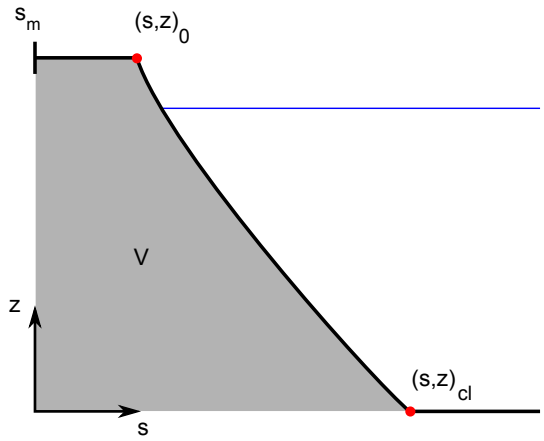

Figure 4.7: *Dean type coastal profile commonly used in the 1D shoreline models. The figure is from Kristensen et al. (2013a).*

1D translation

The 1D translation is the simplest version of the 1D shoreline model. It is assumed that the coastal profile maintains it's form and response to erosion/deposition is a landward/seaward displacement of the entire profile. This model type has been used extensively throughout this study. It has been used to simulate morphological evolution behind offshore breakwaters (see chapters 7 and 6), response to groynes (see chapters 5 and 8) and finally it has been used to simulate shoreline evolution along the coast east of Dunkerque, France in chapter 9.

The profile volume (the shaded area in figure 4.7) may be calculated in terms of the profile parameters by integration i.e.:

$$V = \int_{s_\mathrm{m}}^{\infty} z - z_\mathrm{cl}\,\mathrm{d}s \tag{4.8}$$

where the value of the lower integration limit, s_m is of minor importance as we will focus on the rate of change in volume. s_m should however in principle be chosen landward of the berm position with the largest expected erosion. Inserting the profile definition from equation 4.7 and evaluating the integral, the profile volume may be calculated in terms of the profile parameters:

$$V = (s_0 + W_\mathrm{act} - s_\mathrm{m})\,h_\mathrm{act} - h_\mathrm{act} W_\mathrm{act} \frac{1}{m+1} \tag{4.9}$$

here we have introduced the active height of the coastal profile, $h_\mathrm{act} = z_0 - z_\mathrm{cl}$, the width of the active profile, $W_\mathrm{act} = s_\mathrm{cl} - s_0$ and we have expressed the average slope of the active profile as $A = h_\mathrm{act}/W_\mathrm{act}^m$.

Changes in volume may now be related to changes in profile parameters by taking the temporal derivative of equation 4.9. For the case the coastal profile translates in the offshore/onshore direction, the only parmeter which is variable in time is s_0. The temporal derivative of equation 4.9 reduces therefore to:

$$\frac{\partial V}{\partial t} = h_\mathrm{act} \frac{\partial s_0}{\partial t} \tag{4.10}$$

This is often combined with equation 4.5, thereby forming the well known 1D continuity equation for a profile which translates in response to erosion/deposition:

$$\frac{\partial s_0}{\partial t} = \frac{-1}{1-n}\frac{1}{h_{\text{act}}}\frac{\partial Q_l}{\partial r} \tag{4.11}$$

1D hinged response

The 1D hinged response assumes that the cross-shore distribution of erosion/deposition is concentrated closer to the shoreline. Basically it is assumed that no changes occur at the depth of closure, and that response to accretion in the hinged profile response will therefore be an increase in profile slope. The 1D hinged profile response may be challenged in cases where the shoreline response is comparable to the width of the active profile. The hinged 1D response has been applied to study morphological evolution around groynes in chapter 8.

Derivation of the hinged profile response is based on the profile volume given in equation 4.9. For the hinged response, changes to profile volume changes both the berm position, s_0 and the width of the active profile width, W_{act}. The temporal derivative of the volume equation reduces therefore to:

$$\frac{\partial V}{\partial t} = \frac{h_{\text{act}}}{m+1}\frac{\partial s_0}{\partial t} \tag{4.12}$$

This may be combined with equation 4.5, thereby forming the 1D continuity equation for a profile with a hinged response to erosion/deposition:

$$\frac{\partial s_0}{\partial t} = \frac{-1}{1-n}\frac{m+1}{h_{\text{act}}}\frac{\partial Q_l}{\partial r} \tag{4.13}$$

1D translation with structural restraints

Applying the 1D translation model when shore parallel structures are present may require that the presence of the structures is accounted for as illustrated in figure 4.8. The figure illustrates how an offshore breakwater may be expected to limit morphological activity seaward of the structure and how a seawall will increase the minimum depth in response to erosion.

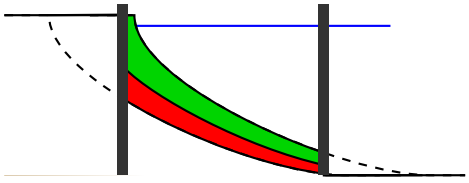

Figure 4.8: *Presence of a seawall or an offshore breakwater may restrain the morphological activity of the coastal profile.*

The 1D translation model with restraints has been applied to an offshore breakwater in chapter 5 and to the dike east of Dunkerque, France in chapter 9.

Evolution of the coastal parameters is performed by use of numerical solution of the problem:

$$V(s_0^{k+1}) = V(s_0^k) + \frac{\partial V}{\partial t}\Delta t \tag{4.14}$$

where the super index indicates the time step, and $\partial V/\partial t \Delta t$ is determined from gradients in the littoral drift according to equation 4.5. The profile volume is calculated according to the definition:

$$V(s_0) = \begin{cases} (s_0 + W_{\text{act}} - s_{\text{m}})\, h_{\text{act}} - \frac{h_{\text{act}} W_{\text{act}}}{m+1} & , \quad \text{type 0} \\ (s_0 + W_{\text{act}} - s_{\text{m}})\, h_{\text{act}} - \frac{h_{\text{act}} W_{\text{act}}}{m+1} \left(1 - \left(\frac{s_{\text{SW}} - s_0}{W_{\text{act}}}\right)^{m+1}\right) & , \quad \text{type 1} \\ (s_{\text{BW}} - s_{\text{m}})\, h_{\text{act}} - \frac{h_{\text{act}}}{(m+1) W_{\text{act}}^{m}} (s_{\text{BW}} - s_0)^{m+1} & , \quad \text{type 2} \\ (s_{\text{BW}} - s_{\text{m}})\, h_{\text{act}} - \frac{h_{\text{act}}}{(m+1) W_{\text{act}}^{m}} \left((s_{\text{BW}} - s_0)^{m+1} - (s_{\text{SW}} - s_0)^{m+1}\right) & , \quad \text{type 3} \end{cases} \tag{4.15}$$

where the 4 different types are defined according to the position of the berm and s_{cl} relative to the position of the seawall and breakwater as sketched in figure 4.9. s_{SW} is the cross-shore position of the seawall and s_{BW} is the cross-shore position of the breakwater.

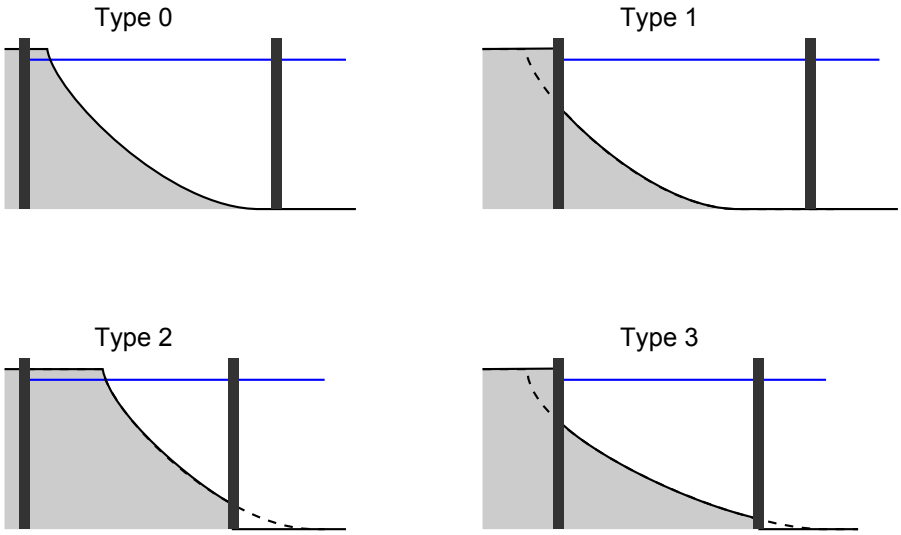

Figure 4.9: *Four different cases are used to calculate the profile volume.*

4.4.2 1.5D morphological model

The 1.5D morphological model was introduces in Kristensen et al. (2013a) as a shoreline model which can handle problems where significant changes to the coastal profile may be expected due to medium/strong 2D effects. The name "1.5D" is used because the shoreline model uses a coastal profile in which the total volume changes according to gradients in the littoral drift, while concurrently allowing changes to the profile to occur according to the spatial distribution of an erosion/deposition field extracted from the 2D coastal model. The 1.5D model deviates therefore from traditional 2D models in the fact that the morphological evolution is described in terms of a number of coastal parameters rather than by changing the bed level of each computational cell.

The 1.5D hybrid morphological model has been applied to segmented coastal breakwaters (see chapter 7) and to groyne fields (see chapter 8). In both cases the model is used to simulate the impact of the structures on the morphology, and littoral drift on idealised cases.

Profile definition

In the 1.5D morphological model, the coastal profile is defined by a number of points which are joined by linear segments. Each point is allowed vertical freedom, thereby allowing the profile

to change form and volume. The points used to define the coastal profile are denoted *coastal parameters* thereby following the jargon used in the 1D shoreline model. Morphological evolution is implemented by use of non-linear optimisation of the vertical position of profile parameters such that the change in profile gives the best fit to the spatial distribution of the erosion/deposition field given by the 2D coastal model. The optimisation is performed successively on each coastal profile in the model domain.

Volume conservation is ensured by introduction of bound parameters. The evolution of a bound parameter is determined such that a specific profile volume is obtained. An example of this principle is shown in (Kristensen et al., 2013a, Appendix A), which is reproduced on page 102.

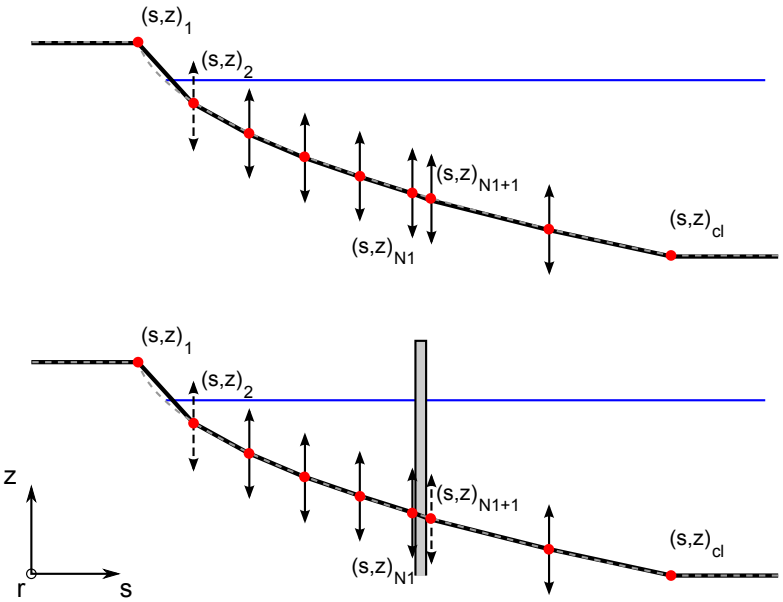

Figure 4.10: *Definition of the coastal profile used in the 1.5D hybrid morphological model. The freedom of the profile is illustrated with the vectors. The dashed vectors indicate that freedom which is bound by continuity.*

The possible definitions of coastal profiles within the 1.5D model are shown in figure 4.10. The first profile is used on an open coast where the profile volume covers the entire coastal profile (therefore including 1 bound parameter), while the second profile is used for profiles which are intersected by a structure thereby dividing the profile volume into a part landward and a part seaward of the structure (this profile has 2 bound parameters). The first profile type is also used for profiles which are limited by a seawall. Figure 4.11 shows an example, where the two types of coastal profile are combined for simulation of a case involving a groyne, a seawall and a detached breakwater. Note that groynes are defined at the interface between morphological elements and the open type coast profile is therefore used for this type of structure.

Optimisation of coastal parameters

The non-linear optimiser is based on the Nelder-Mead algorithm, which can be used on an arbitrary number of degrees of freedom. In Lagarias et al. (1999) it is discussed that the method can only be proven to have strict convergence in convex problems of 1 dimension. Application of the optimiser to simulation of morphological evolution around coastal breakwaters in Kristensen et al. (2013a) indicates however that the method does seem to converge towards the solution of a traditional 2D

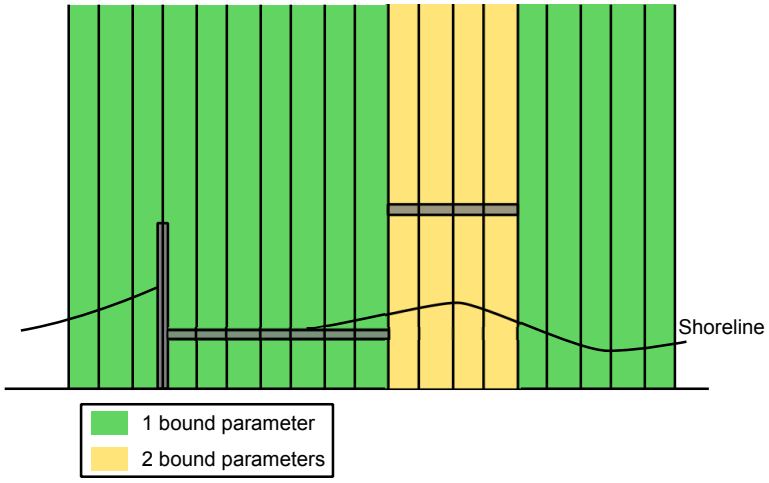

Figure 4.11: *The type of coastal profile is defined during model setup and depends on whether the profile is intersected by a structure (in the surf zone) or not.*

model when the number of profile parameters is increased. In Kristensen et al. (2013a) degrees of freedom ranging from 3 to 20 were considered.

The non-linear optimisation may formally be defined as:

$$\psi_j^{k+1} = \text{argmin}\left(\varepsilon\left\{\psi_j^k, \psi_j^{k+1}, \partial z/\partial t \Delta t\right\}\right) \tag{4.16}$$

where ψ_j^k is a vector containing the coastal parameters of the jth profile at time step k. $\partial z/\partial t$ is the rate of bed level change of the computational elements located inside the jth control volume. Identification of the computational elements is based on the position of their element centre, as illustrated in figure 4.12. Δt is the morphological time step, and ϵ is the area weighted rms-difference between the future parametric coastal profile and the profile obtained with the erosion/deposition field simulated by the 2D coastal model. ε is evaluated at the centre of the computational elements.

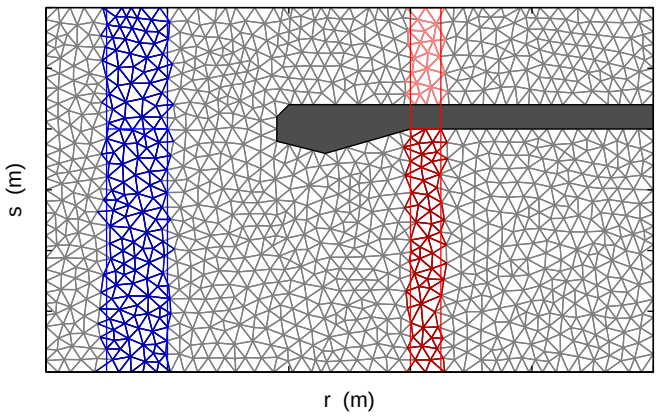

Figure 4.12: *Identification of computational elements enclosed by the control volume of a coastal profile is based on the element centres. Examples are: Free profile (blue) and profile which is intersected by a breakwater (red).*

The bound parameters for ensuring continuity are derived using the trapezoidal rule of integration.

For an open profile consisting of cl points, the profile volume is calculated as:

$$V = (s_1 - s_{\mathrm{m}})\,(z_0 - z_{\mathrm{cl}}) + \frac{1}{2}\sum_{i=2}^{cl}(s_i - s_{i-1})\,(z_i + z_{i-1} - 2z_{\mathrm{cl}}) \tag{4.17}$$

Given a profile volume, V, the bound parameter may be isolated from the expression above and used for calculating the value of the bound parameter, the bound parameter is said to be *reconstructed*. Reconstruction of the bound parameters is introduced as a method for ensuring that the non-linear optimiser only evaluates problems where the volume is conserved.

Tests have shown that the method is insensitive to the position of the bound parameter in the profile. The bound parameter has however been defined as the landward most wet coastal parameter within a control volume as indicated in figure 4.10.

The size of the computational cells is generally selected such that the alongshore width of the morphological control volume is 2-3 times larger. This ensures that the erosion/deposition field within a control volume contains a fair amount of cells for the optimisation, while the morphological model is capable of resolving local features which are propagating in the solution. When the control volume is too narrow, it may occur that parts of the coastal profile are not resolved thereby allowing the profile parameters to attain non-physical values without affecting ϵ. Conversely, too large an alongshore width of the control volume, reduces the ability of the model to propagate undulations because erosion and subsequent deposition is located within the same control volume, a principle which is sketched in figure 4.13.

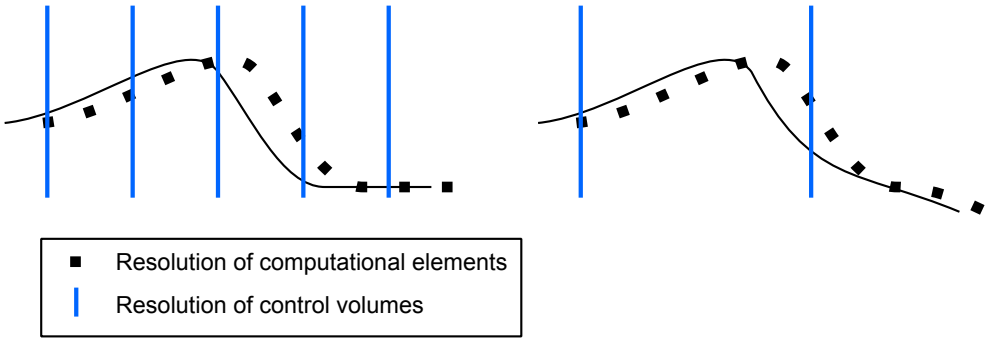

Figure 4.13: *The non-linear optimiser cannot resolve propagation of certain features if the alongshore width of the morphological control volume is too large compared to the alongshore resolution of the computational elements.*

Cross-shore diffusion

A cross-shore redistribution of sediment within the coastal profile is introduced in order to weakly force the coastal profile towards an equilibrium profile. The cross-shore redistribution is implemented as a diffusion type model similar to that proposed by Capobianco et al. (1994) and used in other types of 2D models such as the one presented in Falqués et al. (2000).

Cross-shore transport formulation

The cross-shore transport is defined as proportional to the longshore transport rate and a function of the deviation of the local profile slope from the slope of the equilibrium profile on the same water

depth, i.e.:

$$q_{\mathrm{crs}} = K \frac{q_{\mathrm{l}}}{\sin\left(\theta_{\mathrm{bc}} - \beta\right)} \frac{\alpha - \alpha_{\mathrm{eq}}}{\alpha_{\mathrm{eq}}} \tag{4.18}$$

where K is a dimensionless diffusion coefficient, θ_{bc} is the angle of wave incidence at breaking, although in practice at the offshore boundary of the model domain and β is the angle of the shoreline normal at the profile where q_{l} is given. The inverse dependency of the angle between waves and shoreline normal is included because the cross-shore transport should be independent on wave angle while the longshore transport is not. α is the local profile slope, and the cross-shore transport will therefore be offshore for cases where the profile is too steep and vice versa. The cross-shore redistribution has been implemented such that q_{l}, α and, α_{eq} are all expressed as functions of the local bed level, z.

In the model results applied to segmented coastal breakwaters (section 7) and groyne fields (section 8), the distribution of q_{l} is extracted from a single profile located at some distance from the structures. This has been done in order to ensure that the distribution of q_{l} matches the actual wave forcing. In hindsight, it may be preferred to extract q_{l} from an external simulation in an idealised domain where the bathymetry fits the equilibrium coastal profile. This will ensure that the applied q_{l} is unaffected by 2D circulation currents which in some cases develops e.g. for the case with $H_{\mathrm{s}} = 1.0$ m in groyne fields in figure 8.8, on page 121 (from Kristensen et al. (2013b)). Development of the 2D circulation currents alters the cross-shore distribution of the littoral drift and thereby also the distribution of the cross-shore diffusion.

Modification to the longshore transport distribution

The distribution of the longshore transport, q_{l} is modified before using it to calculate the cross-shore diffusion. The modifications are shown in figure 4.14 and are outlined in the following: The cross-shore diffusion is assumed to be significant near the shoreline, while the longshore transport signal decreases towards the shoreline. $q_{\mathrm{l}} = q_{\mathrm{max}}$ is therefore applied landward of the point where the peak longshore transport occurs. Furthermore, q_{l} should not be lower than 10% of the peak transport, q_{max}. The example of the modifications to q_{l} is shown for a case with $H_{\mathrm{s}} = 1.5$ m, $T_{\mathrm{p}} = 8$ s, $\theta_0 = 30\,\mathrm{deg}$ on a profile with $A = 0.095$ and $m = 0.67$. The transport rates are given in $\mathrm{m}^3/\mathrm{yr/m}$ assuming a porosity of $n = 0.4$.

Calculating the equilibrium profile slope

In the application of the 1.5D model the equilibrium profile is assumed to be a Dean type power profile as given by equation 4.7. The local slope of the equilibrium profile expressed as function of the bed level is then given by:

$$\alpha_{\mathrm{eq}}(z) = -Am \left(\frac{z_0 - z}{A} \right)^{(m-1)/m} \tag{4.19}$$

The result is obtained by first evaluating the derivative, $\mathrm{d}z/\,\mathrm{d}s$ and then substituting $s - s_0 = \left(\left(z_0 - z\right)/A\right)^{1/m}$.

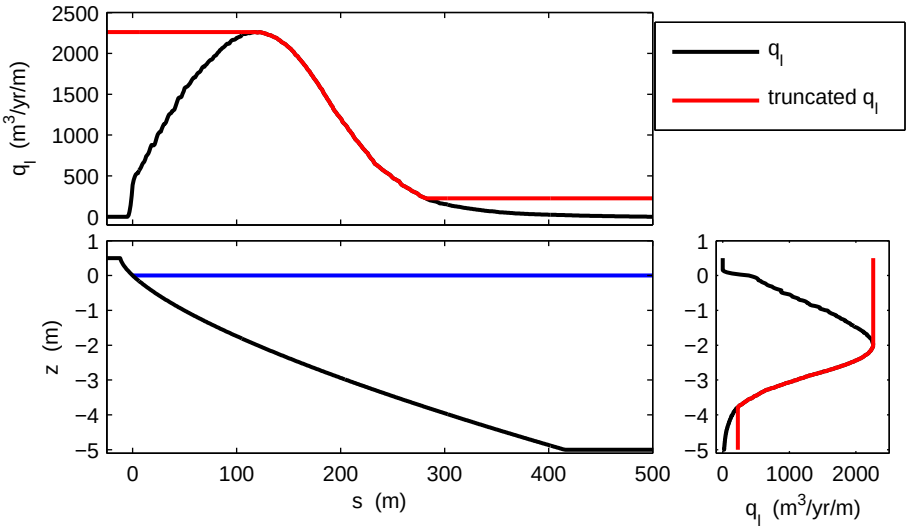

Figure 4.14: *The distribution of q_l is modified landward of the peak in transport and for rates smaller than 10% of the transport peak before using it in equation 4.18.*

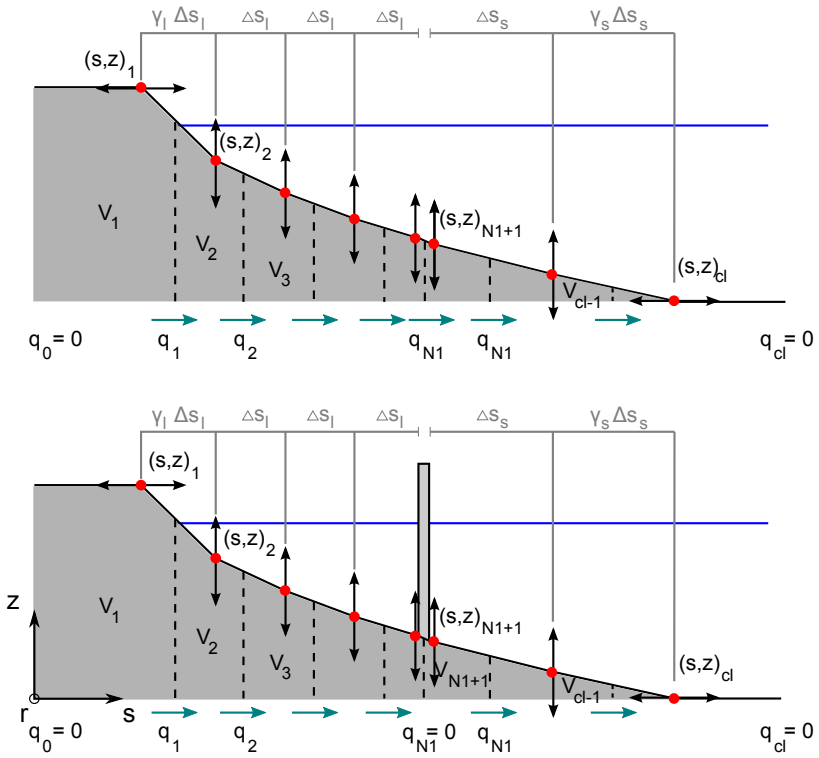

Figure 4.15: *The coastal profile is sub-divided into smaller sections when introducing a cross-shore transport used to force the profile towards an equilibrium profile.*

Morphological evolution model

The morphological evolution model due to cross-shore diffusion is based on subdivision of the coastal profile into smaller control volumes (sub-CV), as shown in figure 4.15. Furthermore, freedom of the coastal profile is defined similar to that in the optimisation method, although here horizontal

freedom of the berm and the foot of the coastal profile is also allowed.

The volume of each sub-CV may be expressed as function of the coastal parameters:

$$V_1 = (s_1 - s_\mathrm{m})(z_1 - z_\mathrm{cl}) + \frac{1}{8}(s_2 - s_1)(z_2 + 3z_1 - 4z_\mathrm{cl})$$

$$V_j = \frac{1}{8}(s_j - s_{j-1})(z_{j-1} + 3z_j - 4z_\mathrm{cl}) + \frac{1}{8}(s_{j+1} - s_j)(z_{j+1} + 3z_j - 4z_\mathrm{cl}) \tag{4.20}$$

$$V_\mathrm{cl} = \frac{1}{8}(s_\mathrm{cl} - s_{\mathrm{cl}-1})(z_{\mathrm{cl}-1} - z_\mathrm{cl})$$

The temporal derivative of the sub-CV's is then:

$$\frac{\mathrm{d}V_1}{\mathrm{d}t} = \frac{1}{8}(5z_1 - z_2 - 4z_\mathrm{cl})\frac{\partial s_1}{\partial t} + \frac{1}{8}(s_2 - s_1)\frac{\mathrm{d}z_1}{\mathrm{d}t}$$

$$\frac{\mathrm{d}V_2}{\mathrm{d}t} = \frac{1}{8}(-z_1 - 3z_2 + 4z_\mathrm{cl})\frac{\partial s_1}{\partial t} + \frac{3}{8}(s_2 - s_1)\frac{\mathrm{d}z_1}{\mathrm{d}t} + \frac{1}{8}(s_3 - s_2)\frac{\partial z_3}{\partial t}$$

$$\frac{\mathrm{d}V_j}{\mathrm{d}t} = \frac{1}{8}(s_j - s_{j-1})\frac{\partial z_{j-1}}{\partial t} + \frac{3}{8}(s_{j+1} - s_{j-1})\frac{\partial z_j}{\partial t} + \frac{1}{8}(s_{j+1} - s_j)\frac{\partial z_{j+1}}{\partial t} \tag{4.21}$$

$$\frac{\mathrm{d}V_{\mathrm{cl}-1}}{\mathrm{d}t} = \frac{1}{8}(s_{\mathrm{cl}-1} - s_{\mathrm{cl}-2})\frac{\partial z_{\mathrm{cl}-2}}{\partial t} + \frac{3}{8}(s_\mathrm{cl} - s_{\mathrm{cl}-1})\frac{\partial z_{\mathrm{cl}-1}}{\partial t} + \frac{3}{8}(z_{\mathrm{cl}-1} - z_\mathrm{cl})\frac{\partial s_\mathrm{cl}}{\partial t}$$

$$\frac{\mathrm{d}V_\mathrm{cl}}{\mathrm{d}t} = \frac{1}{8}(s_\mathrm{cl} - s_{\mathrm{cl}-1})\frac{\partial z_{\mathrm{cl}-1}}{\partial t} + \frac{1}{8}(s_{\mathrm{cl}-1} - s_\mathrm{cl})\frac{\partial s_\mathrm{cl}}{\partial t}$$

This coupled system may formulated on the matrix form:

$$\frac{\mathrm{d}}{\mathrm{d}t}\bar{V} = \bar{\bar{A}}\frac{\mathrm{d}}{\mathrm{d}t}\bar{\psi} \tag{4.22}$$

where $\bar{V}$ is a vector composed of the volumes of the sub-CV's, $\bar{\bar{A}}$ is a system matrix and $\bar{\psi} = [s_1, z_2, \ldots, z_{\mathrm{cl}-1}, s_\mathrm{cl}]^T$ is a vector with the time varying coastal parameters. The elements in the system matrix are also time varying because both horizontal and vertical freedom is included. The matrix equation is however evaluated using an Explicit Euler scheme in which the system matrix is treated as constant and it is therefore evaluated at the known time step:

$$\frac{\mathrm{d}}{\mathrm{d}t}\bar{V^k} = \bar{\bar{A}}^k\frac{\psi^{k+1} - \psi^k}{\Delta t}$$

where the super index refers to the time step. The LHS of the equation is determined from the divergence of the cross-shore transport which is calculated by equation 4.18 at the interface of each sub-CV. The local profile slope is therefore simply the slope of the linear segment between two points on the profile. For profiles where a breakwater is present, the cross-shore transport is set to zero at the interface located at the structure.

Handling presence of a seawall
If a seawall is present, this may be handled by changing the freedom of the point $(s,z)_1$ from being horizontal to vertical when cross-shore diffusion has caused the point to migrate landward of the seawall. The change in vertical freedom changes the temporal derivatives of V_1 and V_2 to:

$$\frac{\mathrm{d}V_1}{\mathrm{d}t} = \frac{3}{8}(s_2 - s_1)\frac{\partial z_1}{\partial t} + \frac{1}{8}(s_2 - s_1)\frac{\partial z_2}{\partial t}$$

$$\frac{\mathrm{d}V_2}{\mathrm{d}t} = \frac{1}{8}(s_2 - s_1)\frac{\partial z_1}{\partial t} + \frac{3}{8}(s_3 - s_1)\frac{\partial z_2}{\partial t} + \frac{1}{8}(s_3 - s_2)\frac{\partial z_3}{\partial t} \tag{4.23}$$

and the vector of free parameters is changed to: $\bar{\psi} = [z_1, z_2, \ldots, z_{\mathrm{cl}-1}, s_{\mathrm{cl}}]^T$.

Handling large shoreline changes
Due to the large changes to s_1 or s_{cl} which occur during the morphological simulations, it has been necessary to implement occasional redistribution of the profile parameters. The redistribution is performed when the distances $s_2 - s_1$ and $s_{\mathrm{cl}} - s_{\mathrm{cl}-1}$ become too small or too large. In most simulations the redistribution occurs for $0.5 \geq \gamma_l \geq 2$ and for $0.5 \geq \gamma_s \geq 2$ with γ_l and γ_s defined in figure 4.15. The points are redistributed evenly between s_1 and s_{N1} for large changes to the shoreline, or they are distributed evenly between $s_{\mathrm{N1}+1}$ and s_{cl} when large changes to s_{cl} has occurred. An alternative method has been investigated, where the cross-shore redistribution was performed during the solution of equation 4.22. The system matrix is however highly non-linear, and the evolution of s_1 and s_{cl} becomes very sensitive to changes in the central part of the profile.

Cross-shore diffusion applied different cases
The cross-shore diffusion model is applied to the four types of coastal profiles which were identified for the 1D model with structural restraints in figure 4.9. The cross-shore redistribution is simulated for a coastal profile which is initially steeper ($A = 0.14$) than the equilibrium profile ($A_{\mathrm{eq}} = 0.07$), thereby causing shoreline erosion. A cross-shore diffusion coefficient $K = 0.02$ is used and q_{l} is shown in figure 4.14 which is based on deep water wave characteristics: $H_{\mathrm{s}} = 1.5$ m, $T_{\mathrm{p}} = 8$ s and $\theta_0 = 30\,\mathrm{deg}$.

The morphological development over 1 year is shown in figure 4.16 for each of the four cases. The mildly sloping equilibrium profile is indicated as a dashed curve in order to illustrate that the coastal profile in fact does converge towards the equilibrium slope. Based on the figure the following observations are made:

- All methods are implemented such that volume is conserved.
- The evolution of s_{cl} is fairly strong due to the zero transport boundary condition applied at the closure depth and the minimum q_{crs} imposed on large water depths.
- The zero transport imposed on interfaces located at a breakwater is clearly seen in the two bottom panels, where a discontinuous profile develops.
- Shoreline erosion in front of a seawall causes the minimum depth to increase, as would be expected. This has been implemented by changing the system matrix in equation 4.22 to account for vertical freedom of s_1 rather than horizontal freedom.
- The 1.5D model may be applied to a larger management schemes by combination of the four basic profile types, as indicated in figure 4.11.

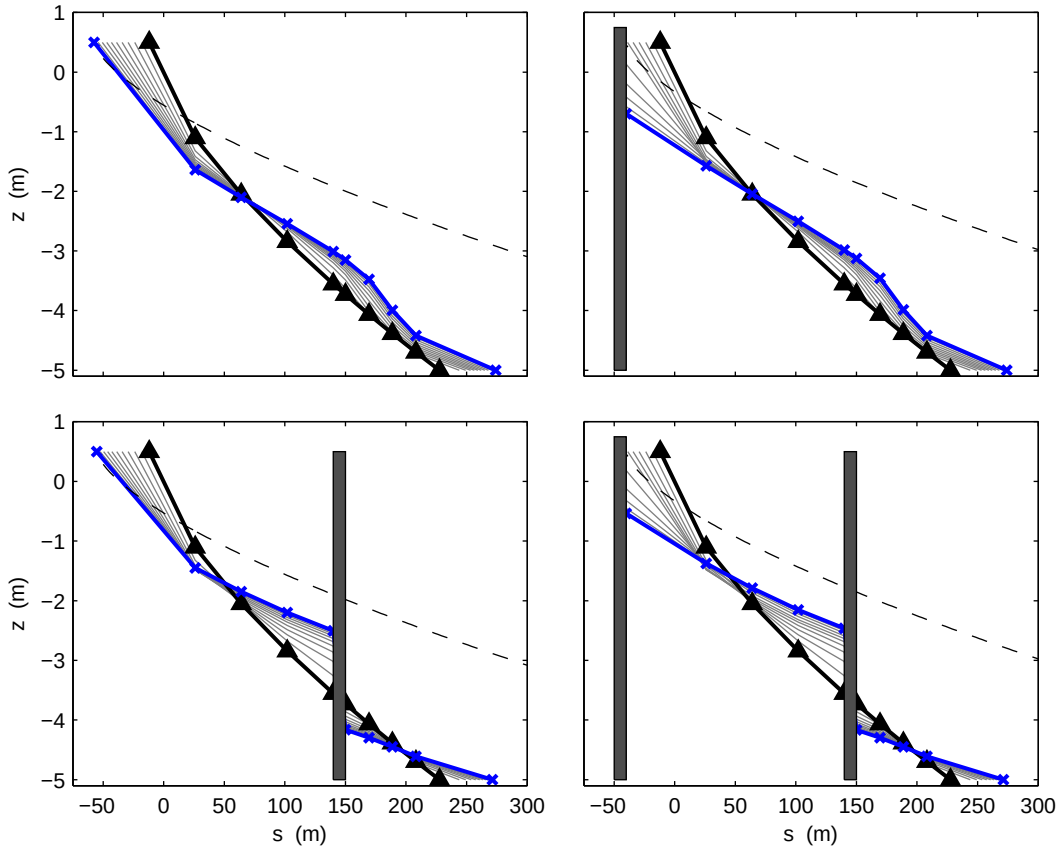

Figure 4.16: *Example of cross-shore diffusion applied to different types of profiles. Top left: Free profile, Top right: Seawall profile, Bottom left: Breakwater profile, Bottom right: Seawall and breakwater profile.*

4.5 Morphological models for local features

Three different types of models for simulation of bar dynamics are presented in the following sections. A comparison of the three models is presented in section 4.5.5.

4.5.1 Profile definition

The models used for morphological evolution of bars are defined to evolve a set of parameters which describe the cross-shore distribution of the profile shown in figure 4.17. The profile is defined by:

$$z_\mathrm{b} = \begin{cases} A_\mathrm{b} \sin^2 \phi_1(s)\,, & s_1 \leq s < s_c \\ A_\mathrm{b} \sin^2 \phi_2(s)\,, & s_\mathrm{c} \leq s \leq s_2 \end{cases} \tag{4.24}$$

where A_b is the bar amplitude, $\phi_1 = \frac{\pi}{2}\frac{s-s_1}{s_\mathrm{c}-s_1}$ and $\phi_2 = \frac{\pi}{2}\frac{s-s_2}{s_2-s_\mathrm{c}}$. ϕ_1 and ϕ_2 are functions of the cross-shore position and the first is used for the part of the profile landward of the crest, while the second is used for the part of the profile seaward of the bar crest. s_c is the cross-shore position of the bar crest. The cross-sectional volume of the bar profile is:

$$V_\mathrm{b} = \frac{1}{2} A_\mathrm{b} W_\mathrm{b}$$

where $W_\mathrm{b} = s_2 - s_1$ is the width of the bar. The skewness of the bar is defined as the ratio

$$\zeta = \frac{s_\mathrm{c} - s_1}{s_2 - s_1} \tag{4.25}$$

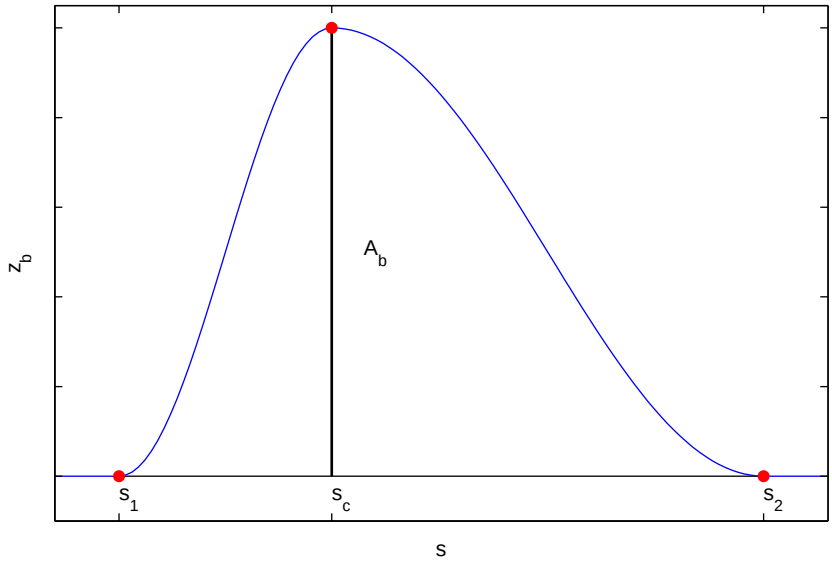

Figure 4.17: *Definition of the parametric profile used to describe bar evolution. The profile is composed of two* $\sin^2$ *contributions.*

4.5.2 Updating bar parameters using streamlines

This bar model is used to simulate alongshore migration of a bar in Kristensen et al. (2010) (reproduced in section 5).

The streamline bar model is a finite difference model, in which the bar parameters, $\psi_\mathrm{b} = [V_\mathrm{b}, s_\mathrm{c}, W_\mathrm{b}, \zeta]^T$ are defined on each coastal profile, see figure 4.18. Update of cross-sectional area of the bar (V_b), is based on gradients in the littoral drift, when integrated over the cross-shore extent of the bar, i.e.:

$$Q_\mathrm{l,b} = \int_{s_1}^{s_2} q_\mathrm{r} \, \mathrm{d}s \tag{4.26}$$

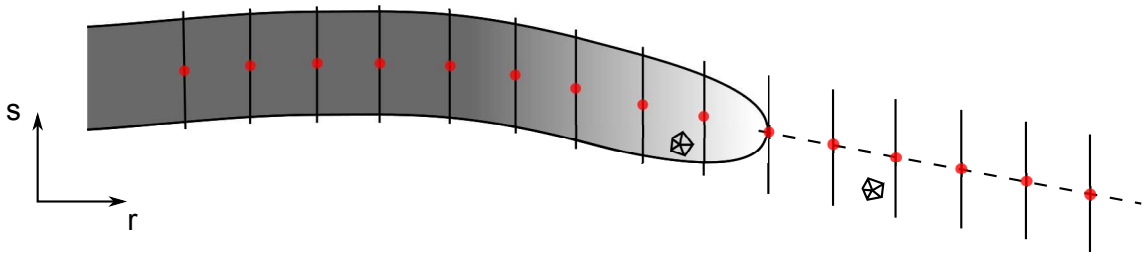

Figure 4.18: *Schematic representation of bar parameters in the streamline model. The parameters are defined on each coastal profile and updated using a finite difference scheme.*

Update of the remaining bar parameters is based on the variation of streamlines in the 2D sediment transport solution. The streamlines are determined by solving the advection equation from three

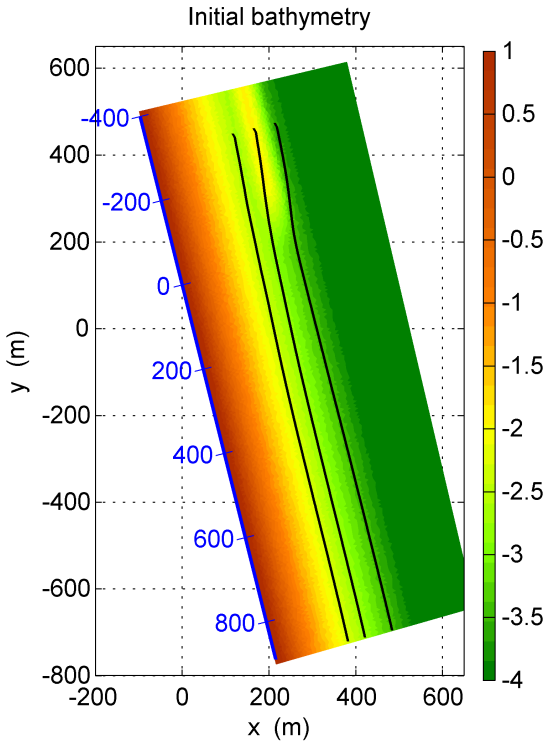

Figure 4.19: *Example of calculated streamlines along a migrating bar. Figure is reproduced from Kristensen et al. (2010). The streamlines start at three characteristic positions on the bar at an upstream profile.*

characteristic points on an upstream coastal profile using a Lagrangian approach. The characteristic points are the inner and outer extent of the bar and the bar crest as shown in figure 4.19.

The bar position, width and skewness are then assumed to converge towards the streamline solution following a response function of the form:

$$\frac{\partial s_c}{\partial t} = \frac{1}{T_{scale}} \left(s_{c,stream} - s_c \right) \tag{4.27}$$

where T_{scale} governs the time scale of the response which is a function of the volume of the bar, causing the bar to react instantly to the streamline solution for cases where the bar volume is zero and at a slower rate when the volume is non-zero. The instant reaction to streamlines has the desirable attribute that it limits gradients in the longshore transport thereby limiting development of bar features located at some distance downstream of the bar front.

4.5.3 Updating bar parameters using optimisation

Evolution of a bar may be calculated by use of non-linear optimisation similar to that which is done in the 1.5D shoreline model. The parametric definition in equation 4.24 is used, to define the form of the bar within control volumes that conform to the cross-shore extent of the bar. This principle is illustrated in figure 4.20, which depicts a bar front and the surrounding control volumes.

The node values of the control volumes are defined as simple averages of the cross-shore extent of the bar parameters in two neighbouring elements. The node value of the control volume in the

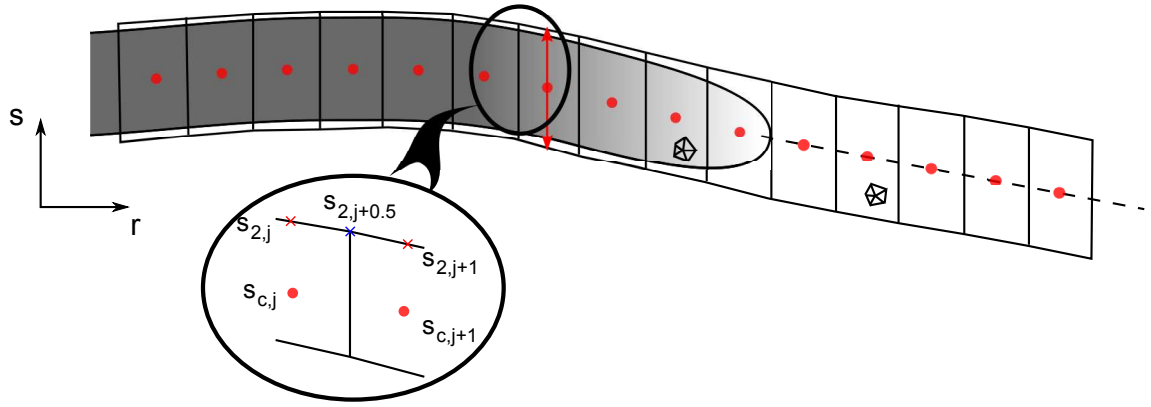

Figure 4.20: *Illustration of the morphological mesh used to describe and evolve bar parameters on. The bar parameters are defined in the centre of the control volumes, and computational elements (elements on which flow, waves and sediment transport are calculated) are associated with a control volume based on the position of their centroid.*

close-up (shown as a cross) in the figure is thus determined as:

$$s_{2,j+\frac{1}{2}} = \frac{1}{2}\left(s_{2,j} + s_{2,j+1}\right) \tag{4.28}$$

where the subscript $s_{2,j}$ is the seaward limit of the bar in the jth control volume. The computational elements of the coastal area model (indicated in the figure as triangular shapes) are associated with a control volume if their centroid is located within the extent of the control volume. The change in bar volume within a control volume is determined as the discrete integration of the contribution from each of the identified computational elements:

$$\frac{\partial V_\mathrm{b}}{\partial t} = \frac{1}{\Delta L_j}\sum_{i}^{N} A_i \frac{\partial z_i}{\partial t} \tag{4.29}$$

where A_i is area of the ith computational element located inside the control volume and $\partial z_i/\partial t$ is the rate of bed level change. ΔL_j is the alongshore length of the jth control volume. The remaining bar parameters are updated by non-linear optimisation such that the imposed response of the bar gives a best fit to the area weighted rms-difference of the erosion/deposition distribution obtained with the identified computational elements.

Optimisation of the bar parameters is only performed for control volumes where the amplitude of the bar is above a specific value. This has proven necessary since a bar of zero amplitude cannot have a unique position, width or skewness. In application of this model in the study reported in Grunnet et al. (2012) (reproduced in section 9), use inverse distance weighted linear extrapolation of the bar position and constant width for control volumes with a small bar amplitude proved to be useful, although this is not guaranteed for other cases. The linear extrapolation of the bar position and constant value extrapolation of bar width has also been used in figure 4.20. Smoothing of the optimised parameters has also proven to be necessary, and has been implemented as a 3-stencil diffusive filter, which primarily affects wave lengths of 2-4 times the resolution of the morphological model.

4.5.4 Updating bar parameters using moments

The evolution of bar parameters may also be determined by use of moments of the erosion deposition field. The *bar moment method* was originally developed as an alternative to the optimisation method in order to achieve a robust integrated approach for detailed evolution of the bar parameters. Derivation of the equations used to solve the problem is however fixed to the selected type of profile, thereby making this method somewhat more difficult to apply to other problems, in contrast to the optimisation method, which is fairly simple to adapt to a new type of freedom and profile definition. Furthermore, the model is not as robust as the optimisation method and has therefore not seen the same amount of application as the optimisation method or the streamline method.

Application of the bar moment method has not been published. A comparative example between bypass of a bar around a groyne is therefore shown in the end of this section. The results are compared with the streamline solution and the optimisation solution.

Model Principle

The spatial distribution of the erosion/deposition field is used to update the parameters which define the bar. It is therefore assumed that the erosion/deposition field near the bar is only affected by the bar dynamics and not by any background shoreline response. Derivation of the coupled system of equations is rather cumbersome and is therefore given in appendix C.

The basis of the method is moments of the bar amplitude of the form:

$$M_i = \int_S s^i z_\mathrm{b}(s,\psi)\,\mathrm{d}s\,, \quad i = 0,1 \tag{4.30}$$

$$M_i = \int_S (s-\delta)^i\, z_\mathrm{b}(s,\psi)\,\mathrm{d}s\,, \quad i = 2,3 \tag{4.31}$$

where z_b is defined in equation 4.24, s defines the cross-shore direction with an arbitrary origin and $\psi = [V, s_1, W_\mathrm{b}, \zeta]^T$ holds the bar parameters. Note however that $V = A_\mathrm{b}W$ is twice the cross-sectional volume of the bar. S covers the cross-shore extent of the bar. The 2nd and 3rd order moments are centred moments, i.e. the centroid location $\delta = M_1/M_0$ is subtracted from s.

Evaluation of the moments given above for the applied profile definition shows that the moments may be determined from the bar parameters and some known functions. These moments may be combined to form so-called *reduced moments* where each order of the reduced moment may be related directly to a single bar parameter (for a given skewness). The change in the reduced moments may also be determined by evaluating the distribution of the erosion/deposition field, thereby coupling the prediction of the 2D coastal model with the parametric model.

Figure 4.21 shows two examples where erosion/deposition distributions are created as the difference in bed level due to a prescribed change in bar parameters, i.e.:

$$\Delta z = z_\mathrm{b}\left(\psi^{k+1}\right) - z_\mathrm{b}\left(\psi^{k}\right)$$

The figure shows the initial form with a thin curve and the prescribed form as points. The evolved form calculated in terms of moments of the erosion/deposition field is shown with a thick curve.

In the first panel the bar width increases uniformly to each side of the crest and the volume is reduced by 10%. The skewness is however maintained. The panel shows that the model may accurately predict the evolution, given that no change in skewness is imposed by the erosion/deposition field and that no noise is contained in the erosion/deposition field distribution. Numerical inaccuracies develop when the skewness changes due to the fact that the 1st, 2nd and 3rd order reduced moments depend on ζ which in the numerical scheme for time integration is taken as invariant.

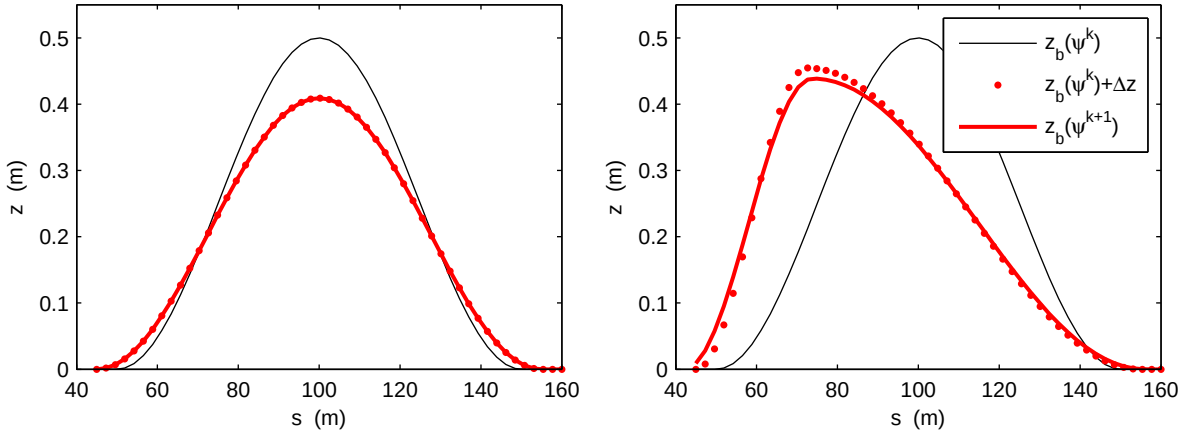

Figure 4.21: *Evaluation of bar moment method to known changes in bar parameters. Thin curve: Initial solution. Points: Target solution. Thick curve: Evolved solution.*

The second panel shows a case where the volume is maintained, the bar width increases and the landward part of the bar migrates onshore. The skewness is in this case reduced, thereby making the bar asymmetric. The comparison between the solution obtained by use of the bar moment method and the intended change, shows that some errors develop, while the overall change in form is obtained.

Discrete integration of erosion/deposition fields

The model parameters are in the bar moment model defined on a grid identical to that of the optimisation method (see figure 4.20). The bar parameters, ψ are therefore defined inside control volumes and evaluation of the integrals shown in equations 4.30 and 4.31 is therefore done as a discrete summation over the computational elements located inside the same control volume:

$$M_{i,k} = \frac{1}{\Delta L_k} \sum_j s_j^i z_\mathrm{b}(s_j, \psi_k) A_j \,, \quad i = 0, 1 \tag{4.32}$$

$$M_{i,k} = \frac{1}{\Delta L_k} \sum_j \left(s_j^i - \delta_k\right)^i z_\mathrm{b}(s_j, \psi_k) A_j \,, \quad i = 2, 3 \tag{4.33}$$

where subscript i refers to the moment order and j identifies the computational elements located inside the kth control volume. A is the area of the computational elements, and ψ_k contains the bar parameters. The alongshore length of the control volume, L_k is introduced because the volume calculations are derived for an alongshore uniform control volume of unit length.

Handling negative volumes

Cases where the bar volume is negative are handled by defining: $\Delta z_\mathrm{b} = -\Delta z_\mathrm{b}$ and $V_\mathrm{b} = -V_\mathrm{b}$. The bar parameters may then be evolved using the same system of equations. It is however necessary

afterwards to correct the change in bar volume using $\Delta V = -\Delta V$, recall that V is the first component in the bar parameters ψ. Figure 4.22 shows an example where evolution of a negative bar volume is handled.

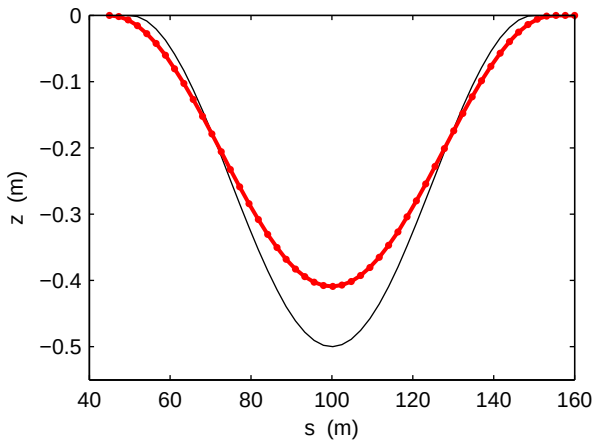

Figure 4.22: *Application of bar moment method to known changes in bar parameters for a negative bar volume.*

For cases where the volume and width of the bar correspond to a bar amplitude abs $(A_b) \leq A_{min}$, only the 0th moment is used to update the bar. This is necessary due to the weak position of the bar when the amplitude is small and it should also avoid cases where the bar volume changes sign during an update.

Landslide mechanism

A slope failure has been included in the bar moment model in order to ensure that the skewness parameter is maintained within the valid limits $0 \leq \zeta \leq 1$. The slope failure mechanism may be applied to both the landward and seaward side of the bar. Only implementation on the landward side is described here.

The maximum slope of the bar is calculated in terms of the bar parameters as:

$$S = \frac{\pi}{2} \frac{V}{\zeta W_b^2} \tag{4.34}$$

A redistribution of sediment is incorporated in case this slope exceeds a user defined maximum allowed slope S_{eq}. The redistribution is implemented as a forced landward migration of the landward section of the bar resulting in a slight reduction in bar height as the bar width increases. The principle is shown in figure 4.23. The implementation over-compensates the redistributed sediment as indicated in the figure. This ensures that the landslide mechanism is not activated at each time step when the slope becomes too steep.

4.5.5 Simulation of bypass of a bar around a groyne

The three bar models are used to simulate a bar which bypasses a groyne. The comparison between the models is performed for waves given on the offshore domain boundary with $H_s = 2.0$ m, $T_p = 6$ s and an angle of wave incidence $\theta_{bc} = 10$ deg. The initial bathymetry is shown in the top panel of figure 4.24. Zero gradient conditions are applied at the upstream boundary and the calculated

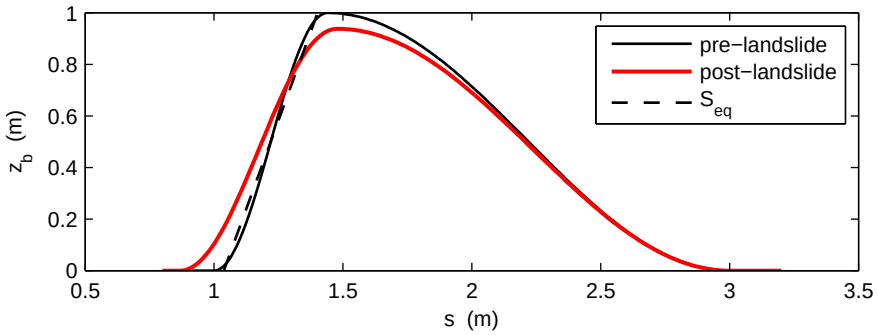

Figure 4.23: *A landslide mechanism is implemented to ensure that ζ is bounded within it's valid limits.*

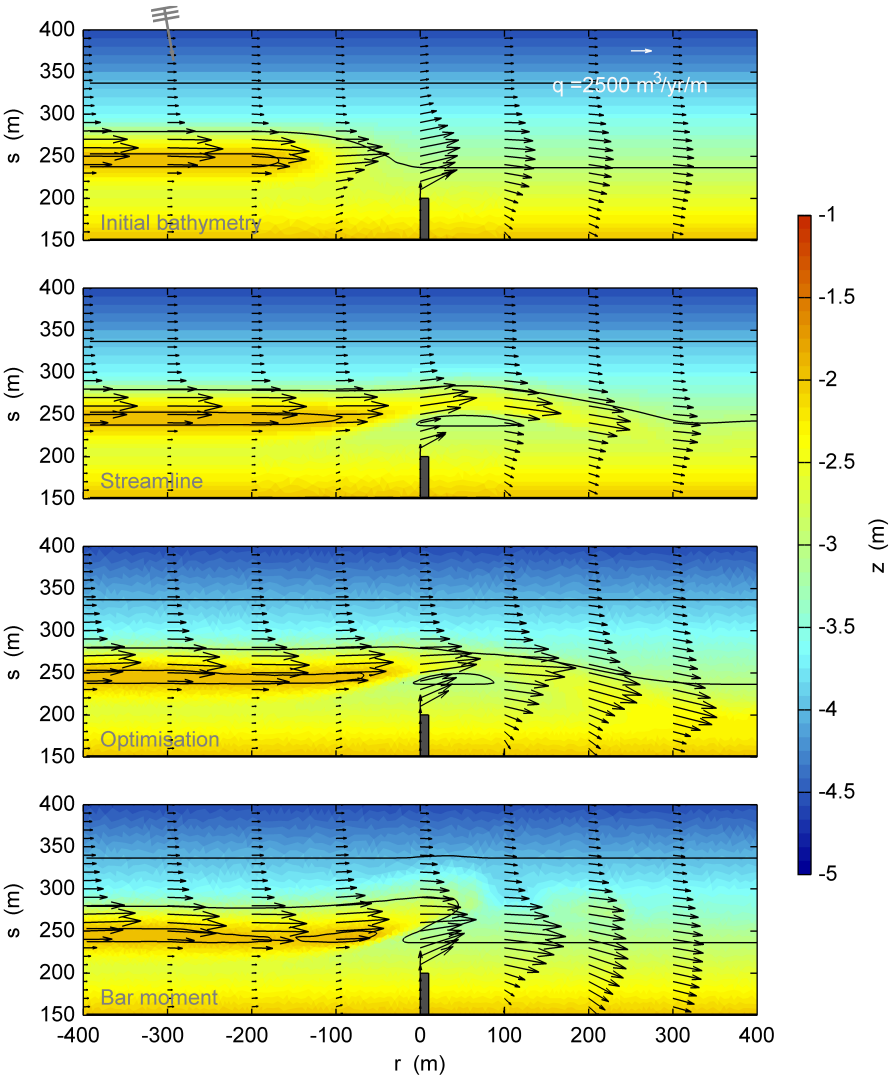

Figure 4.24: *Comparison of simulated bathymetry calculated by three different bar models after 30 days.*

morphological parameters are subject to a blending function over the first 100 m in order to maintain the bar amplitude, position and width at the upstream boundary. A morphological time step of 2 hours is used in the simulations.

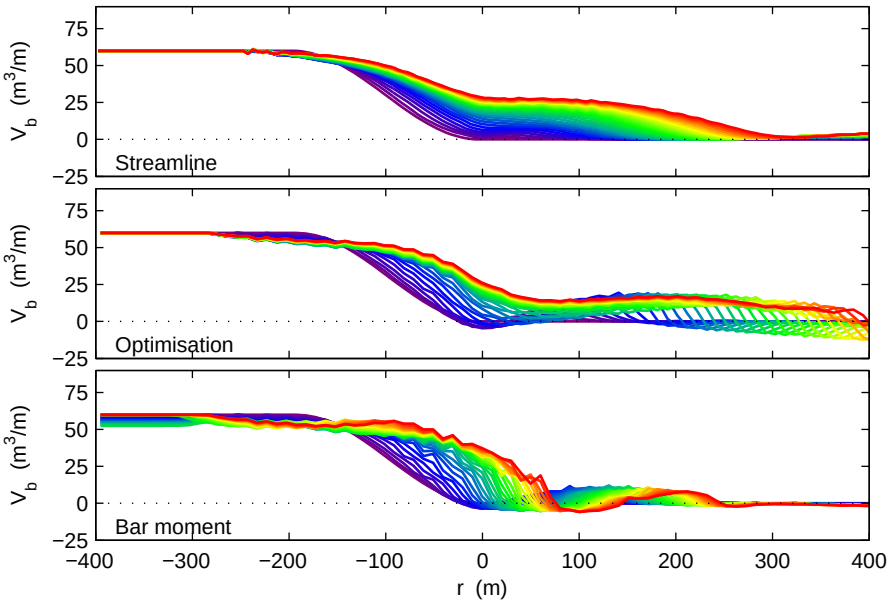

Figure 4.25: *Comparison of computed alongshore distribution of profile volume for every 1 day. The final solution is shown after 30 days. Each colour is associated with a specific time step.*

A snapshot of the computed 2D solution after 30 days for each of the three bar model implementations is shown in figure 4.24. The figure shows that the first two model types predict more or less a similar morphological evolution of the bar, with a sudden depression in the bar close to the groyne and a landward pointing bar front downstream of the groyne. The calculated evolution of the bar-moment method is however significantly different, and is characterised by an inability of the model to bypass the groyne. It has not been possible to identify the reason for this surprising behaviour. Comparing the transient evolution of the bar volume (see figure 4.25) shows that the initial evolution of the bar volume is similar for all three models, thereby indicating that the inability of the bar-moment method is not directly related to the method, but rather a problem which occurs after some time. The comparison of the temporal evolution of the bar volume in the figure shows furthermore that some differences between the streamline model and the model using the optimisation method exist: The alongshore migration of the streamline method occurs in a more smooth manner.

Concluding remarks

The bar model using the optimisation method and the bar-moment model were originally developed in order to handle cases where the sediment transport is not necessarily oriented along the bar. Cases with longshore bars and development of rip currents have therefore also been studied using these two models. A great amount of stabilisation and filtering was however required for these studies and they are therefore not presented. It is however observed from these results, that the optimisation method generally seems more robust compared to the bar-moment model. Use of optimisation of the bar parameters is therefore favoured over the bar-moment model.

Effect of increasing freedom of streamline model

The streamline model is furthermore compared with the result of a traditional 2D model and with an extension to the streamline model, in which a trough has been added to the active profile.

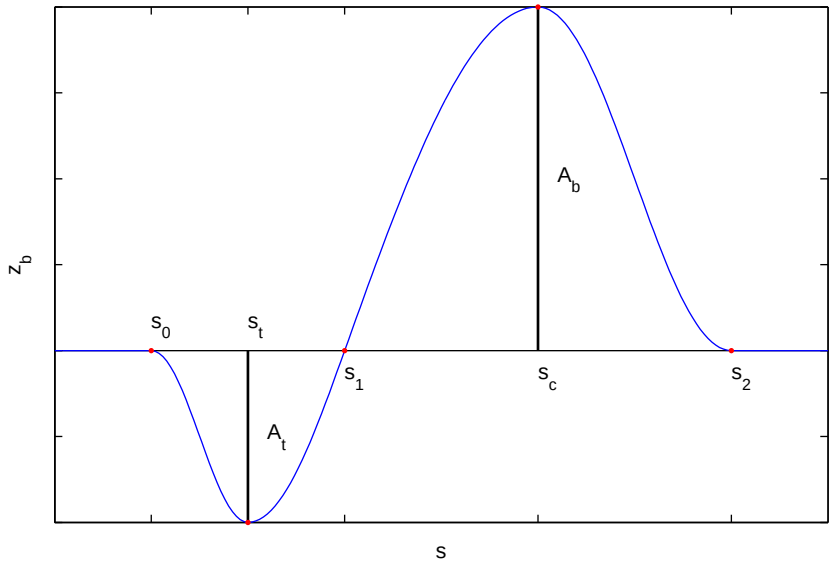

Figure 4.26: *Definition of the bar-trough profile.*

The volume of the trough is updated based on longshore gradients in the locally integrated longshore transport and due to supply of sediment over the landward edge of the trough. The width of the trough is fixed, because the streamline along the landward edge of the trough is not smooth enough to be used. Figure 4.26 shows the definition of the bar-trough profile.

A simulated bathymetry is shown in figure 4.27 for each of the three cases after 30 days. The top panel shows the result obtained with the traditional 2D model, the second panel is the streamline result with a bar and the third panel shows the result obtained with the streamline model where a trough is added to the profile definition. The three results are compared in more detail in figure 4.28, where selected coastal profiles are plotted together.

It is interesting to note from the two figures, that the streamline bar model predicts results which are reasonably close to the predictions of the traditional 2D model. The alongshore migration rate of the bar seems to be well represented by the model, just as the cross-shore position of the bar is also reasonable. Adding the trough allows local erosion between the groyne and the bar which decreases contraction of streamlines and therefore moves the bar slightly further landward at $r \simeq 0$ m. The eroded volumes inside the trough seem reasonable for the profiles close to the groyne i.e. for $r = 0, 75, 200$ m.

The application the streamline method suggests therefore that it may be used to calculate migration and bypass of a bar. It is furthermore possible to remove noise in the solution by use of a parametric description. The streamline method is however restricted by the fact that it requires the longshore transport on the bar to be oriented along the bar. Cases where crescentic features develop due to 2D circulation cannot be handles by the streamline approach. The streamline bar model is therefore primarily applicable to prediction of the migration rate of a bar front.

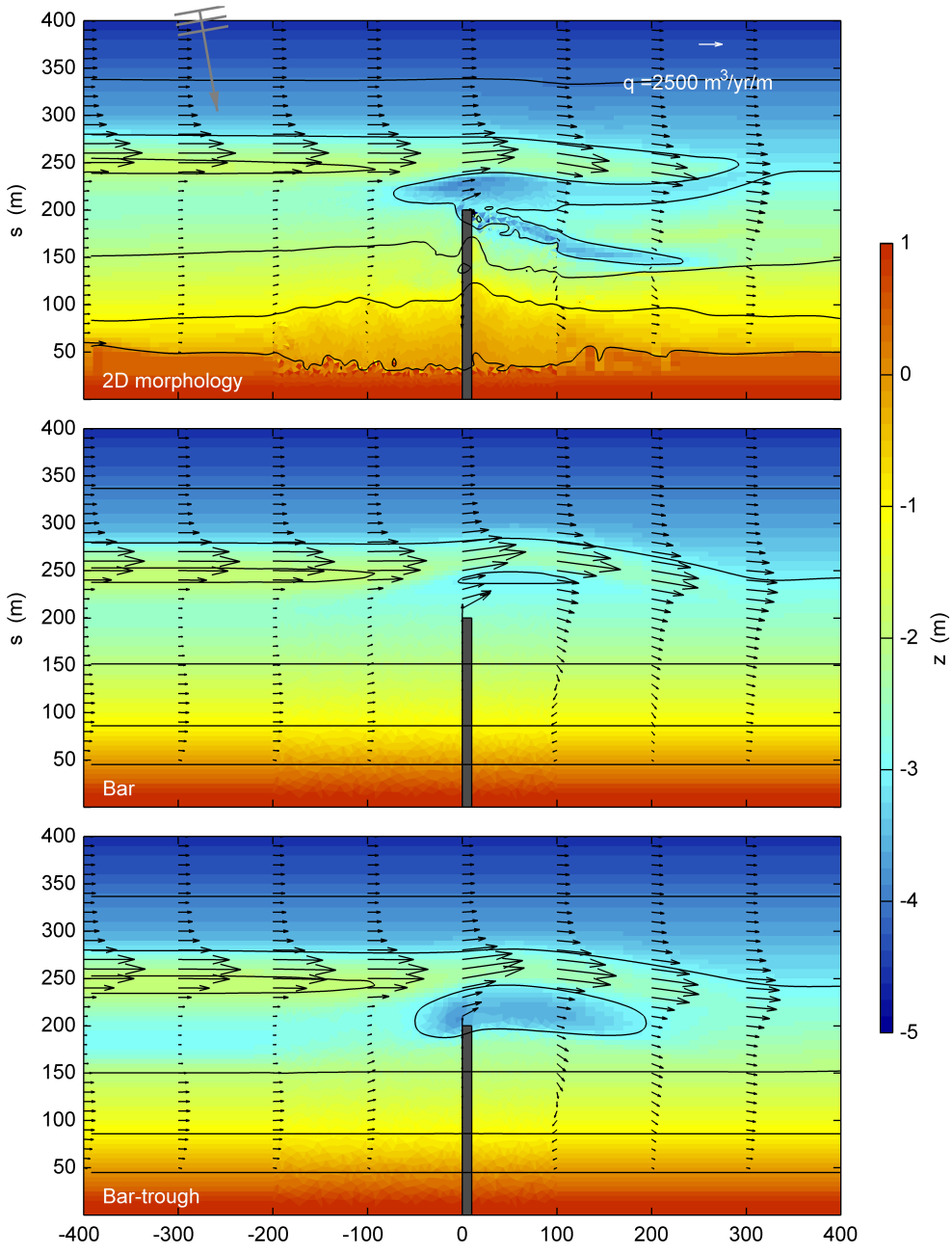

Figure 4.27: *Comparison of simulated bypass of a bar around a groyne after 30 days. Bed contours are shown for every 1 m.*

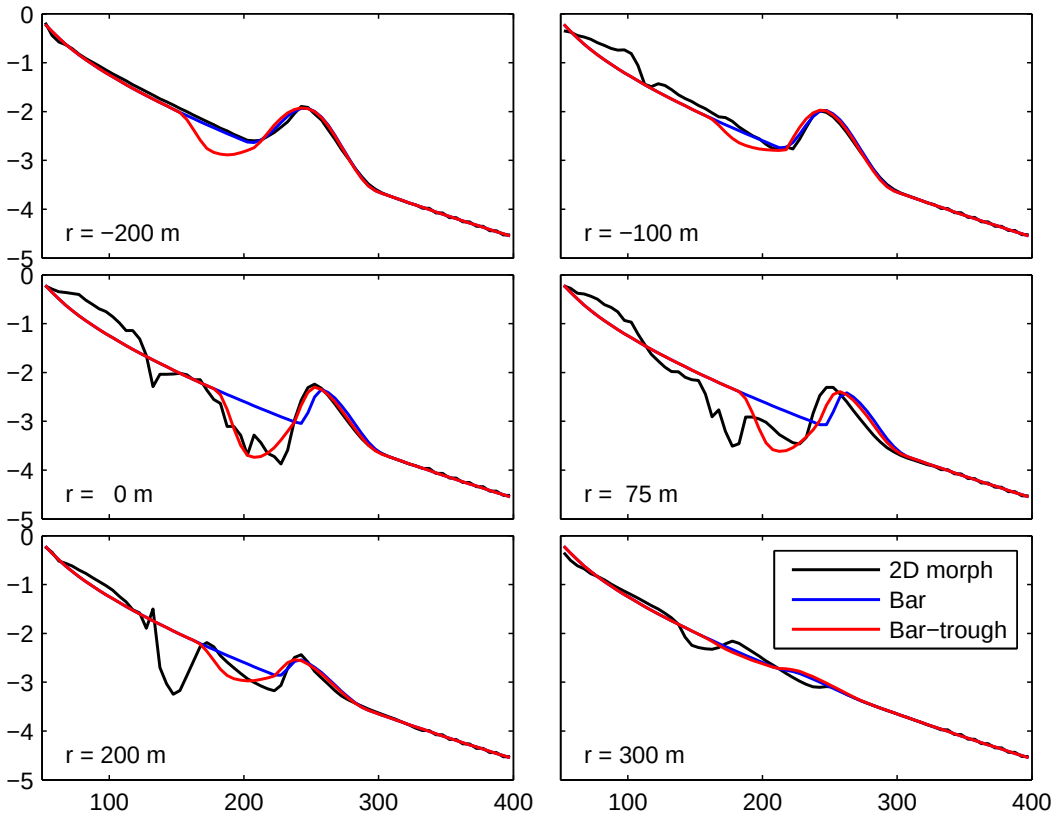

Figure 4.28: *Comparison of coastal profile from simulated bypass of a bar around groyne after 30 days.*

Chapter 5

Longterm Morphological Modelling

Conference proceedings paper from The 32nd International Conference on Coastal Engineering 2010, Shanghai, China. Authors: Sten Esbjørn Kristensen[1], Rolf Deigaard[2], Martin Taaning[3], Jørgen Fredsoe[1], Nils Drønen[3] and Jacob Hjelmager Jensen[3]. Citation: Kristensen et al. (2010)

Abstract

A morphological modelling concept for long term nearshore morphology is proposed and examples of its application are presented and discussed. The model concept combines parametrised representations of the cross-shore morphology, with a 2DH area model for waves, currents and sediment transport in the surf zone. Two parametrisation schemes are tested for two different morphological phenomena: 1) Shoreline changes due to the presence of coastal structures and 2) alongshore migration of a nearshore nourishment and a bar by-passing a harbour. In the case of the shoreline evolution calculations, a concept often used in one-line modelling of cross-shore shifting of an otherwise constant shape cross-shore profile is applied for the case of a groyne and a detached breakwater. In the case of alongshore bar/nourishment migration an alternative parametrisation is adopted. All examples are presented, analysed and discussed with respect to the question of realistic representation, time scale and general applicability of the model concept.

Keywords: Coastline model, Morphology, Groyne, Breakwater, Nourishment, Bar migration

5.1 Introduction

Shoreline morphology is the result of nearshore waves and currents acting on the coastline. Due to breaking of the waves and the currents generated close to the shore, longshore sediment transport is generated, and redistribution of the beach material will occur along the shoreline - from updrift areas, where the beach is eroded and the shoreline retreats, to downdrift areas, where the eroded beach material is accreted. Erosion corresponds to increasing longshore transport, whereas accretion corresponds to decreasing longshore transport, i.e. the shoreline evolution is connected

[1]Department of Mechanical Engineering, Technical University of Denmark, DK-2800 Kgs. Lyngby, Denmark
[2]DHI, Agern Allé 5, DK-2970 Hørsholm, Denmark

to gradients in the longshore transport rates. In order to assess the long-term evolution of the shoreline models for these phenomena must be formulated.

In order to formulate useful shoreline evolution models several issues have to be dealt with. Firstly a quantitative model for describing the longshore transport is needed. This includes the issue of incorporating the main physical mechanisms most important for the longshore transport and the alongshore gradient in the transport. Secondly a way of coupling the sediment transport and the changing shoreline morphology must be formulated. Thirdly the issue of computational time - i.e. the model should be able to produce plausible results within a reasonable (CPU) time horizon - should be dealt with.

Furthermore, it is important to assess the situation to be modelled, in order to make sure that the model resolves the physics governing the specific case (different important examples could be: Long-term predictions of the effect of coastal structures, assessment of effects of changes in wave climate or the effect of beach nourishments on the coast). The problem of formulating a plausible shoreline evolution model can be approached in different ways. In the following a short summary of the most common model types for calculating shoreline response is given, to give the relevant background for describing the shoreline model concept which is the subject of the present paper.

5.1.1 Simple one-line models

The one-line model assumes that the shape of the coastal profile is maintained, and that continuity is obtained by shifting the entire cross-shore profile - shift in the onshore direction corresponds to erosion and shift in the offshore direction corresponds to accretion. This parametrisation of the morphology yields the following version of the sediment continuity equation:

$$\frac{\partial s_0}{\partial t} = \frac{-1}{1-n}\frac{1}{h_{\text{act}}}\frac{\partial Q_{\text{l}}}{\partial r} \tag{5.1}$$

where s_0 is the shoreline position relative to some predefined alongshore axis, n is the porosity, Q_{l} is the solid volume sediment transport in the alongshore direction and h_{act} is the active height of the profile. This simple relation was first proposed by Pelnard-Considére (1956).

The sediment transport models typically implemented in one-line models determine the longshore transport rate at a given point on the shoreline adopting the local wave climate and the local shoreline orientation, and does therefore typically not incorporate memory effects from updrift locations.

Some transport formulations used for one-line modelling are empirical formulas (e.g. the CERC formula) while other are more complex models based on sub-models of the physical processes, Deigaard et al. (1986a). In the latter case the sediment transport is calculated on the basis of an actual coastal profile, which - combined with the assumption of alongshore uniformity in all flow quantities - transform waves from offshore to the shoreline (refraction, shoaling and breaking), calculate a longshore current driven by gradients in radiation stresses and model the concentration of suspended sediment in combined waves and current, to finally obtain the cross-shore distribution of longshore sediment transport. Integration across the profile of the longshore transport then gives a longshore transport rate that can be used as input to the shoreline model. Common for all of the

longshore sediment transport models (being it empirical or process based ones) typically used in one-line modelling, is that effects of local non-uniform wave fields (e.g. caused by coastal structures or offshore reefs), current inertia and refraction, streamline contraction and flow recirculation are not inherent in the models. These effects must be included through explicit schemes either as simple reduction factors on the transport or by modifying the wave climate locally due to refraction and/or diffraction Hanson (1989); Steetzel and Wang (2003).

5.1.2 N-line models

An interesting extension of the shoreline model is the n-line model or multi-layer model, in which the coastal profile is schematised by a series of lines/layers. The layers are mutually coupled through a cross-shore transport formulation, which will force them towards an equilibrium configuration. The longshore transport is determined for each point along the shoreline and for each layer based on the angle between the incident waves and the local orientation of the shoreline normal. The n-line model concept has been developed in order to handle cross-shore transport in the simplified shoreline models, and examples of this are the model of Bakker (1969) and the PonTos-model by Steetzel and Wang (2003).

5.1.3 2D area models

A second class of morphological models is the 2DH/Q3D area models. In these model types the determination of wave and flow fields are typically based on phase averaged formulations, which allow larger time step increments compared to phase resolved models. The 2DH area models typically calculate the transformation of wave energy, wave angle and wave period from an off-shore boundary to the shoreline (wave refraction, shoaling, diffraction and breaking), and use this information to drive a flow model - both over a given bathymetry - to give the depth averaged current field in two horizontal dimensions. Based on the areal distribution of wave characteristics and current field, the areal distribution of the sediment transport field is evaluated. The divergence of the sediment transport field over each computational cell yields the rate of change of the local bed level, which is used to update the morphology for the next time step.

Different approaches to calculate the sediment transport in these model types are reported in the literature, ranging from empirical formulas see e.g. Roelvink et al. (2006); Soulsby (1997) to sophisticated intra-wave, quasi-3D models for the local hydrodynamics (undertow, streaming, wave-current boundary layers, wave generated turbulence, etc.) and sediment suspension, to get the total sediment transport (see e.g. Fredsoe and Deigaard (1992)). Common to these model types is that they are not - as is the case in the one-line model - bound to the assumption of alongshore uniformity, but include effects of non-uniformity in the bathymetry and they may also incorporate the presence of coastal structures sheltering/reflecting the waves and block the currents.

In principle such a model type would yield a very good basis for simulations of the detailed morphological evolution around say a breakwater, and has proven in many cases to give good results over a shorter time scale (e.g. Brøker et al. (2007); Drønen and Deigaard (2007)). There are however some inherent issues that have to be solved before the model type will be feasible for long term simulations. First, the CPU time is still a limiting factor when running such a model for many years and decades. Furthermore, the cross-shore profile may degenerate when run over a long period of time, and will in all cases need a large degree of calibration to produce reasonable results. Also discussions on the numerical diffusion, numerical instability (Callaghan et al. (2006); Johnson and Zyserman (2002)) and numerical stiffness add some questions to the applicability of this model type for long term morphological runs.

5.2 Introduction of the model concept

In the present paper a model concept is formulated as a hybrid of the detailed 2DH area model (for waves, currents and sediment transport) and a geometric simplification and hence parametrisation of the morphology (the one-line model is an example of this).

The main idea is to use a 2DH area model to represent the hydrodynamics and the sediment transport over a generally non-uniform bathymetry including effects of blockage of waves/current by coastal structures - and to couple this information with a morphological updating scheme based on a simplified parametrisation of the morphology.

The one-line model concept is one example of a parametrised morphological scheme used for shoreline evolution, but the basic idea can be used to construct other morphological parametrisations - either when approaching different morphological phenomena or if sophistications of the one-line parametrisation are sought. Generally, the main challenge for the modeller in the present model context is to choose a parametrisation of the morphology that resembles the real morphology best.

In order to connect the two modelling approaches, the morphological evolution is determined on the basis of the cross-shore integrated longshore sediment transport, and the update of the morphology from one time step to the next is carried out by updating a single or few morphological parameters which characterise the coastal profile rather than the bed level in individual mesh elements.

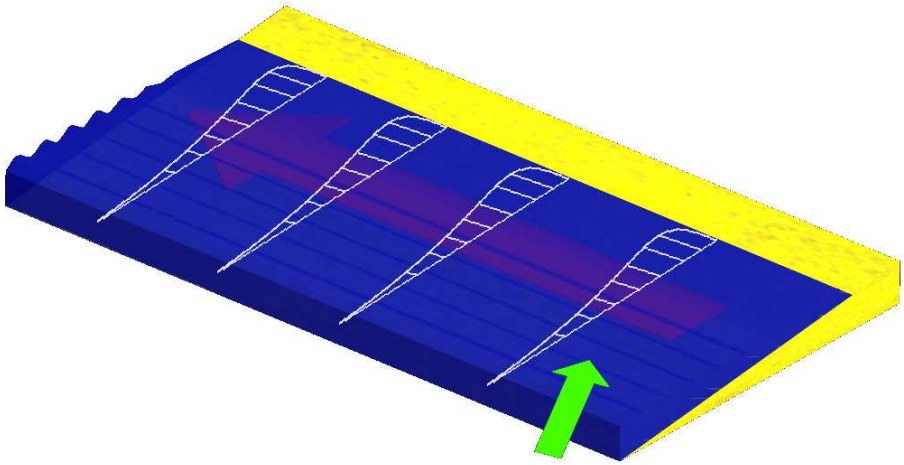

Figure 5.1: *The 2DH sediment transport field determined by a 2DH model is converted into a 1D longshore drift by integration of the transport along coastal profiles.*

The same ideas were in principle used by Hansen et al. (2004) to study three-dimensional bar morphology, and the present study can be seen as a continuation of investigating the principles used in that study.

In the present paper two different morphological parametrisation schemes for two different situations have been tested. Shoreline response is calculated using a scheme similar to the one-line model. Alongshore migration of bars and nourishments are calculated using an alternative scheme, where the morphology is parametrised differently to resolve that specific situation.

Given the simplifications introduced by the parametrisation of the morphology, the model concept has several advantages seen in the context of long-term modelling: 1) The 2DH models give a more realistic description of the horizontal spatial effects on the flow and sediment transport compared to the simple one-line models, 2) long-term degeneration in the cross-shore profile is avoided and 3) CPU time is significantly lower compared to a full 2DH/Q3D morphological model.

5.2.1 Implementation of the model concept

The model concept is in principle not bound to any specific coastal model system. The numerical implementation presented here is based on a combination of scripts and functions interacting with the coastal model system MIKE21 FM from DHI. The coupled model system of DHI consists of a spectral wave module MIKE21 SW, which solves a transport equation for the wave action density, a 2DH depth integrated flow model MIKE21 HD/FM that solves the non-linear shallow water equations and a sediment transport module MIKE21 STP, which calculates the sediment transport based on the values of local hydrodynamic quantities.

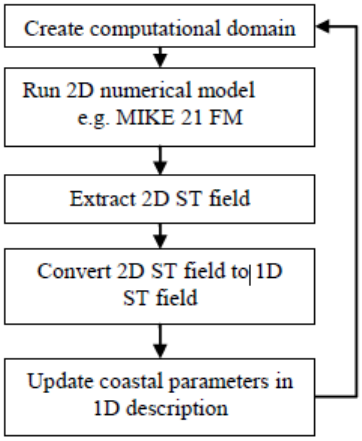

Figure 5.2: *Flowchart of the morphological model.*

The model system is used to determine the 2DH sediment transport field, and the morphological feedback is performed by cross-shore integration of the longshore transport, updating the coastal parameters and writing the updated bathymetry to a new mesh file. The morphological loop is closed by calling the model system once again.

5.3 Application of the model - shoreline evolution

The model concept is applied to the case of shoreline evolution around coastal structures. Two cases are considered where an idealized coastline is interrupted by a coastal structure: In the first example a groyne field is considered and in the second example the case of an offshore breakwater is considered.

5.3.1 Coastline evolution around a groyne field

A groyne field is used in the first example. It is assumed that the form of the coastal profile is maintained throughout the domain. The morphological feedback is thus introduced by shifting the shoreline in the on-/offshore direction depending on whether there is erosion or deposition, as indicated in Figure 5.3. The rate of on-/offshore migration of the shoreline is determined from the 1D continuity equation given in equation 5.1.

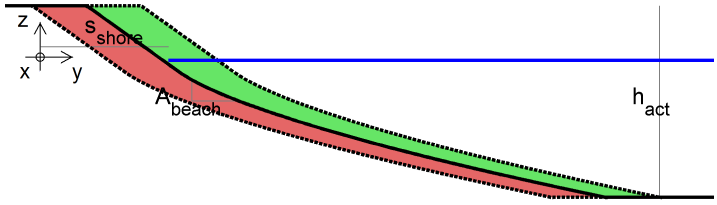

Figure 5.3: *The form of the coastal profile may be maintained, while satisfying sediment continuity by shifting the profile in the on-/offshore direction.*

The result of applying the morphological model to a groyne field, where an infinite number of groynes are represented by periodic boundary conditions on the lateral boundaries, is shown in figure 5.4. A wave climate consisting of 2 waves approaching the shoreline from +15 deg and +25 deg from the initial shore normal is used (a positive angle means that the wave direction is rotated anticlockwise compared to a shore-normal approach). The significant wave height is in both wave conditions 1.5 m at the offshore boundary, and the peak wave period is 7 s. The groyne is long compared to the surf zone width. The 2DH transport field is indicated in the two bottom panels as black vectors, while the longshore variation of the integrated longshore drift is shown in the top panels. Both figures show that the groyne decreases the transport locally - becoming zero at the groyne location - and that the transport recovers downdrift the groyne.

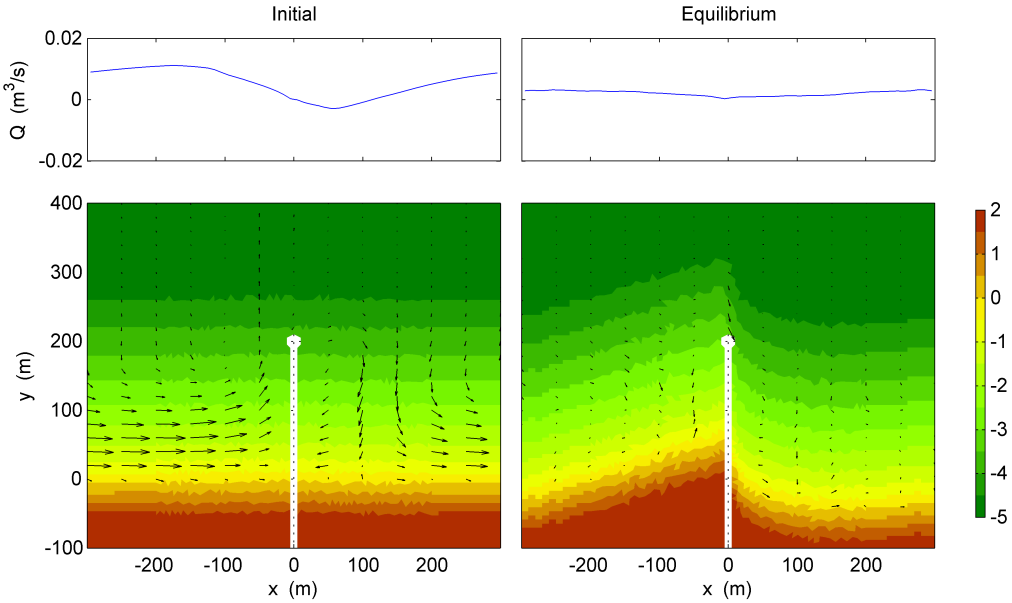

Figure 5.4: *Morphological evolution around a groyne in a groyne field (periodic BC on West and East boundaries). Left panel: Initial bathymetry, Right panel: Equilibrium bathymetry. Colours indicate the bed level in metres. The top panels show the instantaneous long shore transport.*

The morphological evolution of the shoreline in the groyne field seems reasonable, because it features upstream accretion and downstream erosion as would be expected for this problem. The equilibrium conditions are according to figure 5.5 obtained after approximately 4 months. The fact that the model is capable of determining an equilibrium solution for a given forcing is interesting because the method may be used to quantify the effect of the groyne field on the shoreline for different

groyne configurations in different wave climates.

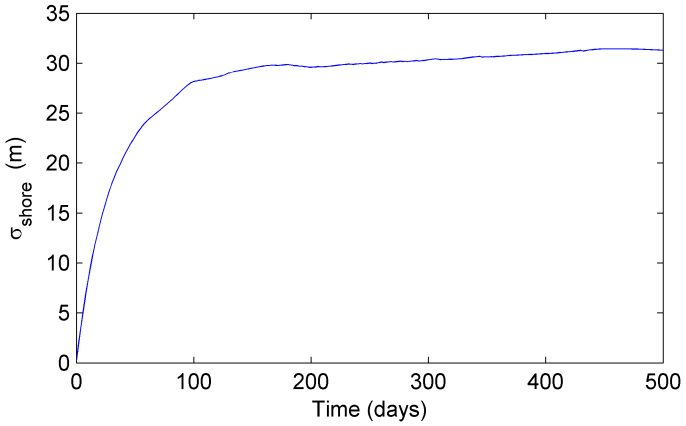

Figure 5.5: *Temporal evolution of the shoreline (rms-value). Equilibrium conditions are obtained after approximately 4 months.*

It should be noted that - as is the case in all one-line modelling - the form of the cross-shore profile is maintained throughout the domain and simulated time, and the model will quantify the morphological change only within the restrictions imposed by the modeller. Possible further development could involve changes to the coastal profile, such as steepening on the upstream side and flattening on the downstream side or development of local erosion at the groyne head.

5.3.2 Coastline evolution behind a breakwater

The next example illustrates the shoreline evolution behind a detached coastal breakwater. The breakwater is constructed on an idealized uniform coastline and subject to a varying wave climate consisting of three waves with the wave directions +10 deg, +5 deg and -5 deg. The significant wave height is 1 m, and the peak wave period is 7 s. The breakwater is positioned in the middle of the active part of the coastal profile, which means that using the same method for updating the shoreline as was done in the case of the groyne, will effectively result in the profile penetrating the structure as the profile moves off-shore, i.e. introducing a flux of sediment through the structure. The sediment flux through the structure is avoided by preventing the model from changing the bathymetry on the seaward side of the structure in profiles where the breakwater is present see figure 5.3.

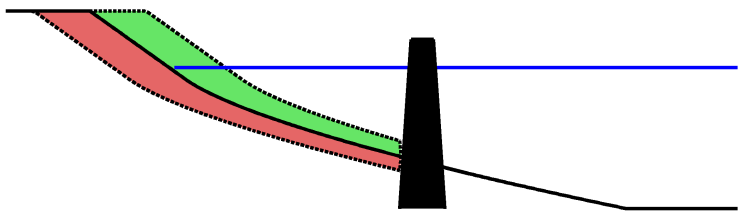

Figure 5.6: *Sketch of a coastal profile where all morphological change is inhibited on the seaward side of a coastal breakwater. The active height of the coastal profile decreases when the shoreline advances. Continuity is therefore obtained through numerical solution.*

The result of using this simple method is shown in figure 5.7. The bottom panel shows the 2D

bathymetry after equilibrium has been reached. The result shows a formation of a tombolo planform behind the breakwater. The planform is asymmetric due to the asymmetric forcing from the waves, and downstream erosion is predicted, up to a distance of 300 m from the structure. The top panels compare this solution with a solution obtained where the sediment flux through the structure is allowed. The comparison shows that that model predicts a decrease in timescale of the morphological development due to the reduction in active height of the coastal profile - which is expected. Furthermore, the maximum accretion of the shoreline behind the breakwater increases because the bed level on the seaward side of the breakwater is maintained.

The example shown in figure 5.7 represents a case where an increase in cross-shore complexity of the morphological evolution improves the result significantly. Promising tests have also been performed with an additional increase in model complexity, where it was made possible for sediment to bypass seaward of the structure. The profile seaward of the structure could also evolve, and if the depth was small enough sediment transport would happen offshore of the breakwater.

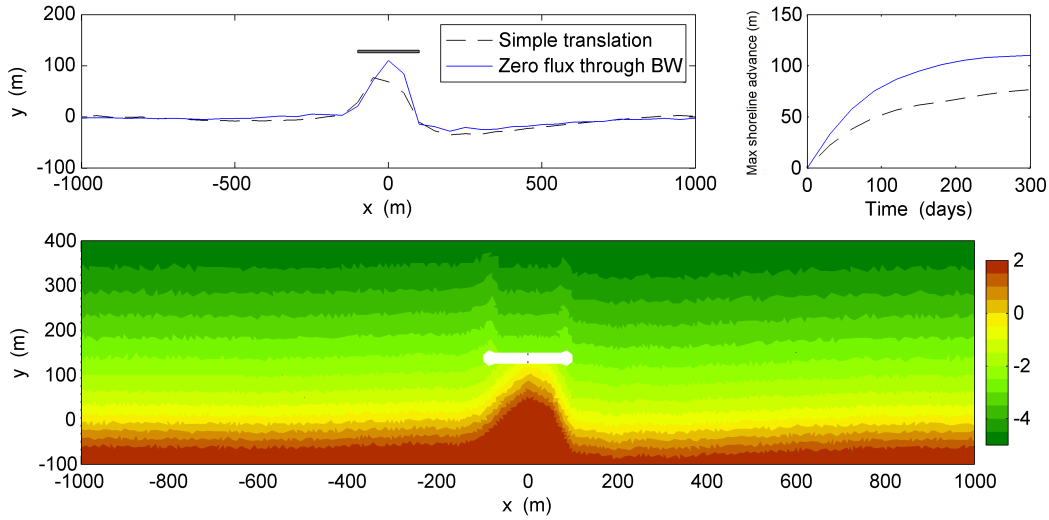

Figure 5.7: *Shoreline evolution behind a breakwater subject to waves from three different directions. The net transport is to the right. A zero sediment flux is imposed through the break water. Colours indicate bed level in metres.*

5.4 Simulations with profile evolution

In order to apply the model concept to a wider range of problems, a simple extension is proposed, where the longshore transport is integrated over part of the coastal profile. The morphological evolution is similarly restricted to this local part of the profile. The extension is visualised in figure 5.8, where the amplitude of a bar is updated.

5.4.1 Morphological evolution of a shoreline nourishment

The model is applied to a case where beach nourishment is performed on an otherwise straight coast. The cross-shore extent of the nourishment is assumed to be limited to the area around the shoreline, as indicated in figure 5.9. Furthermore it is assumed that the nourishment consists of sand which is similar to the existing sand, and that the nourished sediment is only redistributed in the longshore direction.

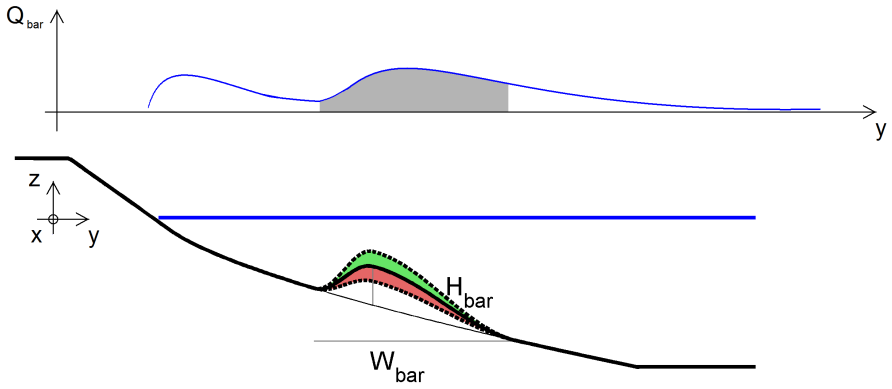

Figure 5.8: *The model concept is used to update local features on the coastal profile. This allows the model to be used on a broader range of problems.*

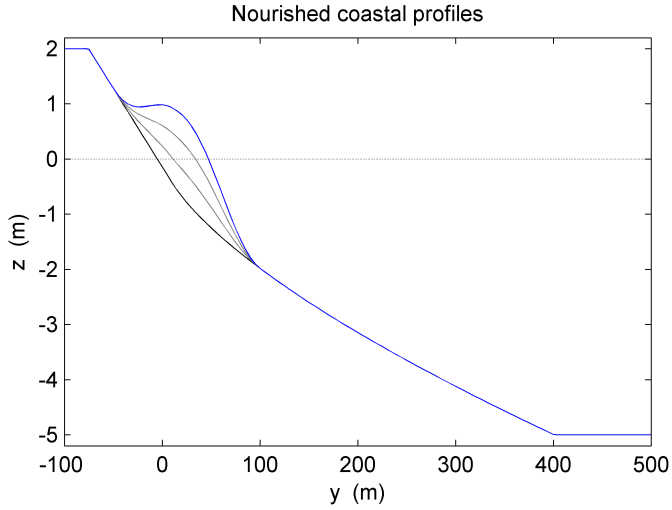

Figure 5.9: *Sketch of the variability of the beach nourishment. The blue line indicates the initial profile in the nourishment area.*

The nourishment is subject to a constant wave climate with a significant wave height of 1.5 m, a peak wave period of 7 s, and waves approaching the shoreline from +10 deg. In a classic one-line model the solution to this type of problem is a diffusive redistribution of the salient formed by the nourishment. This is because the 1D model will predict the transport to be only a function of the coastline orientation and predict the same transport rate on a non-nourished profile as it would on a profile on a central section of the nourishment. Figure 5.9 shows the model prediction. Immediately after construction, the model predicts a rapid diffusive redistribution of the nourishment at the two ends of the nourished area in the same manner as would be expected from a classic 1D model. With time the variation in the longshore transport becomes distributed over the entire length of the nourishment, and the whole nourishment migrates in the downdrift direction while it is still being smoothed out. The movement of the centroid of the nourishment shows a constant migration rate of 0.9 m/day for this configuration.

It is important to describe the life time of a nourishment. This may be done in terms of the re-

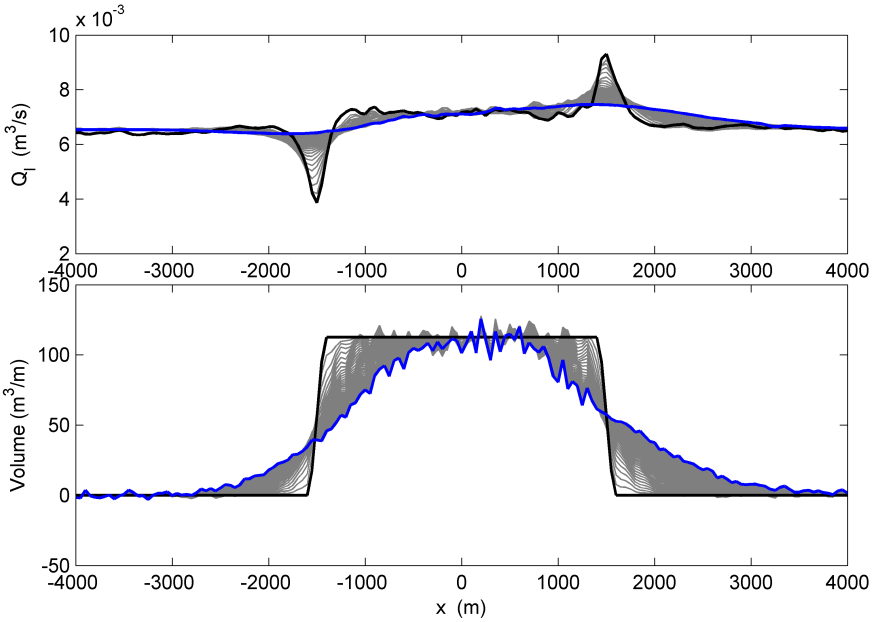

Figure 5.10: *Time stack of the simulated longshore transport and the nourishment volume. Black curve: Initial condition, Blue curve: Final condition.*

maining relative volume of nourished sediment within the original nourishment area. Dean and Yoo (1992) show that the life time of a nourishment is dependent on the length of the nourishment. A long nourishment will have a substantially longer life time than a shorter but otherwise similar nourishment. Figure 5.11 shows a comparison between different nourishments. The only difference between the nourishments is the length. The volume of the nourishment per unit length is constant, and the total volume is therefore proportional to the length. The model clearly predicts an increase in life time for the nourishment as the length is increased - which is expected.

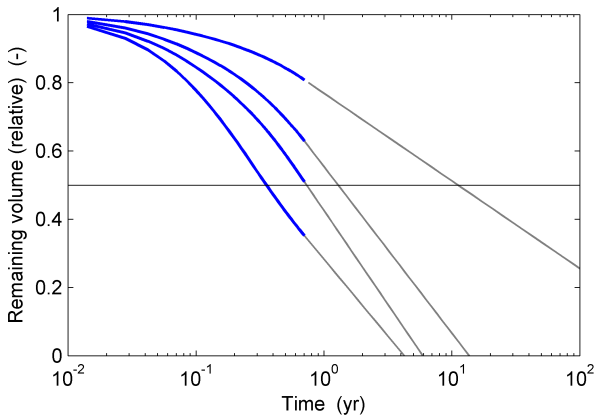

Figure 5.11: *Comparison of the physical performance of different nourishments. Only the length of the nourishment project is varied. The lengths shown in the figure are: L=800 m, L=1200 m, L=1600 m and L=3000 m. Blue curves: Simulations, Grey curves: Extrapolations.*

5.4.2 Alongshore migration of a bar

The model concept may be applied to a more complex problem like the alongshore migration of a bar. In the case considered an alongshore uniform bar is present at the upstream end of the domain. The bar extends into part of the domain and there will be large gradients in the longshore transport along the bar, which will grow into the domain. Constant wave conditions are given at the offshore boundary with significant wave height of 2 m, a peak wave period of 6 s and the angle between the approaching waves and the shoreline normal is +49 deg. Due to the steady supply of sediment into the domain from updrift the bar will grow in the downdrift direction. The model addresses the questions of the migration rate and the shape of the growing bar. The sediment transport near the tip of the bar is described from the pattern of the depth integrated wave-driven currents. As a first approach the cross-shore location of the bar inside the domain is therefore determined from the flow field, which in turn to a large degree is determined by the location of the bar at the upstream boundary of the model domain. The cross-shore migration of the bar is therefore determined by the streamlines extending from each side of the bar on the upstream boundary as indicated in figure 5.12. The cross-shore position of the bar follows a simple response function which resembles that was used by Plant et al. (1999) and Hansen et al. (2004).

$$\frac{\partial s_{\text{bar}}}{\partial t} = \frac{1}{T_{\text{scale}}} \left(s_{\text{stream}} - s_{\text{bar}} \right) \tag{5.2}$$

where s_{bar} represents the cross-shore location of the bar, s_{stream} is the cross-shore location of the streamline and T_{scale} is a time scale which remains to be specified. Plant et al. (1999) suggests that $1/T_{\text{scale}}$ should be a growing function of the incident wave height, because larger wave heights will lead to a larger intensity of the cross-shore transport. The intensity of the longshore transport may also be used as proxy for the time scale of cross-shore movement. In this simple example where the wave climate is constant the time scale for the cross-shore movement is taken to be a function of the bar volume only. T_{scale} is therefore selected such that it spans the range from zero (in practice one time step in the morphological model) to a user specified maximum value T^*_{scale}. In this simulation a value of 15 hours has been used for T^*_{scale}. The bar will thus react instantly to the streamlines for profiles where the bar height is zero, and it will react according to T^*_{scale} for profiles with a volume corresponding to the updrift bar.

The simulation result is illustrated in figure 5.13. The left panel shows the initial bathymetry while the right panel shows the bathymetry after 45 days. The figure shows that the model predicts an alongshore migration of the bar, and that the bed level along the bar crest is maintained (see figure 5.14). The cross-sectional form of the bar is maintained because it is prescribed in the same manner as it was for the nourishment shown in figure 5.9. This increases effectively the stability of the model and makes it more robust and applicable for long term simulation. The alongshore migration of the bar is approximately 16 m/day.

The smooth variation of the cross-shore position of the bar is a direct result of using streamlines to determine the cross-shore forcing. Over the head of the bar the streamlines are deflected towards the shore because the onshore forcing by radiation stresses cannot be balanced by the wave set-up alone. A circulation current is rather generated, which drives a net onshore current over the head of the bar. The morphological model forces the head of the bar to migrate rapidly onshore during the first couple of days, after which the distance from the shoreline to the head of the bar remains almost constant as shown in figure 5.15 where a schematic visualisation of the bar position is shown at different time steps.

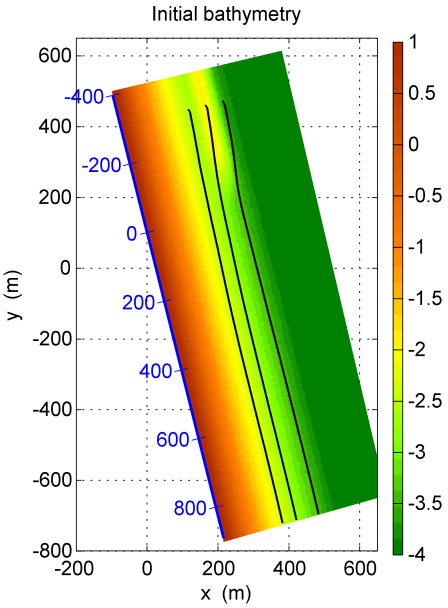

Figure 5.12: *2D plot of the initial bathymetry with an alongshore migrating bar. Colours show bed level in metres, and the three black curves indicate streamlines which define cross-shore forcing of the bar.*

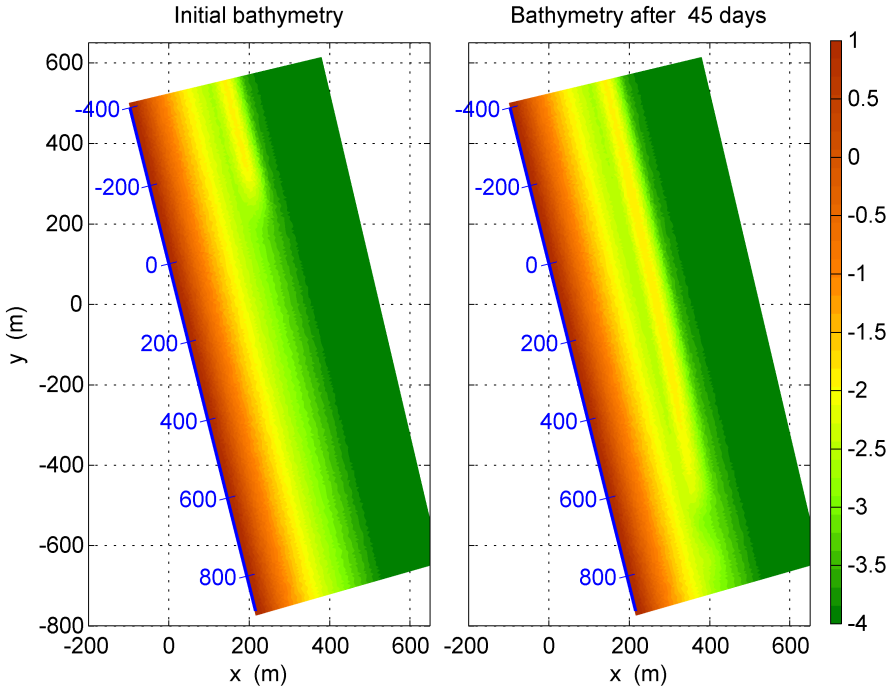

Figure 5.13: *Comparison between the initial bathymetry and the simulated bathymetry after 45 days. Colours indicate bed level in metres. The blue scale defines an r-axis which runs parallel to the shoreline.*

The lack in cross-shore forcing from undertow means that the trunk section of the bar does not return to the same cross-shore position as it is on the upstream boundary. The position of the

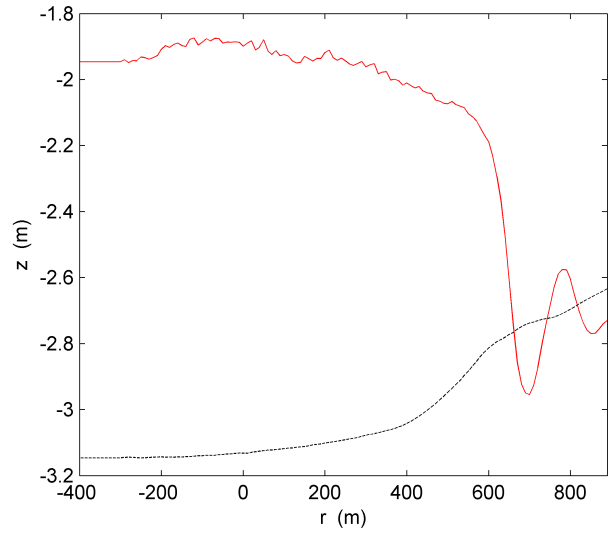

Figure 5.14: *Longshore configuration of the bed level after 45 days of simulation. The bed levels are shown along the bar crest (red curve) and the corresponding bed level for the original unbarred coastal profile (black curve).*

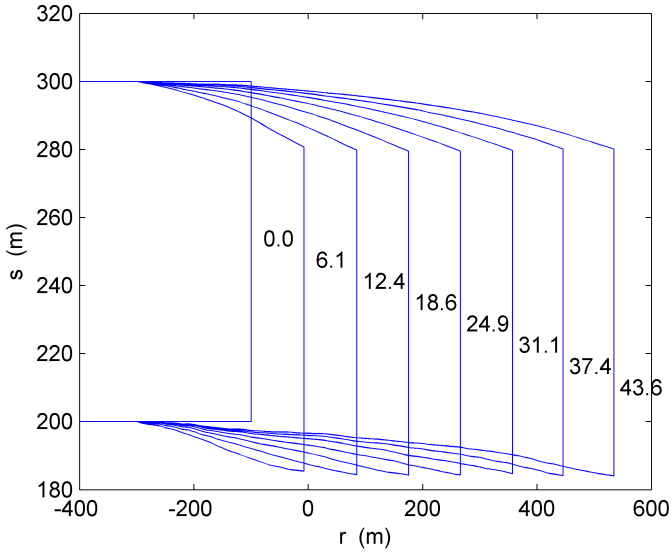

Figure 5.15: *Schematic representation of the bar position at different time steps. The numbers in the plot indicate the number of days simulated. The r-axis is the longshore axis, and the s-axis is the cross-shore axis.*

bar can be maintained by introducing a forcing of the bar towards the "equilibrium cross-shore position" for the profiles away from the head of the bar resulting in the solution shown in figure 5.16. The added forcing towards the equilibrium position is of the form:

$$\frac{\mathrm{d}s_{\mathrm{bar}}}{\mathrm{d}t} = \frac{1}{T_{\mathrm{scale}}} \left(\zeta \mathrm{mean} \left(s_{\mathrm{eq}}, s_{\mathrm{stream}} \right) + \left(1 - \zeta \right) s_{\mathrm{stream}} - s_{\mathrm{bar}} \right) \tag{5.3}$$

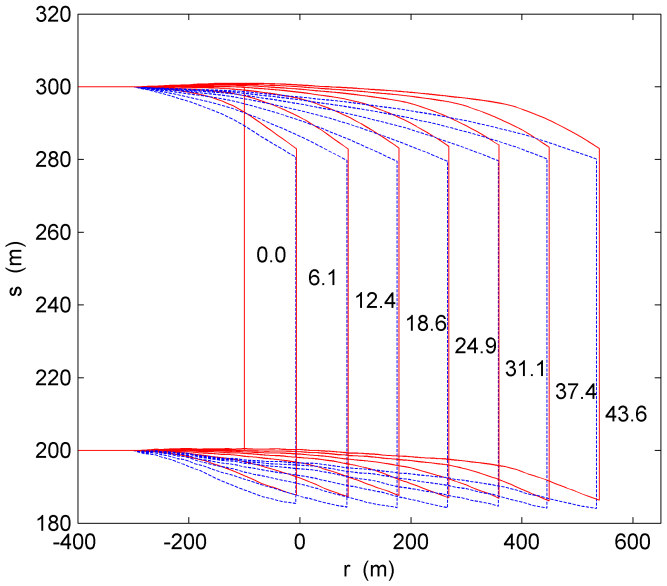

Figure 5.16: *Schematic representation of the bar position at different time steps. The numbers in the plot indicate the number of days simulated. Blue dashed curve: Bar position when following streamlines (result from figure 5.15). Red solid curve: Bar position with an added forcing towards the upstream cross-shore position.*

The result of the added cross-shore forcing is that the bar now migrates into the domain with a constant planform as indicated in figure 5.17. The result is obtained through a rule-based forcing based on the assumption that for the given wave conditions an equilibrium position exists for a longshore bar, and that it tends to return to this position.

5.4.3 Bypass of bar at a harbour

A simulation of the morphological development of a bar that bypasses the harbour Hvide Sande at the Danish North Sea coast is performed in order to determine whether the streamline approach described previously gives reasonable results. This particular problem has been examined by Grunnet et al. (2009) in a study to investigate a revised harbour layout with improved conditions for bypass of sediment. In the original work of Grunnet et al. (2009) the 2DH/Q3D model was validated against field measurements from several storm events. One of these events is selected, where a single bar bypassed Hvide Sande harbour during 5 days in 2003.

In this case the morphological evolution on a real coast with a complex bathymetry is simulated. The coast is not easily parametrised due to the marked variation in coastal profiles at the open coast and those at the harbour. The morphological development of particular interest for this problem is however the migration of the longshore bar. The coastal parameters being updated are the cross-shore position of the bar and the bar height. These parameters may be used to describe the evolution of the bar over the domain. The bar is therefore added onto an inactive bathymetry which essentially is the initial 2D bathymetry where the bar feature is removed in the active part of the domain, see Figure 5.18. The bar parameters are then reconstructed corresponding to the initial bathymetry before the storm. The reconstructed bathymetry is very close to the initial surveyed bathymetry, and contains the same volume of sediment in the bar.

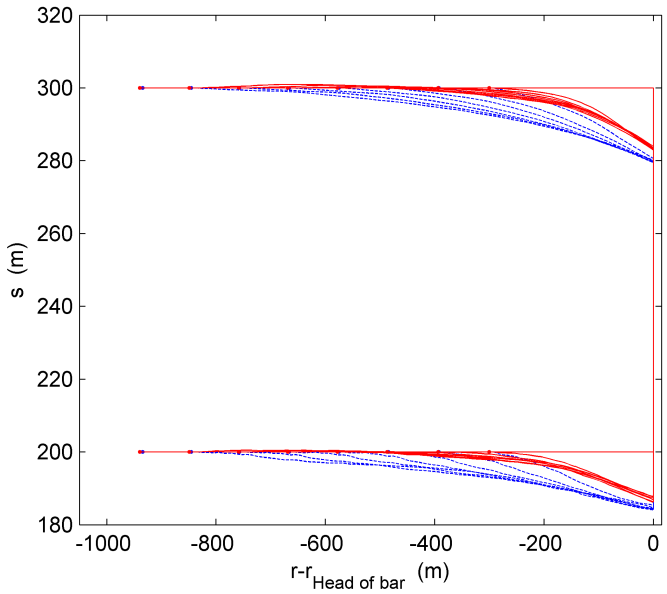

Figure 5.17: *The form of the migrating bars. The effect of the added cross-shore forcing is that the bar now migrates into the domain with a fixed planform. The origin of the horizontal axis is at the instantaneous position of the bar front. Blue dashed curve: Bar position when following streamlines. Red solid curve: Bar position with an added forcing towards the upstream cross-shore position.*

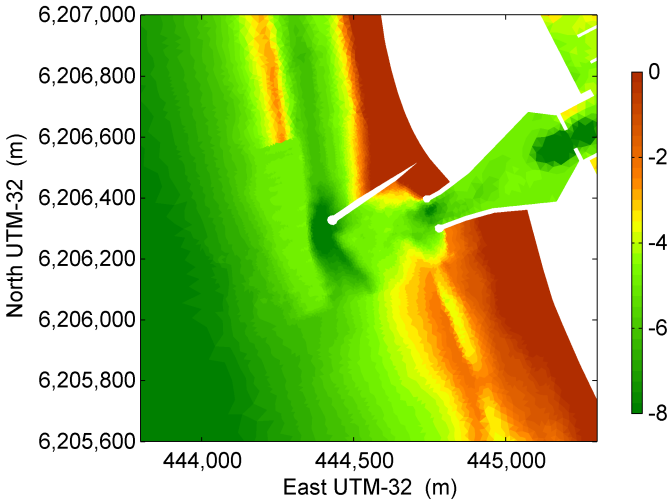

Figure 5.18: *An inactive bathymetry is constructed where the bar features on the active part of the profile are removed. Colours indicate bed level in metres.*

The motivation for using the inactive bathymetry is that the complexity of the coastal configuration is easily maintained, while the bar is allowed to migrate freely over the bathymetry. The simulation with the model describes only the dynamics of the bypass bar and does not reflect other changes in the coastal profile.

Figure 5.19 shows the surveyed conditions after the storm together with the result obtained from Grunnet et al. (2009) and that obtained with the present model concept. The head of the bar is

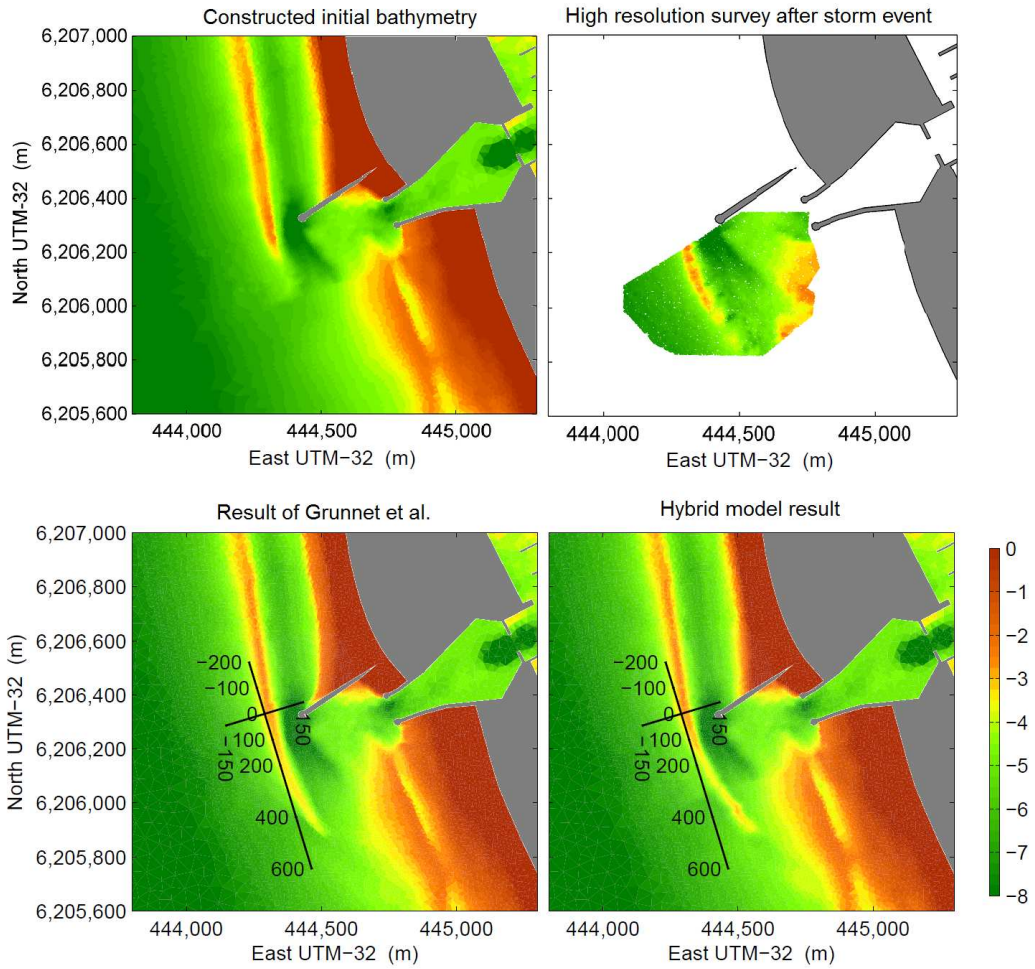

Figure 5.19: *Comparison between surveyed and modelled post storm bar configuration. The pre storm bathymetry is also shown in the top left panel. All colours indicate bed level in metres.*

initially located at the 100 m mark on the rs-coordinate system shown in the figure. During the 5 day storm with wave heights up to 4.5 m the bar migrated approximately 400 m. The features of the bar simulated by the present model resemble those seen in the survey (and in the more detailed morphological simulation), where the bar tends to turn towards the shoreline, and the cross-sectional form of the bar seems to be maintained. There is a tendency for the hybrid model to move the bar too far onshore, possibly because the effect of cross-shore sediment transport processes has not been considered. The bathymetry is quite complex and almost continuous dredging is carried out. It is therefore not possible to prescribe an equilibrium location for the bypass bar and only the streamlines have been used to determine the evolution of the planform of the bar.

5.5 Discussion and conclusions

A morphological modelling concept has been developed, which uses detailed two-dimensional area models to describe the wave-, current- and sediment transport fields. When making the morphological update the evolution of the coastal profile is restrained by allowing only one or two degrees of freedom, such as the coastline position or the volume/position of a bar. The morphological evolution

is therefore based on integrated sediment transport rates and rule-based descriptions of the profile evolution. The concept tries thus to bridge the gap between existing detailed two-dimensional morphological models and simple one-line models for the coastline evolution. The primary motivation of the concept is to (1) improve the calculated longshore transport compared to that determined by conventional 1D transport models and (2) allow simulations over longer time spans by restraining the distortion of the coastal profile which often occurs in two-dimensional models.

In the calculation of the longshore transport the model includes more physical processes than one-line models for coastline evolution. In the littoral drift models used with one-line models the longshore transport depends only on the orientation of the coastline relative to the incoming waves. In the two-dimensional models effects included are: e.g. inertia effects in the longshore current, horizontal circulation currents, effects of non-parallel bed contours on the wave field and the lee-side effect of structures on the longshore transport.

In detailed morphological models the description of the cross-shore transport is still not accurate enough to make realistic simulations of the evolution of a coastal profile over long periods. Typically the bars in a profile will be smoothed out or they will be too peaked. The bars will also often tend to migrate in the offshore direction only. For longer term modelling it can therefore be worth to abandon the profile modelling and use a schematized profile in the simulations in order to maintain a realistic shape of the profile during an extensive simulation period.

In addition the limitations put on the evolution of the coastal profile allows for much longer morphological time steps compared to the refined two-dimensional models. This will allow for longer simulations to be made in an ordinary engineering study and will make it possible to simulate a larger number of different cases.

Acknowledgements

The first author has been supported by a grant from the Danish Agency for Science Technology. This work has been partly supported by the Danish Council for Strategic Research (DSF) under the project: Danish Coasts and Climate Adaptation - Flooding risk and coastal protection (COADAPT), project no. 09-066869.

Chapter 6

Morphological Modelling of the Response to a Shipwreck - A Case study at Cape Town

Conference proceedings paper from The 33rd International Conference on Coastal Engineering 2012, Santander, Spain. Authors: Sten Esbjørn Kristensen[1], Rolf Deigaard[2], Nils Drønen[2], Jørgen Fredsoe[1], Stephen Luger[3] Citation: Kristensen et al. (2012)

Abstract

A simulation of the morphological development and degrade of a salient behind a shipwreck located north of Cape Town, South Africa is presented. The morphological model is based on a hybrid morphological model concept which combines a 2D coastal model for calculating sediment transport with a simplified 1D morphological evolution model for the coastline. The model concept is applied to the case study in order to show how the modelling concept may be applied to real coastlines with general bathymetric features. The results show that the model captures the overall morphological response fairly well without the need for extensive calibration which is often required by traditional 2D morphological models. This is attributed by the authors to the fact that the sediment transport description is based on a process based model that captures the most important features, while neglecting the often challenging description of the cross-shore sediment transport.

Keywords: Hybrid morphological model, Breakwater, Shoreline modelling, Seli 1

6.1 Introduction

Shoreline evolution is affected by gradients in the littoral drift. Accurate calculation of the littoral drift along the shoreline is therefore important in order to establish a morphological model which

[1]Department of Mechanical Engineering, Technical University of Denmark, DK-2800 Kgs. Lyngby, Denmark
[2]DHI, Agern Allé 5, DK-2970 Hørsholm, Denmark
[3]Prestedge Retief Dresner Wijnberg, Marina Centre, West Quay Rd, Cape Town, South Africa

can give reasonable predictions of the shoreline evolution. Several types of models for calculating the littoral drift along a coast have been developed, some of these are empirical methods based primarily on the angle between the approaching waves and the the shoreline normal (e.g. CERC) and other models are based on a mix between processes and empirical relations (e.g. LITLINE by DHI and Unibest-CL+ by Deltares). The process based shoreline models typically solve the wave action equation for calculating the wave height distribution over an alongshore uniform discrete coastal profile and use derived radiation stress gradients to force a flow model which is based on the alongshore uniform depth-integrated momentum equation and continuity equation. Application of process based models for coastline evolution is thus possible because the area over which the models are solved on is reduced compared to a full 2D solution as is done in area models such as MIKE21 FM and Delft 3D. Effects from coastal structures on the littoral drift need however to be incorporated by use of additional models, since these effects are not included in the 1D solution due to the alongshore uniform assumption.

Process based area models have no need for incorporating additional models for effects of coastal structures since effects of alongshore non-uniformity are inherent in this type of model. An accurate calculation of the effect of coastal structures on the littoral transport may therefore be obtained by extracting the transport signal from the solution of a coastal area model. The extracted transport signals may be used as basis of a 1D morphological model which can be used to evolve the shoreline in time by shifting the entire coastal profile onshore/offshore thus reflecting erosion/accretion respectively (see figure 6.1 for an illustration of the concept). We will call this concept a hybrid morphological model because it couples a coastal area model for waves, flow and sediment transport with a 1D morphological shoreline model.

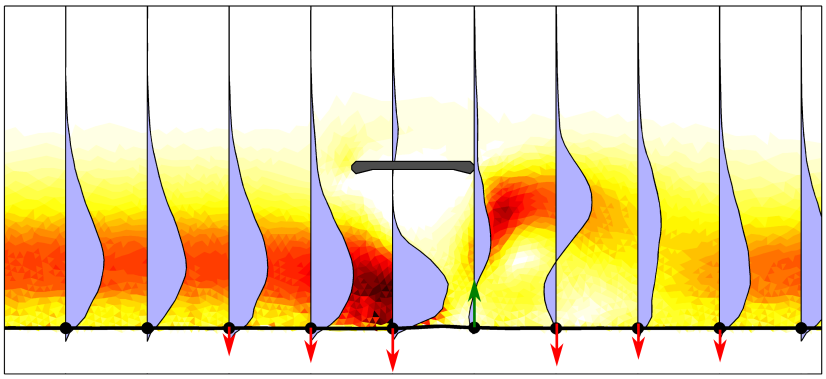

Figure 6.1: *Illustration of the hybrid morphological modelling concept. A coastal area model is used to calculate a sediment transport field based on the existing shoreline. The transport is extracted along profiles, and alongshore differences in transport give rise to a change in shoreline position as indicated by the red and green arrows. The 2D coastal model and the 1D shoreline model are coupled to form a hybrid morphological model.*

The hybrid morphological model is the next obvious step from the existing state-of-the-art shoreline models towards the full 2D coupled models. Development of hybrid morphological model concept is motivated by previous observations which show that 2D coastal models presently predict reas-

onable alongshore variations of the littoral drift during the initial phase of a full 2D morphological simulation. Maintaining a reasonable variation of the littoral drift is however complicated after some time unless the 2D coastal model is carefully calibrated such that the form of the coastal profile is maintained.

The hybrid morphological model concept allows the 2D coastal model to quantify the alongshore erosion/deposition field while the 1D morphological model defines the sediment distribution within the coastal profile. Introduction of a simplification to the morphological development of the bathymetry removes thus the requirement for careful calibration of cross-shore processes, thereby in principle making the model easier to use while obtaining accurate predictions of the shoreline evolution.

6.1.1 Previous application of the hybrid model concept

The hybrid morphological concept is first applied by Hansen et al. (2004) where it is used to simulate bar dynamics with formation of rip channels and interaction with a river mouth. The model was shown to predict a dynamic equilibrium where the bar-rip system migrates along the shoreline. Kærgaard (2011) uses the hybrid morphological concept to predict evolution of shoreline undulations and sandy spits for shorelines subject to very oblique wave incidence. In the study of Kærgaard (2011) special attention is given to a moving grid which enhances the models computational efficiency while including the effect of curvature on the result. A case study from the West Coast of Namibia, Africa shows that the model predictions are reasonably accurate in terms of measured spit dimensions.

Various adaptations of the hybrid morphological model to different coastal problems involving both hard and soft shoreline management schemes are presented in Kristensen et al. (2010). The study shows both examples of how the concept may be used to quantify morphological development and how variation in the number of degrees of freedom in the morphological model will affect the end result. The strength of the hybrid morphological model concept is demonstrated in Drønen et al. (2011) where the model concept is applied to offshore breakwaters. The morphological model is first validated against the gradual formation of a salient behind an offshore breakwater. It is then used to simulate shoreline evolution behind a new future breakwater configuration. In the study they show that the model concept is robust and reliable.

Additional validation of the model concept is however still required and this paper presents a recent addition to this by showing the adaptation of the model to a ship-wreck located off the beach of Table View approximately 10 km north of Cape Town, South Africa. The model concept is applied with a minimum of calibration but is still capable of obtaining reasonable agreement with shoreline response seen on aerial photos.

6.2 Numerical model

The hybrid morphological model is implemented in a framework inside Matlab. The model calls the coastal area model MIKE21 FM from DHI. The coastal area model consists of a spectral wave model for transformation of waves, a non-linear depth integrated flow model and a process based sediment transport model STP which calculates the transport given the local wave and flow characteristics.

The 1D morphological model updates the shoreline position relative to a linear baseline and is based on gradients in the littoral drift following the 1D continuity equation:

$$\frac{\partial s_0}{\partial t} = \frac{-1}{1-n}\frac{1}{h_{\text{act}}}\frac{\partial Q_l}{\partial r} \tag{6.1}$$

where s_0 is the shoreline position and r is an alongshore coordinate. n is the porosity which is included because the sediment transport model STP calculates transport in solid volume. h_{act} is the height of the active profile.

The littoral drift Q_l is calculated by numerical integration of the longshore transport extracted along coastal profiles from the output of the coastal area model. The alongshore gradient is evaluated by use of a first order upwind finite volume scheme and an explicit Euler scheme is used for time integration. The combination of the first order upwind scheme for spatial gradients and the explicit Euler scheme for time integration leads to a robust and dissipative solver, which is favourable in the morphological simulations.

6.3 Case study - SELI 1, Cape Town

6.3.1 A brief history of the shipwreck

The grounded ship was a Turkish bulk carrier called Seli 1 and it ran aground on September 7th 2009 during a storm. The ship is 177 m long and is located approximately 500 m from the shoreline at a water depth of 9 m (this is based on a survey of the area from 2006). The Seli 1 was abandoned by the owners when it was realised that it could not be re-floated. Although the ships cargo was removed within 2009 due to the risk of pollution, the wreck itself remained on the ground because the structure of the ship was too damaged to risk a re-floatation. Work on dismantling the ship started therefore in 2010. In April 2011 only the hull remained and it is expected to be removed by the winter storms such that the wreck is removed completely at the end of 2012.

6.3.2 The site - Table Bay

The wreck is located in Table Bay which is enclosed by two rocky headlands; Mouille Point to the south and Bloubergstrand to the north. The two headlands are separated by a long curved beach which is supplied with a limited amount of sediment from the Diep river, Harris (1993). The beaches in Table Bay are sheltered by the headland to the south and by Robben island which is located 8 km west of Blouberg strand. Figure 6.2 shows an overview of Table Bay and a close-up of the area where the ship is stranded.

The waves in the area are composed of locally generated wind waves and swell waves generated by distant storm centres in the southern latitudes Harris (1993). The combination of the swell waves from the south-west and the headland to the south means that there tends to be an increase in breaking wave height along Table Bay going from south to north. This results in a sorting of the sediment with fine sediment $d_{50} = 0.15$mm in the south to $d_{50} = 0.4$mm in the north measured at the mean water level.

There is a steady net littoral drift towards the north although winter storms (May-September) cause a significant increase in the gross-transport. The northward net transport leads to a general erosional trend in the southern part of the bay, although the bay as a whole is stable.

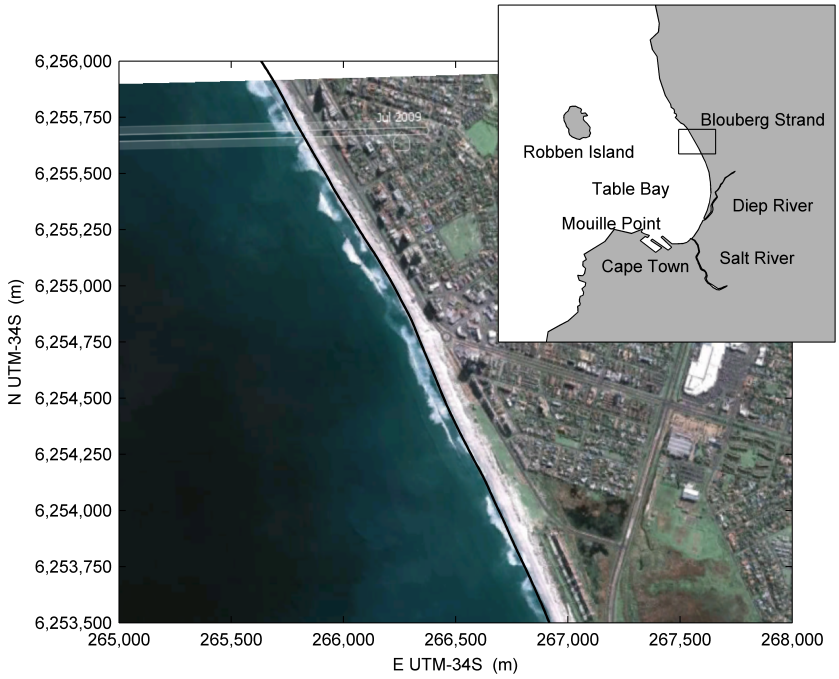

Figure 6.2: *Overview of Table Bay. The average shoreline in the area where the Seli 1 is stranded is shown in the aerial photo supplied by Google Earth. There tends to be a local change in shoreline orientation in this area.*

6.3.3 The beach at Table View

Extra attention is given to the beach at Table View because the Seli 1 is stranded at this location. The aerial photo of the beach shown in figure 6.2 shows the condition of the beach (in 2009) prior to the grounding of the Seli 1 together with the average shoreline which is based on photos from years 2000-2002,2004-2006,2009. The accuracy of the average shoreline is not more than say 20m since processes from tides, wind setup, swash and wave setup complicate detection of the shoreline from aerial photos. The average shoreline shows that it tends to be s-shaped thus the beach north of the wreck is more narrow than the beach south of the wreck. The shoreline variability in the aerial photos does not suggest an erosive or depositional trend in the area, and the shoreline is therefore expected to be in equilibrium with the wave climate prior to the grounding of the Seli 1, albeit some periodic variability due to bar-rip migration and seasonal shift in transport direction may exist.

6.4 Model setup

6.4.1 Wave climate

A two year record of the wave climate approximately 50 km West-South-West of the Seli 1 is used to generate an annual wave climate. The wave climate is a hindcast record provided by the National Centers of Environmental Prediction (NCEP) and includes significant wave height, peak wave period, mean wave direction, wind speed and direction at 3-hourly intervals. The offshore wave and wind climates are shown in figure 6.3 as a wave rose and a wind rose respectively. The wave rose is dominated by waves from the south-west which are swell waves with wave periods

ranging from 9 s to 18 s. Waves generated locally are primarily from the south-east and directed away from Table Bay. The wave period of the locally generated waves extends down to about 4 s.

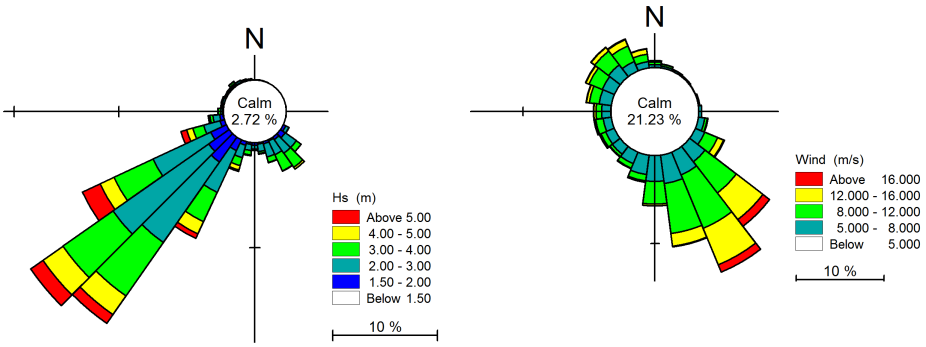

Figure 6.3: *Diagrams of the wave (left) and wind (right) records from NCEP. The parameters are extracted at E* 18° *S* 34°*.*

The seasonal variability of the wave climate is illustrated in figure 6.4 in terms of monthly averages and standard deviations. The figure shows that there tends to be slightly larger waves during the winter months (May-September). The increase in monthly standard deviation of the wave height (σ_H) during the winter indicates that the storms are primarily located in this period. The mean wave direction is turned approximately 15 deg counter clock-wise during the spring months in response to the waves being locally generated rather than being dominated by swell waves. This may also be seen by the sudden increase in directional variability for this period which is attributed to a shift towards wind generated waves rather than the unidirectional swell waves. The seasonal variability is not taken into account in the morphological simulations.

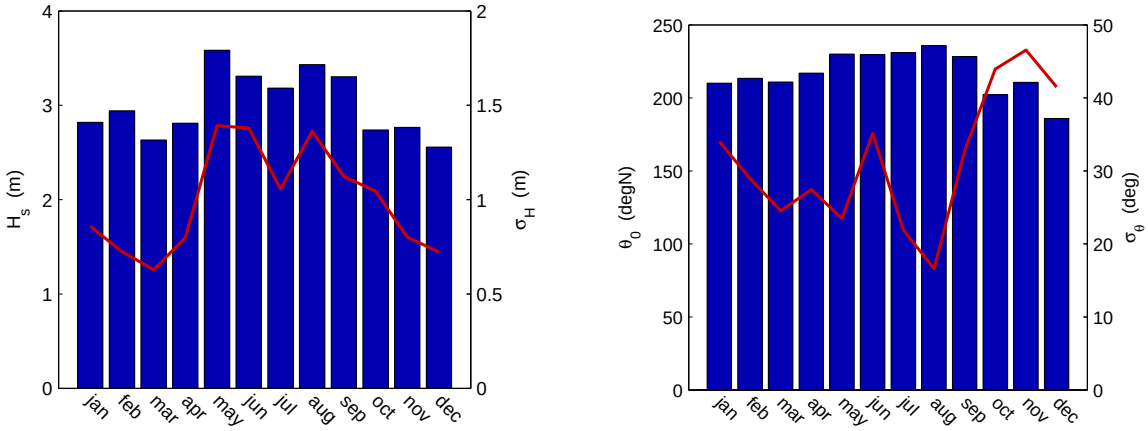

Figure 6.4: *Seasonal variability of the offshore wave climate. Bar plots show monthly averages while the red curves are the monthly standard deviations.*

Wave transformation

The recorded wave climate is condensed into a schematic wave and wind climate which can then be used to transform waves from an offshore location to a near-shore location inside Table Bay. The schematic wave climate is constructed by dividing the offshore wave climate into bins of similar wave direction and wave height. The wave height bins are equidistantly spaced by 0.5 m. The

bins for wave direction are spaced by 5 deg for waves from south-west and west and 25 deg for wave from the north-west. The annual duration of each wave class is determined and the schematic wave climate is constructed from the class mean values of the binned wave climate. The wave climate used in the morphological simulations consists of 103 wave events with durations ranging from 0.1% (9 h) to 3.85% (14 days). This wave climate contains 80% of the full time series. Figure 6.5 shows the wave rose of the binned wave climate. The wave rose is similar to the wave rose of the raw offshore climate shown in figure 6.3 except for the exclusion of wave events with offshore propagating waves.

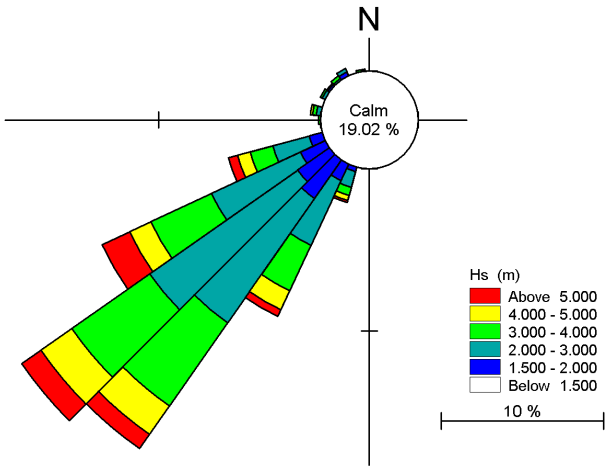

Figure 6.5: *Wave rose of the binned wave climate. The wave climate consists of 103 events and contains events corresponding to 80% of the duration of a year.*

Each wave event in the binned wave climate is associated with a class mean wind speed and wind direction. The class mean wind characteristics are constructed as simple averages of the wind speed and direction occurring concurrently with wave climates falling inside a specific wave bin. This simple method does lead to somewhat arbitrary forcing conditions when the climate is dominated by swell waves but it is nonetheless used because a better cross-correlation of the wind and wave climate would significantly increase the number of wave events thus reducing the efficiency of the model.

The schematic offshore wave climate is transformed into Table Bay by use of a full spectral wave model by DHI: MIKE21 SW. The model is run without feedback from hydrodynamics and each wave event is treated as a quasi-steady sea-state. The model is run with default/recommended settings for coastal application and no calibration is performed in this step. Figure 6.6 shows the bathymetry on which the offshore wave climate is transformed into Table Bay. The limits of the local domain used in the morphological simulations (described in the following section) is indicated by a black polygon. The transformed wave climate is indicated by the three wave roses along the offshore extent of the local domain. Comparing this figure with the wave rose of the schematic offshore wave climate in figure 6.5 shows clearly how the spreading of the wave climate inside Table Bay is reduced considerably due to refraction and due to sheltering from Robben island and the headland west of Cape Town. Furthermore; going from the southern part of the Bay towards north, the wave height tends to increase and the average wave direction turns anti clock-wise. The shoreline inside Table Bay is therefore oriented more or less perpendicular to the transformed wave

climate thus suggesting that the net littoral drift is fairly small. This agrees well with the previously stated observations of the bay.

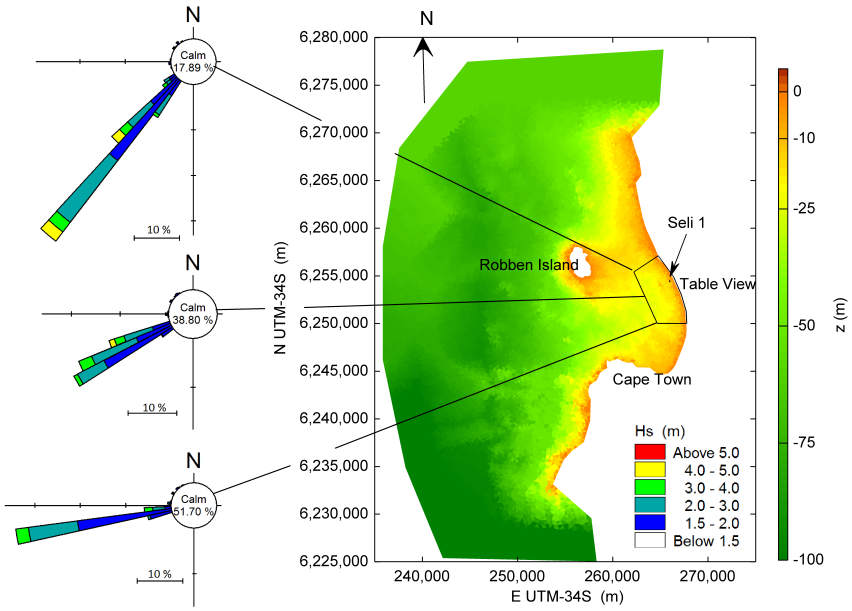

Figure 6.6: *Global bathymetry used to transform the offshore wave climate into Table Bay. The result of the wave transformation is shown in terms of the wave roses. The black polygon indicates the extent of the local domain in which morphological simulations are performed. Vertical datum is given in metres relative to MSL.*

6.4.2 Domain for morphological simulations

The morphological simulations are performed on a local domain. The local domain spans 7 km along the shoreline of Table Bay and extends 3 km into the bay. The domain is resolved by a fine 7-15 m triangular mesh in the near-shore area and a coarse triangular grid in the rest of the domain. The local domain is composed of an inactive part which covers bed levels below the depth of closure and an active part which is defined in terms of a parametric power profile which is added onto the inactive part, see figure 6.7. The active power profile is given by:

$$z = z_0 - A\,(s - s_0)^m \tag{6.2}$$

where z_0 is the berm level, s_0 is the cross-shore position of the berm and A, m are profile parameters. The active and the inactive part are combined to form the 2D bathymetry on which wave, current and sediment transport fields are calculated by the coastal area model.

The bathymetry of the inactive part is determined from a local survey of the area from 2006 which prior to interpolation onto the mesh is smoothed while retaining overall features of the measurement. The form of the active profile is chosen to be constant alongshore and is based on profiles extracted along the area and displaced towards a common origin. The profile parameters $A = 0.9$ and $m = 0.4$ are calculated as a best fit (see figure 6.8) to the entire dataset given a berm height $z_0 = 3$ m and a closure depth $z_{cl} = -5$ m. This closure depth is chosen because the survey from the area shows that the coastal profiles are generally composed of a steep upper shoreface which flattens at around $z = -5$ m followed by a lower shoreface with a mildly steep bed level gradient.

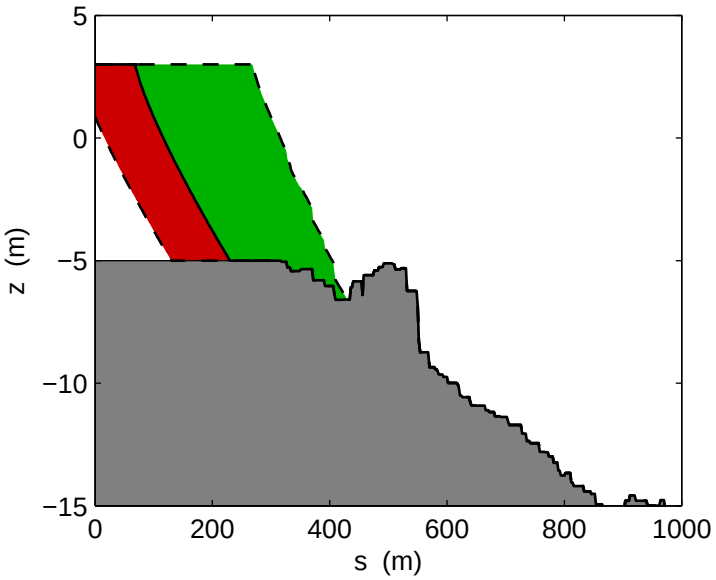

Figure 6.7: *The coastal profile is composed on an inactive part (grey area) and an active part which responds to erosion/deposition by moving onshore or offshore respectively (red and green areas).*

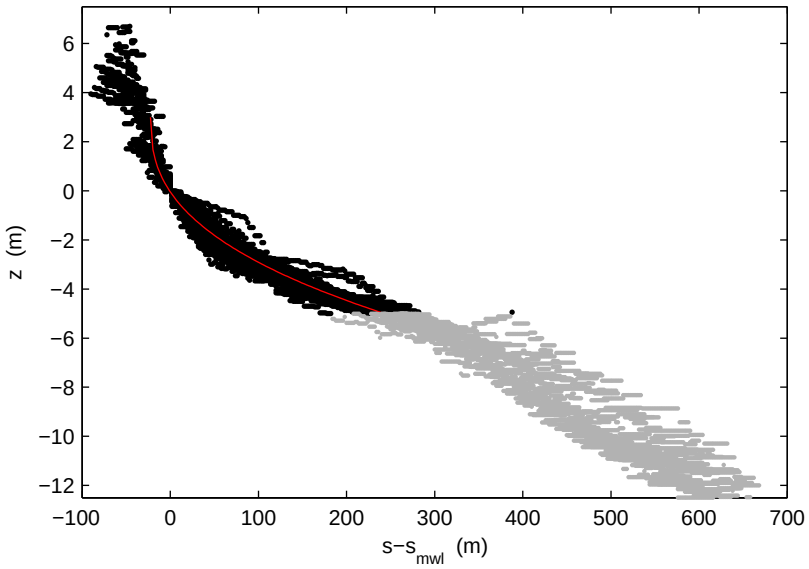

Figure 6.8: *Comparison of the active profile against profiles generated from a field survey from 2006. The profile parameters of the active profile (A and m) are chosen as the best fit to the extracted data.*

6.5 Morphological simulations

6.5.1 Baseline - conditions prior to grounding of Seli 1

The morphological model is set up to simulate shoreline evolution of the beach at Table View without the presence of the shipwreck in order to ensure that the transformed wave field is reasonable. The initial shoreline is determined from an aerial photo taken in 2009 a month prior to grounding of the ship. This shoreline is very similar to the average shoreline shown in figure 6.2.

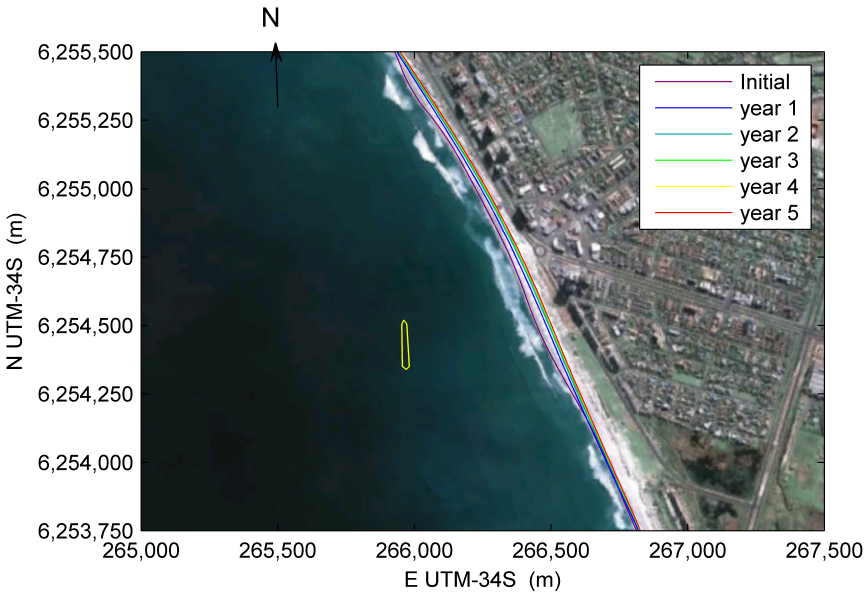

Figure 6.9: *Simulated shoreline for baseline conditions (situation prior to grounding of the Seli 1). The model tends to overestimate erosion of the shoreline but reaches an equilibrium within 5 years of simulation.*

The morphological model responds rapidly to the initial shoreline which is not in equilibrium with the wave forcing, but reaches an equilibrium within 5 years. The most pronounced feature of the morphological response is a removal of undulations on the initial shoreline and erosion of the beach in the area north of the future location of the shipwreck, see figure 6.9. As a matter of interest, this simulation shows also that the morphological model predicts a short transition from one shoreline orientation to another at the same position as is seen on the aerial photos. Simulations where the direction of the wave climate and the features of the inactive bathymetry are changed suggest that this sudden change in shoreline orientation is closely related to a shoal located at a water depth of 10-13 m roughly 1 km south-west of the future position of the wreck.

6.5.2 Morphological response to shipwreck

The impact of the shipwreck on the shoreline is determined by adding the shipwreck to the computational domain. The presence of the wreck causes sheltering from the approaching waves as would be the case from an offshore breakwater. The impact of the shipwreck on the littoral drift causes a salient to form as shown in figure 6.10. The figure compares the simulated shoreline against an aerial photo taken from the area a year after the grounding of Seli 1. The comparison shows that the morphological model gives a reasonable estimate of the salient amplitude and width, although the alongshore position of the salient tends to be located slightly too far to the south.

The position of the salient is fairly stable in the simulation due to the random permutation of the wave climate which therefore suppresses salient movement due to long periods with wave attack from a certain direction. Tests where the shoreline shown in figure 6.10 is used as initial condition and subject to constant waves from north and south show that the salient tends to move downstream, approximately 50 m and that the salient amplitude also decreases slightly. The salient response to the constant wave climate is in both cases approximately 2 months which makes it probable that

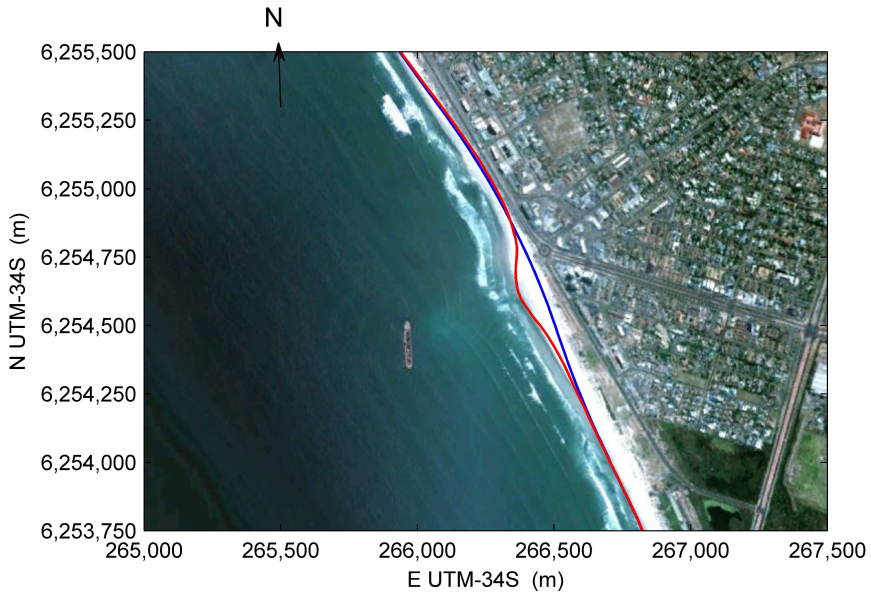

Figure 6.10: *Planview of the simulated formation of a salient in the shadow zone behind Seli 1. Red curve: Equilibrium position. Blue curve: Initial condition.*

seasonal variation will allow the salient some activity. The variability in salient position is however too weak to describe the discrepancies seen in figure 6.10.

6.5.3 Morphological response to removal of shipwreck

Removal of the shipwreck has been simulated with the morphological model showing that the salient disappears within a year. Aerial photos from 2011 show that the ship is broken into several pieces thus allowing an increase in penetration of wave energy into the shadow zone. The salient is at this point no longer easily identifiable. The predicted rapid disappearance of the salient seems therefore most likely.

6.6 Conclusion

Process based area models for coastal sediment transport are generally well suited for predicting the longshore transport and it's distribution across the profile. Their prediction of the cross-shore transport is however rarely sufficiently accurate to simulate the long-term evolution of the coastal profile. The hybrid morphological model uses therefore only the the longshore transport variation for calculating evolution of the shoreline. This leads to a robust morphological model which can be applied with a fair amount of confidence to coastline evolution involving offshore breakwaters. This is illustrated by the case study presented in this paper and by the study presented in Drønen et al. (2011).

Acknowledgements

The first author has been supported by a grant from the Danish Agency for Science Technology and Innovation and by a grant from Otto Mønsteds Fond. This work has been partly supported by

the Danish Council for Strategic Research (DSF) under the project: Danish Coasts and Climate Adaptation - Flooding risk and coastal protection (COADAPT), project no. 09-066869.

Chapter 7

Hybrid Morphological Modelling of Shoreline Response to a Detached Breakwater

Accepted Journal paper in Coastal Engineering 2013, vol. 71. Authors: Sten Esbjørn Kristensen[1], Nils Drønen[2], Rolf Deigaard[2], Jørgen Fredsoe[1]. Citation: Kristensen et al. (2013a)

Abstract

We present a new type of model for calculating morphological changes induced by the presence of breakwaters. The model combines a process based area model, used to calculate the sediment transport field in the two horizontal dimensions, with a simplified morphological updating scheme where the evolving cross-shore profile is described by a limited number of parameters. The hybrid morphological model is a strong tool for medium term and long-term modelling because it is cost effective while containing important features of the sediment transport description. Two versions of the model are developed in order to study the evolution of beach morphology: One suited for offshore breakwaters (1D model) and one mainly dedicated to coastal breakwaters ("1.5D" model).

The version for offshore breakwaters is first presented and tested against field observations of salient evolution. The model is then applied to a model study of the principle correlations between evolving salients (spatial and temporal scales), the characteristic dimensions of the breakwater (distance to shore and alongshore length) and wave climate (wave height, normal and oblique wave incidence).

The second version is applied to investigate in more detail the evolving morphology behind coastal breakwaters. It is demonstrated how the model is able to calculate the evolution of either salient or tombolo planforms, and furthermore it is shown that the results are in reasonable agreement with existing rules.

Keywords: Breakwater, morphological response, shoreline, equilibrium, salient, tombolo

[1]Department of Mechanical Engineering, Technical University of Denmark, DK-2800 Kgs. Lyngby, Denmark
[2]DHI, Agern Allé 5, DK-2970 Hørsholm, Denmark

7.1 Introduction

Detached breakwaters are typically constructed to shelter an area from waves or to promote shoreline accretion either as a measure against local shoreline erosion or to increase the recreational value of a beach. A criterion for success of the breakwater design will often be linked to the shape and dimensions of the coastal planform developing behind the structure, and the erosion of the adjacent coastline downdrift the structure. Application of engineering models which can predict the resulting coastal accretion and erosion can therefore be important for the planning and design of detached breakwaters. There are basically three types of engineering models for predicting the morphological impact of coastal structures on the coastline: empirical models, physical models and numerical models.

Empirical models are formulated as rather simple relations between the geometry of the breakwater and the resulting shoreline evolution. Some of the empirical models use wave diffraction theory to predict an equilibrium shoreline, Hsu et al. (2003); McCormick (1993) while other models estimate the type and dimensions of the coastal accretion based on analysis of field data, Pope and Dean (1986) or results from numerical models Hanson and Kraus (1990).

Physical models have over the last half a century contributed significantly to the understanding of the hydrodynamic processes around breakwaters, see e.g. Gourlay (1974); Mory and Hamm (1997). Physical models are however costly and their applicability is constrained by scaling problems for the sediment, because the model material will be so fine that it becomes cohesive. Use of physical models for morphological studies is therefore generally recommended to be done in large scale testing facilities. Alternatively lightweight sediment can be applied, but this can cause other severe problems in the representation of the sediment transport in the model, Ilic et al. (2005).

Numerical morphological models can be one-, two- and in rare cases three- dimensional. A 1D model calculates the distribution of the littoral drift along the shoreline and assumes that the entire coastal profile is translated in the offshore or onshore direction reflecting deposition or erosion respectively. The 1D models are computationally very efficient and can be used to simulate morphological evolution over several decades. They are however often limited by the assumptions of the form of the coastal profile and of alongshore uniformity in the longshore transport calculations, and they do not incorporate inertia effects of the longshore flow and surf zone circulation generated by alongshore set-up gradients. Examples of 1D models which have been applied to studies in many different coastal areas around the world are GENESIS, Hanson and Kraus (1990, 2011) or the model complex LITPACK of DHI.

A two-dimensional morphological model describes the wave, current and sediment transport fields over an area and calculates the erosion and deposition pattern over the area from the divergence of the sediment transport field. The wave transformation from offshore is carried out on a 2D bathymetry and includes processes like shoaling, refraction, diffraction, breaking and possible energy transfer from the wind. The current in the surf zone is mainly driven by the forcing from the breaking waves, but tide and wind can also be included. The sediment transport is calculated from the wave and current field and its divergence determines the rate of bed level change. The bed level is updated in each morphological time step and the whole sequence of models is repeated. Examples of 2D models are given in Lesser et al. (2004); Zyserman and Johnson (2002) and in Nam et al. (2011). The two-dimensional models are thus much more detailed than the one-dimensional models and it could be expected that they would be superior for all applications. Two-dimensional

models are however primarily used for short to medium term simulations, partly because they are computationally costly and partly because accumulation of small errors leads to degeneration of the coastal profile: a 2D model cannot maintain a realistic coastal profile if drastic morphological changes occur.

Attempts to address some of these limitations of the 2D models are: The computational efficiency of 2D morphological models can be improved by use of a morphological speed up factor, taking advantage of the very slow morphological evolution compared to the rapid response of the hydrodynamics, by reducing the actual time series of the waves to a schematised wave statistics and by use of parallel computing. Degeneration of the 2D bathymetry due to accumulation of noise may be addressed by use of higher order numerical schemes, Callaghan et al. (2006); Long et al. (2008) or by use of filters, Nam et al. (2011) thus retaining the overall features. Degeneration of the coastal profile in long term morphological simulations is linked to the inaccuracy in prediction of the cross-shore sediment transport which should maintain the coastal profile. Research in improving the cross-shore transport predictions has therefore focused on adding new processes such as effect of bed slope, higher order boundary layer effects and Q3D effects to the transport description, Drønen and Deigaard (2007); Fredsoe and Deigaard (1992). Despite the efforts the morphological models still continue to degenerate the coastal profile when significant morphological evolution occurs. Therefore impressive comparisons of calibrated area models against experimental data may be shown after a limited amount of time, while the long term morphological response where an equilibrium state is obtained are rarely seen.

Rather than adding new processes to the sediment transport description the present work focuses on a hybrid model concept, which couples a 2DH coastal model, which simulates the hydrodynamics and sediment transport over the bathymetry of the model area, with a morphological scheme that constrains the number of degrees of freedom for the profile, Kristensen et al. (2010). The main advantages of the hybrid model concept over traditional 2D models is that 1) the profile distortion can be limited considerably because a parametric evolution is imposed on the profile and 2) CPU time is reduced because larger morphological time steps can be used since the morphological elements are larger than the elements on which hydrodynamics and waves are solved.

The first application of the hybrid morphological concept was given in Hansen et al. (2004) where it was used to simulate bar dynamics with rip channel formation and interaction with a river mouth. By combining a 2DH sediment transport model with a behaviour oriented model describing the equilibrium position of the bar it was found that a dynamic equilibrium can be obtained, where the bar and rip channels migrate along the shore. Kærgaard (2011) used the hybrid model concept to simulate evolution of sandy spits which are formed due to an instability which occurs for very oblique wave incidence. In the work of Kærgaard (2011) special attention has been given to development of a moving computational mesh in order to optimise the computational efficiency of the model. The applicability of the hybrid model concept to a range of different coastal problems is illustrated in Kristensen et al. (2010) showing how different parametric formulations can be used to simulate evolution around hard and soft coastal protection solutions. The simplest example of a parametric morphological scheme is an adaptation of the one-line model where the bathymetry is updated by shifting the entire profile offshore or onshore reflecting deposition or erosion respectively. Drønen et al. (2011) presented the strength of this scheme for an application of the hybrid model concept to an engineering problem: The morphological model was first validated against a measured shoreline advance behind an offshore breakwater and was then used to predict the salient formation

behind a new possible breakwater configuration. In this application the simulations cover many years and the model concept was proven to be robust.

Scope of present work

The present work focuses on morphological evolution around offshore and coastal breakwaters. A 1D formulation is used for the morphological evolution around offshore breakwaters while a formulation which allows 2D changes of the costal profile to occur is used for coastal breakwaters. The more complex model is defined as a 1.5D hybrid morphological model because it allows 2D morphological evolution by changing the form of the coastal profile rather than by updating the bed level of discrete mesh elements. The details of the hybrid morphological modelling concept are described and an analysis of the model sensitivity to changes in wave climate and breakwater configuration in relation to the resulting equilibrium planform behind the breakwater is presented.

7.2 Numerical Model

7.2.1 Coastal area model for the sediment transport field

The 2D coastal model used for calculating the wave, current and sediment transport field is the commercial code (MIKE21 FM) developed by DHI. In the present application the spectral wave module MIKE21 SW is used for transformation of the waves from offshore and description of the detailed nearshore wave field. The hydrodynamic module MIKE21 HD is used to calculate surface elevation and currents, which in the present applications are wave-driven, and the sediment transport module MIKE21 ST is finally used to calculate the sediment transport field. The model system is solved on a flexible 2D grid which can include triangular and quadrilateral elements.

The spectral wave module solves the wave action balance equation using a directional decoupled parametric formulation, following Holthuijsen et al. (1989). The wave transformation incorporates effects of energy dissipation due to wave breaking and bottom friction, energy transfer due to depth refraction and diffraction and energy supply due to action of wind. Wave breaking is determined using the dissipation model of Battjes and Janssen (1978). The radiation stress tensor is determined from the integrated energy spectrum and is used to drive the flow.

The hydrodynamic module solves the non-linear shallow water equations (Saint-Venant equations), which consist of the local continuity equation and the momentum equation formulated in a Cartesian coordinate system. Bed friction is described by the Manning equation with a Manning number corresponding to a Nikuradse bed roughness of 0.25 m. This rather high bed roughness has been chosen because no model for the increased apparent roughness caused by the combined wave-current boundary layer is included in the flow modelling. Lateral stresses due to viscous friction, turbulent friction and momentum exchange due to organised water motion are included as an eddy viscosity with a constant value of 0.5 m^2/s.

The sediment transport model is a 1DV intra-wave model for sand transport under the combined action of waves and current. It calculates the vertical distribution of the sediment concentration by solving the diffusion equation, Deigaard et al. (1986b); Fredsoe et al. (1985). The instantaneous bed shear stress is obtained from the Fredsoe (1984) model for turbulent boundary layers in combined waves and current. The near bed concentration used as boundary condition for the suspended sediment calculation is based on the instantaneous Shields parameter, Engelund and Fredsoe

(1976). Bed load transport is calculated using the approach of Engelund and Fredsoe (1976). The sediment transport model is used in a relatively simple form; first order Stokes theory is used to describe the oscillatory component of the near bed orbital motion and the sediment transport is taken to be in the mean current direction omitting so-called Q3D effects.

7.2.2 Parametrised morphological update of bed

Two different formulations are used for the morphological evolution. A 1D parametric model is used for offshore breakwaters, i.e. breakwaters located outside the surf zone, while a 1.5D model which includes profile evolution is used for breakwaters located inside the surf zone. Both models are implemented as Matlab functions which read and process output and input files used by the MIKE21 FM coastal model. The two morphological models and the results obtained with each of them are presented separately in the following parts.

7.3 Offshore breakwater - 1D morphological model

7.3.1 Model formulation

Definitions

The first version of the model is intended for offshore breakwaters. The profile shape is assumed not to be disturbed by the presence of the breakwater. In the present simulations a Dean type power profile has been used to describe the coastal profile. The profile is applied between the level of the berm, z_0 and the level of closure depth z_{cl} (see figure 7.1):

$$z(s) = z_0 - A\,(s - s_0)^m \tag{7.1}$$

s_0 is the cross-shore position of the berm and A is the profile parameter which controls the slope of the coastal profile.

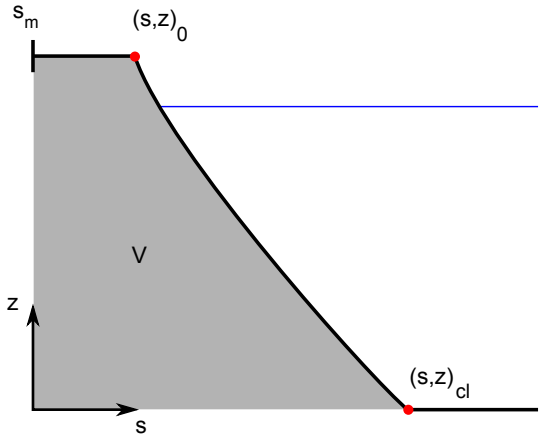

Figure 7.1: *A Dean type power profile is used for describing the coastal profile in the morphological simulations with an offshore breakwater*

For the sake of convenience a coordinate system (r, s) is introduced with the r-axis oriented along the main direction of the coast and a cross-shore s-axis oriented in the offshore direction, see figure 7.2.

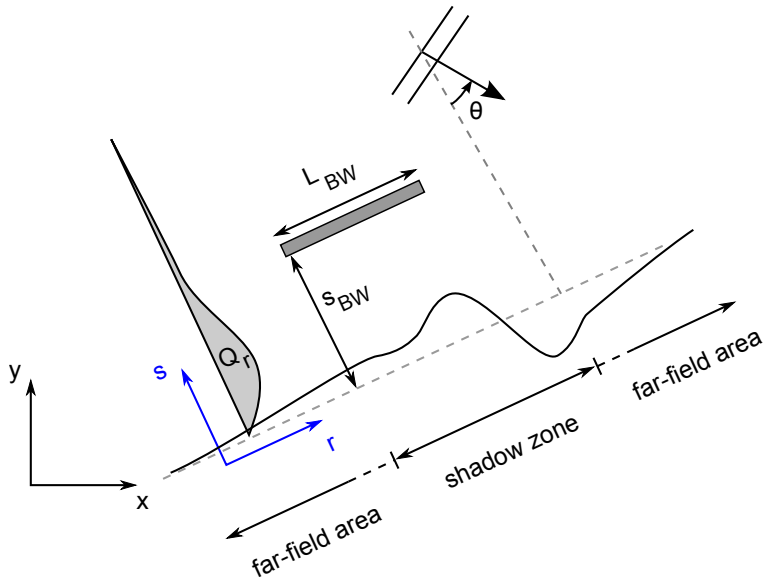

Figure 7.2: *Definition of a local coordinate system, breakwater dimensions and shoreline areas around a detached breakwater. θ is the angle between the incoming waves and the shoreline normal of the general shoreline*

Numerical model

The model is run in a sequential way. First the area model is run over the bathymetry for the given time step to determine wave field, wave generated currents and sediment transport. Then the longshore transport rates are determined by integrating the sediment transport field from the model over transects in the surf zone normal (along the s-axis) to the baseline

$$Q_{\mathrm{r}} = \int_{s_0}^{s_{\mathrm{lim}}} \bar{q}_{\mathrm{st,MIKE21}} \cdot \bar{n} \, \mathrm{d}s$$

Because only the shoreline position is allowed to change, the rate of change in profile volume (given as the gradient in the longshore transport) is related to a rate of change in shoreline position by:

$$h_{\mathrm{act}} \frac{\partial s_0}{\partial t} = \frac{-1}{1-n} \frac{\partial Q_{\mathrm{r}}}{\partial r} \tag{7.2}$$

Where n is the porosity of the deposited sediment. This equation is used to update the shoreline position and a new bathymetry for the next time step is constructed applying the profile assumption described above.

In order to dissipate high frequency alongshore spurious oscillations (numerical noise) the littoral drift is filtered using a 3-stencil filter. Gradients in the littoral drift are evaluated using a first order upwind finite volume scheme and the time integration is evaluated by use of an explicit Euler scheme.

7.3.2 Simulations of the morphological response to offshore breakwaters

As an example the morphological response to offshore breakwaters located 500 m from the shoreline is determined using the 1D hybrid model in a 3000 m long periodic domain. The periodic boundary conditions represent the situation with many equally spaced breakwaters, one for every 3000 m.

The active height of the coastal profile is 5 m ($z_{\mathrm{cl}} = -4$ m)) and a profile parameter $A = 0.12$ with $m = 0.67$ is used. The average slope $(z_0 - z_{\mathrm{cl}}) \,/\, (s_{\mathrm{cl}} - s_0)$ is then: 1/50. A uniform grain size distribution is assumed with a mean grain diameter of 0.2 mm. The alongshore resolution of the morphological model is 20 m for profiles located at some distance from the breakwater while it is 10 m for profiles near the breakwater.

A symmetric two sea-state wave climate is used to obtain a wave climate with no net transport. An offshore wave climate with a significant wave height $H_{\mathrm{s}} = 1.5$ m, peak wave period, $T_{\mathrm{p}} = 8$ s and a mean wave direction normal to the shoreline of $\theta_0 = 0 \pm 15\,\mathrm{deg}$ is used. Each sea state is represented by an energy spectrum with a directional spreading of $\sigma_{\mathrm{w}} = 19\,\mathrm{deg}$.

The wave climate is represented by two different wave directions because this is a better representation of the wave climate on a real coast with a low annual littoral drift compared to using a single sea state with normal incident waves. The double sea state representation of the wave climate introduces some amount of diffusion of small instabilities and allows inertia effects such as recovery of the littoral drift to be resolved by the coastal model. The model is run with the two conditions alternating in each morphological time step.

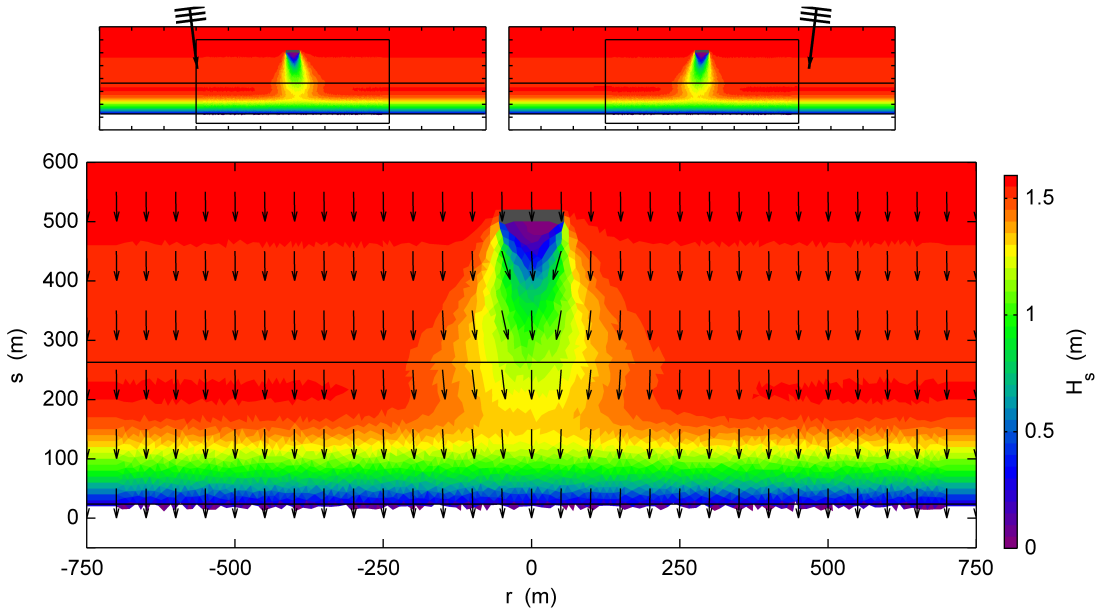

Figure 7.3: *Wave field around breakwater due to two slightly different angles of wave incidence at each time step. Top panels: Instantaneous wave fields during each of the first two time steps for the full domain. Lower panel: Close-up of the average wave field. Vectors indicate mean wave direction and contour lines indicate bed level at the mean water level and the closure depth. The wave annotations at the top panels indicate instantaneous wave incidence at the offshore boundary.*

The initial mean wave field in figure 7.3 shows that the recovery wave height behind the breakwater is approximately 80% of the undisturbed wave height before wave breaking. Reduction in wave height and deflection of the waves behind the breakwater has drastic effects on the wave-driven currents and the littoral drift behind the breakwater. The littoral drift is reduced in the centre of the shadow zone behind the breakwater, while it is increased near the boundaries of the shadow zone as indicated in figure 7.4 in which a close-up of the average transport field is shown together

with instantaneous transport fields. The initial effect of the breakwater is to cause deposition of sediment in the shadow zone, while erosion occurs in the neighbouring coastal profiles. The equilibrium bathymetry is shown in figure 7.5 where a salient has formed. The size of the gross transport is approximately the same in the equilibrium configuration as in the initial conditions with sediment transport occurring only landward of the breakwater. The average transport is however reduced to zero everywhere in the equilibrium conditions because the formation of the salient allows the littoral drift to recover downstream of the breakwater in a smooth manner. The equilibrium bathymetry is shown after 6 years of morphological evolution although most of the morphological changes occur within the first couple of years as indicated in figure 7.6 which shows the variation of the maximum shoreline advance and shoreline retreat with time.

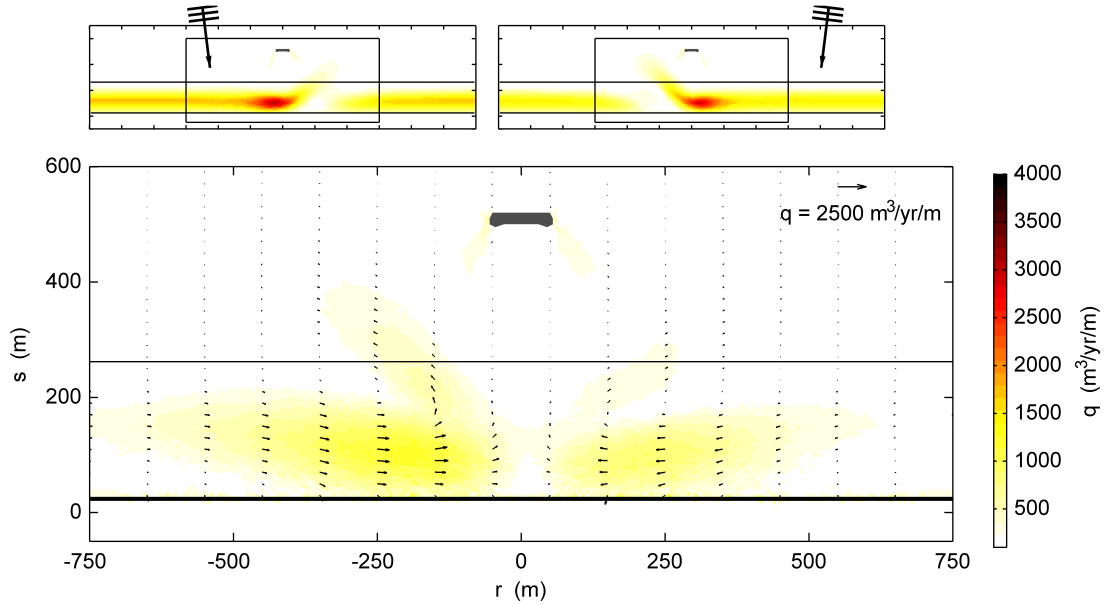

Figure 7.4: *Net sediment transport field at the first two time steps. The instantaneous transport fields are shown in the two upper panels. Vectors indicate direction and magnitude of the net sediment transport. Offshore wave angle incidence is* $\theta_0 = 0 \pm 15\,\mathrm{deg}$.

The behaviour of the morphological model correlates well with observations of Nir (1982) where field observations suggest that an initial rapid morphological evolution is replaced by seasonal variations in salient size and position.

If the mean wave direction deviates from the shore normal the mean littoral drift will be different from zero. The effect of this is that the position of the salient moves downdrift in response to the position of the shadow zone and that the salient becomes asymmetric with the downdrift side forming a larger angle with the original coastline. The mean littoral drift is reduced and correspondingly the far-field shoreline (shoreline updrift and downdrift the structure) is turned slightly up against the incident waves. Figure 7.7 shows the equilibrium transport fields and the equilibrium shoreline obtained for a case where the offshore wave incidence angle relative to the initial shoreline normal is $\theta_0 = 50 \pm 15\,\mathrm{deg}$. The average transport shown in the lower panel is constant throughout the domain while the upper panels show that the gradients in the littoral drift correspond to an alternating updrift and downdrift migration of the salient in each of the two sea-states.

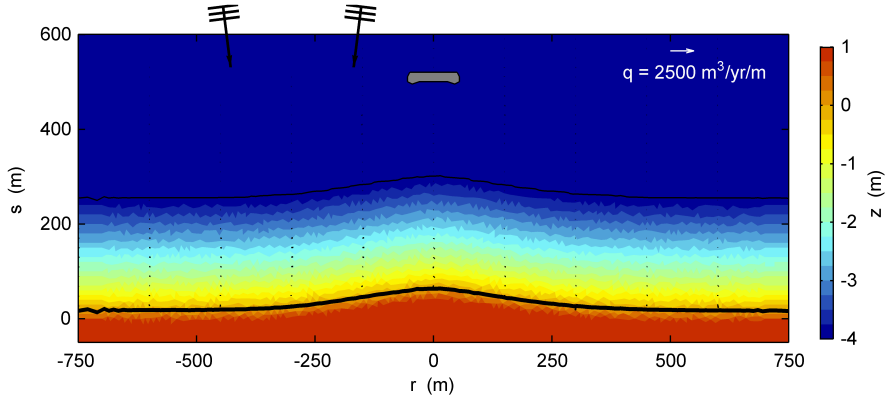

Figure 7.5: *Equilibrium bathymetry obtained after 6 years of morphological evolution for a double sea-state wave climate with* $\theta_0 = 0 \pm 15\,\mathrm{deg}$.

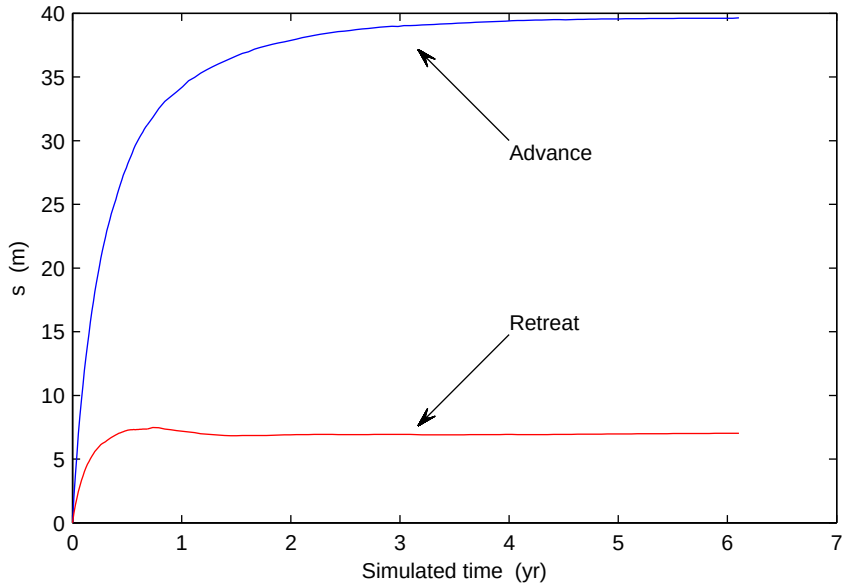

Figure 7.6: *Time series of the maximum berm advance and the maximum berm retreat.*

7.3.3 Case study: Salient formation behind a shipwreck

The 1D hybrid morphological model is applied to a case study at Cape Town where a grounded bulk carrier: Seli 1, has caused a salient to form, see Kristensen et al. (2012) for details. The 177 m long ship is located 500 m from the shoreline at a water depth of 9 m and ran aground on September 2009. A regional bathymetry used to transform offshore waves into the bay is created based on sea chart data and a local survey of the area from 2006. The shallow part of the profile (water depths smaller than 5 m) is described parametrically with a Dean type profile with a profile parameter $A = 0.90$ and $m = 0.40$. A mean grain diameter of 0.4 mm is used based on sediment samples taken from the high, mean and low water line in the area.

A local annual wave climate is synthesized by binning a two year climate supplied by the National Centers for Environmental Prediction (NCEP) and transforming this into the bay. The annual

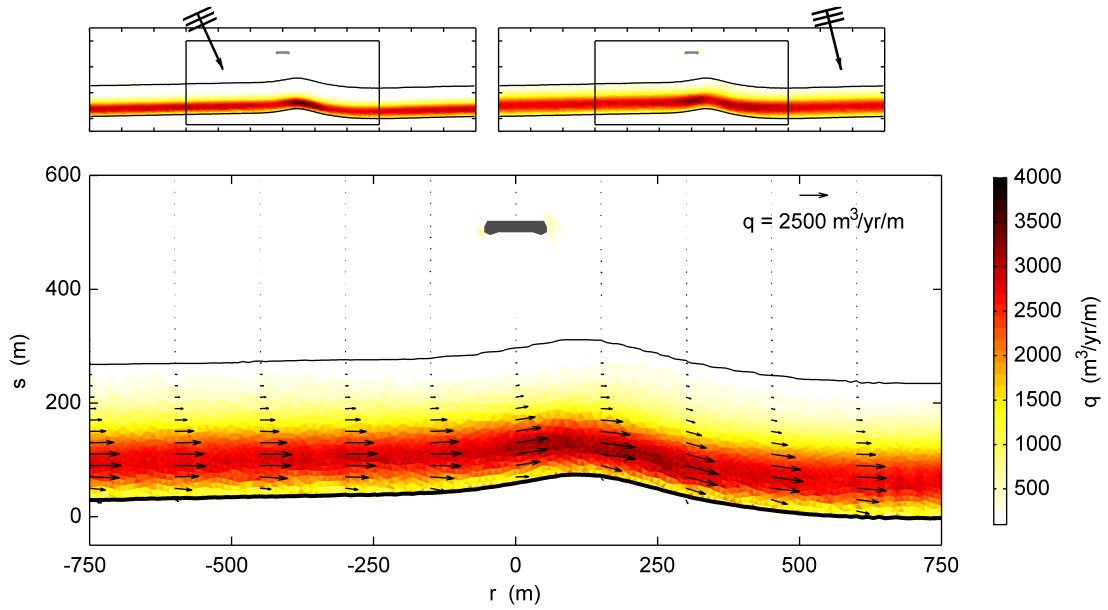

Figure 7.7: *Average and instantaneous sediment transport fields under equilibrium conditions for oblique wave incidence,* $\theta_0 = 50 \pm 15$ deg.

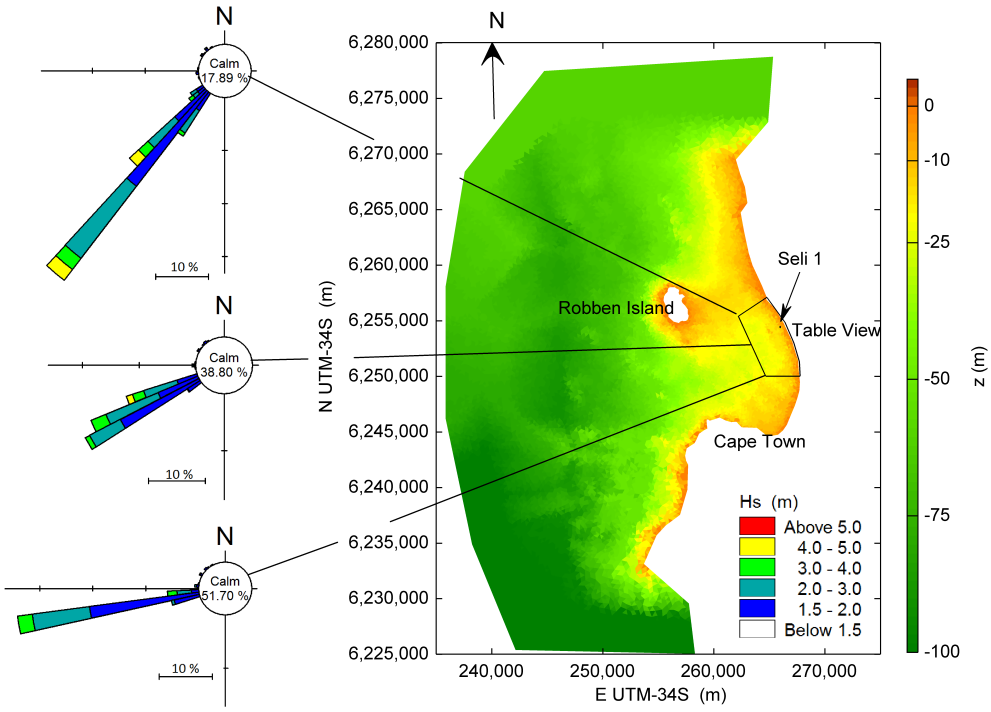

Figure 7.8: *Bathymetry of Table Bay and the area west of Cape Town. Waves are transformed from offshore to a local domain located inside Table Bay using MIKE21 SW.*

wave climate is dominated by 10-14 s swell waves from the south-west which primarily occur in the winter months, May-September. Examples of the transformed wave climate used in the

morphological simulations are shown in terms of 3 wave roses in figure 7.8.

The presence of the shipwreck forms gradients in the littoral drift in a manner similar to an offshore breakwater. The shoreline is initially gently curved following the shoreline from an aerial photograph taken in 2009 prior to the grounding of Seli 1. The shoreline responds to the shipwreck and the morphological model predicts a stable planform within the first year, see figure 7.9. Comparing the calculated shoreline response with the image in the figure shows that the model predicts the salient amplitude and width reasonably well. The result of the morphological model shows despite the small discrepancies that the model represents the most important processes and it gives therefore a good estimate of the morphological effect of offshore structures without use of extensive calibration.

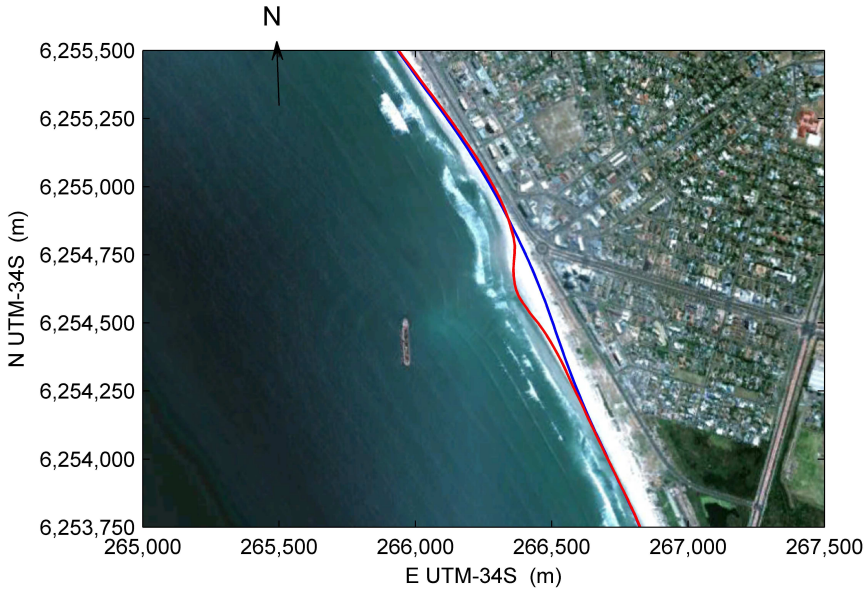

Figure 7.9: *Simulated shoreline after 1 year. Blue curve: Initial shoreline. Red curve: Simulated shoreline. The rectified image is supplied by Google Earth. The image is from November 2010.*

7.3.4 Planform sensitivity analysis, mean wave direction normal to the shoreline

Increasing the spreading of the wave direction would increase the littoral drift under each of the two individual sea-states and widen the footprint of the breakwater on the shoreline. The variation in equilibrium salient planform is therefore analysed from results obtained by the model for the wave climates listed in table 1 and for varying breakwater configurations (defined by the dimensionless quantity λ):

$$\lambda = \frac{L_{\mathrm{BW}}}{s_{\mathrm{BW}}} \tag{7.3}$$

The salient width is defined as the width of a square which has the same area and amplitude as the salient. The actual width is approximately twice the width of the rectangle depending on the peakedness of the salient (see the lower left panel in figure 7.10). The morphological simulations show that the salient width in general increases with the distance of the breakwater to the initial

Table 7.1: *Net normal waves are generated using a two bin wave climate. Transport rate is given in deposited volume assuming a porosity $n = 0.4$. θ_{bc} is the wave angle on the offshore boundary of the model domain. Offshore wave parameters are: $H_s = 1.5$ m, $T_p = 8$ s and $\sigma_w = 19$ deg.*

θ_0 (deg)	θ_{bc} (deg)	Q_{gross} (m^3/s/yr)
0 ± 15	0 ± 7.1	220,000
0 ± 30	0 ± 13.9	350,000
0 ± 50	0 ± 21.5	410,000

shoreline and the angle between the two incident sea states. The impact of breakwater length increases for a small directional spreading of the incident waves but is generally of minor importance. These observations indicate that the salient width may depend on the geometric shadow zone created by the breakwater.

$$W_{shadow} = L_{BW} + 2s_{BW} \tan \theta_{bc} \tag{7.4}$$

where θ_{bc} is the near shore incident wave angle for the two sea states considered. The salient width is made dimensionless by dividing the salient width with W_{shadow}. Figure 7.10 shows the dimensionless salient width as function of λ for varying angles between the two sea states. The figure shows that the dimensionless salient width is weakly affected by variations of the angle between the two sea states. The decrease in dimensionless salient width for increasing λ is associated with a decrease in salient peakedness for increasing λ.

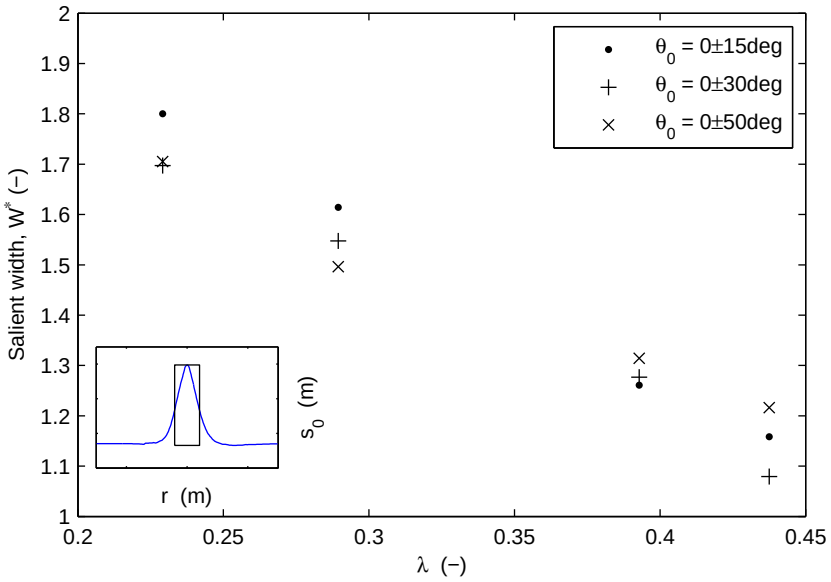

Figure 7.10: *The salient width is defined as a displacement width as indicated in the lower left panel. The salient width is made dimensionless by dividing with the width of the geometric shadow zone.*

The salient amplitude increases weakly with the spreading of the annual wave climate while it is a strong function of λ. This result correlates well with existing empirical rules in which λ is a key parameter for determining the type of planform, Pope and Dean (1986); Rosen and Vajda (1982).

7.3.5 Planform sensitivity analysis, mean wave direction oblique to the shoreline

The morphological response to an offshore breakwater where the annual littoral drift is non-zero is composed of two parts namely formation of a salient in the shadow zone behind the breakwater and turning of the far-field shoreline as shown previously in figure 7.7. The combination of the salient formation and the turning of the far-field shoreline makes it difficult to define the characteristics of the salient itself as was done in the previous section. The cross-shore and longshore position of the shoreline extremes (see lower left panel in figure 7.11) are therefore used to quantify salient changes to varying wave angle incidence and domain length. The results are based on a 110 m long offshore breakwater located 380 m from the initial shoreline with offshore wave conditions $H_s = 1.5$ m, $T_p = 8$ s, $\sigma_w = 19$ deg.

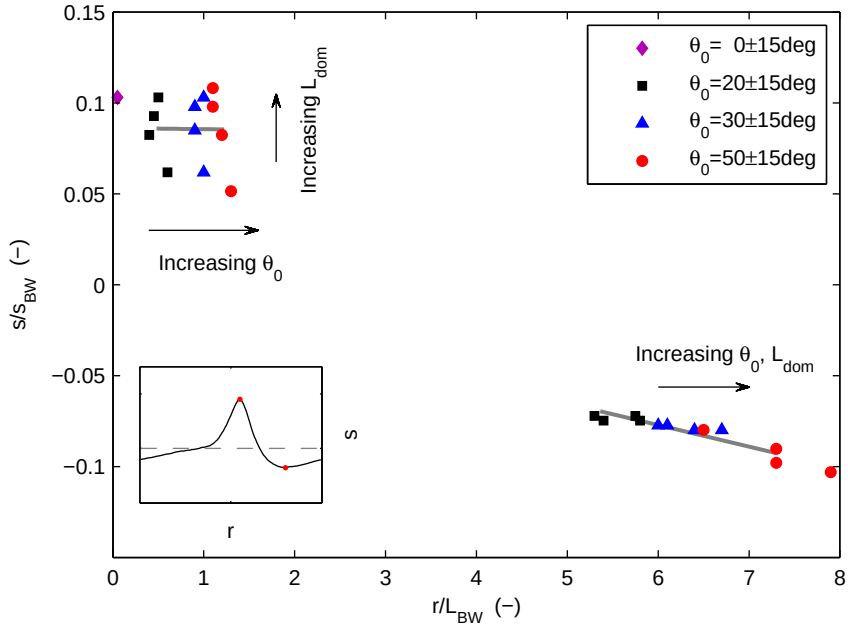

Figure 7.11: *Simulated extremes of equilibrium berm position for varying wave incidence and domain length. The thick grey curves are trend lines for increasing wave incidence.*

Figure 7.11 shows that increasing the angle of wave incidence causes: 1) downstream movement of the salient and 2) increase in salient width (when using the alongshore distance between two shoreline extremes as a measure of the salient width). These effects are illustrated by the two trend lines which are calculated using least squares fit of parametrisations of the shoreline extremes, i.e. $r = r(\theta)$ and $s = s(\theta)$. Each of the trend lines vary from $\theta_0 = 20 \pm 15$ deg to $\theta_0 = 50 \pm 15$ deg. The impact of the domain length of the position of the shoreline extremes may not directly be identified in the figure. The cross-shore position of the maximum salient advance varies however with the domain length as shown by the arrows in the figure. The results indicate therefore that the salient amplitude effectively increases as the domain length increases.

Figure 7.12 shows the equilibrium transport relative to the undisturbed transport as function of the ratio domain length over breakwater length. The figure shows that the morphological model predicts a decrease in the equilibrium transport as the domain length increases relative to the

breakwater length, i.e.

$$\frac{Q_{\text{eq}}}{Q_0} = 1 - \exp\left(-0.6\left(\frac{L_{\text{dom}}}{L_{\text{BW}}} - 1\right)^{0.4}\right) \tag{7.5}$$

The decrease in equilibrium littoral drift updrift and downdrift of the breakwater is obtained by changing the orientation of the far-field shoreline as is the case in traditional one-line models while transport in the shadow zone depends on the salient characteristics. The results from figures 7.11 and 7.12 indicate therefore that an increase in domain length will decrease the turning of the far-field shoreline and increase the salient amplitude.

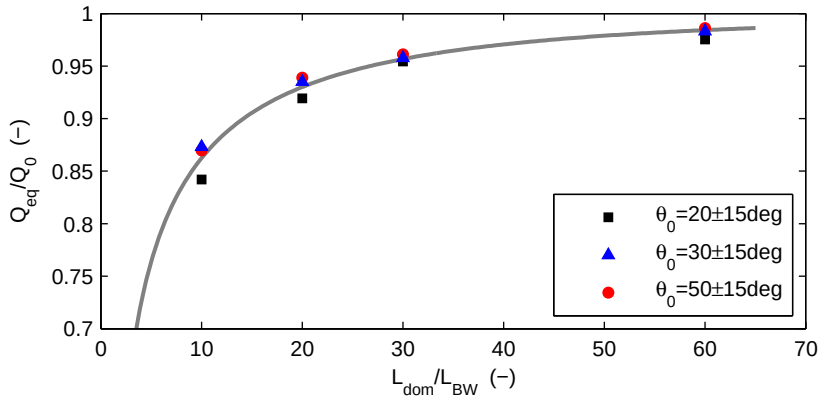

Figure 7.12: *Calculated reduction in littoral drift as function of the breakwater length to domain length ratio. Increasing the domain length reduces the relative impact of the breakwater on the littoral drift.*

7.3.6 Prospects for the 1D hybrid morphological model

The simplicity and robustness of the 1D hybrid morphological model makes it an interesting engineering tool for predicting shoreline response to offshore breakwaters. The model is capable of obtaining equilibrium conditions where gradients in the littoral drift are negligible in a periodic domain both for an average littoral drift close to zero and a non-zero average littoral drift. The model can be adapted to real cases as is shown in the case study from South Africa and in the case study presented in Drønen et al. (2011). It can be used with a fairly high confidence to predict morphological evolution behind offshore structures because it uses a detailed 2D coastal model for calculating the sediment transport. Simulation of morphological evolution around coastal breakwaters i.e. structures located inside or near the surf zone, Mangor (2004) is however not advisable with the model since gradients in the longshore transport landward and seaward of the structure in this case will be different. Handling morphological evolution around coastal breakwaters requires therefore an increase in the number of degrees of freedom of the coastal profile.

7.4 Coastal breakwater - 1.5D morphological model

7.4.1 Numerical model

Profile evolution caused by 2DH circulation is included in the morphological model used for coastal breakwaters by introducing a number of points along the profile. The points are joined by linear segments and can be moved vertically in order to reflect erosion or deposition in the profile as

indicated by the vectors in figure 7.13. The position of the points defines thus the coastal profile and will henceforth be the profile parameters. We will define this morphological concept as a 1.5D model.

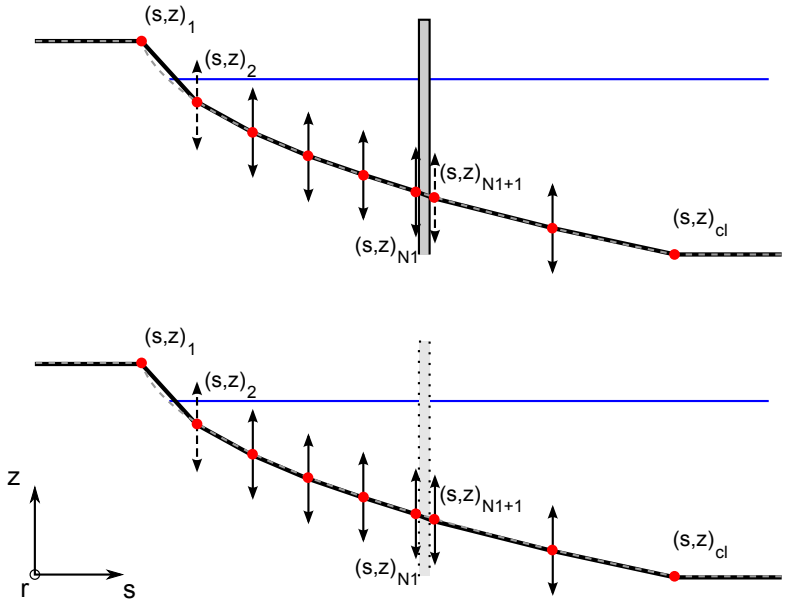

Figure 7.13: *The coastal profile used in simulations with the 1.5D morphological model is defined by a number of points joined by linear segments. Profile evolution is carried out by allowing vertical freedom of the points. Dashed vectors indicate bound parameters see appendix 7.A for details.*

The actual updating of the profile parameters is done using non-linear numerical optimisation of the parameters such that the evolution of the profile has the best fit to the erosion/deposition field predicted by the 2D coastal model. Volume conservation is ensured during the optimisation based on gradient in the littoral drift. Appendix 7.A gives a brief description of the principles behind the optimisation and the method for ensuring volume conservation.

Changing the number of points on the coastal profile will modify the morphological response of the model. Figure 7.14 shows snapshots of simulated bathymetries for a varying value of N_1 (number of coastal parameters landward of the breakwater) after roughly 4 months of morphological evolution. Offshore wave conditions are $H_s = 1.5$ m, $T_p = 8$ s and $\theta_0 = 50 \pm 15$ deg. The simulated bathymetries show some common characteristics i.e. deposition of sediment at the shoreline in the shadow zone forming a salient, deposition of sediment thus forming a plateau on the landward side of the breakwater, general erosion in the deeper part of the coastal profile downdrift of the breakwater and seaward deflection of the bed contours updrift of the breakwater. Use of a few degrees of freedom causes the model to distribute erosion/deposition over larger sections of the coastal profile acting as a cross-shore filter but also in some cases leading to arbitrary results (e.g. formation of a bar downstream of the breakwater for $N_1 < 10$). More importantly the shape of the salient changes for low values of N_1 with the salient being most pronounced for large values of N_1. Comparing the alongshore variation of the profile volume shows however that the erosion/deposition are similar regardless of the value of N_1, see figure 7.15. The 2D model differs somewhat from the 1.5D results, but this is attributed to the lack in morphological activity above mean sea level.

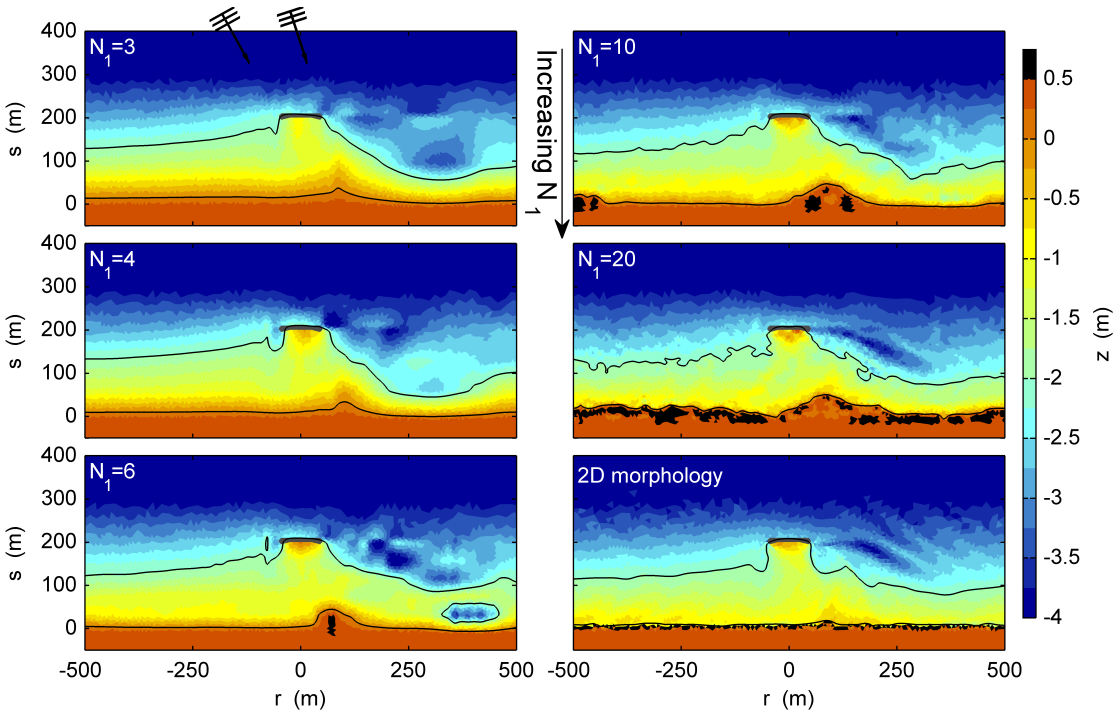

Figure 7.14: *Close-up of the morphological response predicted behind a 100 m long breakwater located 200m from the shoreline after approximately 4 months of wave incidence for different degrees of freedom. N_1 is the number of points landward of the breakwater. The computational domain is 2000 m long and periodic.*

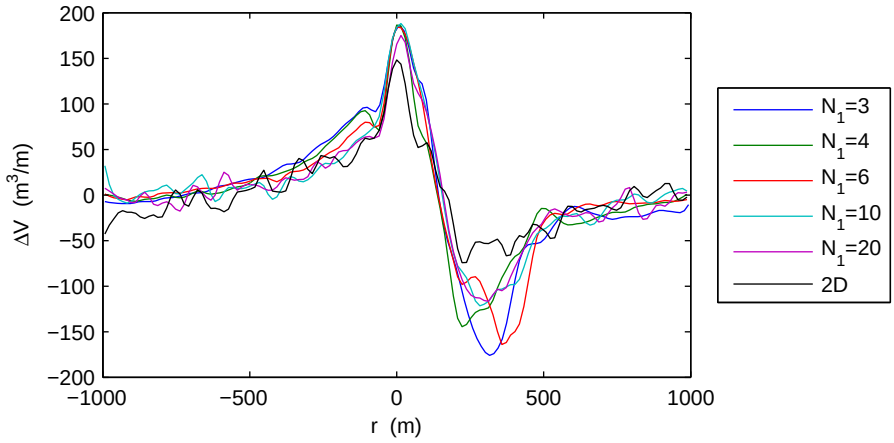

Figure 7.15: *Alongshore variation of the change in profile volume after 4 months of simulation for the cases shown in figure 7.14.*

Cross-shore redistribution of sediment

General degeneration of the coastal profile occurs for all the cases shown in figure 7.14. The degeneration of the profile is caused both by numerical errors which accumulate over time and due to the fact that cross-shore processes which can otherwise maintain the form of the profile are not resolved

by the model. Including cross-shore processes (Q3D) in the model is not expected to improve the representation of the profile. Long-term profile simulations require extensive calibration of a model for the specific location and wave forcing being treated as discussed in Roelvink and Reniers (2011). The calibration may be done in a 1D profile model while it is hardly possible for a Q3D model. The coastal profile is instead maintained by adding a cross-shore diffusion of the deviation from the equilibrium profile after each morphological time step similar to that used by van den Berg et al. (2011); Falqués et al. (2000). The cross-shore diffusion represents non-resolved cross-shore processes and acts as a practical remedy for maintaining the coastal profile. The cross-shore transport is defined such that it will be directed offshore in areas where the local profile slope is steeper than the corresponding local equilibrium slope and vice versa.

$$q_{\mathrm{crs}} = K \frac{q_{\mathrm{l}}}{\sin\theta} \frac{\alpha - \alpha_{\mathrm{eq}}}{\alpha_{\mathrm{eq}}} \tag{7.6}$$

K is a positive dimensionless cross-shore diffusion coefficient. q_{l} is the undisturbed littoral transport ($\mathrm{m}^3/\mathrm{s/m}$) and θ is the angle between the incident waves and the shoreline normal at breaking (in practice the wave angle on the offshore domain boundary). The cross-shore transport magnitude is represented as the littoral drift divided by $\sin\theta$ because the cross-shore transport should be more or less independent on θ whereas the littoral drift is not. The terms in the second fraction represent the relative deviation of the cross-shore bed level gradient from of the equilibrium bed level gradient.

Gradients in the cross-shore transport are used to update the vertical position of the central points $(z_j, j = 2, \ldots, cl-1)$ and the horizontal position of the outermost profile parameters, s_1 and s_{cl}. The morphological update is performed by solving a system of linear and non-linear equations as described in Appendix 7.B.

The morphological update used in the 1.5D hybrid model is thus composed of two steps. The first step uses non-linear optimisation to update the coastal profile in accordance with changes predicted by the 2D coastal model. The second step is composed of a redistribution of sediment based on solving a diffusion problem which will force the profile towards the form of an equilibrium profile.

Effect of cross-shore diffusion coefficient

The cross-shore diffusion coefficient, K is in this study chosen to be constant along the shore. K should be small enough to allow 2D circulation currents to modify the coastal profiles while it should be large enough to maintain the cross-shore profile at some distance away from the breakwater. Figure 7.16 shows simulated bathymetries for varying values of K for $N_1 = 6$. The top left panel shows a comparative result obtained with the 1D morphological model. The figure shows that increasing K will increase the shoreline response and will reduce the local deposition on the landward side of the breakwater. The shoreline response will for a large diffusion coefficient be greater than the shoreline response obtained with the 1D morphological model because the closure depth effectively is reduced for profiles intersecting the breakwater and because areas of erosion/deposition are located at different alongshore coordinates landward and seaward of the breakwater.

Simulations where the morphological time step is varied for a strong $(K = 1)$ and a weak $\left(K = 10^{-2}\right)$ cross-shore diffusion show that the maximum morphological time step for a stable result increases with the cross-shore diffusion coefficient. This is consistent with the observations related to the

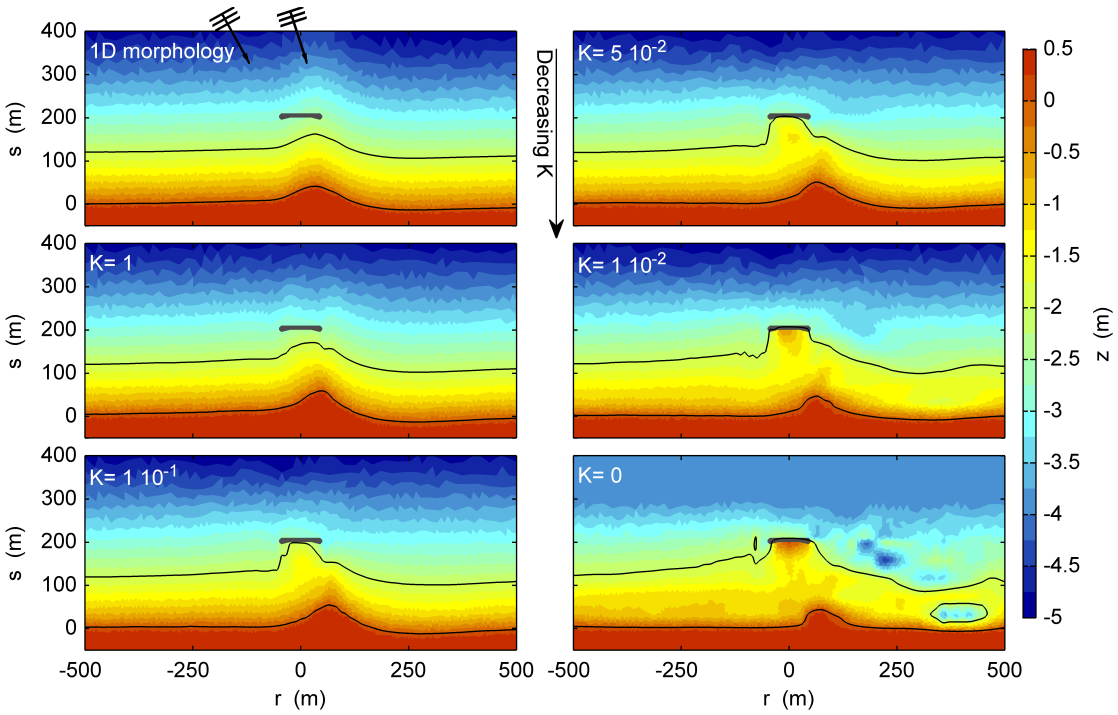

Figure 7.16: *Close-up of the morphological response predicted behind a 100 m long breakwater located 200 m from the initial shoreline after approximately 4 months of wave incidence for different values of cross-shore diffusion, K. $N_1 = 6$. The result is obtained on a 2000 m long periodic domain.*

maximum time step for changes to N_1 because increasing K will suppress formation of local bathymetric features. For the case with $K = 1$ a stable morphological time step of 24 h can be used (which is similar to that used in the 1D morphological model) while the morphological time step needs to be reduced to 6 h for $K = 10^{-2}$ with an alongshore discretisation, $\Delta r = 10$ m.

7.4.2 Morphological response to a coastal breakwater

Similar to an offshore breakwater a coastal breakwater causes deposition updrift of the structure and in the shadow zone while erosion occurs in the area downdrift the structure. The far-field areas will behave similarly to that which is seen in the offshore breakwater i.e. the bed contours turn against the incoming waves. The area of accretion in the shadow zone will however differ slightly and it is convenient to divide it into a part close to the shoreline (the salient) and a part further seaward (the plateau). Salient formation occurs in response to wave diffraction and refraction as discussed in e.g. Rosen and Vajda (1982), while deposition in the plateau occurs because the sudden decrease in wave height going from an undisturbed profile to a profile in the shadow zone reduces the sediment transport capacity. Deposition of sediment in the plateau stops at some point because the water depth has decreased to a value for which sediment transport resumes. Tombolo formation is determined from the interaction between accumulation in the salient area and the plateau area.

The 1.5D hybrid morphological model is used to illustrate how deposition in the two areas in the shadow zone are affected by varying breakwater configuration λ, varying wave angle incidence θ_0

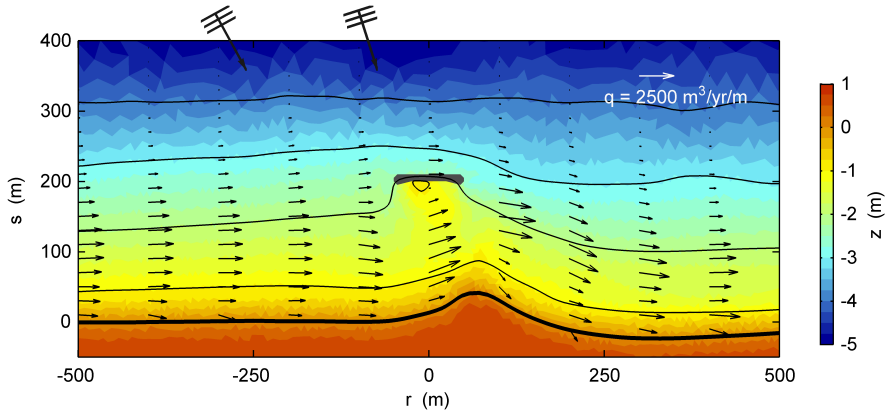

Figure 7.17: *Close-up of the equilibrium bathymetry for a 100 m long breakwater located 200 m from the initial shoreline subject to waves from* $\theta_0 = 50 \pm 15$ deg.

and for varying distance to the shoreline relative to the surf zone width. Offshore wave conditions with $H_s = 1.5$ m, $T_p = 8$ s and $\sigma_w = 19$ deg are used. The simulations are performed on a Dean type coastal profile with the profile parameter $A = 0.095$ and $m = 0.67$ corresponding to an average slope of 1/77 and with 0.20 mm sediment. A fairly weak cross-shore diffusion coefficient $K = 2{\cdot}10^{-2}$ is used. The morphological response to the breakwaters is simulated in a periodic domain with a domain length of 2000 m. The alongshore discretisation of the morphological model is 10-15 m and a total number of $cl = 10$ points is used to define the coastal profile. A morphological time step of 6 h is used in the simulations. All simulations start with an initially straight shoreline.

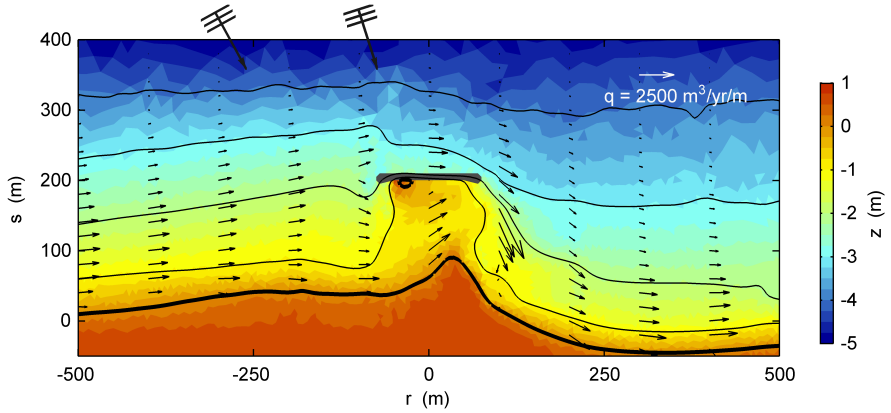

Figure 7.18: *150 m long breakwater located 200 m from the initial shoreline subject to waves from* $\theta_0 = 50 \pm 15$ deg. *The shoreline advance increases and the water depth on the plateau decreases compared to the 100 m long breakwater.*

Breakwater dimensions

Simulated equilibrium bathymetries are shown for two different breakwaters with $\lambda = 0.5$ in figure 7.17 and $\lambda = 0.75$ in figure 7.18. The wave angle incidence is $\theta_0 = 50 \pm 15$ deg in both cases and both cases result in formation of a salient. Comparing the two cases shows that the salient is more pronounced and that the water depth in the plateau is lower for the long breakwater. The shallow water depth in the plateau is controlled by the decreased wave activity in the shadow area and by

the fact that breaking waves on the undisturbed upstream profiles continue to drive a flux of water through the shadow zone thus inhibiting further deposition.

Angle of wave incidence

Decreasing the angle of wave incidence for the breakwater shown in figure 7.18, results in tombolo formation, as shown in figure 7.19. The tombolo formation occurs because the salient is located further upstream, thus making it easier to close the gap between the salient and the breakwater and because the forcing from the breaking waves on the neighbouring profiles decreases thereby allowing an even smaller water depth on the plateau. The transition from salient to tombolo occurs suddenly after a long period with a slow monotonic salient growth and a gradual decrease in water depth in the plateau area.

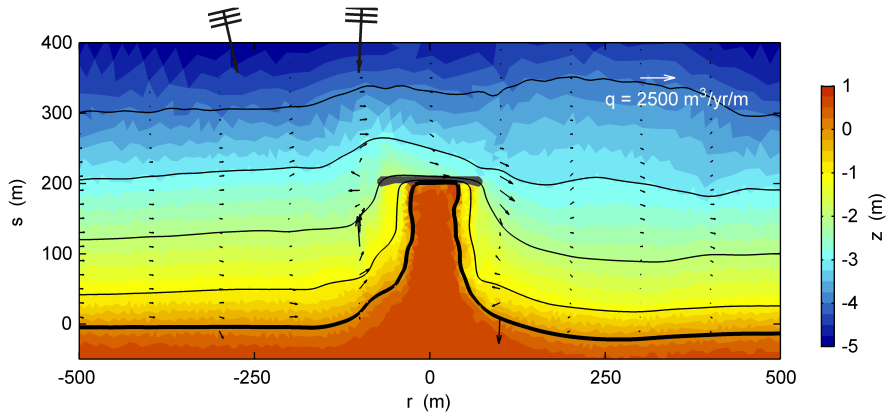

Figure 7.19: *150 m long breakwater located 200 m from the initial shoreline subject to waves from* $\theta_0 = 10 \pm 15\,\text{deg}$. *A tombolo forms because the salient merges with the plateau. Bypass of sediment starts to occur after the model has decreased the water depth seaward of the breakwater.*

Breakwater position relative to surf zone width

The cross-shore position of the breakwater relative to the surf zone width is according to Mangor (2004); Suh and Dalrymple (1987) important for the possibility of tombolo formation. Tombolo formation is apparently favoured for breakwaters located inside the surf zone. The mechanism behind this may be linked to the interaction between the two depositional areas; the salient and the plateau. A breakwater located inside the surf zone causes deposition in the plateau area while a breakwater located outside the surf zone primarily causes deposition in the salient due to changes in recovery of wave height. This may be further enhanced by the flux of water being more prone to bypass on the seaward side of the breakwater for a breakwater located inside the surf zone. Additionally, the ratio between the breakwater distance and the surf zone width seems to change the degree of turning of the far-field bed contours. Figure 7.20 shows the simulated equilibrium bathymetry for a breakwater with $\lambda = 0.75$ subject to waves with $\theta_0 = 50 \pm 15\,\text{deg}$. Comparing this result with that obtained in figure 7.18 (same λ and θ_0) shows that the depth contours are not turned as much for the breakwater located well inside the surf zone. This is in accordance with the observations from the 1D hybrid morphological model, where the degree of turning of the far-field shoreline is determined by the relative impact of the breakwater on the littoral drift.

Shoreline equilibrium after tombolo formation

The rate of downdrift shoreline retreat increases after a tombolo is formed regardless of the amount of bypass because bypassed sediment returns to the shoreline at some distance downstream of the

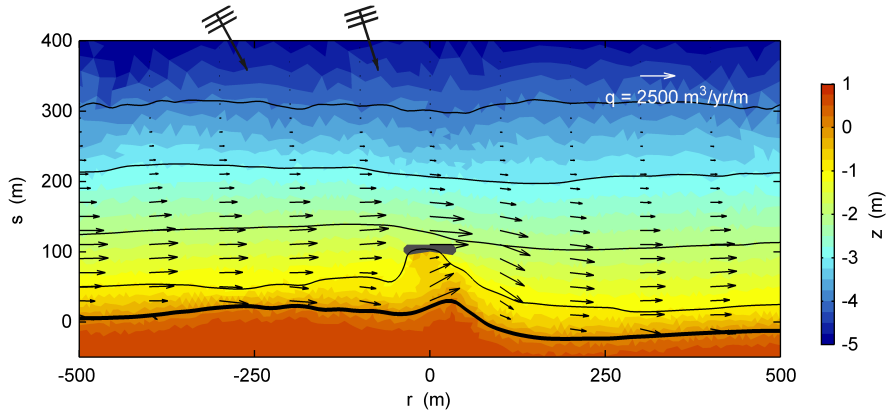

Figure 7.20: *75 m long breakwater located 100 m from the shoreline subject to waves from* $\theta_0 = 50 \pm 15\,\text{deg}$. *The depth contours seaward of the breakwater are mildly affected. The shoreline itself is only turned mildly against the waves due to the relative small impact of the breakwater on the littoral drift.*

breakwater while recovery of the littoral drift close to the shoreline starts earlier. Figure 7.21 shows a simulated bathymetry for a 100 m long breakwater located 100 m from the initial shoreline where a tombolo has formed and strong lee side erosion has forced the shoreline to retreat roughly 50 m. The tombolo is according to the morphological model stable despite the strong lee side erosion because the high angle of wave incidence creates a large calm area along the downstream side of the tombolo.

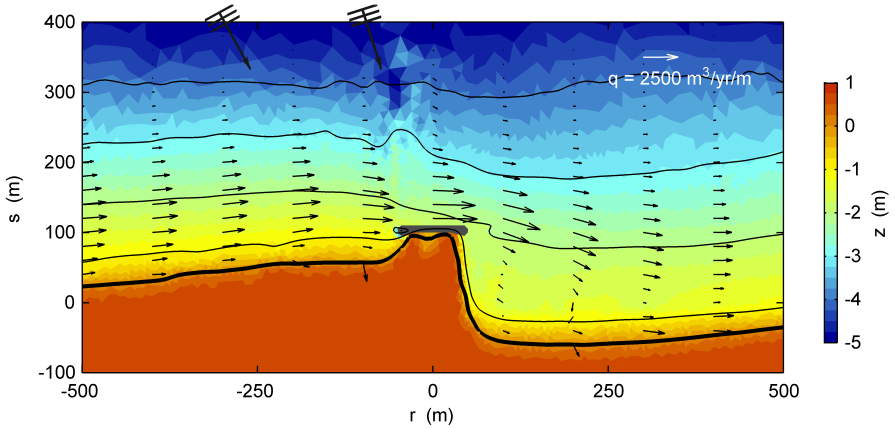

Figure 7.21: *100 m long breakwater located 100 m from the initial shoreline with an offshore wave angle incidence of* $\theta_0 = 50 \pm 15\,\text{deg}$

Equilibrium planform behind coastal breakwater

Simulated salient advance behind coastal breakwaters performed with the 1.5D hybrid morphological model are shown in figure 7.22. The results agree reasonably with laboratory results obtained by Rosen and Vajda (1982) and field observations of Nir (1976) which are also shown in the figure.

The simulations show that λ is the governing parameter controlling tombolo formation, although the wave incidence is also important and that the 1.5D morphological model generally predicts

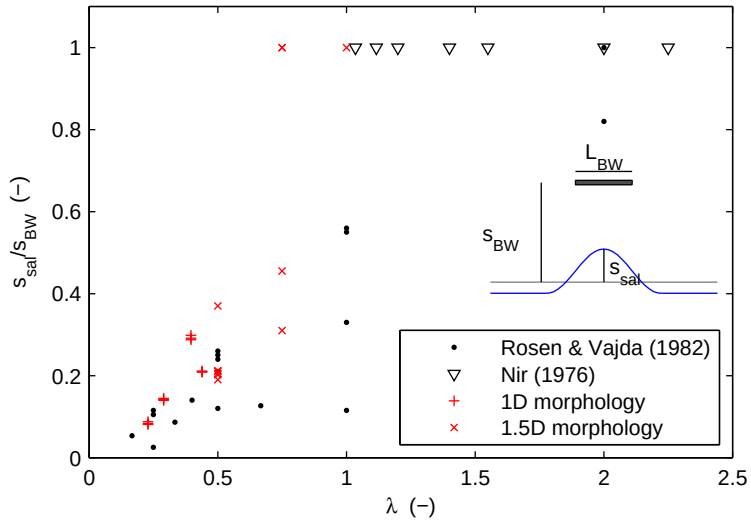

Figure 7.22: *Comparison of simulated salient advance with laboratory results of Rosen and Vajda (1982) and the field data of Nir (1976).*

salient formation for $\lambda \geq 0.75$. Existing rules predict tombolo formation for $\lambda \geq 1$, Mangor (2004) although the exact limits are subject to a large degree of uncertainty as illustrated in Axe et al. (1996) where it is observed that the onset of tombolo formation previously has been reported for λ between 0.67 and 2.5 while salient formation begins for λ between 0.5 and 1.5.

7.5 Discussion

The main motivation of the hybrid modelling approach is linked to an increase in computational efficiency of coastal morphological modelling and to a reduction of profile degeneration when simulating morphological evolution over long time scales. The 1D hybrid morphological model fulfils these goals by reducing the degree of freedom of the coastal profile to a single parameter, while the 1.5D model restrains the added freedom to the coastal profile by use of a simple cross-shore transport formulation.

The 1.5D hybrid morphological model allows a smooth transition from a 1D to a 2D morphological model thus illustrating changes in the properties of the morphological model as the degree of freedom is changed. In this study it is found that increasing the degree of freedom of the morphological model improves the ability of the model to represent local erosion/deposition features thus making the morphological features more pronounced. Decreasing the freedom of the model will conversely cause the model to distribute erosion/deposition according to the restrictions imposed on the coastal profile rather than due to the erosion/deposition field predicted by the detailed 2D coastal model. Increasing the cross-shore diffusion causes erosion/deposition to occur more uniformly over the profile which effectively increases the maximum allowed time step for a stable model because formation of small perturbations is restricted.

In order for the 1.5D hybrid morphological model to be an interesting engineering tool it must be both robust, reliable and CPU efficient. A compromise between each of the three desirable

attributes is obtained by changing the degrees of freedom and the stabilisation of the model. The implemented cross-shore diffusion represents stabilisation of the model and has been chosen such that it is a function of the instantaneous littoral drift and an inverse function of the angle between waves and shoreline normal at breaking. This formulation is used in an attempt to obtain a stabilisation mechanism where a single parameter can be used regardless of the flux of energy approaching the shoreline. For the cases in the present study it seems that the diffusion coefficient $K = 0.02$ can be used in order to obtain reasonable values.

A quasi-steady state of the hydrodynamics (waves and currents) is simulated for each sea-state and the morphological evolution due to the sea-state is applied to the model instantly before starting simulation of a new sea-state. The computational efficiency of the model is obtained because the morphological time step is significantly larger than the time scale in which quasi-steady hydrodynamic conditions develop. The ratio between the morphological time step and the time scale for quasi-steady conditions to develop can be compared with the morphological speed-up factor known from traditional 2D models. For the cases presented in this study the hybrid model can use morphological speed-up factors ranging from 3 (still water conditions used initially) to 72 (hot-start of initial hydrodynamics from most recent similar sea-state, 1D morphology). For morphological simulations of real engineering problems the range of allowable morphological speed-up may vary even more because sea-states with nearly calm conditions may use very large morphological time steps e.g. on the order of weeks, Grunnet et al. (2012); Kristensen et al. (2012). The maximum allowed morphological time step in the 1.5D hybrid morphological model is typically lower than that used in the 1D hybrid morphological model which means that the morphological speed-up of the 1.5D model becomes comparable to that which can be used in traditional 2D models.

Consequently, the 1D hybrid morphological model is an interesting candidate as a future engineering model where 1D and weak 2D morphological response is expected because the model outperforms both the traditional 1D and 2D model in terms of the three desirable attributes of an engineering model. The 1.5D hybrid morphological model performs well but does not outperform traditional 2D models in terms of computational efficiency. It is however our opinion that the cross-shore diffusion improves the ability of the 1.5D hybrid morphological model to maintain the cross-shore profile and therefore improves the model's applicability to long-term morphological simulations compared to traditional 2D models.

7.6 Conclusion

The results of morphological evolution presented here are obtained by use of a hybrid modelling concept where a deterministic 2D sediment transport model is combined with a simplified morphological scheme. The case study from South Africa and the application of the model concept presented in Drønen et al. (2011) show that the hybrid model has reasonable predictive capabilities in terms of development of salient characteristics. The robustness of the model concept where a constant profile is assumed (1D morphology) allows it to be applied to real engineering problems using relatively simple schematised wave climates because processes which maintain the cross-shore profile are not required to be resolved.

The results from the study of breakwater length and distance to shoreline obtained with the 1D

hybrid morphological model indicate that the breakwater length to distance ratio, λ is an important descriptive parameter for the equilibrium planform. An increase in λ (e.g. increase in breakwater length) will increase the aspect ratio of the salient thus increasing the amplitude of the equilibrium planform. On shorelines with a non-zero annual drift, the salient moves downdrift when the angle of wave incidence increases and the far-field shoreline turns against the incident waves. The degree of turning of the far-field shoreline depends both on the angle of wave incidence and on the relative impact of the breakwater on the forces driving the littoral drift.

Simulations with coastal breakwaters show that the 1.5D hybrid model may distinguish between the type of planform which develops and that the resulting planform is governed by the breakwater length to distance ratio. Oblique wave incidence may alter the resulting planform type primarily because the salient is moved further downdrift thus making it more difficult to close the gap between the salient and the breakwater.

Acknowledgements

The authors would like to thank Eng. Stephen Luger for raising our attention to the salient formation behind the Seli 1 at Cape Town, South Africa and for supplying the information needed to calculate the morphological response behind the wreck. The first author has been supported by a grant from the Danish Agency for Science Technology and Innovation. This work has been partly supported by the Danish Council for Strategic Research (DSF) under the project: Danish Coasts and Climate Adaptation - flooding risk and coastal protection (COADAPT), project no. 09-066869.

7.A Optimisation of coastal parameters in the 1.5D morphological model

The coastal parameters used to define the coastal profile are optimised by use of a non-linear optimiser such that the imposed morphological change gives the best fit to the discrete change calculated by the detailed 2D sediment transport model. The principle is illustrated in figure 7.23 in which the profile for simplicity is defined by two parameters which are allowed freedom along the horizontal axis. The figure illustrates how the parametric profile (black curve) is optimised such that it matches the discrete update to the profile predicted by the 2D model (black points).

The optimisation is performed using the *Nelder-Mead algorithm*, a non-linear method that uses a set of basic operations to search an n-dimensional space for a minimum value, see Lagarias et al. (1999). The optimisation method may formally be written as:

$$\psi_j^{k+1} = \text{argmin}\left(\varepsilon\left\{\psi_j^k,\, \psi_j^{k+1},\, \frac{\partial z}{\partial t}\Delta t\right\}\right) \tag{7.7}$$

where ψ_j^k is a vector containing the coastal parameters of the jth profile at time step k. $\partial z/\partial t$ is the rate of bed level change calculated by the 2D coastal model and Δt is the morphological time step. ε is the area weighted rms-difference between the future parametric coastal profile and the profile obtained with the erosion/deposition field simulated by the 2D coastal model. The profile optimisation is performed using the rate of bed level change signal from 2D mesh elements which

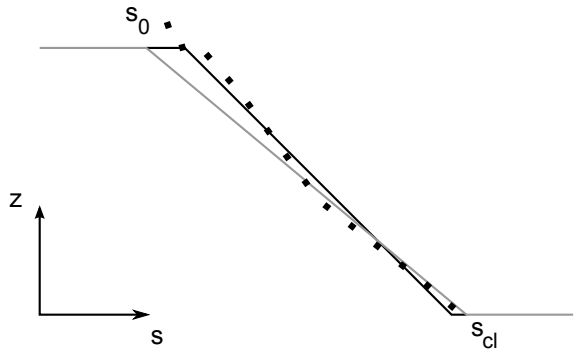

Figure 7.23: *Morphological evolution is performed by evolving the coastal parameters by use of a non-linear optimiser. The optimal solution is the solution where the difference between the signal from the 2D coastal model (points) and the signal from the parametric model (black curve) is minimal.*

are located within a morphological section.

Volume conservation is included by reducing the size of ψ and determining the last parameters so that the total volume change in the profile is equal to divergence of the sediment flux over the faces of a morphological section. The parameters used for obtaining volume conservation are denoted bound parameters, $\hat{\psi}$.

Typically a profile will have only one bound parameter, but the conservation of volume may be imposed in several sections of the profile, for example, distinguishing between the part of the profile landward of the breakwater and the part of the profile seaward of it. Introduction of bound parameters ensures that the non-linear optimisation method only evaluates sets of profile parameters where volume conservation is fulfilled. This principle is illustrated in figure 7.24 where a profile described by two parameters, s_0 and s_{cl} will have one free parameter $\psi = s_0$ and the bound parameter $\hat{\psi} = s_{\mathrm{cl}}$. The solutions that fulfil a specific volume will in this case be given by a straight line in the (s_0, s_{cl})-space. The optimal solution will then be the solution along the bold curve which has the lowest error where the error, ϵ is indicated by the thin contour lines. The figure illustrates that the set of parameters which gives the smallest error is not necessarily the same set which fulfils volume conservation.

7.B Adding a cross-shore diffusion towards the equilibrium profile

A cross-shore transport is defined in order to maintain the coastal profile by forcing it towards an equilibrium profile. The cross-shore transport is defined on a grid as indicated in figure 7.25. The transport is defined as zero at the landward and seaward boundaries of the profile and at the interface located inside the breakwater. The cross-shore position s_1 and s_{cl} are made free to accommodate for erosion/deposition in the outermost profile sections thereby incorporating a method for updating the shoreline position in time.

The profile evolution is implemented by setting up a system of equations for the profile volumes V_1 to V_{cl}, e.g. the volume in the central part of the profile may be determined as:

$$V_j = \frac{1}{8}\left(s_j - s_{j-1}\right)\left(z_{j-1} + 3z_j - 4z_{\mathrm{cl}}\right) + \frac{1}{8}\left(s_{j+1} - s_j\right)\left(z_{j+1} + 3z_j - 4z_{\mathrm{cl}}\right) \tag{7.8}$$

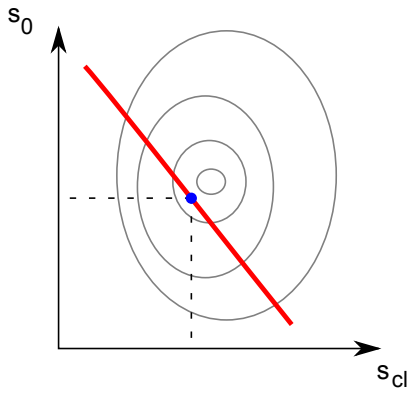

Figure 7.24: *Illustration of parameter space for a profile like the one shown in figure 7.23. Optimisation is only performed for parameter sets which fulfil local continuity (bold curve). The optimal solution is the solution on the bold curve which gives the lowest value of ϵ (thin curves are iso-lines of ϵ)*

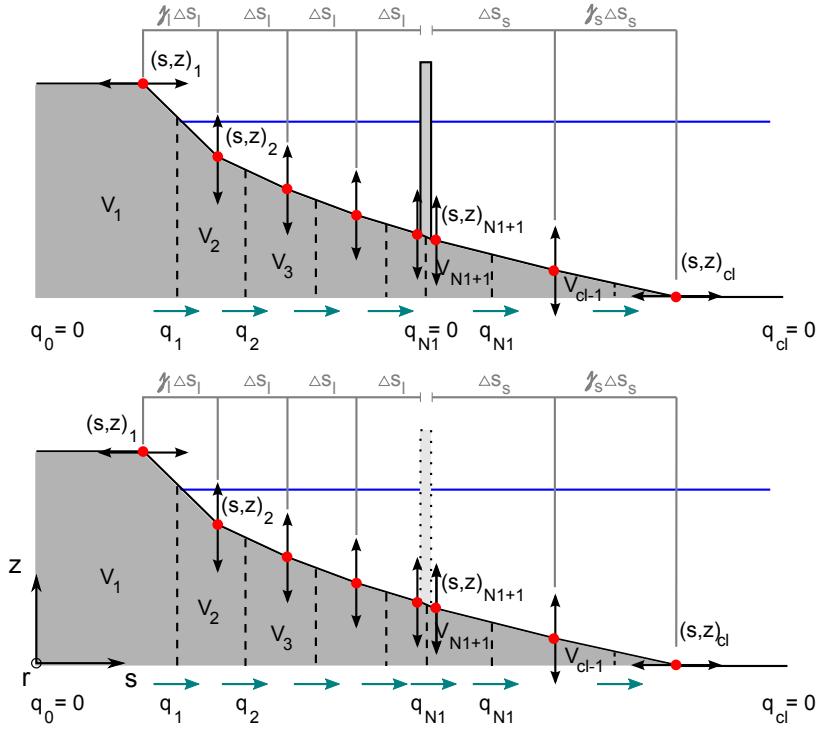

Figure 7.25: *The cross-shore transport is defined on a staggered grid in order to force the profile towards the equilibrium profile by diffusion. The cross-shore transport is defined zero at interfaces located inside the breakwater and at the landward and seaward boundaries.*

Each of the equations are differentiated with respect to time resulting in a system of linear ($j = 3, \ldots, \mathrm{cl}-2$) and non-linear ($j = 1, 2, \mathrm{cl}-1, \mathrm{cl}$) equations on the form:

$$\frac{\mathrm{d}}{\mathrm{d}t}\bar{V} = \bar{\bar{A}}\frac{\mathrm{d}}{\mathrm{d}t}\bar{\psi} \tag{7.9}$$

where the left-hand side is the vector of volume change determined as the divergence of the cross-shore transport along the coastal profile and $\bar{\psi} = [s_1, z_2, z_3, \ldots, z_{\mathrm{cl}-1}, s_{\mathrm{cl}}]^T$ are the free parameters.

Time integration of is performed using an explicit Euler scheme.

Large shoreline changes and changes to the cross-shore position of the closure point are handled using an equidistant redistribution of the otherwise fixed profile parameters, thus limiting γ_l and γ_s (see figure 7.25) within a specified interval.

Chapter 8

Hybrid Morphological Modelling of Shoreline Response to a Groyne Field

Unpublished, intended as journal paper in Coastal Engineering 2013, in a reduced form.
Authors: Sten Esbjørn Kristensen[1], Nils Drønen[2], Rolf Deigaard[2], Jørgen Fredsoe[1].
Citation: Kristensen et al. (2013b)

Abstract

The 1.5D hybrid morphological model presented in Kristensen et al. (2013a) is used to simulate morphological response to groyne fields with impermeable groynes. The model combines a 2D coastal model (MIKE21 FM), to calculate a 2D sediment transport field, with a simplified scheme for the morphological update.

The 1.5D hybrid morphological model is used to study the principal response to changes in groyne dimensions (length, spacing, orientation and shape) and wave climate (wave height, direction and period). This analysis shows that groyne length and surf zone width (governed by wave height) significantly affect the morphological response with the largest re-orientation of bed contours occurring for groynes which block the littoral drift completely and for large angles of wave incidence.

Finally it is proposed that initial design of groyne fields may be based on a combination of the two dimensionless quantities: groyne spacing over groyne length and the (initial) relative geometric bypass transport, in order to obtained a specific relative reduction in littoral drift. The relative geometric bypass transport is determined as the part of the undisturbed littoral drift located seaward of the groyne tip divided by the total undisturbed littoral drift.

Keywords: Hybrid morphological model, Groyne field, Shoreline modelling, Initial design

8.1 Introduction

Groynes are structures normal to the shoreline which block the littoral drift partially or completely. The structures are typically used as part of a coastal management strategy in order to maintain the

[1]Department of Mechanical Engineering, Technical University of Denmark, DK-2800 Kgs. Lyngby, Denmark
[2]DHI, Agern Allé 5, DK-2970 Hørsholm, Denmark

beach on which they are constructed or to manage the magnitude of the littoral drift. In modern beach management strategies, single groynes may be constructed as headlands in order to create smaller littoral cells in the groyne compartments in which the beach may turn against the locally prevailing wave direction, Mangor et al. (2008) or as terminal structures which limit the amount of sediment deposited in tidal inlets and navigation channels Basco and Pope (2004); Grunnet et al. (2009).

Groyne fields are traditionally constructed on shorelines with a significant annual littoral drift (relative to the gross transport) where a reduction in the littoral drift is desired, or as short closely spaced constructions which fix the beach position, CEM (2002a). Construction of groyne fields may be combined with nourishment schemes in order to minimize downdrift erosion during the transient and long term response of the shoreline Kraus et al. (1994); Mangor (2004).

Modern design guidelines for groyne fields recommend that the groynes should only act as a template for the subaerial beach (fixing the shoreline locally) while providing unrestricted bypass, Basco and Pope (2004); CEM (2002a). This should be obtained by use of permeable groynes with a limited length and an alongshore spacing of $L_{\text{space}}/L_{\text{g}} = 2 - 4$. Here L_{space} is the alongshore spacing of the groynes and L_{g} is the groyne length measured from the design shoreline to the groyne tip. The groyne performance should then according to CEM (2002a) be measured in terms of the minimum beach width retained by the groynes and by the amount of bypass.

Formation of rip current along groynes, as reported by Aelbrecht and Denot (1999); Pattiaratchi et al. (2009); Trampenau et al. (2004); Wind and Vreugdenhil (1986), is in the literature often associated with a negative impact on groyne functioning. Formation of the rip current creates an offshore transport of sediment which causes loss of sediment within the groyne compartment and ultimately a reduction in groyne performance. The reduced groyne performance is reported for long groynes due to offshore loss of sediment, Kraus et al. (1994). Hanson and Larson (2004) argue that offshore loss of sediment may be enhanced if the time scale of the shoreline response inside a groyne compartment is long compared to the time scale of the changes in transport direction because the strength of the rip current increases when waves approach the shoreline at an oblique angle.

Reduced effectiveness is also reported for short groynes, because the upstream rip current not only diverts sediment offshore but also causes local erosion while located inside the surf zone, a process which is described in Deigaard et al. (1999) for rip-currents in breaker bars. The rip current upstream of short groynes reduces the re-orientation of bed contours as reported in numerical studies, Johnson (2004); Walker et al. (1991) and in experimental studies, Badiei et al. (1994); Hulsbergen et al. (1976). Johnson (2004) speculates therefore that rough wave conditions may lead to upstream erosion while the usual picture of updrift accretion and downdrift erosion is obtained during mild wave conditions.

8.1.1 Present study

The present study concerns modelling of the morphological response to impermeable groynes. The article includes an initial sensitivity study in which wave height, period and angle of incidence are varied along with groyne length, alongshore spacing and orientation. The objective of the initial sensitivity study is twofold. 1) It gives an opportunity to understand processes which are important for the morphological evolution around groynes and the effect of changing groyne design. 2) The model behaviour is validated against the expected response.

The results are based on morphological simulations with a so-called 1.5D hybrid morphological model, which is composed of a depth integrated area model for waves, flow and sediment transport and a simplified morphological updating scheme which allows shoreline and profile changes due to 2D circulation created by the presence of impermeable structures.

8.1.2 Hybrid morphological modelling concept

The hybrid morphological modelling concept is used because it uses the detailed description of the littoral drift from a coastal area model, which includes effects such as streamline contraction and development of 2D circulation currents. The simplified morphological scheme allows the model to use large morphological time steps and it reduces degeneration of the coastal profile. As described in Kristensen et al. (2013a), we distinguish between a 1D implementation and a "1.5D" implementation.

The simplest version of the hybrid morphological concept is the 1D morphological shoreline evolution model which is discussed in Kærgaard (2011); Kristensen et al. (2010). Validation of the 1D hybrid morphological model against case studies are given in Drønen et al. (2011); Kærgaard (2011); Kristensen et al. (2012). In all three studies the concept is shown to be robust and reliable for morphological simulations extending over years, decades and centuries. The studies involve evolution of sandy spits due to oblique wave incidence and shoreline evolution behind offshore breakwaters. The robustness of the 1D hybrid concept combined with the fact that the model resolves transient response of the shoreline allows the model to be used as decision support tool for design of coastal management strategies as illustrated in Drønen et al. (2011); Grunnet et al. (2012). A refined version of the hybrid morphological concept is presented in Kristensen et al. (2013a) as the 1.5D hybrid morphological model. The 1.5D hybrid morphological model allows relaxation of the robustness of the morphological model by allowing profile changes to occur due to 2D circulation currents. This allows the model to be applied to cases such as coastal breakwaters. The study Kristensen et al. (2013a), shows that the 1.5D hybrid morphological model may predict the equilibrium planform (salient/tombolo) for varying breakwater dimensions and characteristics of the wave forcing.

In the present study, the 1.5D hybrid morphological model developed in Kristensen et al. (2013a) is used with minor changes to simulate morphological evolution around groynes. This study should therefore apart from discussing morphological processes and effects around groyne fields also investigate application of the 1.5D hybrid morphological model to a larger range of different coastal structures.

8.2 Numerical model

The hybrid morphological model is composed of two overall models: a 2D coastal model (MIKE21 FM) and a morphological module which implements the hybrid concept. Each of the two overall models are treated separately and it should be emphasized that any 2D coastal model can in principle be used within the hybrid morphological modelling framework.

8.2.1 2D coastal model for sediment transport

The 2D coastal modal used for calculating wave, current and sediment transport field uses three modules. The detailed nearshore wave field is calculated by use of the spectral wave module, MIKE21 SW. The hydrodynamic flow module MIKE21 HD is used to calculate surface elevation

and depth integrated currents, which are driven by gradients in radiation stresses computed from the nearshore wave field. The sediment transport is calculated by MIKE21 ST which uses local flow, wave and sediment characteristics to calculate the sediment transport at each computational cell. The model system is solved on a flexible 2D grid which can include both triangular and quadrilateral elements.

The spectral wave module solves the wave action balance equation using a directional decoupled parametric formulation, following Holthuijsen et al. (1989). The wave transformation incorporates effects of energy dissipation due to wave breaking and bottom friction, energy transfer due to depth refraction and diffraction and energy supply due to action of wind. Wave breaking is determined using the dissipation model of Battjes and Janssen (1978). The radiation stress tensor is determined from the integrated energy spectrum and is used to drive the flow.

The hydrodynamic module solves the non-linear shallow water equations, which consist of the local continuity equation and the momentum equation formulated in a Cartesian coordinate system. Bed friction is described by the Manning equation with a Manning number corresponding to a Nikuradse bed roughness of 0.25 m. This rather high bed roughness has been chosen because no model for the increased apparent roughness caused by the combined wave-current boundary layer is included in the flow modelling. Lateral stresses due to viscous friction, turbulent friction and momentum exchange due to organised water motion are included as an eddy viscosity with a constant value of 0.5 m^2/s.

The sediment transport model is a 1DV intra-wave model for sand transport under the combined action of waves and current. It calculates the vertical distribution of the sediment concentration by solving the vertical transport equation, Deigaard et al. (1986b); Fredsoe et al. (1985). The instantaneous bed shear stress is obtained from the Fredsoe (1984) model for turbulent boundary layers in combined waves and current. The near bed concentration used as boundary condition for the suspended sediment calculation is based on the instantaneous Shields parameter, Engelund and Fredsoe (1976). Bed load transport is calculated using the approach of Engelund and Fredsoe (1976). The sediment transport model is used in a relatively simple form; first order Stokes theory is used to describe the oscillatory component of the near bed orbital motion and the sediment transport is taken to be in the mean current direction omitting so-called Q3D effects.

8.2.2 Hybrid morphological model

The morphological model is implemented in a Matlab framework which reads, processes and writes from and to input/output files used by the 2D coastal model. The general concept behind the hybrid morphological model is illustrated in figure 8.1. Basically; morphological changes are imposed on larger sections in this case defined by coastal profiles which extend from the shoreline out to the depth of closure. The alongshore distribution of change in profile volume is calculated as the divergence of the 1D littoral drift which is determined by integration of the sediment transport field calculated by a 2D coastal model along the coastal profiles.

In the 1D hybrid morphological model, changes in profile volume are directly related to a change in shoreline. In the 1.5D hybrid morphological model, local changes to the coastal profile are imposed according to the cross-shore distribution of the erosion/deposition field, while satisfying the change in volume for each coastal profile in accordance with the aforementioned gradient in the littoral

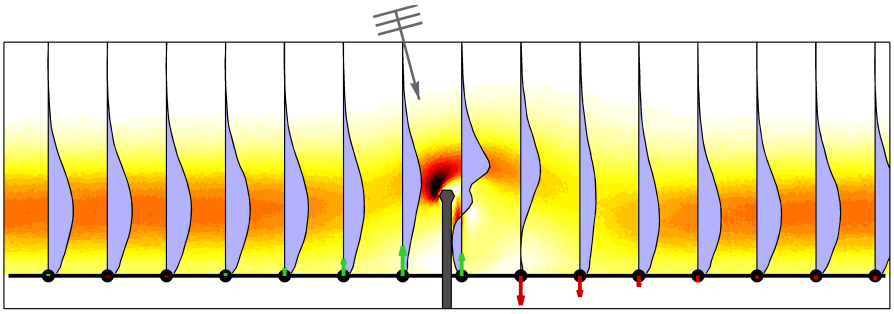

Figure 8.1: *Illustration of the hybrid morphological concept. Morphological change to the 2D bathymetry is based on longshore gradients in the integrated longshore transport. This is illustrated here as changes in shoreline position.*

drift. A brief summary of the 1.5D morphological model is given in the following, details may be found in Kristensen et al. (2013a).

The coastal profile is discretised by a number of points which are connected by linear segments. Morphological evolution is allowed only, by changing the vertical position of the points, as indicated by the vectors in figure 8.2. The morphological evolution uses non-linear optimisation of vertical position of the points, such that a best fit against the spatial distribution predicted by the 2D coastal model is obtained. The freedom of a single point is however bound by continuity thereby ensuring that the non-linear optimisation method only evaluates cases where volume conservation is fulfilled. A simple example of this is given in (Kristensen et al., 2013a, Appendix A). It is shown in Kristensen et al. (2013a) that the morphological evolution obtained with the optimisation method converges towards the solution obtained with a traditional 2D morphological model given a sufficient number of profile parameters.

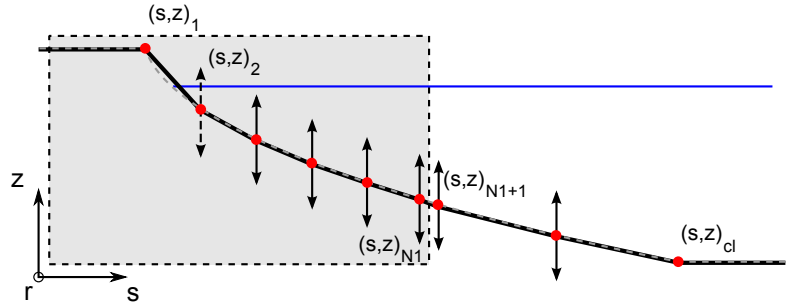

Figure 8.2: *Definition of the coastal profile in the 1.5D hybrid morphological model. The dashed vector indicates degree of freedom which is bound by volume conservation within the coastal profile.*

In order to reduce drift in profile parameters, which eventually leads to non-physical coastal profiles, a cross-shore redistribution of sediment is implemented, following the ideas used by Capobianco et al. (1994); Falqués et al. (2000). The redistribution of sediment assumes that cross-shore transport processes will maintain a specific form of the coastal profile. This is implemented by defining a cross-shore transport which is a function of the deviation of the simulated coastal

profile slope from that of the equilibrium profile slope:

$$q_{\mathrm{crs}} = K \frac{q_{\mathrm{l}}}{\sin\theta} \frac{\alpha - \alpha_{\mathrm{eq}}}{\alpha_{\mathrm{eq}}} \tag{8.1}$$

where K is a dimensionless diffusion coefficient which can be used to impose a weak or a strong redistribution of sediment towards the equilibrium profile. q_{l} is the longshore transport ($\mathrm{m}^3/\mathrm{s/m}$) extracted from the 2D model as function of the local water depth and θ is the angle between the incident waves at wave breaking and the local orientation of the shoreline normal. α is the local bed slope and the final part of the right hand side is therefore the relative deviation of the local bed slope from the equilibrium bed slope. The cross-shore redistribution ensures that the cross-shore transport is onshore when the the local bed slope is too mild and vice versa. A moving shoreline is introduced in the cross-shore redistribution of sediment as described in Kristensen et al. (2013a). A value of $K = 0.02$ is adopted from Kristensen et al. (2013a) who found that this value ensured that coastal profiles located at some distance from detached breakwaters were maintained without having too strong an effect on the profiles located at the structures.

8.3 Model setup

8.3.1 Coastal profile and sediment properties

The initial coastal profile used in all simulations is defined as a Dean type power profile of the form:

$$z(s) = \begin{cases} z_0 & s < s_0 \\ z_0 - A\,(s - s_0)^m & s_0 \leq s_0 < s_{\mathrm{cl}} \\ z_{\mathrm{cl}} & s_{\mathrm{cl}} \leq s \end{cases} \tag{8.2}$$

where $(s, z)_0$ denotes the berm position which is taken to be 0.5 m above MSL. The profile slope is determined by the profile parameters $A = 0.095$ and $m = 0.67$ corresponding to a profile with a mean slope of 1/75. The depth of closure is if nothing else is mentioned, taken as $z_{\mathrm{cl}} = -5$ m. Sediment with a mean grain size $d_{50} = 0.2$ mm, a geometric spreading $d_{16/84} = 1.5$ and a porosity of $n = 0.4$ is used for the entire domain.

8.3.2 Wave forcing

Wave conditions are given at deep water and linear shoaling and refraction is used to transform them onto the offshore boundary of the model domain. Typically waves with significant wave height $H_{\mathrm{s}} = 1.5$ m, peak wave period $T_{\mathrm{p}} = 8$ s and directional spreading of the instantaneous wave energy spectrum $\sigma_{\mathrm{w}} = 19\,\mathrm{deg}$ are used. Wave angles are given relative to the initial shoreline normal with values: $\theta_0 = 15, 30$ or $50\,\mathrm{deg}$. In contrast to the alternating wave forcing used in Kristensen et al. (2013a), a constant wave forcing is used in this study. The alternating waves were originally introduced in order to study morphological evolution around breakwaters on shorelines with a small annual littoral drift. This particular case is however of little interest in the present application. Furthermore use of the alternating waves may for groyne fields result in an overestimation the offshore transport due to rip currents because the difference in morphological response time of the shoreline will be too large compared to the angular variation of the incident waves.

8.3.3 Periodic boundary conditions

The model assumes periodic boundary conditions on the model boundaries perpendicular to the shoreline. The simulated cases presented in this study correspond therefore to the morphological

response around a groyne located in the central part of a long groyne field. The periodic boundaries combined with a zero supply of sediment through the offshore boundaries ensures also that the total sediment volume does not change in time. Effects such as gradual filling of a groyne field are therefore not treated in this study.

8.3.4 Definition of morphological model

The hybrid morphological modelling concept is generally challenged by the fact that the choice of freedom to the coastal profile may affect the simulated equilibrium solution. This has been illustrated in previous studies, Kristensen et al. (2010, 2013a) and it will be repeated here for simulation of the morphological response to groynes in a long groyne field. A case with a 200 m long groyne located in a periodic domain which is 2000 m long has therefore been used as benchmark for 5 different implementations of the hybrid model. The tests include both changes to the freedom of the coastal profile (1D and 1.5D) and changes to the formulation of the baseline itself (1D).

Varying freedom of the coastal profile

The response of the coastal profile may within a 1D model be either implemented as a *translation* of the entire profile (panel A in figure 8.3) or as a response where the profile is *hinged* at the depth of closure contour (panel B in figure 8.3).

In the case where profile translation is applied, the slope (and therefore width) of the profile is constant. The shoreline response is in this case related to gradients in the littoral drift through the 1D continuity equation:

$$\frac{\partial s_0}{\partial t} = \frac{-1}{1-n}\frac{1}{h_{\text{act}}}\frac{\partial Q_{\text{l}}}{\partial r} \tag{8.3}$$

where n is the porosity and h_{act} is the active height of the profile measured as the vertical distance from the berm level to the level of the closure depth.

For the case where the hinged profile response is used, the profile slope becomes steeper in response to accretion and more gentle in response to erosion, thereby changing the width of the active profile. The hinged response is related to gradients in the littoral drift through the 1D continuity equation:

$$\frac{\partial s_0}{\partial t} = \frac{-1}{1-n}\frac{m+1}{h_{\text{act}}}\frac{\partial Q_{\text{l}}}{\partial r} \tag{8.4}$$

where m is the exponent of the power profile, which is defined invariant to changes in profile slope.

Finally a 1.5D implementation is used where the profile shape in principle develops according to the accretion/erosion field determined by the 2D coastal model (panel E in figure 8.3). Profile evolution may therefore include a mix of the translation and hinged response.

The simulated shoreline evolution and changes to profile volume are shown in figure 8.4 after 2 years where all solutions are close to an equilibrium. Comparing the solutions for the 1D translation with the 1D hinged response shows that the shoreline response is significantly smaller when the profile responds as a translation. This is due to the characteristics of this particular case where upstream deposition is strongest near the shoreline while the response in the deeper parts of the profile is limited. Forcing the profile to translate causes thereby an overestimation of the deposition in the deeper part of the profile. This causes a reduced seaward migration rate for the transient part of

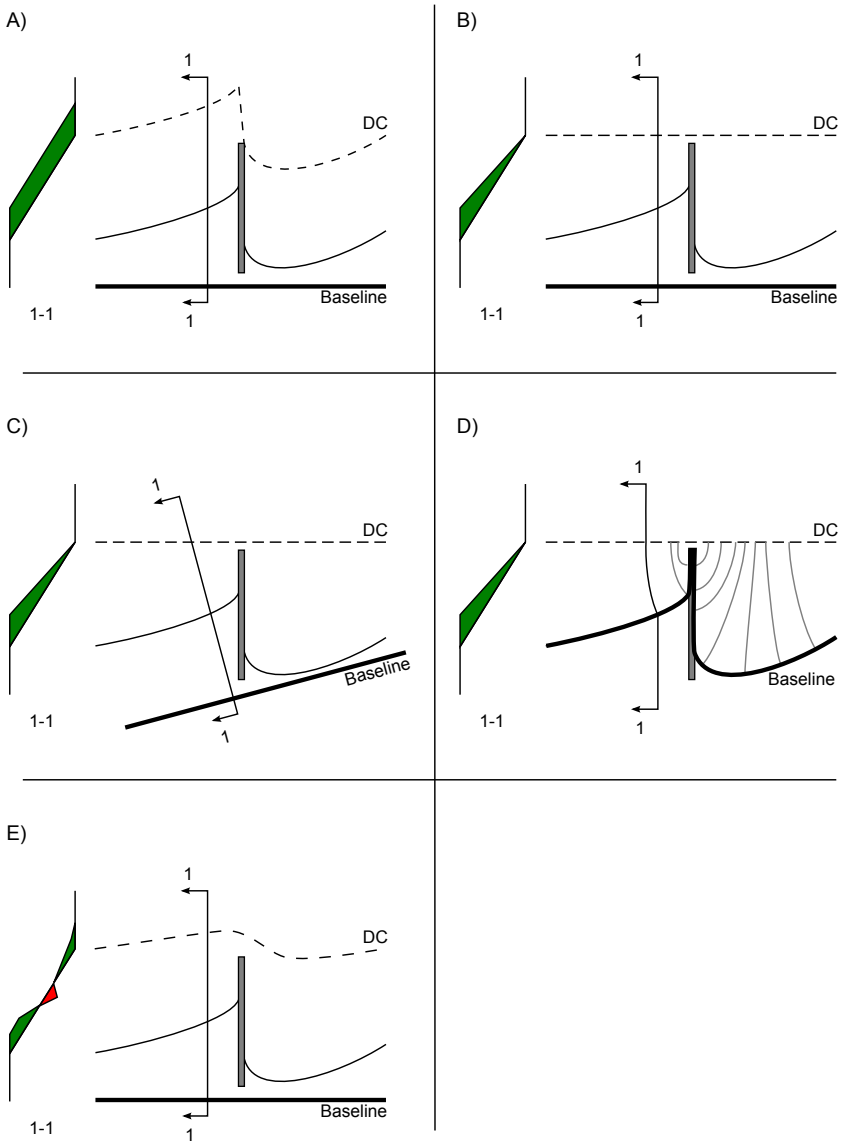

Figure 8.3: *Five different implementations of the hybrid morphological model used to simulate shoreline evolution around a groyne. A) 1D translation of profile, B) 1D profile is hinged at depth of closure, C) Rotated baseline, 1D profile is hinged at depth of closure, D) 1D curved mesh following shoreline and groyne, E) 1.5D*

the solution due to continuity. More importantly, the overestimated deposition reduces the water depth at the groyne tip thereby increasing the bypass transport effectively reducing the equilibrium shoreline response.

The 1.5D model allows erosion and deposition to occur within the same coastal profile and it gives therefore a better representation of the morphological development around the groyne. The shoreline response shown in figure 8.4 shows also that the model predicts a discontinuous shoreline over the groyne and that the shoreline response is generally stronger compared to the two 1D cases. The response of the 1D hinged model is however very similar to the shoreline response of the 1.5D model for profiles located at some distance from the groyne.

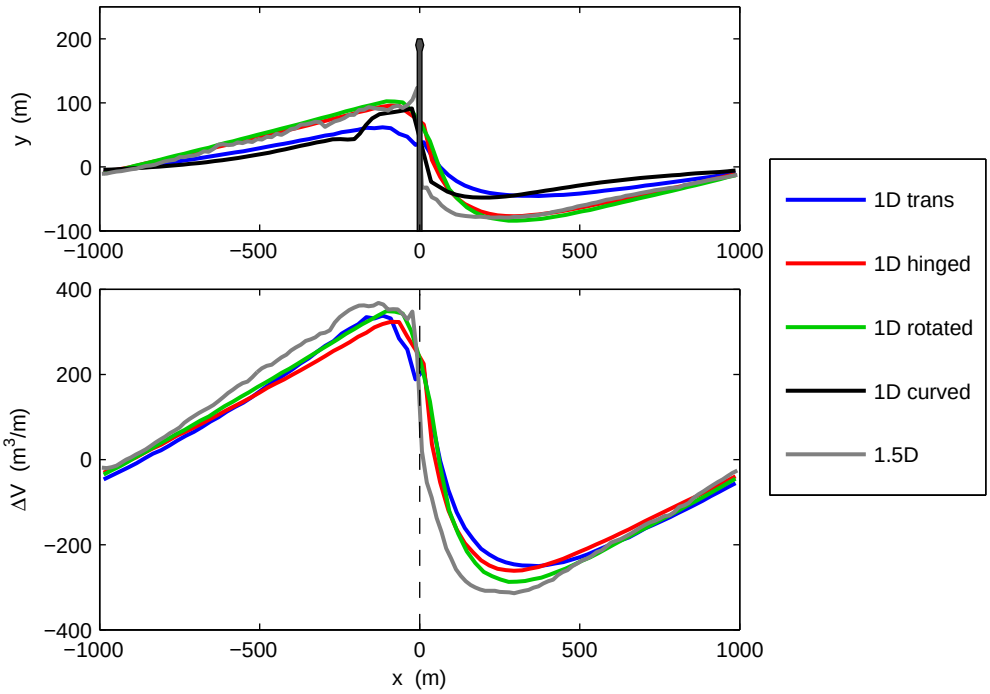

Figure 8.4: *Comparison of simulated shoreline evolution and change in profile volume after 2 years predicted by 5 different implementations of the hybrid morphological model. The result 1D curved is shown after just 6 months due to model breakdown.*

The change in profile volume shown in the lower panel of the figure yields a more integrated estimate of the morphological evolution. The figure shows interestingly that all three models give similar results, although the response of the 1.5D model is slightly stronger.

The case presented here is representative for several of the morphological simulations presented in this study. In terms of freedom of the coastal profile it may therefore be expected that the 1D hinged model is superior to the 1D translation model for representing profile response around the groynes used in this study. It may however be expected that the 1D translation model is superior for other cases, e.g. when the groyne is longer than the width of the active profile. Use of a model type which can represent both a hinged response, a translation or a mix of the two, is clearly favourable.

Varying formulation of the baseline

The morphological mesh is generally based on a straight baseline which is aligned with the initial shoreline. Use of a straight baseline simplifies the definition of the morphological model because the alongshore width of the coastal profile is constant (in the cross-shore direction) and it simplifies description of the 2D bathymetry because a cartesian coordinate system may be introduced. The straight baseline fixes however the orientation of the coastal profiles, thereby causing an alongshore redistribution of gradients in the littoral drift when the baseline is oblique to the shoreline.

Two new variations of the 1D hinged profile response are therefore formulated. The first is based on a straight baseline which is rotated such that it follows the orientation of the "anticipated" equilibrium shoreline as shown in panel C in figure 8.3. The second variation is a preliminary model

which is based on a curved baseline that follows the shoreline and groyne. In the curved baseline model the width and cross-shore variation of the coastal profiles are controlled by the local shoreline variation as illustrated in panel D in figure 8.3. The curved baseline is introduced because it is intuitive to describe the depth variation of a strongly curving coast along a curve related to the local shoreline orientation rather than along a straight line with an arbitrary orientation. Furthermore in the present implementation, coastal profiles have also been added along the trunk section of the groyne in order to increase resolution in an area where large variation to the morphology may be expected. The curved baseline implementation is however substantially more complex, and problems with sediment continuity and stability are present. It is included in this study only to allow a discussion of using such a principle. An overview of the curved baseline model may be found in appendix 8.A.

Comparing the predicted shoreline response of the 1D hinged and the 1D hinged model with a rotated baseline (1D rotated) shows no difference in solution. Presently the rotated coordinate system has been turned 7 deg, and it seems that this does not affect the solution.

The calculated shoreline variation using the curved baseline is shown after just 6 months due to model breakdown. The predicted shoreline is therefore not "as developed" as that of the other solutions and it's variation is questionable due to volume conservation problems. The shoreline variation shows however one interesting characteristic, namely a clear discontinuous feature over the groyne, which is similar to that predicted by the 1.5D model. By introducing the curved baseline, the resolution along the trunk section of the groyne may be improved, and this seems to make the model capable of representing 2D features which are otherwise restricted to the 1.5D model (compare the 2D plots of simulated bathymetries for the 1.5D model in the middle panel of figure 8.6 and that of the 1D curved solution in figure 8.21).

The variations to the baseline definition have shown that the orientation of the straight baseline has a limited effect for the cases simulated in this study. Application of the curved baseline model is not feasible as it presently is inconsistent and unstable. Instead the 1.5D model is applied using a straight baseline which is oriented along the initial straight shoreline.

8.3.5 Wave reflection

An initial test of the effect of including reflection along the trunk section of the breakwater is performed in order to asses the impact of applying wave reflection in the 2D coastal model. This is done because there are some uncertainties as to the nature of the effect predicted by the 2D coastal model in case of a partially standing wave field. The question is raised because the applied intra-wave sediment transport model is developed for unidirectional waves and not bidirectional partially standing waves, where transport may be strongly affected by streaming circulation patterns as discussed in e.g. Gíslason et al. (2009).

Including wave reflection will locally cause a slight increase in wave height and a change to the wave direction near the groyne. The increased wave height increases the instantaneous Shields parameter thereby increasing the near-bed sediment concentration. However as indicated in figure 8.5 (top and middle panel) the wave reflection changes the radiation stress gradients in a manner which effectively reduces the offshore transport due to changes in the depth integrated velocity in the upstream rip current. Allowing morphological evolution indicates that there, for this particular case, is a limited effect of wave reflection, see bottom panel in figure 8.5. The limited effect is expected to be a combination of the local effect that wave reflection has on the sediment transport field,

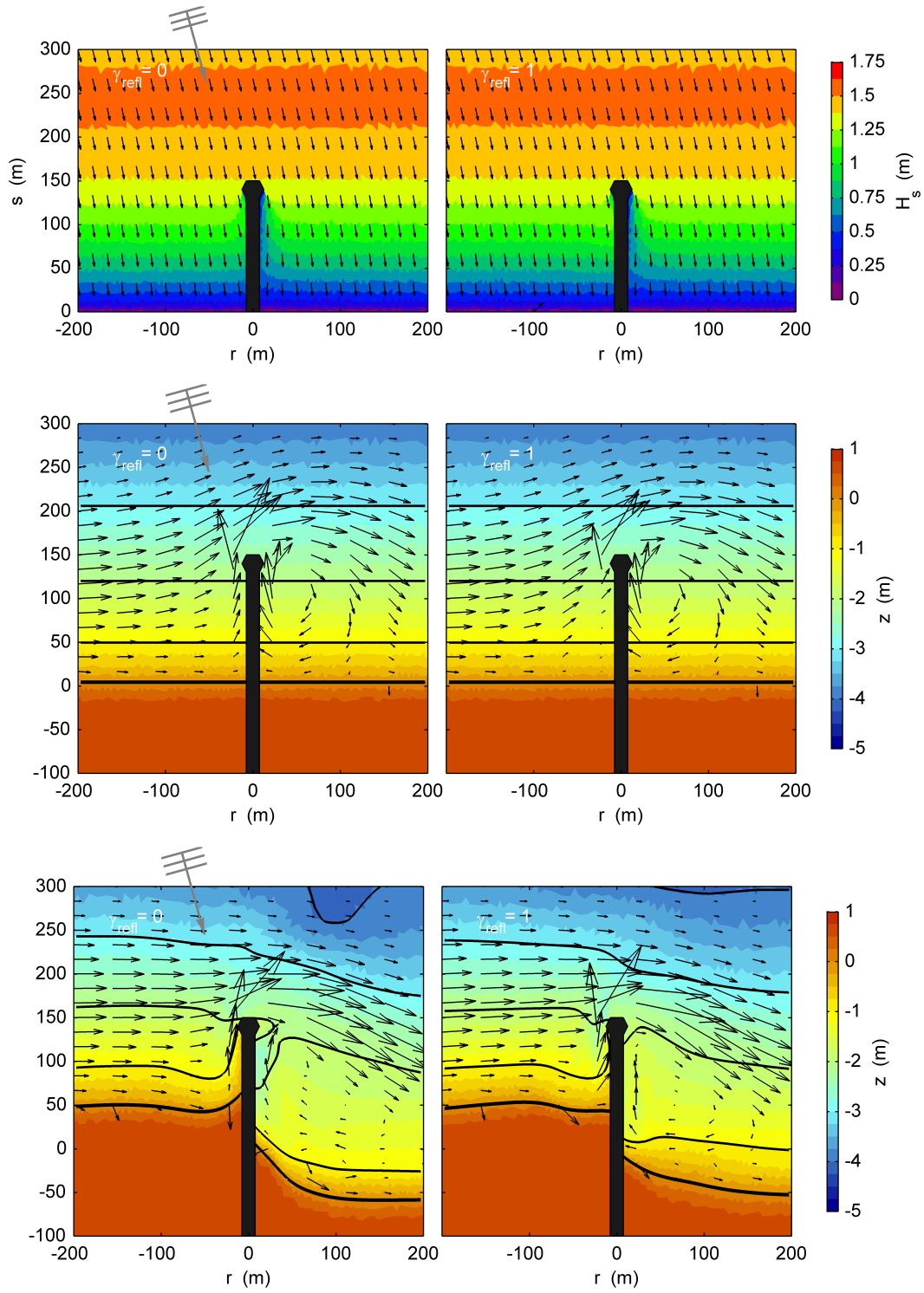

Figure 8.5: *Effect of adding wave reflection to the groyne. Top: Initial wave field. Middle: Initial sediment transport field. Bottom: Equilibrium bathymetry and sediment transport field. Bed contours are shown for every 1 m with the still water line in bold.*

and because morphological evolution has allowed re-orientation of the shoreline thereby creating a more streamlined bypass of transport on the upstream side of the groyne.

Obviously, the effect of adding wave reflection is more significant for groynes extending far into the surf zone and for cases where the re-orientation of bed contours is limited thereby favouring the continual existence of a rip current. Furthermore the alongshore extent of the area affected by wave reflection may generally be taken as very limited due to the acute angle which generally exists between the incident waves and shore-normal groynes.

For the simulations presented here a wave reflection coefficient of $\gamma_{\text{refl}} = 0.7$ has been used. This rather high value corresponds to smooth impermeable structures with a 1/1 slope, CEM (2002b).

8.4 Morphological response to groyne fields

The 1.5D model is used to simulate the equilibrium response to impermeable groynes in a groyne field. The simulations examine the response predicted by this model type to different groyne sizes and to variations in wave climate. The results are used to discuss general morphological behaviour to impermeable groynes. The morphological model has been run until equilibrium conditions have been reached. Determination of whether equilibrium conditions have been reached is based on a pragmatic evaluation of the temporal evolution of the littoral drift.

8.4.1 Groyne length

The hybrid morphological model generally predicts upstream accretion and downstream erosion in response to the placement of a groyne. The groyne length affects the magnitude of impact on the morphological evolution as shown in figure 8.6 where three different groyne lengths are considered. Increasing the groyne length increases the depth at which a clear correlation between cross-shore displacement of depth contours and distance to the groyne is seen. Also the shoreline response increases with groyne length as a result of the increased impact of the groyne on the littoral drift. The shoreline response is in this study defined as the largest cross-shore distance between the shoreline for profiles with accretion and profiles with erosion.

The time scale of the morphological development (evaluated as the time needed to obtain a steady littoral drift) increases also. This is a direct effect of the increasing amount of volume being redistributed for increasing groyne length. While it hasn't been quantified, the fact that sediment is moved from an increasing water depth as the groyne length increases means also that onshore transport occurs at a lower rate, thereby increasing the time scale of morphological development even further.

For the cases presented in the figure the 100 m long groyne reaches an equilibrium within 2 years, while it is nearly 3 years for the 200 m long groyne. The equilibrium conditions of the 350 m long groyne are obtained after 7 years although some alongshore variations in littoral drift continue to exist due to formation and propagation of undulations in the solution with the 350 m long groyne.

Profile response

The profile response at three characteristic longshore locations is shown for the three different groyne lengths in figure 8.7. The figure shows that the response of the coastal profile generally is a mix between the hinged response and translation. Accretion causes therefore an increase in profile slope while erosion flattens the coastal profile. For the long groyne however, offshore diversion of sediment creates a shoal, which locally flattens the profile.

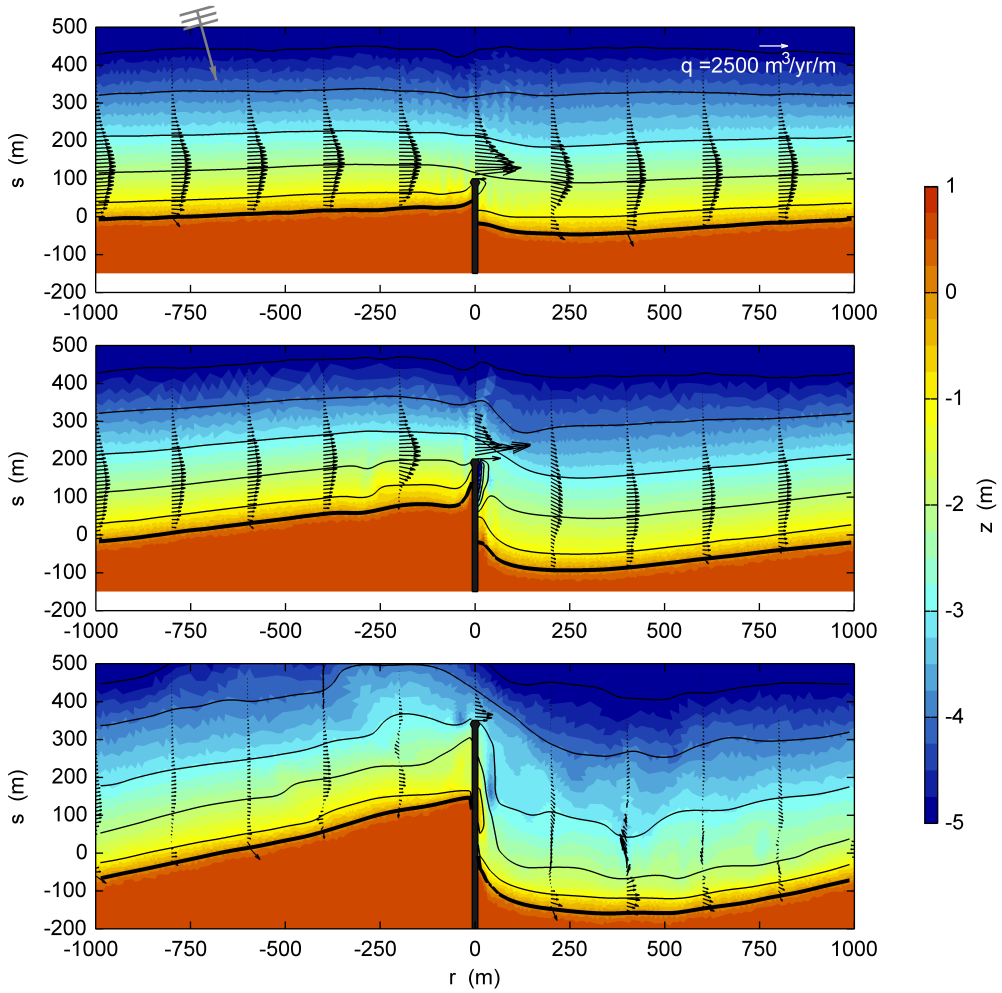

Figure 8.6: *Simulated bathymetry for three different cases where the groyne length varies. Top panel:* $L_g = 100$ *m, Middle panel:* $L_g = 200$ *m, Bottom panel:* $L_g = 350$ *m.*

8.4.2 Wave height

Changes to wave height affects the width of the surf zone and the alongshore forcing due to wave breaking. Increasing the wave height should therefore decrease the impact of the groyne on the littoral drift and morphological changes seaward of the groyne should decrease similar to that which is observed when changing the groyne length.

Figure 8.8 shows simulated bathymetries for three different deep water wave heights, $H_s = 1.0, 1.5, 2.0$ m in a groyne field with 150 m long groynes. The figure shows that the shoreline response generally decreases with increasing wave height in response to the decreasing impact of the groyne on the littoral drift.

Based on the three simulation results it is also found that the time scale of the morphological development decreases with increasing wave height. This follows directly from the fact that the

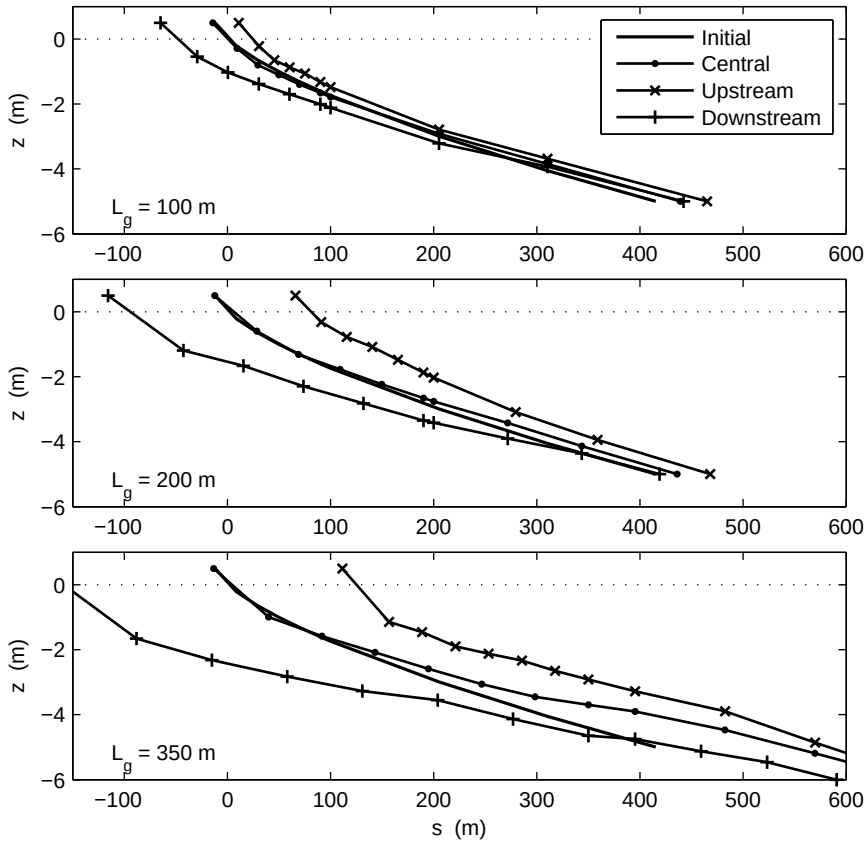

Figure 8.7: *Comparison of simulated coastal profiles at three characteristic locations for each of the three different groyne lengths.*

littoral transport increases greatly with increasing wave height, while the amount of volume being redistributed decreases.

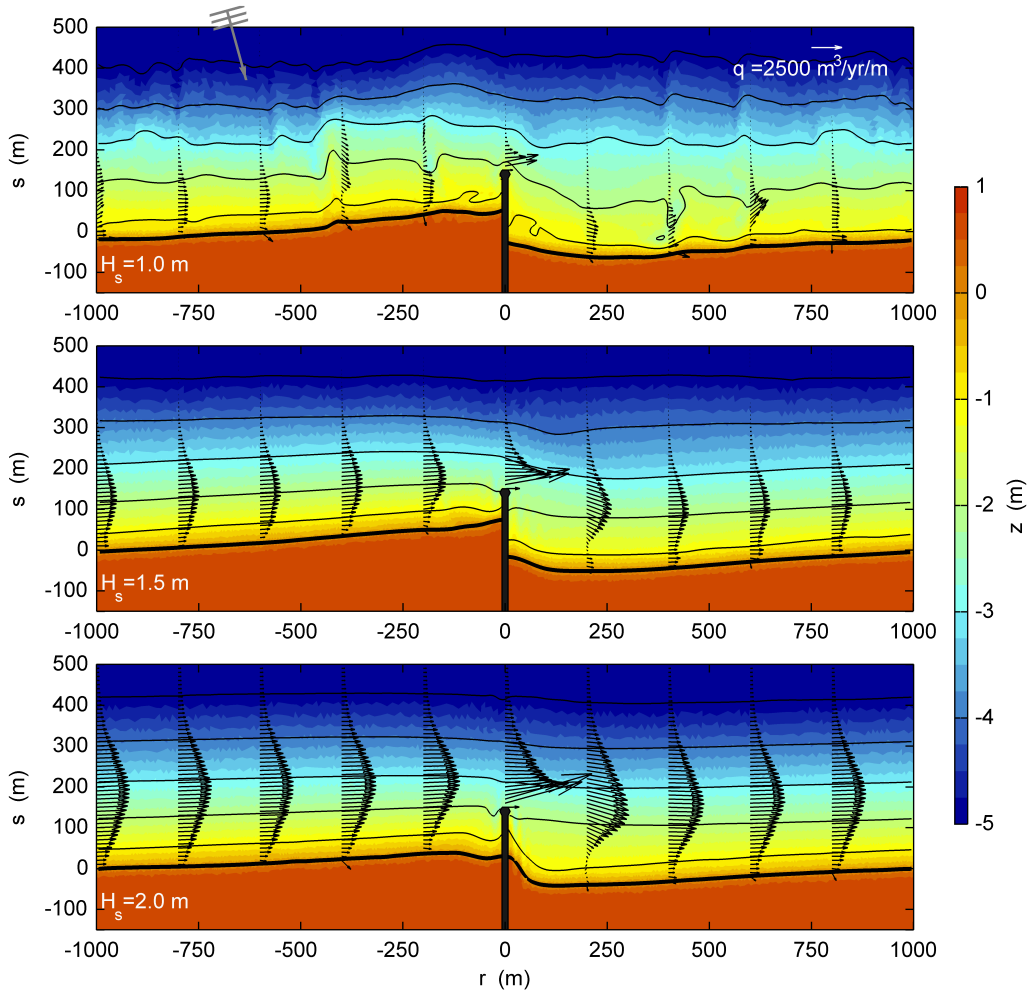

Figure 8.8: *Simulated bathymetry for three different offshore wave heights:* $H_s = 1.0, 1.5, 2.0$ *m (top to bottom). The groynes are 150 m long and the groyne spacing is 2000 m*

8.4.3 Wave direction

The angle of prevailing wave incidence is a fundamental parameter in design of equilibrium beaches where the annual littoral drift is small because the shoreline in this case is expected to be defined by the angle of wave incidence. The shoreline normal is however not expected to be aligned with the incident waves for groyne fields if a significant bypass transport is intended. The shoreline normal will in this case also be a function of other parameters such as the groyne length and the surf zone width as is seen in the preceding sections.

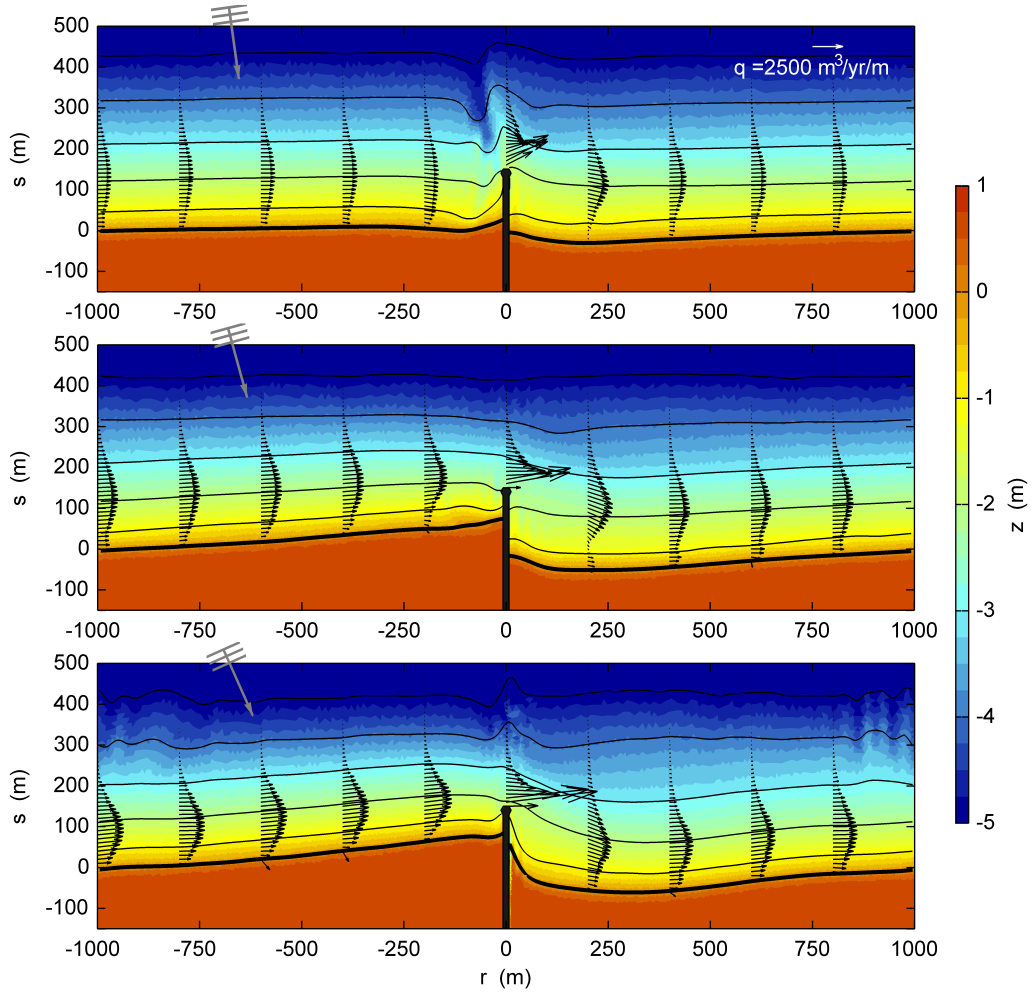

Figure 8.9: *Simulated morphological evolution for three different angles of wave incidence. Top to bottom:* $\theta_0 = 15, 30, 50\,\text{deg}$. *Results are shown after approximately 2 years, where most morphological changes have occurred.*

Simulations where the deep water angle of wave incidence is varied shows however that there is a clear effect on the equilibrium shoreline orientation. Increasing the angle of wave incidence increases the re-orientation of the shoreline as shown in the simulated equilibrium cases in figure 8.9. The degree of re-orientation of the shoreline is quantified in table 8.1 as β which is calculated using the equilibrium shoreline variation at some distance from the groyne. β is smaller than the angle

of wave incidence given at the offshore boundary although it seems remarkably sensitive for small wave angles.

Apparently for the case with $\theta_0 = 15\,\text{deg}$ (upper panel in the figure) a significant amount of sediment is deposited seaward of the groyne in contrast to the two other cases where the depth contours seaward of the groyne tip are more streamlined.

Table 8.1: *Wave forcing and calculated equilibrium parameters for a 150 m long groyne subject to waves of three different angles of incidence.*

θ_0 (deg)	$H_{\text{s,bc}}$ (m)	θ_{bc} (deg)	β (deg)	Q_{eq} (m^3/yr)	Q_0 (m^3/yr)	Q_{eq}/Q_0 (-)
15	1.52	7.9	2	232.000	285.000	0.81
30	1.45	15.4	6	314.000	402.000	0.78
50	1.29	24.0	8	328.000	415.000	0.79

As a matter of interest, table 8.1 shows that the relative reduction in equilibrium transport is more or less unaffected by the angle of deep water wave incidence, a result which is also reported in Kristensen et al. (2013a) for segmented offshore breakwaters.

8.4.4 Wave period

Variations in wave period greatly affect the wave climate given at the offshore boundary of the model domain since the systematic variation of wave climate in this study is based on variation of the deep water wave characteristics. An attempt to study the morphological response to different wave periods may therefore not be a function of the wave refraction pattern around the groyne but rather a result of linear shoaling and refraction from deep water to the closure depth. The wave parameters applied at the offshore boundary (at a water depth of 5 m) are listed in table 8.2. As shown in the table, waves with a peak wave period, $T_{\text{p}} = 6$ s have the largest angle of wave incidence and the smallest wave height, while the opposite is the case for $T_{\text{p}} = 10$ s. Based on the previously observed response to variations in wave height and wave direction alone, it may be expected that the re-orientation of the shoreline is greatest for the short waves. The computed equilibrium conditions shown in figure 8.10 shows in fact that the greatest re-orientation of the shoreline occurs for the short waves.

Table 8.2: *Wave forcing and calculated equilibrium parameters for a 150 m long groyne subject to waves of three different wave periods, with deep water angle of wave incidence, $\theta_0 = 30\,\text{deg}$.*

T_{p} (deg)	$H_{\text{s,bc}}$ (m)	θ_{bc} (deg)	Q_{eq} (m^3/yr)	Q_0 (m^3/yr)	Q_{eq}/Q_0 (-)
6	1.36	19.8	262.000	332.000	0.79
8	1.45	15.4	314.000	402.000	0.78
10	1.57	12.5	367.000	466.000	0.79

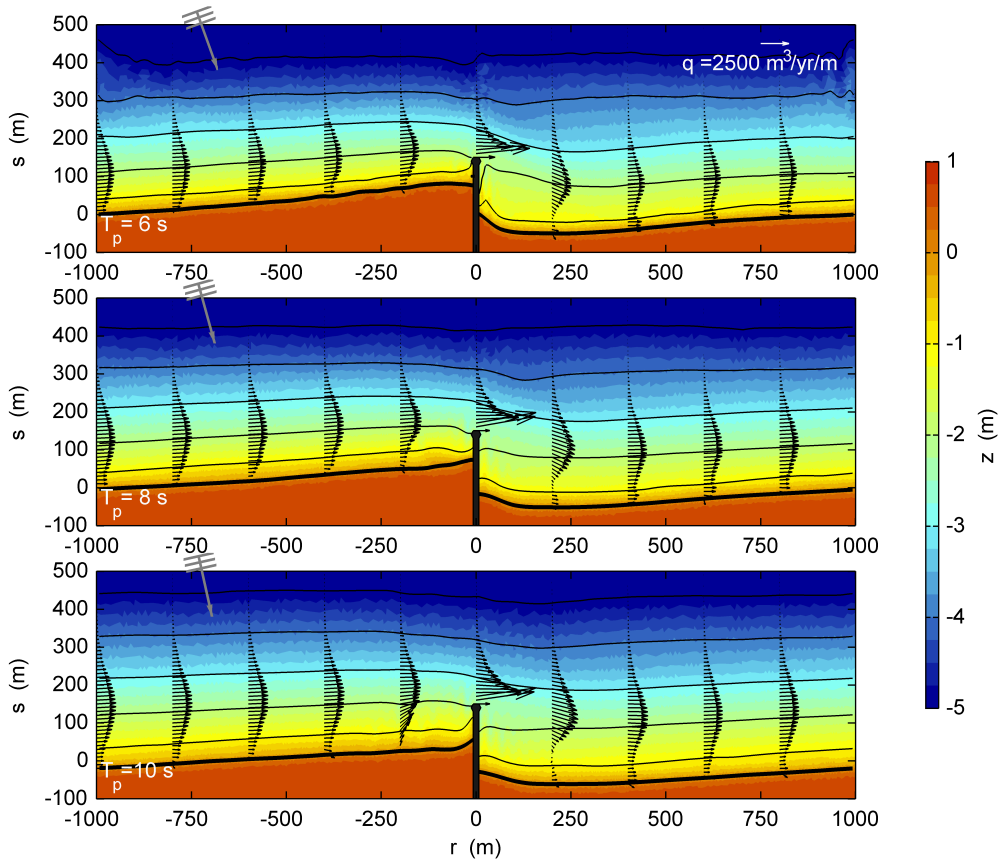

Figure 8.10: *Simulated morphological evolution for three different wave periods. Results are shown after approximately 2 years, where most morphological changes have occurred.*

8.4.5 Groyne spacing

The equilibrium littoral drift increases generally with increasing groyne length. For an increase in groyne spacing the upstream shoreline may migrate further upstream, thereby increasing sediment bypass. As figure 8.11 shows, the increased equilibrium transport may however also be obtained due to a decrease in re-orientation of the bed contours (going from $L_{\text{space}} = 2000$ m to $L_{\text{space}} = 3000$ m).

Secondly, for groyne spacings smaller than a length scale related to the recovery length of the littoral drift, re-orientation of the bed contours within the groyne compartment may be inhibited completely, as shown in figure 8.12.

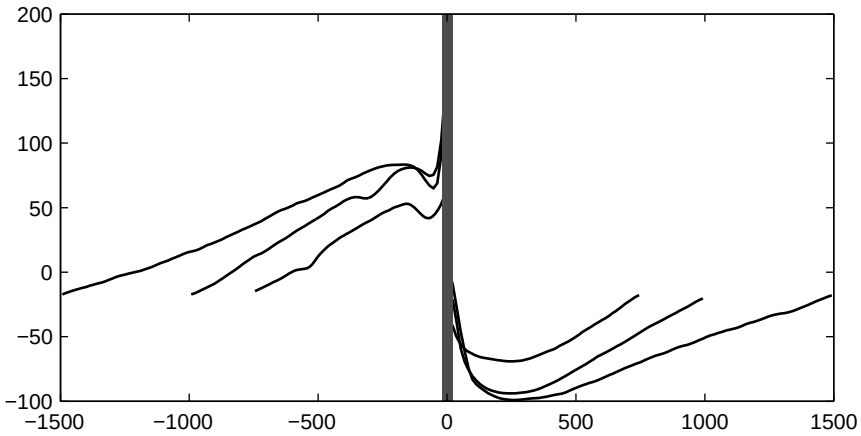

Figure 8.11: *Comparison of simulated shorelines for varying groyne spacing,* $L_{\text{space}} = 1500, 2000, 3000$ *m.*

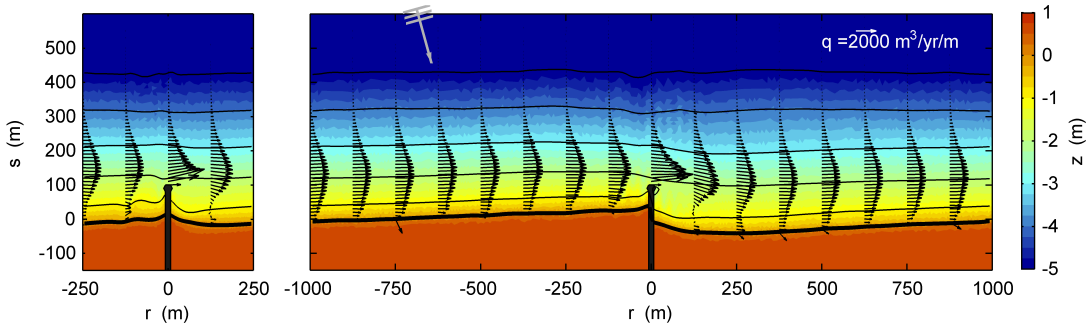

Figure 8.12: *Comparison of shoreline response at equilibrium conditions for two different groyne spacings. Left:* $L_{space} = 500$ *m, Right:* $L_{space} = 2000$ *m.*

8.4.6 Varying groyne design

The design of the groyne may be varied by inclining it against or with the dominant wave direction or by addition of a breakwater thus forming a T-groyne. Changing the design of the groyne will influence the impact of the groyne on the equilibrium bathymetry. Simulation of the impact of changing the groyne design has been performed within the hybrid modelling framework by defining coastal profiles which are intersected by the groyne or breakwater as breakwater profiles. Breakwater profiles are characterised by the fact that no cross-shore sediment transport is allowed

through the intersecting structure and that the profile may be discontinuous over the intersecting structure.

Table 8.3: *Comparison of effect of changing the groyne design. Initial water depth at groyne head is* $h_{g,0} = 2.5\ m$.

Type	s_{up} (m)	s_{down} (m)	$h_{\text{g,eq}}$ (m)	Q_{eq} (m^3/yr)
Simple	74	-52	2.3	314,000
T-groyne	141	-73	2.2	278,000
Inclined up	103	-62	2.6	314,000
Inclined down	81	-57	2.2	312,000
Headland	58	-58	2.5	313,000

The resulting morphological evolution as predicted by the 1.5D model is shown for each of the cases in figure 8.13. The most noticeable difference is the added accretion imposed by the T-groyne which also has the largest shoreline response and the greatest reduction in littoral drift, see table 8.3. For the case of the headland, it seems that a more streamlined design improves bypass thereby minimising the shoreline response. Use of streamlined design of coastal structures such as harbours and headlands has in fact been applied over the last decade in an attempt to minimize downstream lee erosion, as discussed in e.g. Brøker et al. (2007). The simulated response seems therefore reasonable.

The difference between each of the solutions is evaluated using an integrated approach in figure 8.14 in which the change in profile volume is shown. Again, it is seen that the solutions in the far-field areas seem to be unaffected by the details of the groyne design apart from the case of a T-groyne. Near the structures it seems that inclining the structure in the direction of the prevailing longshore transport increases sheltering in the lee of the structure thereby favouring deposition and reducing downstream erosion compared to the variation when the groyne is inclined against the prevailing longshore transport.

The increased deposition in the lee of the +10 deg inclined structure may however be affected by the definition of the morphological mesh because a similar study where the baseline is oriented normal to the groyne (thereby avoiding coastal profiles which are intersected by the groyne) does not show the same strong amount of accretion (see figure 8.15). The results shown in the figure indicate therefore that there may be some artificial effects on the resulting morphological response due to the definition of the morphological mesh. Similar effects may also affect the strong additional accretion around the T-groyne, although this has not been quantified. It is however our belief that these artificial effects will primarily modify the solution locally around the groyne, while the general trends such as reduction in littoral drift are not affected.

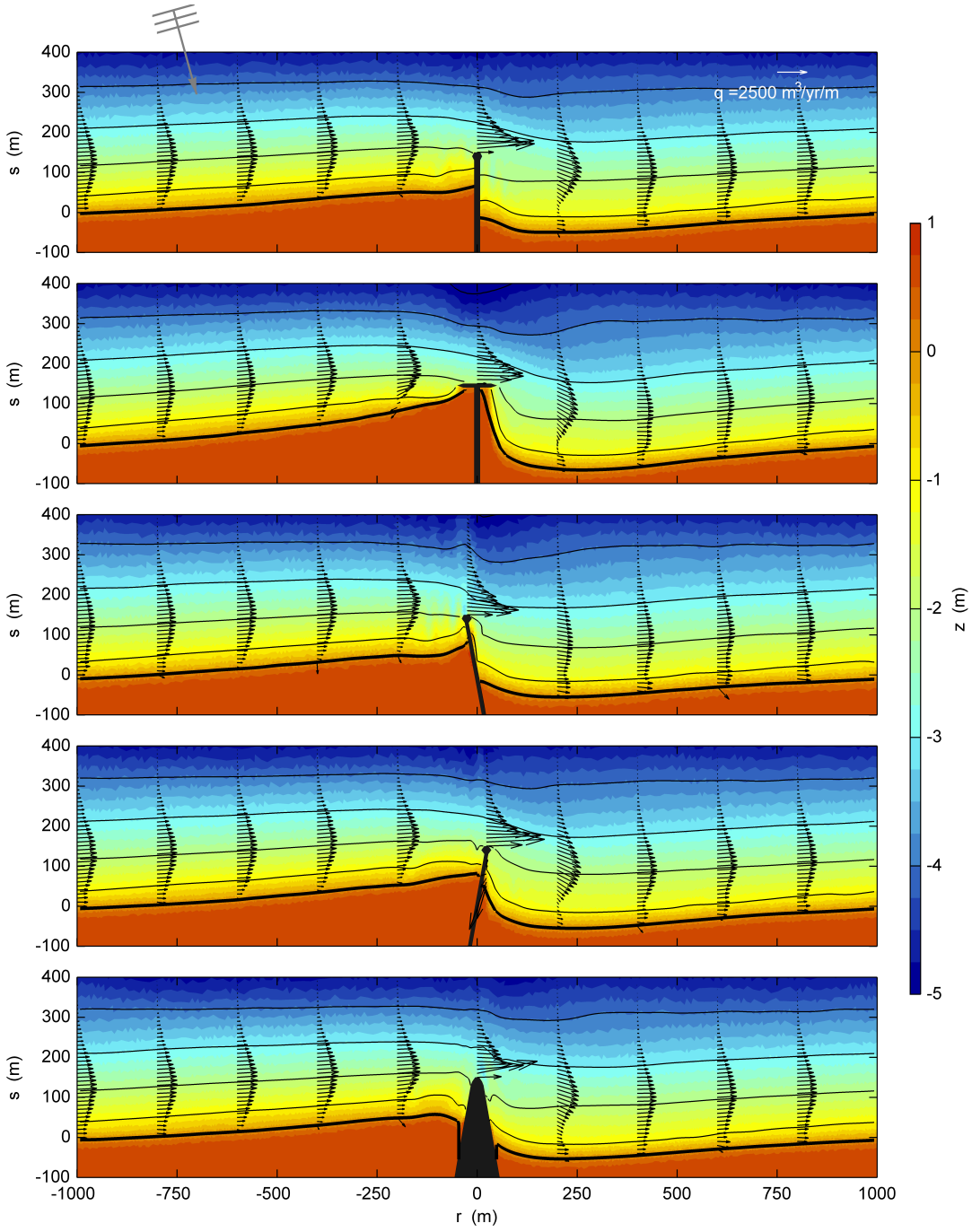

Figure 8.13: *Simulated bathymetries around groynes of varying geometries. From top to bottom: 1) Simple groyne, 2) T-groyne, 3) Groyne inclined* $-10\,\mathrm{deg}$*, 4) Groyne inclined* $+10\,\mathrm{deg}$*, 5) Headland.*

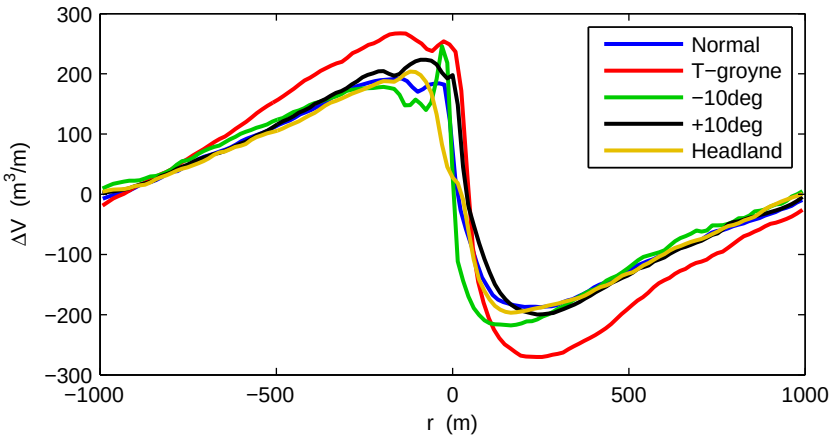

Figure 8.14: *Comparison of alongshore distribution of change in profile volume for varying groyne geometry.*

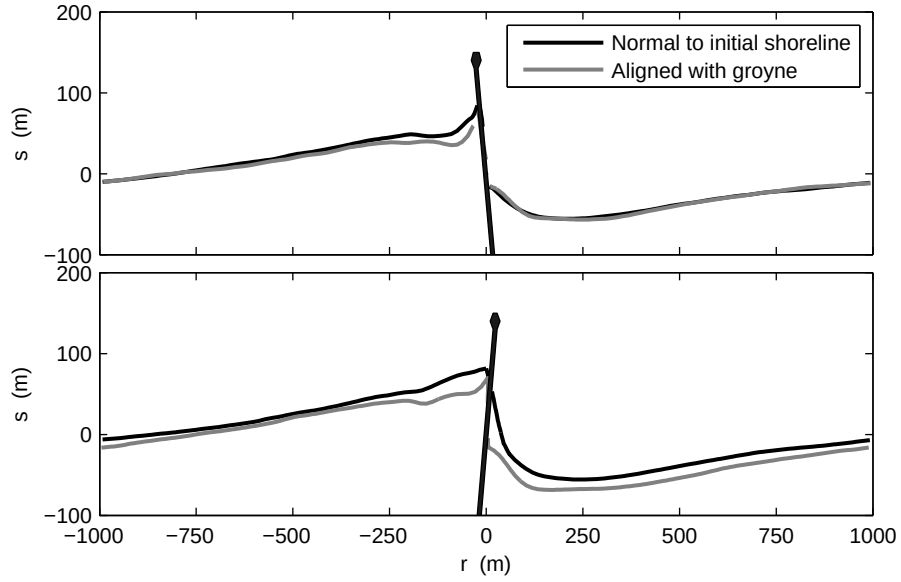

Figure 8.15: *Comparison of the effect of changing the orientation of baseline and thereby the orientation of the coastal profile.*

8.5 Reduction in littoral drift

The reduction in littoral drift at equilibrium conditions relative to the undisturbed case may be an important design parameter in cases where a stretch of coast under erosion due to gradients in the littoral drift is stabilised by construction of a groyne field. As an example, a groyne field with an exaggerated efficiency may be costly to construct and costly to maintain due to excessive erosion downdrift the groyne field. A conceptual discussion on the basic functioning of groyne fields is attempted in the following. The purpose of the discussion is to establish general relations between the reduction in littoral drift and characteristic length scale of a groyne field.

8.5.1 Conceptual function of groyne fields

The functioning of groynes is conceptually divided into two overall groups depending on the groyne length relative to the surf zone width[3]. This is done because the preceding sensitivity study has clearly shown that the characteristics of the morphological response is different for groynes which block the transport completely compared to groynes which allow a significant amount of bypass.

Short groynes

Short groynes, that is groynes which are short compared to the surf zone width, reduce the littoral drift by blocking the part of the transport field located landward of the groyne tip. The amount of bypass may therefore be determined as the shaded area of the undisturbed littoral drift field in the top panel of figure 8.16. Increasing the groyne spacing may lead to recovery of the littoral drift within the groyne compartment, which therefore would question this geometric calculation of the bypassed transport. However re-orientation of the bed contours means that the littoral drift within the groyne compartment continues to be limited. The limited effect of short groynes on the seaward depth contours means the short groynes primarily fixate the beach while the reduction in littoral drift is greatly affected by the geometric bypass rate, Q_{geo} regardless of the groyne spacing.

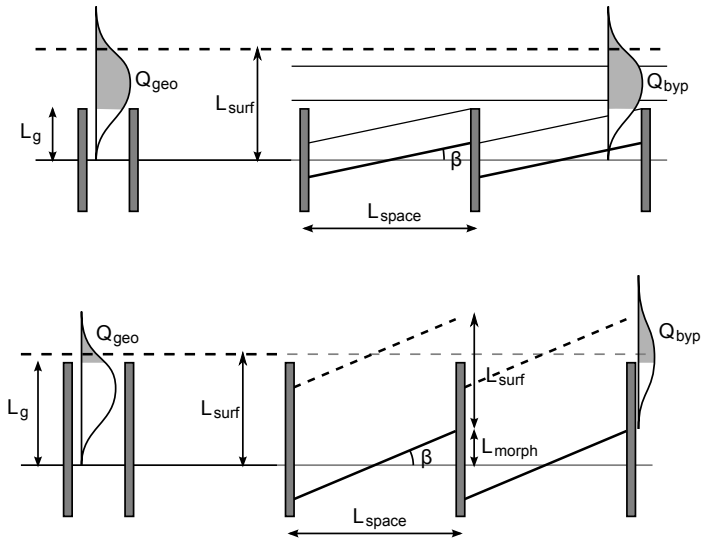

Figure 8.16: *Characteristic length scales associated with groynes in groyne fields. Top: Short groynes. Bottom: Long groynes.*

[3]The surf zone width is in this context taken as the cross-shore distance over which 80% of the littoral drift is contained, Mangor (2004)

Long groynes

Long groynes are groynes with a length which is comparable to the surf zone width. The long groynes block initially most of the littoral drift and they favour therefore a strong re-orientation of bed contours on the entire active profile. However the strong re-orientation of the bed contours will also move the entire littoral zone seaward at the upstream part of the groyne (see bottom panel of figure 8.16), thereby increasing bypass of sediment. The equilibrium solution for the long groynes is therefore a complex balance between the degree of re-orientation of the bed contours (which decreases littoral drift) and the seaward deflection of the littoral drift field (which increases the amount of bypass). The resulting equilibrium transport for long groynes is therefore greatly affected by the groyne spacing, groyne length and angle of wave incidence since these three parameters have been shown to affect the re-orientation of the shoreline.

8.5.2 Simulated reduction in littoral drift

Based on the conceptual discussion on functioning of groynes, the relative reduction in littoral drift may be expected to be sensitive to the ratio surf zone width to groyne length, in which the effect of the seaward displacement of the surf zone at the upstream side of the groyne is included, ie.:

$$\Omega_1 = \frac{L_{\text{surf}} + L_{\text{morph}}}{L_{\text{g}}} \tag{8.5}$$

In accordance with the idealised sketch in figure 8.16 the seaward displacement of the upstream surf zone may be taken as:

$$L_{\text{morph}} = \frac{1}{2} L_{\text{space}} \tan\theta_{\text{br}}$$

where θ_{br} is the wave angle of incidence at wave breaking on the initial (undisturbed) shoreline, which is used as a characteristic angle for the maximum change in shoreline orientation at equilibrium conditions. L_{morph} is defined in this way for two reasons: 1) The actual shoreline change is not known a priori and 2) the length scale is meant as a measure of potential shoreline change because this must be related to the actual shoreline change.

For Ω_1 tending towards unity, it may be expected that no bypass occurs because the geometric surf zone width (including morphological response) does not extend seaward of the groyne tip. For large values ($\Omega_1 >> 1$) bypass occurs, either because the groyne length is short compared to the surf zone width ($L_{\text{surf}} \simeq L_{\text{morph}}$), or because the groyne spacing is large enough to facilitate a significant seaward displacement of the upstream shoreline ($L_{\text{morph}} \simeq L_{\text{g}}$). Using this concept, the simulated relative reduction in littoral drift is shown as function of Ω_1 in figure 8.17.

Interestingly enough, it seems that this quantity may be used to describe the relative reduction in littoral drift for a wide range of groyne dimensions, spacings and for some different wave heights and angles of incidence. It is expected that the slope of the curve may depend on other parameters such as bed friction since this parameter has a strong effect on the recovery length of the flow. For the present dataset a best fit to the data is found to be:

$$\frac{Q_{\text{eq}}}{Q_0} = 1 - \exp\left(-1.15\left(\Omega_1 - 1\right)^{0.72}\right) \tag{8.6}$$

Examining the data-set in figure 8.17 shows that the relative bypass transport is high for cases where the relative geometric bypass rate, $Q^*_{\text{geo}} = Q_{\text{geo}}/Q_0$ is also high (Q^*_{geo} is indicated by the

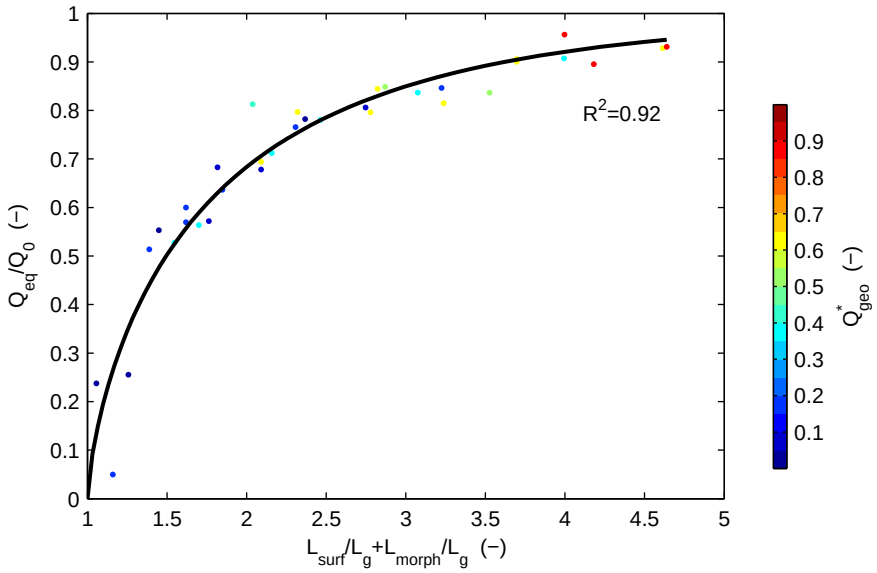

Figure 8.17: *Simulated relative reduction in littoral drift as function of dimensionless groyne impact. The solid curve is a best fit to the dataset with an exponential function.*

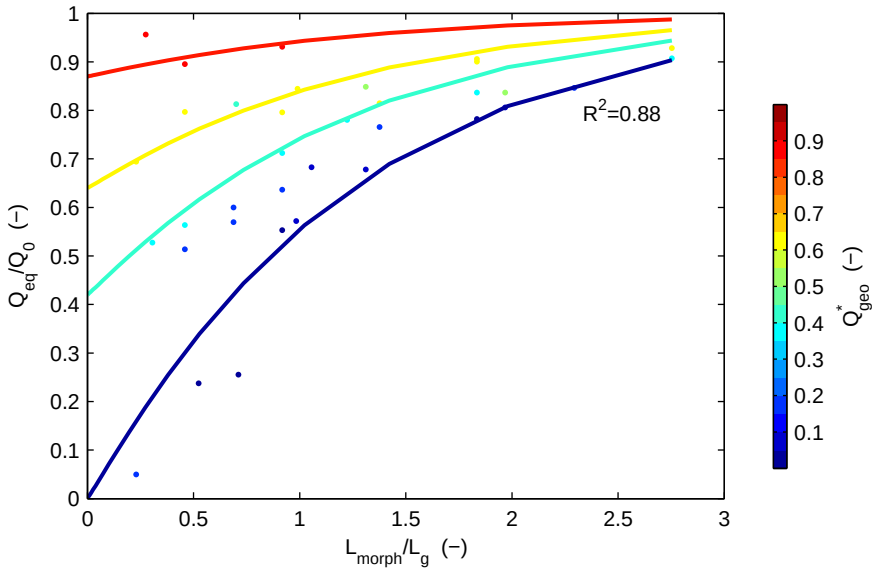

Figure 8.18: *Reduction in littoral drift as function of dimensionless groyne spacing and geometric bypass. The functional form of eq. 8.7 is shown for* $Q^*_{\text{geo}} = 0, 0.42, 0.64, 0.87$ *which are typical values from the dataset.*

colour of the data points). In fact, following the conceptual discussion from section 8.5.1, it may be expected that the equilibrium bypass transport should not be able to be reduced below the geometric bypass regardless of how closely the groyne are spaced. Increasing groyne spacing may increase the transport, although it can never exceed that of the undisturbed transport rate. Following this, it may be realised that groynes which are long compared to the undisturbed surf zone width may have a large range of different equilibrium solutions to the littoral drift depending on the groyne

spacing, while short groynes will not. Separation of the different effects related to $L_{\mathrm{surf}}/L_{\mathrm{g}}$ and to $L_{\mathrm{morph}}/L_{\mathrm{g}}$ is done in figure 8.18 with the best fit to an exponential function of the form:

$$\frac{Q_{\mathrm{eq}}}{Q_0} = Q^*_{\mathrm{geo}} + \left(1 - Q^*_{\mathrm{geo}}\right)\left(1 - \exp\left(-0.8\frac{L_{\mathrm{morph}}}{L_{\mathrm{g}}}\right)\right) \tag{8.7}$$

While the functional description of the data is not as good when the two contributions are separated, this form clearly illustrates the importance of the groyne length relative to the surf zone and it also clearly shows the dependence to changes in groyne spacing.

8.6 Discussion

The 1.5D hybrid morphological model developed for morphological simulations around coastal breakwaters and presented in Kristensen et al. (2013a), is used to simulate the morphological response to groyne fields. The morphological model does not require any changes because the freedom of the coastal parameters for a detached breakwater are not significantly different from the freedom needed for groynes.

Profile distortion

In the 1.5D hybrid model, the response of the points defining the coastal profile is coupled along the entire profile from the shoreline to the depth of closure. Therefore in some cases where the littoral drift occurs only on the upper part of the active profile, the position of the points on the lower part of the profile tend to drift in time. The cross-shore redistribution was therefore included as a method for reducing the drifting profile in the study of Kristensen et al. (2013a). The cross-shore redistribution is intended as a weak correction to the to profile which should not significantly affect the "true" erosion/deposition field computed by the 2D coastal model. In Kristensen et al. (2013a) is was found that a cross-shore diffusion based on the longshore transport and a diffusion coefficient gave satisfactory results. In this study the same method has been adopted with reasonable success although for cases where the wave height is small, the cross-shore redistribution seems inadequate. It may therefore be necessary either to implement another more physically based formulation of the cross-shore transport or simply modify the closure depth according to the wave climate in future applications of this model type.

Effect of periodic boundary conditions

Periodic boundary conditions have been used in all the simulations presented in this study. The results obtained here correspond therefore to the morphological response obtained in the central part of a groyne field. The periodic boundary conditions ensure that a static equilibrium may be obtained in contrast to the solution near the upstream and downstream end of the groyne field. The solution is in this area inherently transient unless the groyne field covers an entire sediment cell. Solution of the transient conditions near either of the two ends of the groyne field may be performed within the hybrid morphological modelling framework. For example, applying constant gradient conditions on the littoral drift (fixing orientation of shoreline normal) can be used at the upstream end of the model domain resulting in a gradual seaward migration of the shoreline, which in the end causes the groyne field to fill or the boundary condition can be applied at the downstream end in which case downstream erosion will continually erode the shoreline.

Use of groyne fields as coastal protection
As described in the introduction to this paper, groynes act primarily by fixing the beach. They cannot be designed to cause local accretion because changes to the direction of the littoral drift will reverse the orientation of the equilibrium shoreline. A beach which was previously wide will thus after a change in direction of littoral drift be narrow. If the aim of a beach protection scheme is to locally increase beach width, then use of detached breakwaters may be advisable since local accretion is certain behind this type of structure. However, protection against a retreating shoreline (due to gradients in the littoral drift) may be treated by use of groyne fields because the groyne field may fix the beach locally. The sediment deficit is not removed by construction of the groyne field, it is simply moved further downstream. It is therefore necessary to address the increased shoreline retreat downstream of the groyne field, either passively as a "managed" retreat or by use of nourishment. Use of the latter approach may be favourable to distributing the nourishment along the entire stretch of the eroding shoreline because it is possible to concentrate the efforts along a smaller area. As pointed out in Mangor (2004) erosion will continue to occur seaward of the groyne tip, which eventually may lead to destabilisation of the groyne head. In Denmark the Coastal Authorities have addressed this issue by a managed retreat and reconstruction of the groyne tip.

8.7 Conclusion

The sensitivity study has shown that increasing the groyne length will increase the shoreline response and the response of depth contours on an increasing water depth. Conversely, an increase in wave height will effectively increase the surf zone width and thereby decrease shoreline response and the response of depth contours seaward of the groyne tip. Both results indicate that the groyne length relative to the surf zone with may be expected to be an important parameter in relation to the morphological response around groynes.

Increasing the deep water angle of wave incidence increases the potential degree of re-orientation of the shoreline and thereby the shoreline response. Re-orientation of bed contours causes the groyne spacing also to have a direct effect on the seaward displacement of the shoreline upstream of the groyne. Therefore, an important parameter for the morphological response in groyne fields must be related to the potential seaward displacement of the shoreline relative to the groyne length, where the first parameter is defined in terms of the groyne spacing and angle of wave incidence.

Compilation of data obtained by use of the 1.5D hybrid model has shown that these two parameters in fact may be combined to describe the relative reduction in littoral drift. Using the obtained functional relationship between the reduction in littoral drift and groyne dimensions it may be possible to quantify groyne dimensions during the initial phase of a design, or it may be used to quantify necessary changes to existing groyne fields which do not function as intended. At the very least the functional relationships can be used to understand the impact of groynes on the littoral drift.

Acknowledgements

The first author has been supported by a grant from the Danish Agency for Science Technology and Innovation. This work has been partly supported by the Danish Council for Strategic Research (DSF) under the project: Danish Coasts and Climate Adaptation - Flooding risk and coastal protection (COADAPT), project no. 09-066869.

8.A 1D curved baseline model

This section gives a brief description of the final implementation of a 1D hybrid morphological model using a curved baseline. The model introduces curved cross-shore profiles as fourth order polynomials in which the polynomial coefficients are related to the shoreline position, local shoreline orientation and orientation at the depth of closure. Additionally, the curvature of the polynomial is modified iteratively in order to avoid overlapping cross-shore profiles.

The morphological evolution model is first presented. Details on how the polynomial coefficients are determined are then given and some snapshots of the results obtained with the model are finally given in the end of this section.

8.A.1 Model description

The model solves the 1D sediment continuity equation using a finite volume method with an upwind flux reconstruction as is done when the baseline is straight. The formulation is however slightly more complex because the alongshore width of the morphological elements varies in the cross-shore direction since the cross-shore profiles are curved. The sediment continuity equation is therefore:

$$\Delta\tilde{V} = \frac{-1}{1-n}\Delta Q_l \Delta t$$

where $\tilde{V}$ is the total active volume in m^3 of the morphological element and ΔQ_l is the divergence of the reconstructed flux over the morphological element faces. The change in shoreline position ($\Delta\epsilon_0$) is assumed to occur normal to the existing shoreline normal and it is calculated for each morphological element by numerical solution of the equation (see also figure 8.19):

$$\tilde{V}\left(\epsilon_0^k + \Delta\epsilon_0\right) - \tilde{V}\left(\epsilon_0^k\right) = \Delta\tilde{V} \tag{8.8}$$

where the superscript k denotes the time step number. The profile volume is calculated using numerical integration:

$$\tilde{V}(\epsilon_0) = \int_{-l}^{\infty} W(\xi) h_{\mathrm{act}}(\xi, \epsilon_0)\,\mathrm{d}\xi$$

h_{act} is a profile height function, which takes arguments, cross-shore distance from the baseline and cross-shore position of berm. ξ is an dummy variable running from some distance landward of the shoreline $-l$ out to the depth of closure beyond which the active height of the profile (h_{act}) is zero. The varying width of the morphological element is included in the function $W(\xi)$.

$\Delta\epsilon_0$ is the change in shoreline position necessary to fulfill continuity. The baseline position is however only updated to reflect this change if the baseline point is not restricted by any structure in which case the baseline point remains at the same position while the function calculating the active height is instead changed in order to obtain continuity. Morphological elements located at the groyne will therefore remain on the groyne until deposition of sediment has updated the active height function to a degree where it is no longer restricted by the groyne.

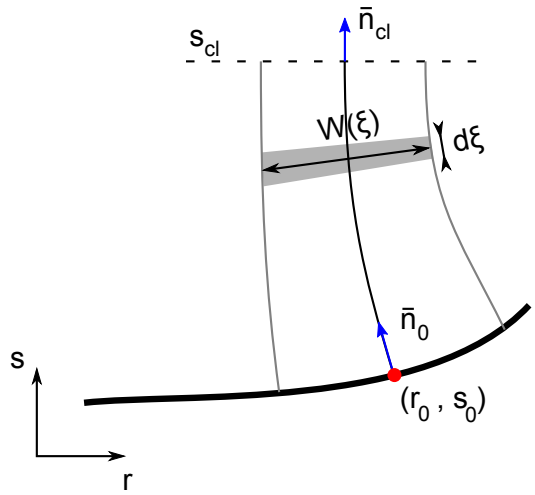

Figure 8.19: *Planview of a curved morphological element. The volume of a morphological element is calculated as the integral of the product of local profile width and local profile height.*

Defining a cross-shore profile as a polynomial

The curved cross-shore profiles are defined as 4^{th} order polynomials of s, where $s \in \{s_0, s_{\text{cl}}\}$.

$$\tilde{r}(s) = as^3 + bs^2 + cs^2 + ds + e \tag{8.9}$$

The polynomial coefficients, a, b, c, d, e are defined in terms of the boundary conditions:

$$\tilde{r}(s_0) = r_0 \ , \lim_{s\to s_0}\left(\frac{\mathrm{d}\tilde{r}}{\mathrm{d}s}\right) = \frac{n_r}{n_s} \ , \lim_{s\to s_{\text{cl}}}\left(\frac{\mathrm{d}\tilde{r}}{\mathrm{d}s}\right) = 0 \ , \lim_{s\to s_0}\left(\frac{\mathrm{d}^2\tilde{r}}{\mathrm{d}^2 s}\right) = \kappa_0 \ , \lim_{s\to s_{\text{cl}}}\left(\frac{\mathrm{d}^2\tilde{r}}{\mathrm{d}^2 s}\right) = 0 \tag{8.10}$$

The $\tilde{r}$ is used to emphasize that it is a polynomial function and not the alongshore coordinate. n_r and n_s are the components of the local shoreline normal and κ_0 is the curvature of the coastal profile at the shoreline, a value which is changed iteratively as will be shown later in the text.

Inserting the boundary conditions into equation 8.9 leads to a coupled system of equations with the solution:

$$\begin{aligned}
a &= \frac{1}{2}\frac{n_r}{n_s}\left(s_{\text{cl}} - s_0\right)^{-3} + \frac{1}{4}\kappa_0\left(s_{\text{cl}} - s_0\right)^{-2} \\
b &= \frac{12a\left(s_{\text{cl}}^2 - s_0^2\right) + \kappa_0}{6\left(s_0 - s_{\text{cl}}\right)} \\
c &= -6as_{\text{cl}}^2 - 3bs_{\text{cl}} \\
d &= -4as_{\text{cl}}^3 - 3bs_{\text{cl}}^2 - 2cs_{\text{cl}} \\
e &= -as_0^4 - bs_0^3 - cs_0^2 - ds_0
\end{aligned} \tag{8.11}$$

8.A.2 Avoiding crossing profiles

It has not been possible to identify a general expression for the curvature of the coastal profile, which ensures non-overlapping profiles. In stead an iterative algorithm is used, where an initial

guess on κ_0 is used as basis for identifying regions where profiles may overlap (indicated with green curves in the top panel in figure 8.20).

$$\kappa_{0,\text{init}} = 0.015 \left(\frac{n_{r,\text{cl}}}{n_{s,\text{cl}}} - \frac{n_r}{n_s} \right)$$

The coefficient in the initial guess is expected to be inverse proportional to the distance $s_{\text{cl}} - s_0$. κ_0 is then changed for each profile within the identified regions, such that the profiles are distributed more evenly. The identification of overlapping profiles and redistribution of them is run successively while overlapping of profiles occurs. The final result is shown in the bottom panel of the figure, where it is seen that the effect of the groyne has spread to profiles located at some distance from the structure.

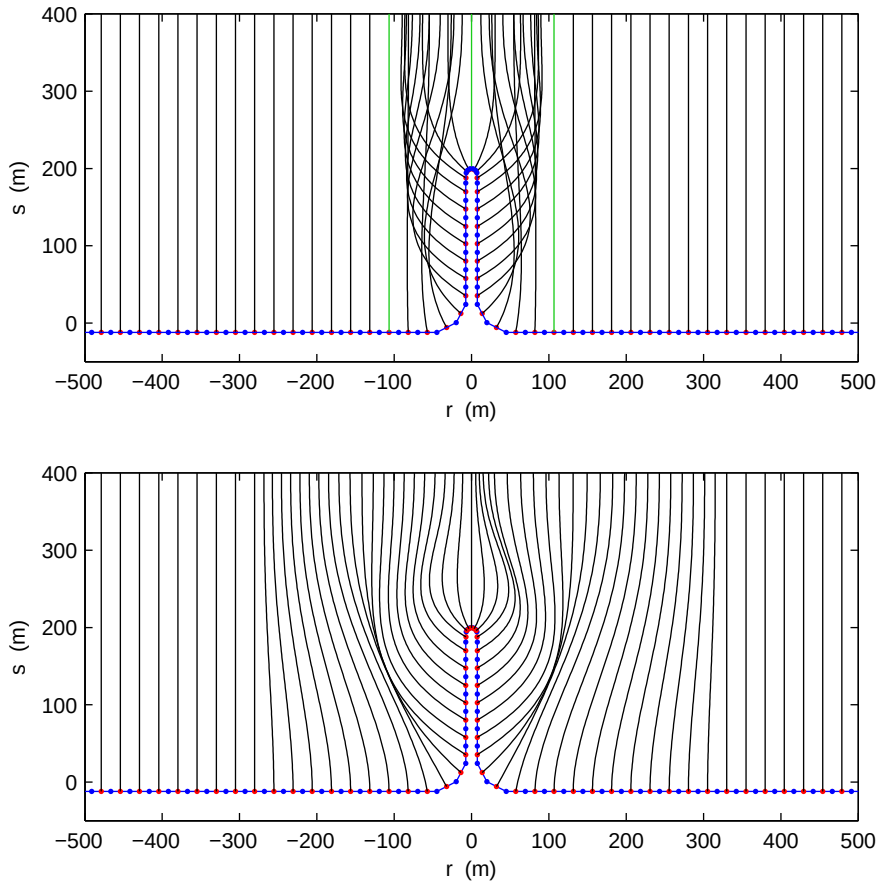

Figure 8.20: *Examples of curved profiles. Top: initial guess on κ_0. Bottom: Solution where κ_0 has been modified to avoid overlapping morphological elements.*

8.A.3 Examples of morphological evolution around a groyne

Figure 8.21 shows the morphological mesh and the bathymetry during initial conditions (top) and after half a year of morphological evolution (bottom). From the initial bathymetry it is seen that alongshore gradients in the bed level exist due to the curved coastal profiles along which the bed level is calculated. This can be limited further by allowing the exponent of the Dean type power profile to vary, although this has not been tested.

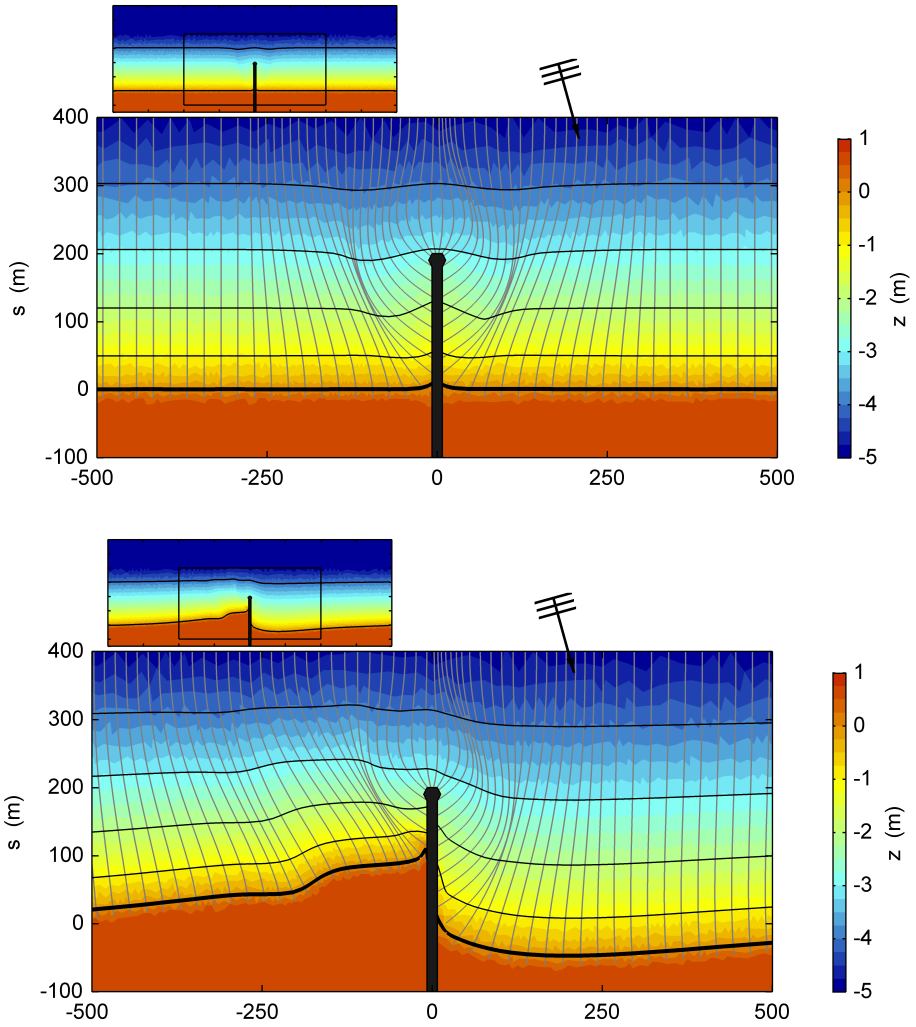

Figure 8.21: *Initial (top) and Final (bottom) bathymetry of a morphological simulation with the 1D hybrid morphological model with a curved baseline. The model breaks down shortly after the final time step.*

The morphological model responds to gradients in the littoral drift by deposition of sediment on the updrift side and erosion on the downdrift side of the groyne as would be expected. The model is furthermore capable of representing the discontinuous shoreline in (r, s)-space by the combination of the shoreline position itself (r_0, s_0) and the distance from the shoreline to the berm (used by the function for the active height of the profile).

The morphological model is however fairly unstable and some changes in the bathymetry are caused by the fact that the coastal profiles are allowed to change position after each morphological update of the shoreline position. Principally it is assumed that the method itself is volume conserving as long as the update of the shoreline position is volume conserving. In reality however, when changing the orientation of the coastal profiles some errors are introduced. Furthermore in order to avoid instabilities is is found necessary to filter the shoreline itself after a number of morphological updates. This introduces volume errors and false alongshore transport redistribution. The 1D

hybrid morphological model with the curved baseline was therefore rejected in this study because it's performance could not match that of the 1.5D model.

Chapter 9

Evaluation of Nourishment Schemes Based on Long-Term Morphological Modeling

Conference proceedings paper from The 33rd International Conference on Coastal Engineering 2012, Santander, Spain. Authors: Nicholas Grunnet[1], Sten Esbjørn Kristensen[1,2], Nils Drønen[1], Rolf Deigaard[1], Caroline Tessier[3] and Nicolas Forain[4]. Citation: Grunnet et al. (2012)

Abstract

A recently developed long-term morphological modelling concept is applied to evaluate the impact of nourishment schemes. The concept combines detailed two-dimensional morphological models and simple one-line models for the coastline evolution and is particularly well suited for long-term simulation. This hybrid concept is here applied to study the decadal morphological evolution of several nourishment scenarios in Dunkerque, France. The morphological simulations successfully allowed identifying the impact of beach versus shoreface nourishment scenarios on the background morphological behaviour of the study site. This study strongly indicates that the hybrid model may be used as an engineering tool to predict shoreline response following the implementation of a nourishment project.

Keywords: Morphological modelling, Nearshore bars, Beach nourishment

9.1 Introduction

The recently developed long-term morphological modelling concept proposed in Kristensen et al. (2010) is used in order to evaluate the impact of nourishment schemes. The concept tries to bridge

[1]DHI, Agern Allé 5, DK-2970 Hørsholm, Denmark
[2]Department of Mechanical Engineering, Technical University of Denmark, DK-2800 Kgs. Lyngby, Denmark
[3]DHI, 2/4 rue Edouard Nignon, 44372 Nantes, France
[4]Grand Port Maritime de Dunkerque, Terre-plein Guillain, 59386 Dunkerque, France

the gap between existing detailed two-dimensional morphological models and simple one-line models for the coastline evolution and hence is referred to as 1-D hybrid modelling. A first promising application of the hybrid model concept as an engineering tool for predicting effects of offshore breakwaters was given in Drønen et al. (2011) and Kristensen et al. (2012, 2013a). The hybrid morphological model has now also been used to simulate morphological response to groyne fields (Kristensen et al. (2013b)). This paper provides an additional application of the morphological modelling concept in relation to the design and optimisation of beach and shoreface nourishment projects. The concept is particularly well suited for long-term simulation and is here applied to study the decadal morphological evolution of several nourishment scenarios in Dunkerque, France.

The Dunkerque East Harbour breakwaters and dredged navigation channel act as sediment traps which effectively block the littoral drift to the downdrift beaches. Erosion has been ongoing for decades along these beaches backed by dikes and has now resulted in a severe marine flooding hazard of the low-lying and densely-populated hinterland. Yearly maintenance dredging is necessary to ensure a safe navigation depth. The high-quality dredged medium sand has traditionally been disposed offshore and thereby lost from the littoral zone. Aware of the interests which could be served by supplying this material onto the eroding beaches, the harbour authorities now wish to implement a scheme that both provides coastal protection to the threatened dikes and acts as a sand by-passing system past the harbour. DHI was commissioned to design such a scheme.

9.2 Study area

9.2.1 Environmental setting

Dunkerque is located on the southern North Sea part of the English Channel (see figure 9.1). Waves are incident from both the North Sea and the North Atlantic Ocean. Ocean waves that have propagated through the English Channel are somewhat attenuated. The mean annual significant offshore wave height at the -20 m isobath is about 0.9 m and the mean annual significant offshore wave period is about 6 s. During severe autumn and winter storms significant wave heights increase up to 4 to 5 m. A corresponding wave rose is also illustrated in figure 9.1.

Tides along the coast at Dunkerque are semidiurnal and macrotidal with a neap tidal range of about 3.5 m and a spring tidal range of about 5.5 m. The flood (ebb) tidal flow is in an ENE (WSW) direction. Associated tidal currents are slightly stronger during flood than during ebb and tidal ellipses are basically oriented parallel to the shore and are flat and rectilinear. At spring tide, the flow velocities at the surface are in the order of 1.4 m/s. Wind-driven currents are generated in the study area as the coastline is oriented parallel to the predominant westerly winds.

The seabed in the shoreface consists mainly of fine to medium sands, ranging from 125 to 500 μm. The beach face is characterized by fine sands ranging from 170 to 200 μm. Beach face slopes are typically ranging from 1/70 to 1/200.

9.2.2 Complex morphodynamic setting

The study area is located immediately east of the eastern breakwater of Dunkerque East Harbour and is characterised by the presence of numerous coastal structures (groynes, breakwaters and dikes), dredged channels and offshore sand banks.

The harbour breakwaters and dredged navigation channel act as sediment traps which effectively block the littoral drift to the downdrift beaches to the east of the harbour entrance. The updrift

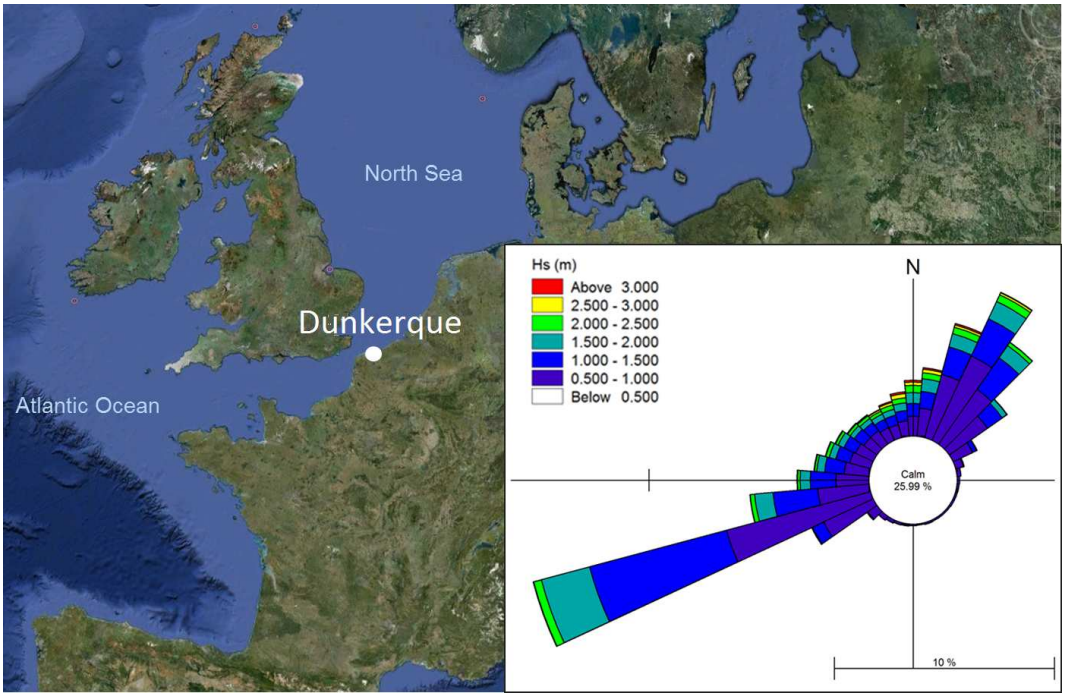

Figure 9.1: *Location of study site and 1979-2002 wave rose off Dunkerque.*

Figure 9.2: *Aerial view of Dunkerque East Harbour with indication of the study area (white box).*

impoundment of sediment and offshore disposal of dredged material has resulted in coastal erosion for decades along the beaches east of the harbour. Figure 9.2 shows groynes and detached breakwaters that are in place to mitigate the erosion. In order to prevent marine flooding of the low-lying and densely-populated hinterland, the beach is also backed by a coastal dike (located inside the white box in figure 9.2). The chronic lowering of the beach face in front of the coastal dike is threatening the safety of the dike and presents a severe marine flooding hazard. Comparison of historical bathymetric surveys yields an erosion on the order of 10,000 m^3/yr on the beach face seaward of the coastal dike.

The offshore bathymetry is characterized by a group of irregular sand banks called the Flemish

banks. These sand banks have a wavelength between 1 km and 10 km, and they are up to several tens of meters high. The sand banks are formed by tide-seabed interactions and are actively maintained by the tidal regime. In the vicinity of Dunkerque these banks are found to be migrating in an overall eastward direction at a rate up to 10 m/yr, Héquette et al. (2008).

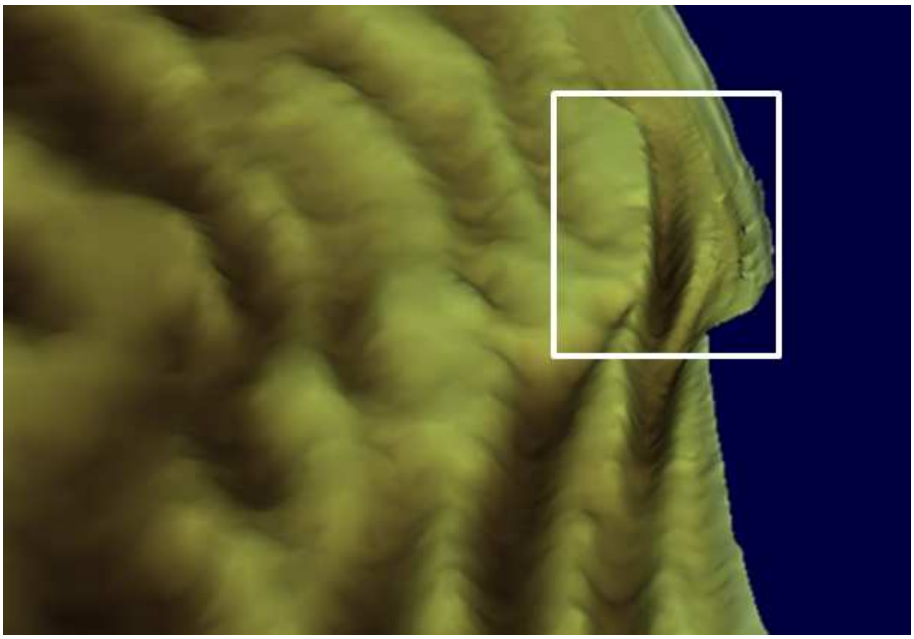

Figure 9.3: *3D representation of nearshore bathymetry off Dunkerque East Harbour: view from west (bottom) to east (top). The white box indicates the study site.*

9.3 Baseline study on a fixed bed

Prior to applying a morphodynamic feedback loop in the hybrid modelling approach, a baseline study was performed based on a 2D approach on a fixed bed. This first modelling step acts as a calibration of the individual wave, flow and sediment transport modules against measured behaviour, a prerequisite to the subsequent long-term modelling of shoreline predictions.

9.3.1 Process-based 2DH modelling

MIKE21 FM modules are used for the 2DH simulations of the wave field, flow field and sediment transport field. No description of the applied conventional wave and flow modules is given here, as these modules are widely reported in the literature. However, a short description of the sophisticated Q3D version of the sediment transport formulation of MIKE21 FM is presented hereafter.

The essence of the Q3D hydrodynamics model in the sediment transport formulation is the solution of the force balance across the water column. The model calculates instantaneous and time-averaged hydrodynamics and sediment transport in two horizontal directions. The temporal and vertical variations of shear stress, turbulence, flow velocity and sediment concentrations are resolved. The time evolution of the boundary layer due to combined wave/current motion is solved by means of the integrated momentum approach of Fredsoe (1984). The force balance includes contributions from the near bed orbital motion, forces associated with wave breaking (gradients of radiation stresses) and the sloping water surface.

The depth-averaged current speed and direction as well as the wave motion defined through a number of general parameters are input parameters to the sediment transport model; these are supplied by the 2DH modules. The sediment transport is then simulated by a time-varying model for the suspended sediment concentration determined from the settling and the vertical turbulent exchange of the sediment and the bed load transport is determined from the instantaneous bed shear stress; see Deigaard et al. (1986a).

9.3.2 Schematisation of forcing conditions

As pointed out by Latteux (1995), a small number of tides can be found to represent the whole spring-neap tidal cycle in such a way that their cumulative effect on bed morphology is similar to the effect of the sum of all tides in the cycle. The range of the selected tide, referred to as the morphological tide, was taken as 10% larger than the mean astronomical tidal range at Dunkerque, following results obtained in Grunnet et al. (2004).

A wave schematisation aims at reducing the wave climate into a choice of representative wave conditions. The choice of representative conditions was based on sediment transport calculations in such a way that the net transport in the study area derived from the whole climate is comparable - in intensity as well as direction - to the one deduced from the set of representative conditions. A choice of 37 representative wave conditions, each representing a directional sector including a range of wave heights and directions, was made to schematise the wave input. The selected wave conditions represent about 70% of the wave climate and approximately 90% of the transport. Each of the individual 37 wave conditions were run for the duration of the predefined morphological tide.

The wind climate was divided in classes of corresponding wave heights and directions.

9.3.3 Model set-up

An unstructured flexible mesh was constructed with a relatively high resolution in the study area on the order of 5 m. The mesh resolution gradually decreases towards the model boundaries and is as large as 250 m offshore and about 50 m along the lateral boundaries. The open sea boundary was located in water depths of approximately 20 m. The Dunkerque model contains about 220,000 computational elements and covers an area of approximately 40 km x 20 km.

The boundary conditions are composed of the schematic wave conditions and the water level variations from the morphological tide. Wind forcing is applied uniformly over the model domain.

An example of the required detailed 2DH approach can be inferred from figure 9.4 which illustrates wave roses along the study area: significant alongshore variability is found as a result of the strong refraction and attenuation of waves propagating over the offshore and shallow sand banks.

9.3.4 Calibration of the area model

The Dunkerque fixed bed model was calibrated against a comprehensive monitoring data set comprised of hourly wave, wind, current and water level measurements, grain size data and nearshore bathymetric surveys. An overall sediment budget was established based on the detailed area modelling of waves, currents and sediment transport over a typical year as represented by the 37 selected wind and wave conditions.

The resulting sediment budget is illustrated in figure 9.5. The figure shows a strong eastward-directed net transport in the tide-dominated zone with transport rates above 150,000 m^3/yr. In

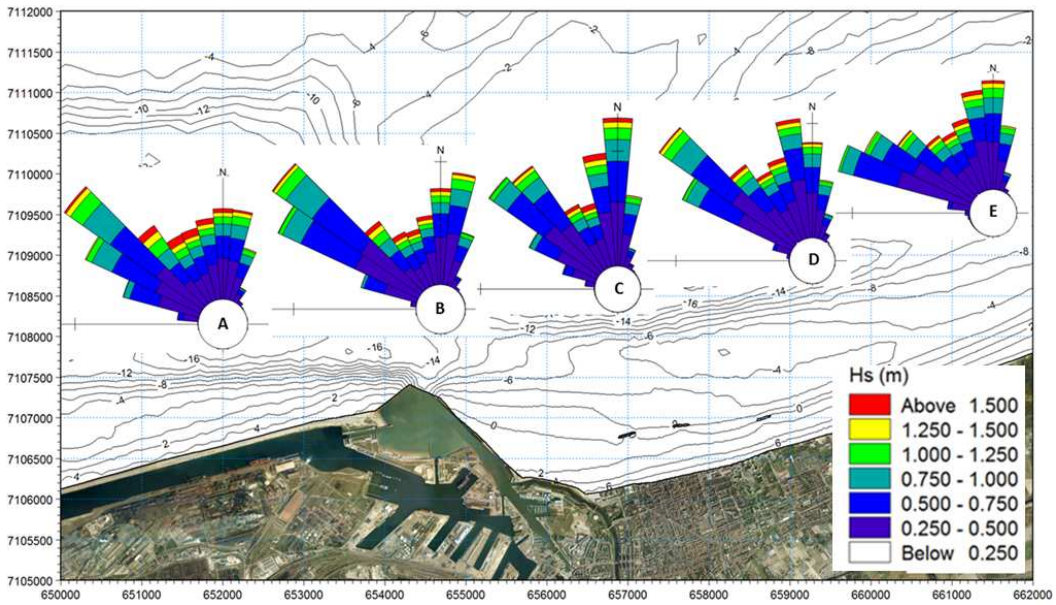

Figure 9.4: *Alongshore variability of 1979-2002 wave roses at selected locations off Dunkerque.*

the wave-dominated zone, net transport rates are also eastward-directed; however these rates are an order of magnitude smaller and found to be below 20,000 m^3/yr. In general, a low morphodynamic activity in the nearshore zone is found and erosion on the order 10.000 m^3/yr in front the coastal dike is confirmed.

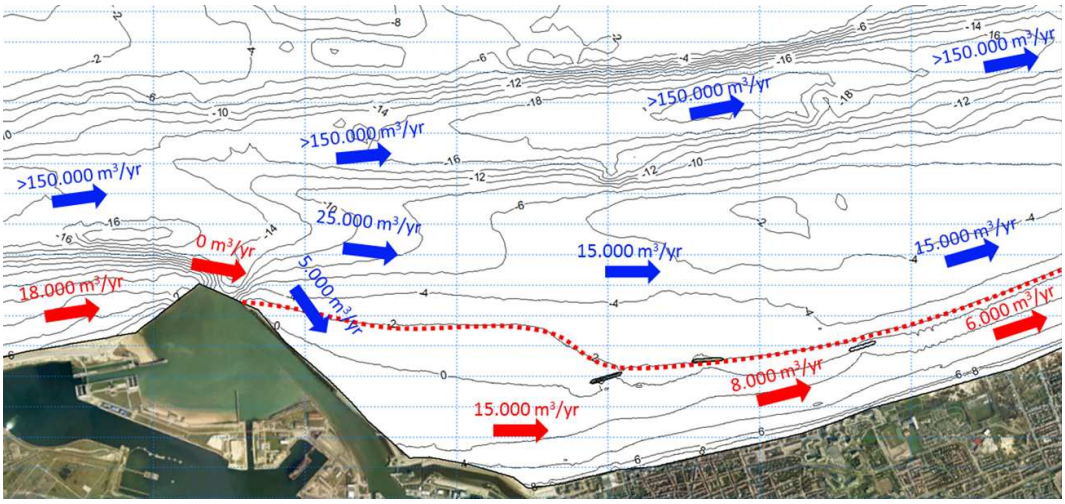

Figure 9.5: *Average yearly net transport rates off Dunkerque. Blue (red) arrows indicate tide dominated (wave dominated) net transport direction. The dotted red line indicates the seaward limit of wave action along the study site.*

9.4 Set-up of morphological model

9.4.1 Hybrid modelling concept

An in-depth description of the hybrid modelling concept is given in Kristensen et al. (2010); in the following, only a brief description is given. The hybrid morphological modelling concept uses detailed two-dimensional area models to describe the wave, current and sediment transport fields. When making the morphological update the evolution of the coastal profile is restrained by allowing only one or two degrees of freedom, such as the coastline position or the volume/position of a bar. The morphological evolution is therefore based on integrated sediment transport rates and rule-based descriptions of the profile evolution. The concept thus tries to bridge the gap between existing detailed two-dimensional morphological models and simple one-line models for the coastline evolution. The primary motivation of the concept is to (1) to improve the calculated longshore transport compared to that determined by conventional 1D transport models and (2) allow simulations over longer time spans by restraining the distortion of the coastal profile which often occurs in two-dimensional models due to difficulties in making a process-based simulation of the profile evolution based on modelling of the cross-shore transport.

For the present study, the morphological development is divided into two parts, namely the development of the shoreline and the development of a shoreface nourishment, each of which is further detailed in the following.

9.4.2 Definition of shoreline model

A linear profile is used to describe the active profile. The profile is defined in terms of a berm level, which is taken to be constant in the entire domain, a cross-shore position of the berm, a profile slope and a level of closure depth. The profile slope and level of closure depth is allowed to vary along the shoreline but is constant in time. The cross-shore position of the berm varies in both space and time. An additional parameter which defines the onshore limit of profile evolution is introduced. This parameter is used in the volume calculations of the coastal profile and allows the morphological model to take lowering of the active height into account for profiles where extensive erosion occurs in front of the dike.

Best fit of the coastal profile to the measured bathymetry yield estimates of the level of closure depth, the berm position and the profile slope. The fitted estimates are used to construct the coastline parameters, and subsequently some amount of smoothing is introduced. Note that the 1D parametric description of a salient behind an existing breakwater limits the representation of the salients to a decrease in profile slope, whereas the measured salient planforms are weakly two dimensional.

The spatial resolution of the coastal morphological elements varies from 50 to 100 m as indicated in figure 9.6. The seaward extension of the morphological grids shown in figure 9.6 is selected for illustrative purposes. The actual seaward extension used in the morphological simulations follow the seaward extent of the active coastal profile. The active height of the coastal profile varies along the modelled shoreline, from 6 m near the harbour of Dunkerque to 10 m near the Belgian border located about 12 km to the east.

The shoreline is updated by solving the 1D sediment continuity equation, where it is assumed that the coastal profile is displaced in the onshore/offshore direction in response to erosion/deposition

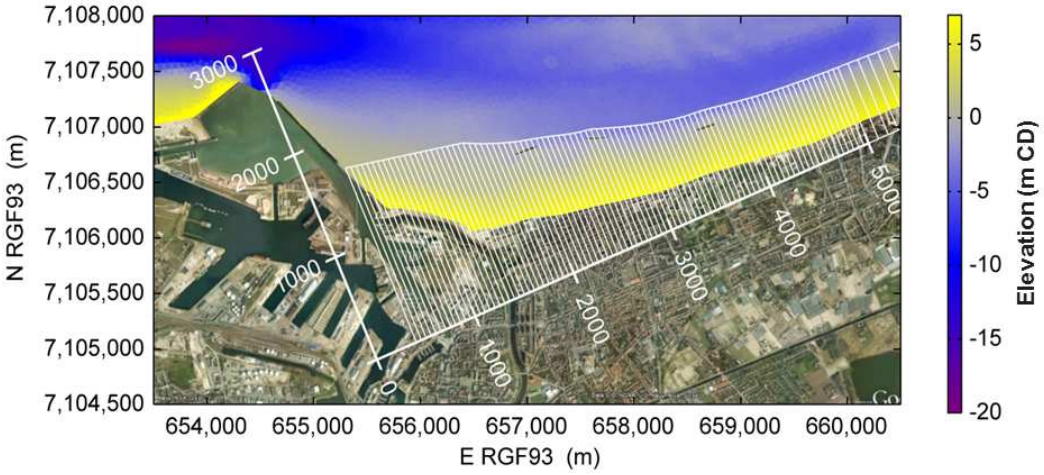

Figure 9.6: *Morphological coastal elements are indicated with white lines (in a locally defined coordinate system) superimposed on a post-nourishment bathymetry.*

respectively. Erosion/deposition is determined from gradients in the littoral drift and from offshore exchange of sediment which is particular important near Dunkerque East harbour due to sediment bypass.

Modified littoral drift

Separation of the longshore transport associated with changes to the upper shoreface from the transport causing morphological changes to the tidal channels and tidal banks has been difficult due to the complex bathymetric pattern in the area, the large tidal variation and significant transport in the tidal channels. A method defined here as the *cancellation method* has therefore been applied. In the cancellation method, the littoral drift used to simulate shoreline evolution, is modelled as the difference in transport between the present shoreline and the baseline shoreline, where the baseline shoreline is represented as the shoreline prior to beach nourishment. It is therefore possible to isolate the effect of nourishment on the shoreline and thereby limit artificial shoreline change in other parts of the model which may otherwise develop when simulating shoreline change over 10 years.

9.4.3 Model for evolution of shoreface nourishment

Evolution of the shoreface nourishment is modelled using a bar model, where the shoreface nourishment is parametrised by defining a cross-sectional volume, a width and a cross-shore position, in sections along the shore. Morphological evolution of the shoreface parameters is imposed by use of non-linear optimisation such that the development of the shoreface nourishment gives a best fit to the distribution of the erosion/deposition field predicted by MIKE21 FM.

The initial volume of the shoreface nourishment is defined invariant, and the morphological model is therefore only allowed to redistribute the nourishment alongshore and cross-shore. Transfer of sediment is however imposed for cases where the shoreface nourishment impinges to the active profile of the shoreline model, thereby feeding the shoreline with sediment and reducing the volume of the shoreface nourishment.

9.4.4 Definition of nourishment scenarios

The abundance of high-quality sandy sediments on site calls for a coastal protection solution based 100% on nourishment. Two types of nourishment scenarios were identified and proposed. The first is based solely on beach nourishment and the second is based on a coupling between beach and shoreface nourishment. Regardless of the nourishment scenario, suitable material for nourishment is available during the yearly maintenance dredging campaigns with borrow site grain sizes in the range 250-400 μm e.g. coarser sediments than the native sediments.

The characteristics of scenario 1 (plan view shown in figure 9.7) are the following:

- Beach nourishment along and parallel to the existing dike in order to obtain the same level of protection along the dike e.g. resulting in a change of depth contour orientation of approx. 20 deg in the study area.
- Nourishment volume of 1,500,000 m^3 distributed over 1,200 m with a 30 m wide dry beach levelled at +7.5 m CD.
- Increased beach slope from 1/200 to 1/70 as a result of coarser sediment.

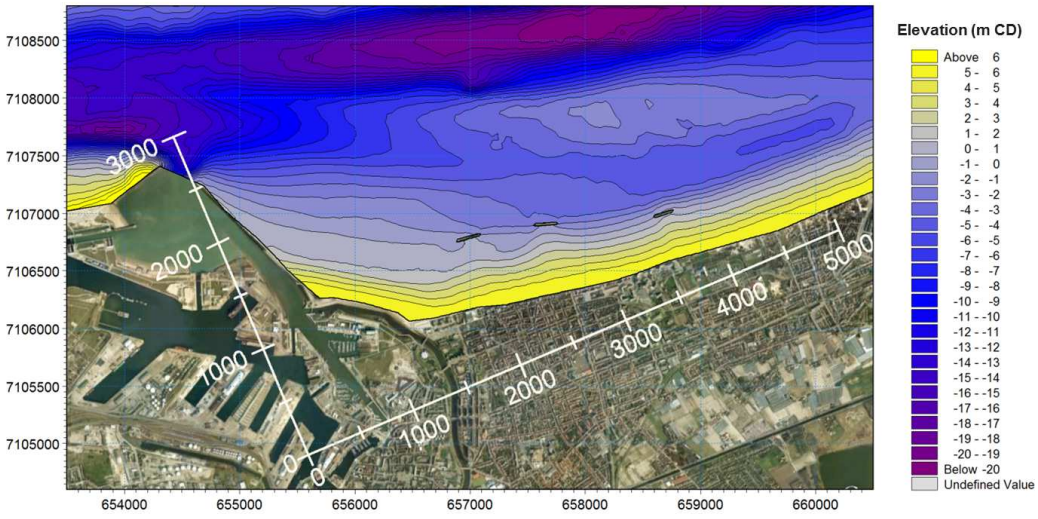

Figure 9.7: *Post-nourishment bathymetry for nourishment scenario 1.*

The characteristics of scenario 2 (plan view shown in figure 9.8) are the following:

- Beach nourishment is identical as in scenario 1.
- Submerged berm located roughly between isobath's 0 m and 3 m CD in front of dike.
- Shoreface nourishment of 700,000 m^3 distributed over 1,000 m.
- Maximum height of nourished berm on the order of 4 m.
- Submerged berm located approx. 500 m from harbour breakwater.

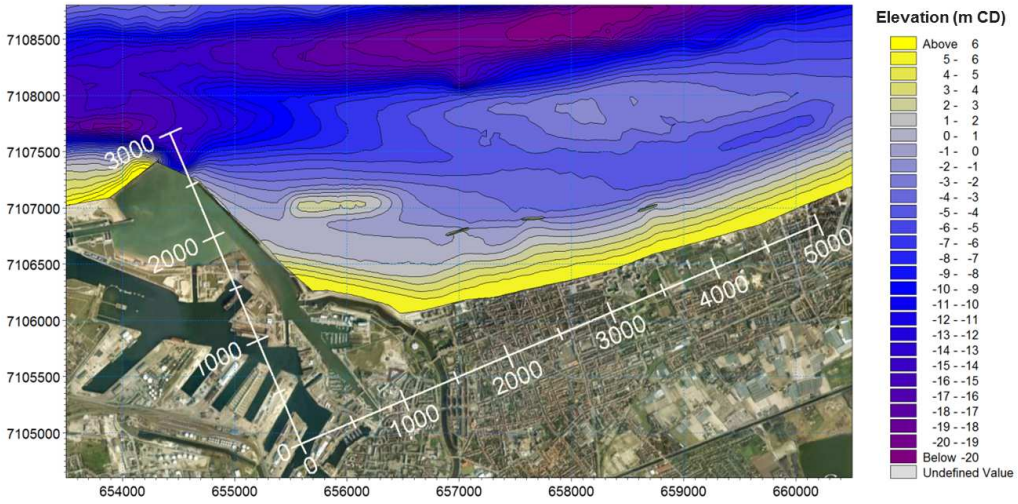

Figure 9.8: *Post-nourishment bathymetry for nourishment scenario 2.*

Although not presented in detail here, a total of five scenarios were defined, two of which are related to scenario 1 and three of which are related to scenario 2. The additional scenarios differ only by their geometric characteristics such as berm location and height and suggested maintenance schemes for the beach nourishment solution.

9.5 Simulation of morphological response

The hybrid modelling approach was used to simulate the morphological response of the various nourishment scenarios. A simulation period of 10 years was selected for all predictions of morphological development. All results shown hereafter are relative to the actual situation: recall that the previously defined cancellation method implies that the natural background morphological behaviour has been removed from all computations. Hence the results here show the relative impact of the nourishment solution. In the following, results are firstly shown individually for the two types of scenarios and secondly compared.

9.5.1 Beach nourishment alone

The bathymetric evolution after 10 years of morphological modelling is presented in figure 9.9 for nourishment scenario 1. The characteristics of the morphological impact are the following:

- Erosion of the western half of the nourished beach with a seabed lowering up to of 0.5 m.
- Accretion of the downdrift beaches to the east with a seabed rise up to 0.5 m.
- The morphological evolution for scenario 1 thus consists in a dynamic response towards a new equilibrium by which a change in orientation of the nourished beach occurs.

9.5.2 Beach and shoreface nourishment coupled

The bathymetric evolution after 10 years of morphological modelling is presented in figure 9.10 for nourishment scenario 2. The characteristics of the morphological impact are the following:

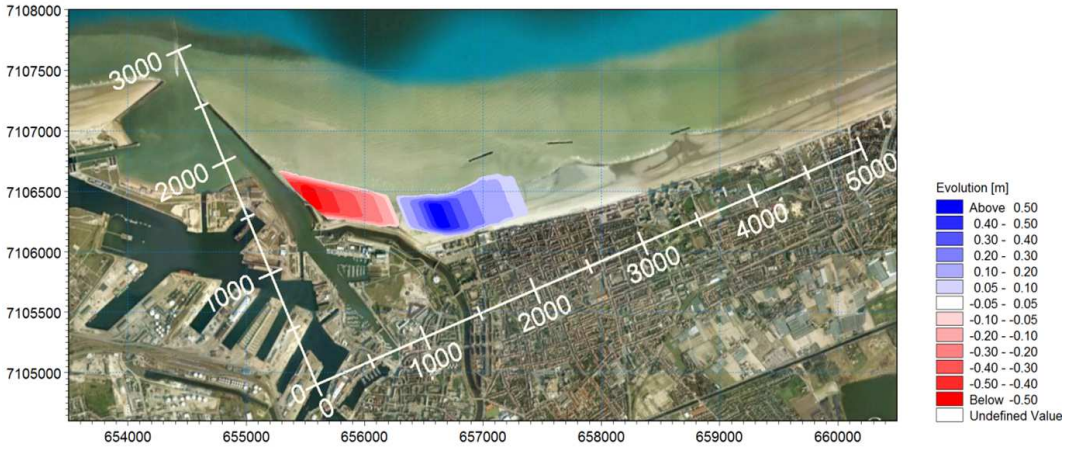

Figure 9.9: *Morphological response after 10 years of simulation: bathymetric evolution for scenario 1.*

- Attenuated erosion of the western half of the nourished beach with a seabed lowering reduced to less than 0.4 m.
- Attenuated accretion of the downdrift beaches with a seabed rise less than 0.4 m.
- Moderate erosion of the beaches in the breakwater area with a seabed lowering up to 0.05 m.
- Onshore and alongshore migration of the shoreface nourishment (very strong migration the first 2-3 years after implementation).
- Perturbation of tidal channel dynamics to the north-east of the nourished berm.

The morphological evolution for scenario 2 thus consists in (1) an attenuated response towards a new equilibrium by which a change in orientation of the nourished beach occurs, (2) a rapid migration of the nourished berm, and (3) a moderate erosion of the beaches further downdrift - note that with an average slope of approximately 1/70, a seabed lowering on the order of 0.05 m corresponds to a shoreline retreat of 3.5 m in 10 years.

9.5.3 Comparison of nourishment scenarios

A comparison of the five modelled nourishment scenarios is given hereafter, however only impacts of scenario 1 and 2 are reported here. The comparison is based on the spatial and temporal evolution of the littoral drift immediately after the implementation of the nourishment and after 10 years of evolution. The analysis covers the coastal stretch impacted by the nourishment e.g. a few kilometres east of the harbour breakwaters. Note that in the applied local coordinate system, the coastal dike is located between 400 m and 1,400 m from the origin.

The positive and negative impacts are significant immediately following the implementation of the various nourishment schemes (see figure 9.11):

- Increased littoral drift for both scenarios as a result of the new shoreline orientation e.g. erosion of the nourished beach on the order of 40,000 m^3/yr and subsequent increased downdrift supply.

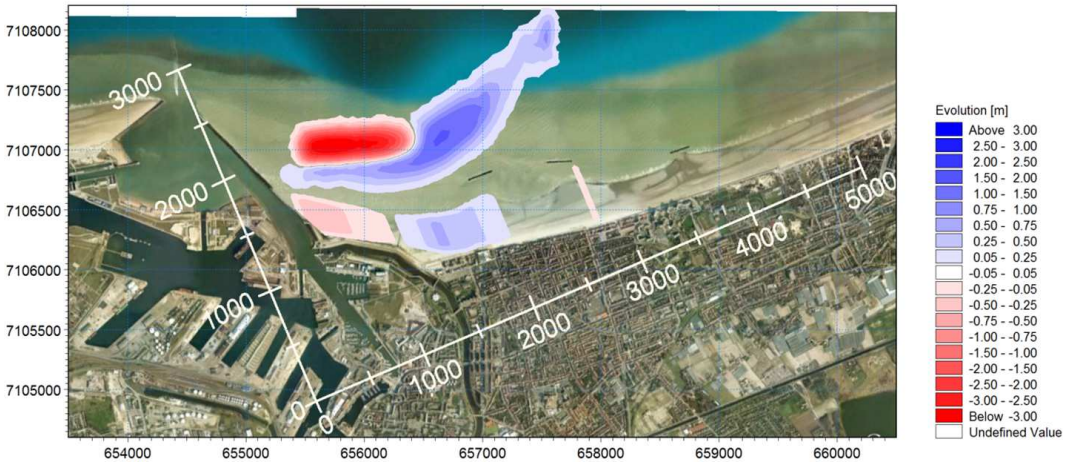

Figure 9.10: *Morphological response after 10 years of simulation: bathymetric evolution for scenario 2.*

- Deposition on the order of 40,000 m^3/yr immediately downdrift of the nourishment for both nourishment scenarios.
- The shoreface nourishment decreases the littoral drift east of the dike (2,000 m to 3,000 m) due to the breakwater effect of the submerged berm.

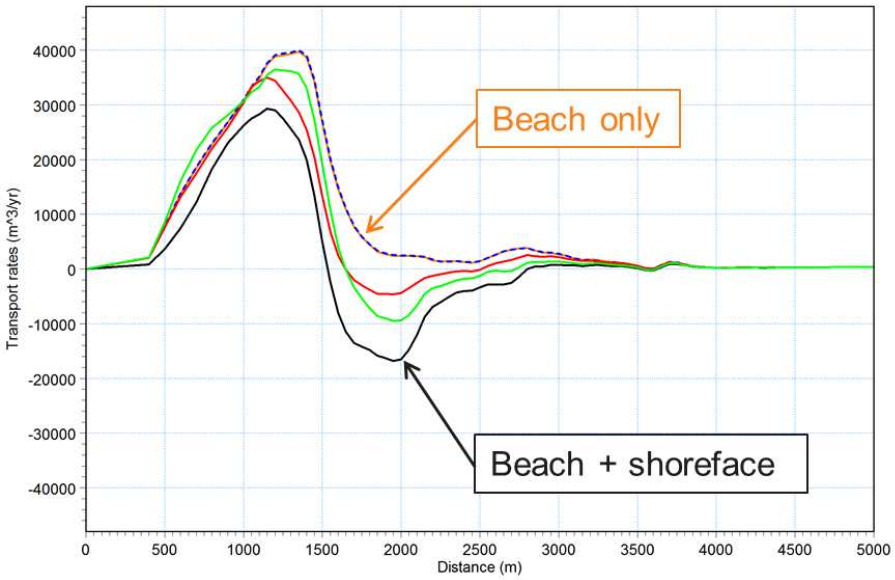

Figure 9.11: *Littoral drift immediately after implementation of nourishment scheme for various nourishment schemes (t = 0 year); nourishment scenarios presented in this paper are highlighted. Positive (negative) transport corresponds to increased (decreased) littoral drift with respect to pre-nourishment situation.*

After 10 years of morphological evolution, the positive and negative impacts of the nourishment scenarios are attenuated (see figure 9.12):

- Continuous erosion of the nourished beach, however at slower rate reduced to approximately 20,000 m^3/yr.
- Downdrift beach tends towards a new equilibrium, leading to a reduction in transport gradients in this coastal stretch.
- Continuous eastward propagation of negative impact of the shoreface nourishment.

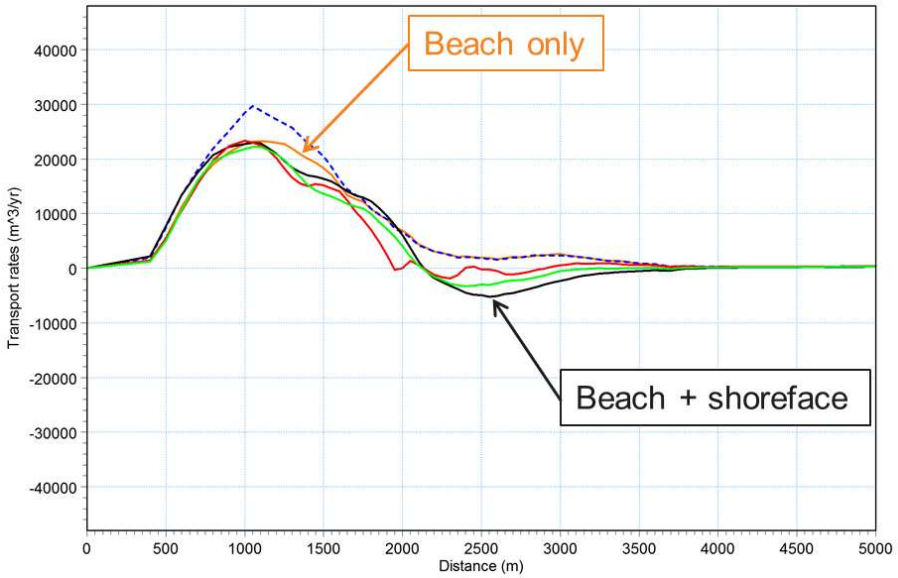

Figure 9.12: *Littoral drift 10 years after implementation of nourishment scheme for various nourishment schemes (t = 10 years); nourishment scenarios presented in this paper are highlighted. Positive (negative) transport corresponds to increased (decreased) littoral drift with respect to pre-nourishment situation.*

The evolution of the nourishment volume in its initial location was also investigated in order to define the required volume necessary to maintain the initial level of protection of the coastal dike constant throughout a 10-year period. An illustration of this evolution is presented in figure 9.13. The figure clearly shows the significant erosion of the shoreface nourishment caused by the rapid migration of the submerged berm. Hence, the level of protection supplied by the shoreface nourishment decreases rapidly in time and the order of magnitude for maintenance nourishment is above 100,000 m^3/yr, specifically in the first years. On the opposite, a moderate and gradually decreasing erosion of the beach nourishment is observed: maintenance nourishment is on the order of 40,000 m^3/yr and decreasing with time.

Based on these results, the pure beach nourishment solution was selected for implementation.

9.6 Conclusions

The hybrid model was successfully applied to predict the 10-year morphological evolution of individual beach and shoreface nourishment projects as well as a combination of these. The morphological modelling conclusively showed that shoreface nourishment is not suited for the present site as (1) the migration of the berm interacts with the tidal channels, (2) the downdrift supply of

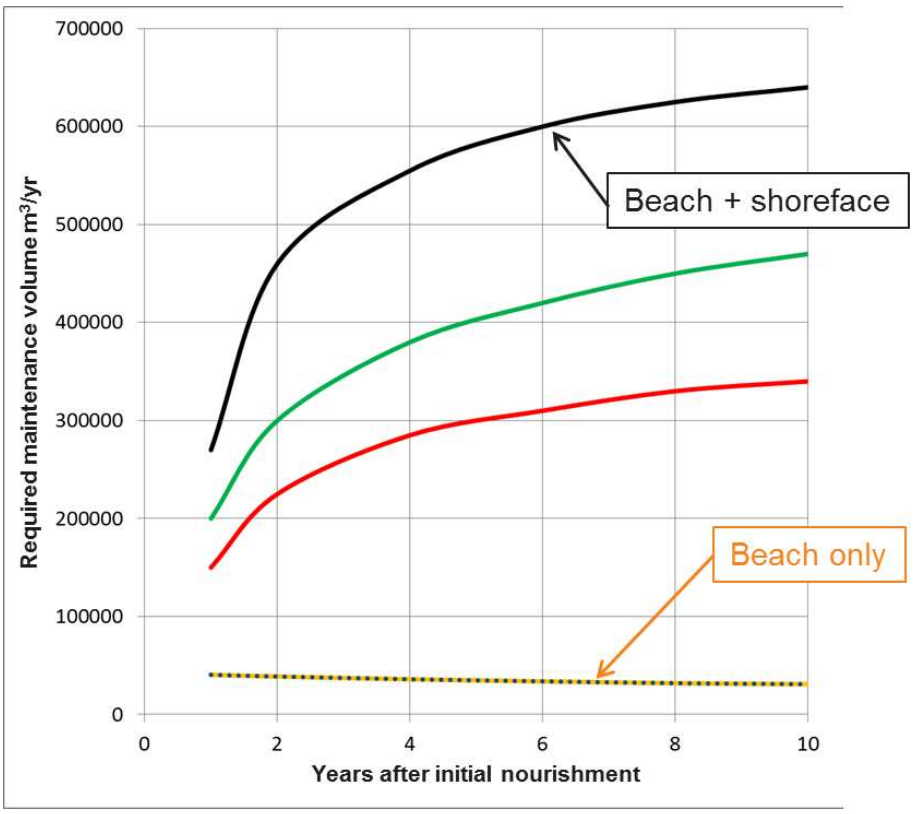

Figure 9.13: *Required maintenance volume to maintain the initial level of protection of the dike.*

sediment decreases, and (3) the required volume to maintain the initial level of protection increases in time. Beach nourishment was consequently selected as the preferred solution as (1) it evolves at a slower rate, (2) increases the downdrift supply of sand, and (3) does not perturbate the background morphological system.

This study strongly indicates that the hybrid model may be used as an engineering tool to predict shoreline response following a nourishment project. The selected nourishment project e.g. the beach nourishment alone, will be fully implemented in 2012 during the yearly autumn maintenance dredging campaigns. A monitoring program has been scheduled to follow the morphological evolution of the nourishment.

Acknowledgements

Dunkerque Harbour is acknowledged for entrusting DHI to apply a research version of the hybrid model concept for this study. The second author was granted a leave of absence from his ph.d. study at the Technical University of Denmark, to participate in application and further development of the hybrid modelling concept to the nourishment schemes in Dunkerque, France.

Chapter 10

Conclusion

Hybrid morphological modelling concept

The modelling concept is intended to bridge the gap between traditional 2D models, and models which are traditionally used for medium term and long-term morphological modelling. This is basically done by allowing morphological evolution in terms of evolving a set of coastal parameters. The evolution of the coastal parameters is based on information determined in a traditional 2D model and from *weak* forcing from behaviour-oriented models.

The key point in hybrid morphological modelling is that it is possible to quantify morphological evolution of certain morphological features using the detailed information contained in a traditional 2D coastal model, while effects from coastal processes which are not accurately described can be prescribed using behaviour-oriented modelling.

Shoreline models

Two types of shoreline models have been developed and examined in this study, a 1D and a 1.5D model. Both models use gradients in the littoral drift to evolve the volume of coastal profiles distributed along a shoreline. The models differ in that the 1.5D model allows the cross-shore distribution of an erosion/deposition field to modify the form of the coastal profile, while the 1D model assumes that changes to shoreline defines changes to the entire coastal profile. The shoreline models may be used to simulate morphological evolution involving substantial shoreline response, including response of the beach up to a given berm level. This is possible without the need for resolving shoreline movement due to tidal action because the effect of such short term processes is prescribed rather than modelled.
The models are used to simulate development towards equilibrium conditions, where gradients in the littoral drift disappear. The fact that the models can be used to predict transient evolution and equilibrium solutions makes them an interesting tool.

Due to it's simplicity, the 1D model is an excellent candidate as an engineering tool within the hybrid morphological modelling concept. By defining active and inactive features, the model may be applied to a wide range of problems. And it may be applied with a high degree of confidence because it is closely linked to a process based 2D sediment transport model. This has been confirmed in three case studies in which the 1D hybrid model has been used with great success as reported

in Drønen et al. (2011); Grunnet et al. (2012); Kristensen et al. (2012).
Work on incorporating the 1D model within MIKE21 FM has therefore also begun, although alternative and more general implementations of the the model are constantly being examined.

Previous attempts at developing multi-line model implementations within the hybrid morphological modelling concept have proven unsuccessful mainly because the solution was found to be very sensitive to the definition of the cross-shore interface between the morphological elements. The 1.5D hybrid model was therefore developed as an attempt to formulate a hybrid model which includes profile evolution, while limiting effects due to the definition of the morphological elements. The 1.5D model has been very useful because it can be applied to problems of a 2D Nature. The model has therefore been used to gather insight to the morphological response around detached breakwaters and shore normal groynes. Future application of the 1.5D hybrid model is however uncertain because it is not a robust as the 1D model.
Possible future derivations of the 1.5D hybrid model could be based on smaller morphological elements which do not span the entire coastal profile, while continuing to act by grouping a number of computational elements.

Bar models
Three different implementations of bar models have been discussed during this study. The focus of the models is to quantify alongshore migration of a bar, since the morphological evolution for this problem is expected to be governed by longshore transport processes and horizontal 2D circulation currents - processes which are well described by the 2D coastal model. The first model (streamline model) is only applicable to alongshore migration of a bar front because it can only handle situations where the longshore transport is aligned with the existing bar. Attempts at applying the two other models (optimisation and bar-moment) to simulate morphological evolution of longshore bars with rip-current development have been undertaken (but not documented) with limited success. The models are constrained by a number of challenges:

- Cross-shore transport processes govern this type of problem, but are ill-described by the applied 2D coastal model
- Behaviour-oriented forcing needs to be strong in order to stabilise the model, thereby violating the principle of applying a *weak* behaviour-oriented forcing to the model
- Complex evolution due to bar-bar interaction (splitting and joining of bars) cannot be described with the present approach
- Separation of morphological evolution of bar and morphological evolution of shoreline has proven difficult in particular for cases where the bar amplitude is small

Hybrid morphological modelling of bar dynamics is therefore far from a mature state and will require both improvements to the existing cross-shore transport calculation and an implementation which is different from the implementations tested in this study. Representing a bar as a coherent two-dimensional structure which is allowed to deform and migrate could as an example be an interesting alternative to the existing representation of the bar which uses a number of cross-sectional profiles for the morphological evolution.
Alternatively, the existing method could be applied to situations where bar dynamics are prescribed rather than modelled. This could be interesting for understanding overall effects of bar dynamics on the littoral drift and subsequent shoreline evolution.

Bibliography

Aagaard, T. and Greenwood, B. (2008), Infragravity wave contribution to surf zone sediment transport - The role of advection, in *Marine Geology*, volume 251, pp. 1–14.

Aelbrecht, D. and Denot, T. (1999), 2D and 3D Modelling of Wave-Driven Currents in Presence of a Groin System in a Tidal Sea, *Coastal Engineering and Marina Developments*, 3:35–44.

Axe, P., Ilic, S. and Chadwick, A. (1996), Evaluation of beach modelling techniques behind detached breakwaters, in Edge, B. L. (editor), *Proceedings of the 25th International Conference on Coastal Engineering*, volume 3, pp. 2036–2049, ASCE, Orlando, Florida.

Badiei, P., Kamphuis, J. W. and Hamilton, D. G. (1994), Physical experiments on the effects of groins on shore morphology, in Edge, B. L. (editor), *Proceedings of the 24th International Conference on Coastal Engineering*, pp. 1782–1796, ASCE, Kobe, Japan, ISSN 2156-1028.

Bakker, W. T. (1969), The Dynamics of a Coast with a Groyne System, in *Proceedings of the 11th International Conference on Coastal Engineering*, pp. 492–517, ASCE, London, United Kingdom.

Basco, D. R. and Pope, J. (2004), Groin Functional Design Guidance from the Coastal Engineering Manual, *Journal of Coastal Research*, SI 33:121–130.

Battjes, J. A. and Janssen, J. P. F. M. (1978), Energy loss and setup due to breaking of random waves, in *Proceedings of the 16th International Conference on Coastal Engineering*, volume 1, pp. 569–587, ASCE, Hamburg, Germany.

van den Berg, N., Falqués, A. and Ribas, F. (2011), Long-term evolution of nourished beaches under high angle wave conditions, *Journal of Marine Systems*, 88:102–112.

Brøker, I., Zyserman, J., Madsen, E. Ø., Mangor, K. and Jensen, J. (2007), Morphological Modelling: A Tool for Optimisation of Coastal Structures, *Journal of Coastal Research*, 23(5):1148–1158.

Callaghan, D. P., Saint-Cast, F., Nielsen, P. and Baldock, T. E. (2006), Numerical Solutions of the Sediment Conservation Law; A Review and Improved Formulation for Coastal Morphological Modelling, *Coastal Engineering*, 53:557–571.

Capobianco, M., Vriend, H. J. D., Nicholls, R. J. and Stive, M. J. F. (1994), Application of a Parametric Long Term Model Concept to the Delray Beach Nourishment Program, in *Coastal Dynamics*, pp. 391–401, ASCE.

Carter, T. G., Liu, P. L.-F. and Mei, C. C. (1973), Mass-transport by waves and offshore sand bedforms, in *Journal of Waterways Harbors and Coastal Engineering Division*, American Society of Civil Engineers.

CEM (2002a), *Coastal Engineering Manual, Part V Chapter 3, Shore Protection Projects*, US Army Corps of Engineers, Washington, DC.

CEM (2002b), *Coastal Engineering Manual, Part VI Chapter 5, Fundamentals on Design*, US Army Corps of Engineers, Washington, DC.

Cowell, P. J., Stive, M. J. F., Niedoroda, A. W., Swift, D. J. P., de Vriend, H. J., Buijsman, M. C., Reed, C. W. and de Boer, P. L. (2003a), The Coastal-Tract (Part 2): Application of Aggregated Modeling of Low-Order Coastal Change, *Journal of Coastal Research*, 19(4):828–848.

Cowell, P. J., Stive, M. J. F., Niedoroda, A. W., de Vriend, H. J. and Swift, D. J. P. (2003b), The Coastal-Tract (Part 1): A Conceptual Approach to Aggregated Modeling of Low-Order Coastal Change, *Journal of Coastal Research*, 19(4):812–827.

DCA (2008), Vestkysten 2008, Technical report, Danish Coastal Authorities, Højbovej 1, DK-7620 Lemvig.

Dean, R. G. and Yoo, C.-H. (1992), Beach-Nourishment Performance Predictions, *Journal of Waterway, Port, Coastal and Ocean Engineering*, 118:567–585.

Deigaard, R., Drønen, N., Fredsoe, J., Jensen, J. H. and Jørgensen, M. P. (1999), A morphological stability analysis for a long straight barred coast, *Coastal Engineering*, 36:171–195.

Deigaard, R., Fredsoe, J. and Hedegaard, I. B. (1986a), Mathematical Model for Littoral Drift, *Journal of Waterway, Port, Coastal and Ocean Engineering*, 112(3):115–128.

Deigaard, R., Fredsoe, J. and Hedegaard, I. B. (1986b), Suspended Sediment in the Surf Zone, *Journal of Waterway, Port, Coastal and Ocean Engineering*, 112(1):115–128.

Deigaard, R., Justesen, P. and Fredsoe, J. (1991), Modelling of undertow by a one-equation turbulence model, *Coastal Engineering*, 15:431–458.

Drønen, N. and Deigaard, R. (2007), Quasi-three-dimensional modelling of the morphology of longshore bars, *Coastal Engineering*, 54:197–215, ISSN 03783839.

Drønen, N., Kristensen, S., Taaning, M., Elfrink, B. and Deigaard, R. (2011), Long term modeling of shoreline response to coastal structures, in *The Proceedings of the Coastal Sediments*, World Scientific, Miami, Florida.

Elfrink, B. and Baldock, T. (2002), Hydrodynamics and sediment transport in the swash zone: a review and perspectives, *Coastal Engineering*, 45:149–167.

Engelund, F. and Fredsoe, J. (1976), A Sediment Transport Model for Straight Alluvial Channels, *Nordic Hydrology*, 7:293–306.

Falqués, A., Coco, G. and Huntley, D. A. (2000), A Mechanism for Generation of Wave-driven Rhythmic Patterns in the Surf Zone, *Journal of Geophysical Research*, 105(C10):24071–24087.

Fredsoe, J. (1984), Turbulent boundary layer in wave-current motion, *Journal of Hydraulic Engineering*, 110(8):1103–1119.

Fredsoe, J., Andersen, O. H. and Silberg, S. (1985), Distribution of Suspended Sediment in Large Waves, *Journal of Waterway, Port, Coastal and Ocean Engineering*, 111(6):1041–1059.

Fredsoe, J. and Deigaard, R. (1992), *Mechanics of Coastal Sediment Transport*, Advanced Series on Ocean Engineering, World Scientific.

Gíslason, K., Fredsoe, J., Diegaard, R. and Sumer, B. M. (2009), Flow under standing waves Part1. Shear stress distribution, energy flux and steady streaming, *Coastal Engineering*, 56:341–362.

Gourlay, M. R. (1974), Wave set-up and wave generated currents in the lee of a breakwater or headland, in Edge, B. L. (editor), *Proceedings of the 14th International Conference on Coastal Engineering*, volume 3, pp. 1976–1995, ASCE, Copenhagen, Denmark.

Grunnet, N., Brøker, I., Clausen, E. and Sørensen, P. (2009), Improving Bypass and Increasing Navigation Depth: A Vision for Hvide Sande Harbour, Denmark, in Mizuguchi, M. and Sato, S. (editors), *Coastal Dynamics*, volume 6, World Scientific.

Grunnet, N., Kristensen, S. E., Drønen, N., Deigaard, R., Tessier, C. and Forain, N. (2012), Evaluation of nourishment schemes based on long-term morphological modeling, in Smith, J. M. (editor), *Proceedings of the 33rd International Conference on Coastal Engineering*, Santander, Spain.

Grunnet, N., Walstra, D. J. R. and Ruessink, B. G. (2004), Process-based modeling of a shoreface nourishment, *Coastal Engineering*, 51(7):581–607.

Grunnet, N. M. and Hoekstra, P. (2004), Alongshore variability of the multiple barred coast of Terschelling, The Netherlands, *Marine Geology*, 203:23–41.

Hansen, H. F., Deigaard, R. and Drønen, N. (2004), A numerical hybrid model for the morphology of a barred coast with a river mouth, in Smith, J. M. (editor), *Proceedings of the 29th International Conference on Coastal Engineering*, pp. 2607–2619, World Scientific, Lisbon, Portugal.

Hanson, H. (1989), GENESIS - A Generalized Shoreline Change Model, *Journal of Coastal Research*, 5(1):1–27.

Hanson, H., Aarninkhof, S., Capobianco, M., Jiménez, J. A., Larson, M., Nicholls, R. J., Plant, N. G., Southgate, H. N., Steetzel, H. J., Stive, M. J. F. and de Vriend, H. J. (2003), Modelling of Coastal Evolution on Yearly to Decadal Time Scales, *Journal of Coastal Research*, 19(4):790–811.

Hanson, H. and Kraus, N. C. (1990), Shoreline response to a single transmissive detached breakwater, in Edge, B. L. (editor), *Proceedings of the 22nd International Conference on Coastal Engineering*, volume 5, pp. 2034–2046, ASCE, Delft, The Netherlands.

Hanson, H. and Kraus, N. C. (2011), Long-term evolution of a long-term evolution model, *Journal of Coastal Research*, SI(57):118–129, ISSN 07490208, 15515036.

Hanson, H. and Larson, M. (2004), Implications of morphodynamic time scale for coastal protection, in Smith, J. M. (editor), *Proceedings of the 29th International Conference on Coastal Engineering*, pp. 2620–2632, World Scientific, Lisbon, Portugal.

Harris, L. B. (1993), The Seaport, Table Bay. An archaeological and historical perspective, ECU Research Report 8, East Carolina University.

Héquette, A., Hemdane, Y. and Anthony, E. J. (2008), Sediment transport under wave and current combined flows on a tide-dominated shoreface, northern coast of France, *Marine Geology*, 249(3-4):226–242.

Holthuijsen, L. H., Booij, N. and Herbers, T. H. C. (1989), A prediction model for stationary short-crested waves in shallow water with ambient currents, *Coastal Engineering*, 13(1):23–54, ISSN 03783839.

Hsu, T. W., Jan, C. D. and Wen, C. C. (2003), Modified McCormicks model for equilibrium shorelines behind a detached breakwater, *Ocean Engineering*, 30(15):1887 – 1897, ISSN 0029-8018.

Hulsbergen, C. H., Bakker, W. T. and van Bochove, G. (1976), Experimental Verification of Groyne Theory, in *Proceedings of the 15th International Conference on Coastal Engineering*, pp. 1439–1457, ASCE, Honolulu, Hawaii.

Ilic, S., Chadwick, A. J. and Fleming, C. (2005), Investigation of detached breakwaters. Part 2 - Morphodynamics, *Proceedings of the Institution of Civil Engineers: Maritime Engineering*, 158(4):163–172, ISSN 17417597, 17517737.

Johnson, H. K. (2004), Coastal area morphological modelling in the vicinity of groins, in Smith, J. M. (editor), *Proceedings of the 29th International Conference on Coastal Engineering*, pp. 2646–2658, World Scientific, Lisbon, Portugal.

Johnson, H. K. and Zyserman, J. A. (2002), Controlling spatial oscillations in bed level update schemes, *Coastal Engineering*, 46(2):109 – 126, ISSN 0378-3839.

Kærgaard, K. H. (2011), *Numerical modeling of shoreline undulations*, Ph.D. thesis, Technical University of Denmark.

Kamphuis, J. W. (1991a), Alongshore Sediment Transport Rate, *Journal of Waterway, Port, Coastal and Ocean Engineering*, 117(6):624–640.

Kamphuis, J. W. (1991b), Alongshore Sediment Transport Rate Distribution, in *Coastal Sediments*, pp. 170–183.

Kraus, N. C., Hanson, H. and Blomgren, S. H. (1994), Modern functional design of groin systems, in Edge, B. L. (editor), *Proceedings of the 24th International Conference on Coastal Engineering*, pp. 1327–1342, ASCE, Kobe, Japan.

Kristensen, S., Deigaard, R., Taaning, M., Fredsøe, J., Drønen, N. and Jensen, J. H. (2010), Long term morphological modelling, in Smith, J. M. and Lynett, P. (editors), *Proceedings of the 32nd International Conference on Coastal Engineering*, ASCE, Shanghai, China, ISSN 2156-1028.

Kristensen, S. E., Deigaard, R., Drønen, N., Fredsoe, J. and Luger, S. (2012), Morphological modelling of the response to a shipwreck - a case study at Cape Town, in Smith, J. M. and Lynett, P. (editors), *Proceedings of the 33rd International Conference on Coastal Engineering*, ASCE, Santander, Spain.

Kristensen, S. E., Drønen, N., Deigaard, R. and Fredsoe, J. (2013a), Hybrid morphological modelling of shoreline response to a detached breakwater, *Coastal Engineering*, 71:13–27.

Kristensen, S. E., Drønen, N., Deigaard, R. and Fredsoe, J. (2013b), Hybrid morphological modelling of the response to groyne fields, unpublished, manuscript intended for Coastal Engineering.

Lagarias, J. C., Reeds, J. A., Wright, M. H. and Wright, P. E. (1999), Convergence properties of the Nelder-Mead simplex method in low dimensions, *SIAM journal on optimization*, 9(1):112–147, ISSN 1052-6234.

Latteux, B. (1995), Techniques for long-term morphological simulation under tidal action, *Marine Geology*, 126(1-4):129–141.

Laustrup, C. and Madsen, H. T. (1998), Evaluation of the Effect of 20 Years of Nourishment, in Edge, B. L. (editor), *Proceedings of the 26th International Conference on Coastal Engineering*, ASCE, Copenhagen, Denmark.

Laustrup, C., Madsen, H. T., Sørensen, P. and Brøker, I. (1996), Comparison of Beach and Shoreface Nourisment Torshmide Tange, Denmark, in Edge, B. L. (editor), *Proceedings of the 25th International Conference on Coastal Engineering*, ASCE, Orlando, Florida.

Lesser, G. R., Roelvink, J. A., van Kester, J. A. T. M. and Stelling, G. S. (2004), Development and validation of a three-dimensional morphological model, *Coastal Engineering*, 51:883–915.

Long, W., Kirby, J. T. and Shao, Z. (2008), A Numerical Scheme for Morphological Bed Level Calculations, *Coastal Engineering*, 55:167–180.

Mangor, K. (2004), *Shoreline Management Guidelines*, DHI Water, Environment & Health, 3rd edition.

Mangor, K., Brøker, I. and Hasløv, D. (2008), Waterfront Developments in Harmony with Nature, *Terra et Aqua*, 111.

McCormick, M. E. (1993), Equilibrium shoreline response to breakwaters, *Journal of Waterway, Port, Coastal and Ocean Engineering*, 119(6):657–670, ISSN 0733950x, 19435460.

Mory, M. and Hamm, L. (1997), Wave height, setup and currents along a detached breakwater submitted to regular or random wave forcing, *Coastal Engineering*, 31(1-4):77–96, ISSN 03783839.

Nam, P. T., Larson, M., Hanson, H. and Hoan, L. X. (2011), A Numerical model of beach morphological evolution due to waves and currents in the vicinity of coastal structures, *Coastal Engineering*, 58:863–876, ISSN 0378-3839.

Nielsen, P. (1992), *Coastal Bottom Boundary Layers and Sediment Transport*, volume 4 of *Advanced Series on Ocean Engineering*, World Scientific.

Nir, Y. (1976), Detached breakwater, groynes and artificial structures on the Mediterranean shore and their influence on the structure of the Israeli shore, Rep 3, 76/2, Ministry of Industry and commerce, Geological institute, marine geology section, Jerusalem.

Nir, Y. (1982), Offshore artificial structures and their influence on the israel and sinai mediterranean beaches, in Edge, B. L. (editor), *Proceedings of the 18th International Conference on Coastal Engineering*, volume 3, pp. 1837–1856, ASCE, Cape Town, South Africa.

O'Hare, T. J. and Huntley, D. A. (1994), Bar formation due to wave groups and associated long waves, in *Marine Geology*, pp. 313–325, Elsevier Science B.V.

Pattiaratchi, C., Olsson, D., Hetzel, Y. and Lowe, R. (2009), Wave-driven circulation patterns in the lee of groynes, *Continental Shelf Research*, 29:1961–1976, ISSN 0278-4343.

Pelnard-Considére, R. (1956), Essai de Theorie de l'Evolution des Forms de Rivage en Plage de Sable et de Galets, *Soc. Hydrotechnique de France, Quatriémes Journees de l'Hydraulique, Les Energies de la mer*, pp. 289–298.

Plant, N. G., Holman, R., Freilich, M. and Birkemeier, W. (1999), A Simple Model for Interannual Sandbar Behaviour, *Journal of Geophysical Research*, 104:15755–15776.

Pope, J. and Dean, J. L. (1986), Development of design criteria for segmented breakwaters, in Edge, B. L. (editor), *Proceedings of the 20th International Conference on Coastal Engineering*, volume 3, pp. 2144–2158, ASCE, Taipei, Taiwan.

Roelvink, D. and Reniers, A. D. (2011), *A Guide to Modelling Coastal Morphology*, volume 12 of *Advances in Coastal and Ocean Engineering*, World Scientific, ISBN 98143-04255.

Roelvink, D., Reniers, A. D. and van Dongern D J Walstra, A. (2006), Modeling of Hurricane Impacts, Interim Report 2, UNESCO-IHE Institute for Water Education.

Roelvink, J. A. (2006), Coastal morphodynamic evolution techniques, *Coastal Engineering*, 53:277–287.

Rosen, D. S. and Vajda, M. (1982), Sedimentological influences of detached breakwaters, in Edge, B. L. (editor), *Proceedings of the 18th International Conference on Coastal Engineering*, volume 3, pp. 1930–1948, ASCE, Cape Town, South Africa.

Rossington, S. K., Nicholls, R. J., Stive, M. J. F. and Wang, Z. B. (2011), Estuary schematisation in behaviour-oriented modelling, *Marine Geology*, 281:27–34.

Soulsby, R. (1997), *Dynamics of Marine Sands*, Thomas Telford Publications, ISBN 072772584X.

Steetzel, H. J. and Wang, Z. B. (2003), Development and application of a large-scale morphological model of the Dutch coast, phase 2: formulation and application of the PonTos-model version 1.4, Technical report, National Institute for Coastal and Marine Management/Rijkwaterstaat-RIKZ.

Stive, M. J. F., de Vriend, H. J., Nicholls, R. J. and Capobianco, M. (1992), Shore Nourishment and the Active Zone: A Time Scale Dependent View, in Edge, B. L. (editor), *Proceedings of the 23rd International Conference on Coastal Engineering*, pp. 2464–2472, ASCE, Venice, Italy.

Suh, K. and Dalrymple, R. A. (1987), Offshore Breakwaters in Laboratory and Field, *Journal of Waterway, Port, Coastal and Ocean Engineering*, 113(2):105–121, ISSN 0733-950X/87/0002-0105.

Trampenau, T., Oumeraci, H. and Dette, H. H. (2004), Hydraulic Functioning of Permeable Pile Groins, *Journal of Coastal Research*, SI 33:160–187.

Villard, P. V., Osborne, P. D. and Vincent, C. E. (2000), Influence of wave groups on SSC patterns over vortex ripples, in *Continental Shelf Research*, pp. 2391–2410, Elsevier Science Ltd.

de Vriend, H. J., Capobianco, M., Chesher, T., de Swart, H. E., Latteux, B. and Stive, M. J. F. (1993), Approaches to long-term modelling of coastal morphology: a review, *Coastal Engineering*, 21:225–269.

Walker, D. J., Dong, P. and Anastasiou, K. (1991), Sediment Transport Near Groynes in the Nearshore Zone, *Journal of Coastal Research*, 7(4):1003–1011.

Wind, H. G. and Vreugdenhil, C. B. (1986), Rip-current generation near structures, *Journal of Fluid Mechanics*, 171:459–476.

Zyserman, J. A. and Johnson, H. K. (2002), Modelling morphological processes in the vicinity of shore-parallel breakwaters, *Coastal Engineering*, 45(3-4):261–284, ISSN 03783839.

Appendix A

Integration of flux over a line

The 2D coastal model used in this study is discretised using a finite volume method on an unstructured mesh. The unstructured mesh defines the computational elements of the mesh and all variables are defined inside these computational elements. The value of the variables is furthermore defined as spatially invariant over the entire extent of the computational element in contrast to finite element methods where the variables vary spatially inside a computational element. Integration of the littoral drift computed by the 2D coastal model is therefore performed assuming that the computed transport is constant inside a computational element.

Extraction of vector quantities from a 2D mesh along a line may be done using two different methods. The first method extracts the vector quantity in a number of discrete points along the line of integration while the second method identifies all 2D elements which enclose parts of the line of extraction and their union length by use of coordinate transformation and linear interpolation. Each of the two methods are described separately in the following sections.

A.1 Extraction and integration using discrete points

This method distributes a number of points along each coastal profile as illustrated in figure A.1. Given the position of the discrete points, the enclosing computational element of each point may be found using standard element searching techniques[1]. The sediment transport vector contained by the identified computational elements is directly assigned to the discrete points, and the littoral drift along a coastal profile may be calculated by numerical integration of:

$$Q_r = \int_{s_0}^{\infty} \bar{q}_{\text{MIK21,st}} \cdot \bar{n} \, \mathrm{d}s \tag{A.1}$$

where $\bar{q}_{\text{MIKE21,st}}$ is the sediment transport assigned to each of the discrete points with the transport given relative to a cartesian coordinate system in (x, y)-space and $\bar{n}$ is the unit vector of the r-axes relative to the (x, y)-system. The numerical integration is performed using the trapezoidal rule of integration.

Use of this integration method requires that a certain cross-shore discretisation of the coastal profile is selected. The resolution of the cross-shore discretisation should be higher than the resolution of the computational mesh to ensure an accurate estimate of the littoral drift.

[1] In this study such a method is supplied with the MIKE21-Matlab API. Matlab has also similar built-in features.

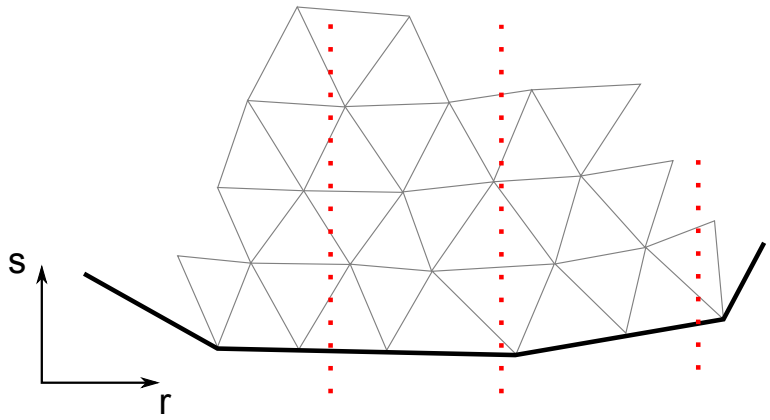

Figure A.1: *Integration of littoral drift using a number of discrete points.*

A.2 Extraction and integration using coordinate transformation

The integration of the transport over a line of extraction is here calculated as a weighted summation of the transport component normal to the line of extraction.

$$Q_\eta = \sum_i^N q_{\eta,i} \Delta L_i \tag{A.2}$$

Q_η is the transport flux over the line of extraction, and $q_{\eta,i}$ are the normal components of the transport in the elements which enclose parts of the line of extraction. The summation length, ΔL_i is the distance between the intersection of the mesh element faces and the line of extraction as indicated in figure A.2.

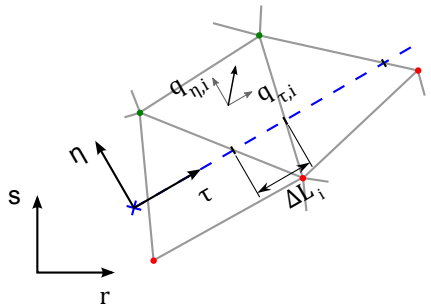

Figure A.2: *The contribution from each computational element which partially enclose the line of extraction is calculated as the product of $q_{\eta,i}$ and the distance between the element faces at $\eta = 0$.*

The summation operation can be perform after having performed the operations:

1. Identification of mesh elements enclosing the line of extraction
2. Calculation of the summation lengths, ΔL_i
3. Calculation of $q_{\eta,i}$

Identification of enclosing computational elements

Identification of the computational elements which partially enclose the line of extraction is based on the coordinates of the nodes, Ω_i, of the i'th element. A computational element which encloses the line of extraction must have nodes which are located on both sides of the line of extraction ($\eta_j \geq 0 \cap \eta_k < 0 \mid j,k \subset \Omega_i$). The computational elements must finally have at least one node which is located between the points that define the line of extraction ($\tau_j \geq 0 \cap \tau_j \leq L_f \mid j \subset \Omega_i$). Computational elements which fulfil these criteria can potentially contribute to the total flux over the line of extraction. Figure A.3 shows an example where the line of extraction is illustrated as a dashed line. The local coordinate system (τ, η) is introduced and mesh nodes which have positive values of η are coloured green while mesh nodes which have negative value of η are coloured red. Computational elements which enclose the line of extraction must therefore have at least one green node and one red node.

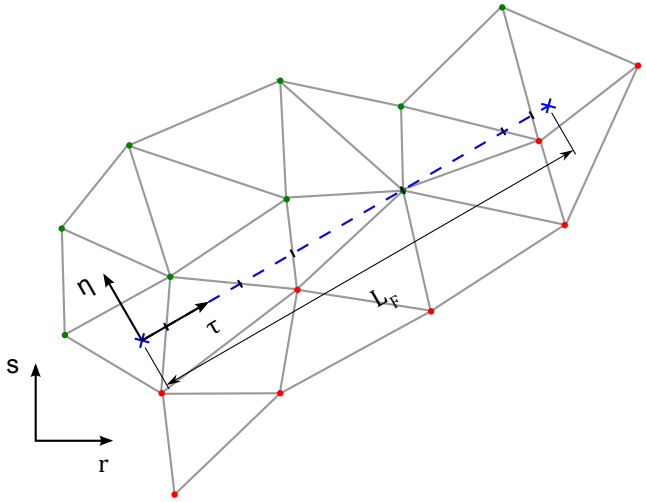

Figure A.3: *Computational elements which partially enclose the line of extraction must have at least one green node and one red node. Green mesh nodes: $\eta \geq 0$, Red mesh nodes: $\eta < 0$.*

Calculation of summation lengths

Points of intersection between a mesh face and the line of extraction are indicated by a solid bar in figure A.3. The τ-coordinate of the intersection is calculated by use of linear interpolation between two neighbouring nodes on the computational element. The point of intersection $(\tau_{12}, 0)$ between nodes 1 and 2 in figure A.4 is thus determined by:

$$\tau_{12} = \tau_1 - \frac{\eta_1}{\eta_2 - \eta_1}(\tau_2 - \tau_1) \tag{A.3}$$

The point of intersection is calculated for all faces of the computational element. The calculated point is valid if it is located on the face of the computational element ($\tau_{jk} \geq \min(\tau_j, \tau_k) \cap \tau_{jk} \leq \max(\tau_j, \tau_k) \mid j,k \subset \Omega_i$) and as long as the point of intersection is located on the line of extraction ($\tau_{jk} \geq 0 \cap \tau_{jk} \leq L_F$).

Each computational element will typically have two valid points of intersection with the line of extraction. The summation length will in this case simply be the absolute difference between the two points of intersection. Computational elements with one valid point of intersection enclose one of the two end points on the line of extraction. The summation length is for this case the minimum

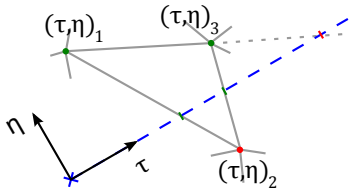

Figure A.4: *The point of intersection is calculated for all faces of a computational element. Green points of intersection: Valid points. Red point of intersection: Invalid.*

distance from the point of intersection to each of the two end points on the line of extraction. Computational elements without any valid points of intersection are located near the end points of the line of extraction but do not enclose it and do as such not contribute to the total flux.

The total flux of sediment over the line of integration is the sum of the individual contributions. It is however ensured that the contributions to the flux are unique since two contributions will exist for the same part along the line of integration in the event that a mesh face is aligned with the line of extraction. The two contributions will in this case be averaged before adding them to the the total flux.

Appendix B

Creating a periodic mesh with conforming elements

Simulation using periodic boundary conditions are possible in MIKE21 FM by modifying the boundary codes in the ascii setup files according to table B.1. Creation of a high quality periodic mesh with conforming computational elements using the existing mesh generation tools supplied by the DHI software is however not possible. Creation of a periodic mesh may therefore be carried out by use of the functions `MakePeriodic1.m` and `MakePeriodic3.m`.

Table B.1: *Boundary codes used to apply periodic boundary conditions.*

Module	Boundary code
Flow model	15
Spectral wave model	8
Sand transport model	4

B.1 Definition of a periodic mesh

A mesh is considered periodic when the face normal and face length of the boundary elements along a pair of periodic boundaries match eg. the face length $L_{E,1}$ is equal to the matching face length $L_{W,1}$ in figure B.1 and the dot product between the two face normal's is -1.

The boundary elements along a pair of periodic boundaries may be linked when the boundary faces conform to each other. Flux reconstruction may then be performed using the same methods as for flux reconstruction over internal element faces.

B.2 Creating a periodic mesh

A robust method for creating a high quality periodic mesh which fulfills the conformity requirement is implemented as the Matlab function `MakePeriodic1.m`. Construction of the periodic mesh includes:

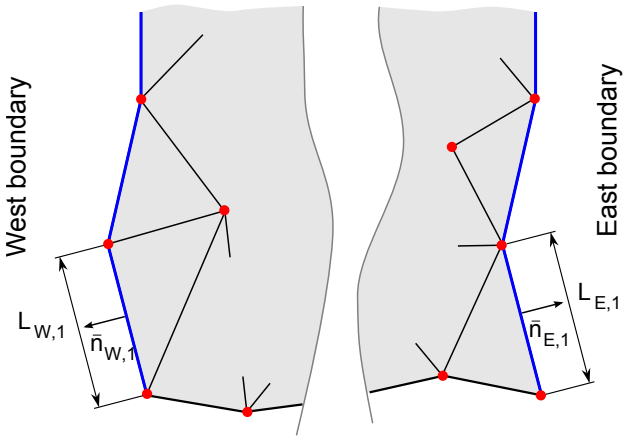

Figure B.1: *Conformity is required by the coastal model between the individual boundary elements along a pair of periodic boundaries. Conformity is obtained when* $L_{W,i} = L_{E,i} \cap \vec{n}_{W,i} \cdot \vec{n}_{E,i} = -1 | i \in \Omega$ *where* Ω *covers the faces defining the periodic boundaries.*

- Identification boundary nodes
- Distribution of new nodes along boundaries
- Creation of additional mesh elements by connecting the new nodes with existing nodes
- Transfer of boundary code of the old nodes to the new nodes

The identification of boundary nodes assumes that the periodic boundaries are linear and that they are oriented along the grid north (s-axis). Boundary nodes are thus all nodes located near the limits of the mesh in the r-axis. The position of the boundary nodes is sorted in ascending order so that the face length may be calculated. The s-position of the new nodes is calculated by stepping along the new boundary. The distance between the new boundary nodes is determined as the average inverse distance weighted average face length of the old boundaries, i.e.:

$$\tilde{L}_W(s) = \sum_i^{N_W} \frac{c^{-1}}{(s - s_i)^2} L_{W,i} \quad , \qquad c = \sum_i^{N_W} (s - s_i)^{-2}$$

is the inverse distance weighted average face length according to the existing nodes on the west boundary. The face length imposed to the new boundary is the simple average between $\tilde{L}_W(s)$ and $\tilde{L}_E(s)$. Use of the inverse distance weighting function allows construction of a new boundary where the face length is adapted to the existing without requiring the same number of faces on the existing east and west boundary. The new nodes are finally positioned at some fixed alongshore distance from the existing boundaries.

The new boundary nodes are connected with the existing nodes by creating new mesh elements. The connection is performed in a two-step method. Existing nodes are numbered j and new nodes are numbered i. Starting from one end of the boundary nodes j and i are connected with the nearest of the two nodes $j+1$ and $i+1$. If node $j+1$ is nearest, then the next element is created by connecting nodes $i, i+1, j+1$, see figure B.2. The algorithm is continued until all new nodes are connected to the existing nodes. The two-step method is performed for both of the two boundaries.

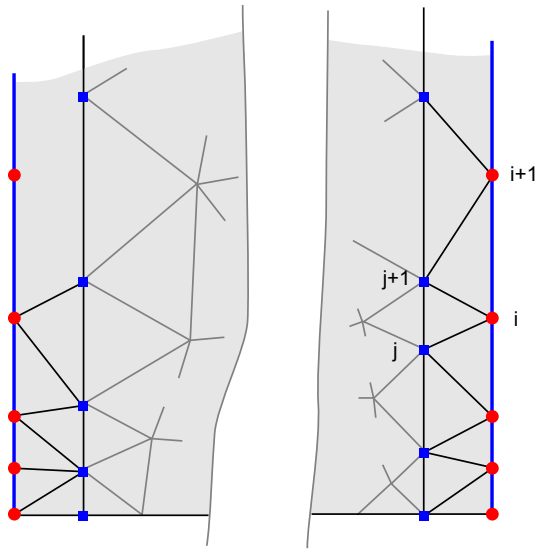

Figure B.2: *Principle in adding new mesh elements along the periodic boundaries. The new boundary nodes (red circles) are connected to old boundary nodes (blue squares) by a two-step algorithm.*

The resulting mesh includes very skew elements at the boundary in case there is a large variation in element size along the boundary or if the the user-specified increase in alongshore extent of the domain is poorly chosen (see example in figure B.3. The mesh may be smoothed by loading it into the MIKE zero mesh generator. Prior to smoothing, mesh nodes located on the non-periodic boundaries (green northern boundary in the figure) should be redistributed manually in order to increase the effectiveness of the mesh smoothing method incorporated into the mesh generator utility. The mesh smoothing should not be allowed to redistribute nodes on the periodic boundaries (blue eastern boundary).

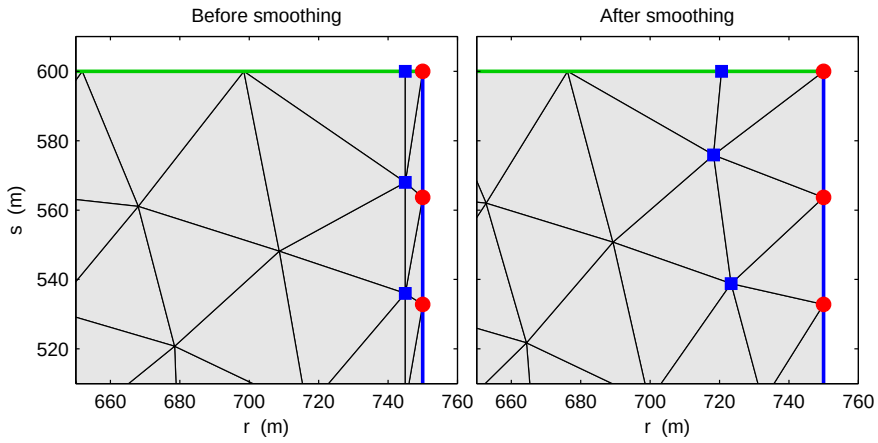

Figure B.3: *Close-up of the North-East corner of a periodic mesh before and after applying smoothing. Skew elements may be created in the process of making a periodic mesh. The skew elements are smoothed using a method available in the MIKE21 mesh generator environment.*

B.2.1 Generalisation of periodic mesh generation

`MakePeriodic1.m` is generalised in `MakePeriodic3.m` such that it allows creation of a periodic mesh which has non-linear boundaries with a general orientation. The general method uses the same principles with the following differences:

Identification of boundary nodes is based on the boundary code value of the nodes. The final North-West node which by definition is numbered according to the offshore boundary code is identified as the node with offshore boundary code which is closest to the seaward most West boundary node.

A local coordinate system may be defined in order to sort the identified boundary nodes in ascending order according to the distance from the shoreline. Default values may be used in all cases where the shore normal is oriented northward.

Direction of extension of the periodic domain may be given explicitly. If none is given, then the extension occurs normal to the offshore direction of the local coordinate system.

Construction of new mesh element faces ensures that the new mesh is periodic. The construction algorithm uses inverse distance weighting functions to calculate the new face length *and* face normal (in practice the face tangent).

Seaward-most face length is modified such that the total length of the new boundaries is identical to the total length of the old boundaries.

Figure B.4 shows an example of an initial mesh which is made periodic. The East and West boundaries are allowed different number of nodes although this is not the case in this example. The orientation of the boundary faces on the initial mesh also do not need to be aligned. It is however recommended that the general orientation of the East and West boundaries is the same. The bottom panel documents that the periodic mesh is in fact valid by plotting the periodic mesh next to itself.

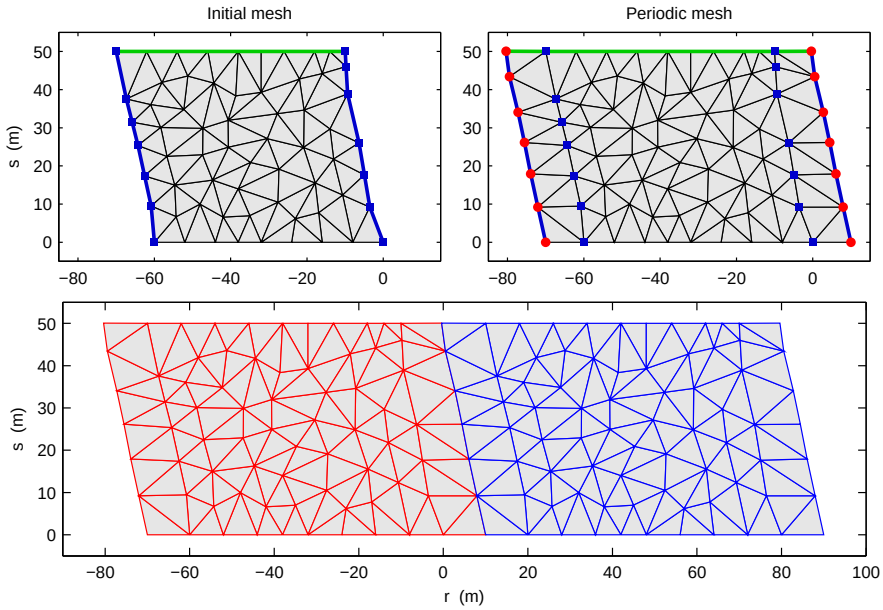

Figure B.4: *Illustration of a general mesh which is made periodic. Top left: Initial mesh. Top right: Periodic mesh. Bottom: Two periodic mesh which are joined.*

Appendix C

Derivation of the bar moment method

This section gives a detailed derivation of the bar moment method described in section 4.5.4. The method uses a coupled system of equations to evolve a set of parameters, which describe a bar on the form:

$$z_\mathrm{b} = f\left(s, \psi\right)$$

where s is the cross-shore position and ψ is a vector which contains the parameters used to construct the bar.

From ordinary statistics it is known that the moments 0 to 3 may be used to describe the following four characteristics of the form of a distribution:

- M_0 characterises the area under the distribution
- M_1 characterises the centroid of the distribution
- M_2 characterises the width of the distribution
- M_3 characterises the skewness of the distribution

The moments are in this context defined as:

$$M_i = \int_S s^i z_\mathrm{b}(s,\psi)\,\mathrm{d}s\,, \quad i = 0, 1 \tag{C.1}$$

$$M_i = \int_S \left(s-\delta\right)^i z_\mathrm{b}(s,\psi)\,\mathrm{d}s\,, \quad i = 2, 3 \tag{C.2}$$

where $z_\mathrm{b}(s)$ is defined by equation 4.24 and S defines the interval over which $z_\mathrm{b}(s) > 0$. The 2nd and 3rd order moments are centred moments, i.e. the centroid location, $\delta = M_1/M_0$, is subtracted from s. The integral may be evaluated by introducing a dimensionless formulation of the bar

form. One possible way to do this is indicated in figure C.1. This corresponds to the dimensionless quantities:

$$
\begin{aligned}
z_b^* &= \frac{z_\mathrm{b}}{A_\mathrm{b}} \\
s^* &= \frac{s - s_1}{W_\mathrm{b}} \quad \Rightarrow \quad s = s^* W_\mathrm{b} + s_1 \\
\zeta &= \frac{s_\mathrm{c} - s_1}{W_\mathrm{b}}
\end{aligned}
$$

And the dimensionless form of the bar may then be described by:

$$
z_\mathrm{b}^*(s^*) = \begin{cases} 0 \quad , & \leq s^* < 0 \\ \sin^2(\phi_\mathrm{a}) \, , & 0 \leq s^* < \zeta \\ \sin^2(\phi_\mathrm{b}) \, , & \zeta \leq s^* < 1 \\ 0 \quad , & 1 \leq s^* < \end{cases} \tag{C.3}
$$

where the arguments to the sine functions are:

$$
\begin{aligned}
\phi_\mathrm{a} &= \frac{s^*}{\zeta} \frac{\pi}{2} \\
\phi_\mathrm{b} &= \frac{s^* - \zeta}{1 - \zeta} \frac{\pi}{2} + \frac{\pi}{2}
\end{aligned}
$$

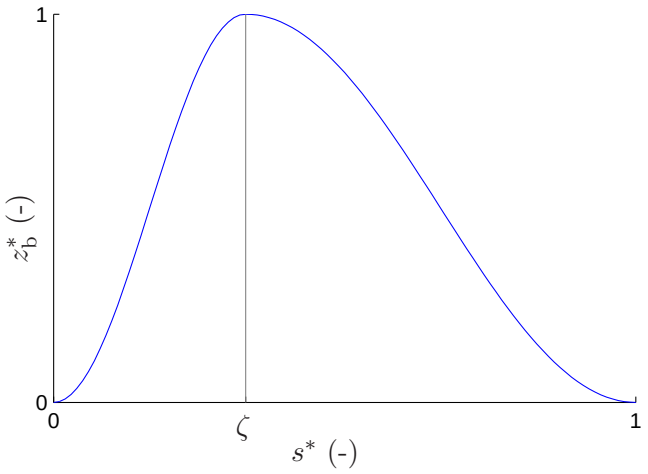

Figure C.1: *The dimensionless form of the bar can be uniquely defined in terms of the skewness parameter, ζ.*

Substituting the dimensionless quantities into the integrals leads to:

$$
\begin{aligned}
M_0 &= \int_{s_1}^{s_2} z_\mathrm{b}(s) \, \mathrm{d}s = A_\mathrm{b} W_\mathrm{b} \left(\int_0^\zeta \sin^2 \phi_\mathrm{a} \, \mathrm{d}s^* + \int_\zeta^1 \sin^2 \phi_\mathrm{b} \, \mathrm{d}s^* \right) \\
&= A_\mathrm{b} W_\mathrm{b} M_0^*
\end{aligned} \tag{C.4}
$$

The dimensionless 0th moment is simply 1/2, but we will retain it's symbol for the sake of completeness. The first order moment evaluates to:

$$\begin{aligned} M_1 &= \int_{s_1}^{s_2} s z_\mathrm{b}(s)\,\mathrm{d}s = A_\mathrm{b} W_\mathrm{b}^2 \left(\int_0^\zeta (s^* W_\mathrm{b} + s_1) \sin^2\phi_a \,\mathrm{d}s^* + \int_\zeta^1 (s^* W_\mathrm{b} + s_1) \sin^2\phi_\mathrm{b}\,\mathrm{d}s^* \right) \\ &= A_\mathrm{b} W_\mathrm{b}^2 M_1^* + A_\mathrm{b} W_\mathrm{b} s_1 M_0^* \end{aligned} \tag{C.5}$$

The dimensionless 1st order moment is purely a function of the skewness parameter, ζ, and is defined as:

$$M_1^* = M_{1,\mathrm{a}}^* + M_{1,\mathrm{b}}^* = \int_0^\zeta s^* \sin^2\phi_\mathrm{a}\,\mathrm{d}s^* + \int_\zeta^1 s^* \sin^2\phi_\mathrm{b}\,\mathrm{d}s^*$$

The second order moment evaluates to:

$$\begin{aligned} M_2 &= \int_{s_1}^{s_2} (s-\delta)^2 z_\mathrm{b}(s)\,\mathrm{d}s \\ &= A_\mathrm{b} W_\mathrm{b}^3 \left(\int_0^\zeta \left(s^* - \frac{M_1^*}{M_0^*} \right)^2 \sin^2\phi_\mathrm{a}\,\mathrm{d}s^* + \int_\zeta^1 \left(s^* - \frac{M_1^*}{M_0^*} \right)^2 \sin^2\phi_\mathrm{b}\,\mathrm{d}s^* \right) \\ &= A_\mathrm{b} W_\mathrm{b}^3 \left(M_2^* - \frac{M_1^{*2}}{M_0^*} \right) \end{aligned} \tag{C.6}$$

where it is used that:

$$(s-\delta)^2 = \left(s^* W_\mathrm{b} + s_1 - s_1 - W_\mathrm{b} \frac{M_1^*}{M_0^*} \right)^2 = W_\mathrm{b}^2 \left(s^* - \frac{M_1^*}{M_0^*} \right)^2$$

The dimensionless 2nd order moment which is purely a function of the skewness parameter, ζ, is defined as:

$$M_2^* = M_{2,\mathrm{a}}^* + M_{2,\mathrm{b}}^* = \int_0^\zeta s^{*2} \sin^2\phi_\mathrm{a}\,\mathrm{d}s^* + \int_\zeta^1 s^{*2} \sin^2\phi_\mathrm{b}\,\mathrm{d}s^*$$

The 3rd order moment evaluates to:

$$\begin{aligned} M_3 &= \int_{s_1}^{s_2} (s-\delta)^3 z_\mathrm{b}(s)\,\mathrm{d}s \\ &= A_\mathrm{b} W_\mathrm{b}^4 \left(\int_0^\zeta \left(s^* - \frac{M_1^*}{M_0^*} \right)^3 \sin^2\phi_\mathrm{a}\,\mathrm{d}s^* + \int_\zeta^1 \left(s^* - \frac{M_1^*}{M_0^*} \right)^3 \sin^2\phi_\mathrm{b}\,\mathrm{d}s^* \right) \\ &= A_\mathrm{b} W_\mathrm{b}^4 \left(M_3^* - 3\frac{M_1^*}{M_0^*} M_2^* + 2\frac{M_1^{*3}}{M_0^{*2}} \right) \end{aligned} \tag{C.7}$$

where the dimensionless 3rd order moment is defined as:

$$M_3^* = M_{3,\mathrm{a}}^* + M_{3,\mathrm{b}}^* = \int_0^\zeta s^{*3} \sin^2\phi_\mathrm{a}\,\mathrm{d}s^* + \int_\zeta^1 s^{*3} \sin^2\phi_\mathrm{b}\,\mathrm{d}s^*$$

C.1 Reduced moments

Inspection of the definitions for the bar moments (equations C.4, C.5, C.6, C.7) shows that the moments cannot directly be related to the characteristics listed in the start of the previous section. We introduce therefore the so-called *reduced moments*, which are denoted by the calligraphic letter: $\mathcal{M}_i$. The reduced moments are combinations of lower order ordinary moments, resulting in a unit identical to that, which they are representing. The reduced 0th order moment is simply defined as:

$$\mathcal{M}_0 = M_0 = A_\mathrm{b} W_\mathrm{b} M_0^* = V M_0^* \tag{C.8}$$

Here a new variable $V = A_\mathrm{b} W_\mathrm{b}$ is defined. V is two times the cross-sectional area of the bar.

The 1st order reduced moment defines the location of the centroid of the bar, and is independent of the bar amplitude. The definition of $\mathcal{F}_1(\zeta)$ is used to show the variation of $\mathcal{M}_1$ with respect to ζ (see figure C.2). The figure shows that the centroid location for the two extremes ($\zeta = 0, \zeta = 1$) is equal to that of a triangle as expected. The corresponding variations of the bar are illustrated in the bottom panel of the figure.

$$\mathcal{M}_1 = \frac{M_1}{M_0} = s_1 + W_\mathrm{b} \frac{M_1^*}{M_0^*} = s_1 + W_\mathrm{b} \mathcal{F}_1 \tag{C.9}$$

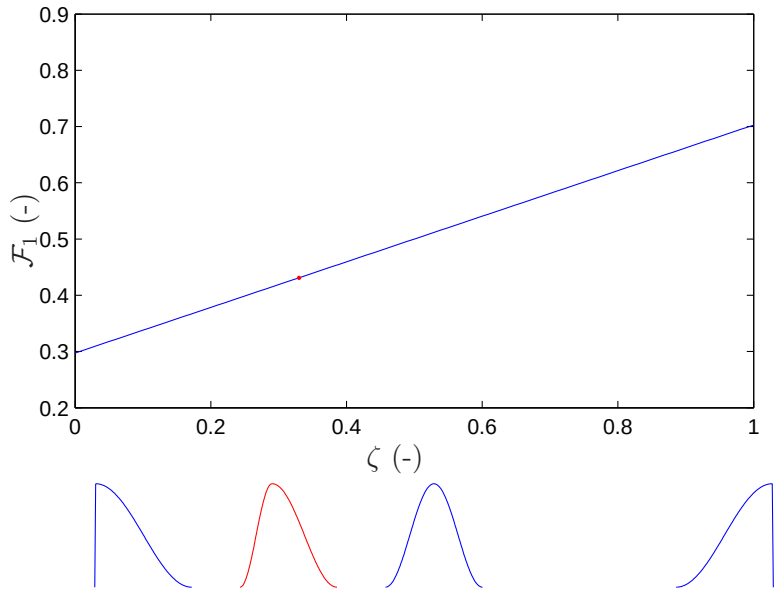

Figure C.2: *Variation of the dimensionless component of the first moment as function of the skewness parameter.*

The 2nd order reduced moment is a linear function of the bar width and a weak function of the skewness parameter. The 2nd order reduced moment is independent of the bar amplitude and centroid position as indicated below.

$$\mathcal{M}_2 = \sqrt{\frac{M_2}{M_0}} = W_\mathrm{b} \sqrt{\frac{M_2^*}{M_0^*} - \left(\frac{M_1^*}{M_0^*}\right)^2} = W_\mathrm{b} \mathcal{F}_2 \tag{C.10}$$

$\mathcal{F}_2(\zeta)$ is introduced in order to show the variation of $\mathcal{M}_2$ as function of the skewness parameter. $\mathcal{F}_2$ is shown in figure C.3. The figure shows that $\mathcal{M}_2$ is typically 19% of the bar width, and that the minimum value is for a bar with zero skewness ($\zeta = 0.5$).

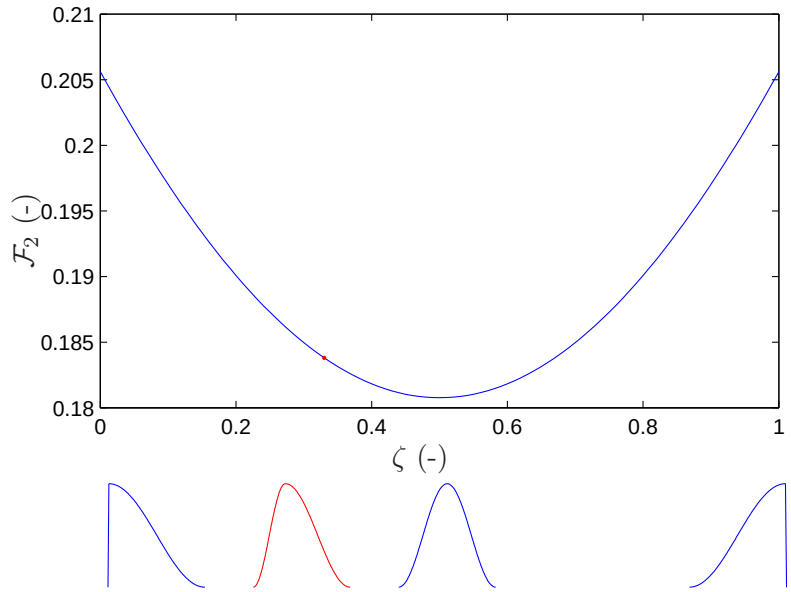

Figure C.3: *Variation of the dimensionless component of the second order moment with the skewness parameter.*

The 3rd order reduced moment is a function of the skewness parameter only. A new parameter, $\mathcal{F}_3(\zeta)$ is introduced for consistency compared to the following two moments although there is no formal difference between $\mathcal{M}_3$ and $\mathcal{F}_3$.

$$\mathcal{M}_3 = M_3\sqrt{\frac{M_0}{M_2^3}} = \left(M_3^* - 3\frac{M_1^*}{M_0^*}M_2^* + 2\frac{M_1^{*3}}{M_0^{*2}}\right)\frac{\sqrt{M_0^*}}{\left(M_2^* - \frac{M_1^{*2}}{M_0^*}\right)^{1.5}} = \mathcal{F}_3 \tag{C.11}$$

Figure C.4 shows the variation of $\mathcal{F}_3$ as function of the skewness parameter. The figure shows a negative relationship between the two parameters, and that $\mathcal{M}_3$ should fall in the range ± 0.6.

C.2 Temporal derivatives of reduced moments

Definitions of the reduced moments in terms of the bar parameters ψ are established in the previous section. The next step is now to establish the temporal derivatives of the reduced moments. This is done in two ways. The first is based on the moments from the previous section, as this will give a formal definition for how the bar parameters will change when the reduced moments change. The second method for determining temporal derivatives is based on how a change in the bar bathymetry z_b will affect the reduced moments, as this is used to couple the signal from a 2D morphological model to the parametric description of the bar profile.

C.2.1 Derivatives in terms of bar parameters

The reduced moments can be defined in terms of the bar parameters, $\psi = [V, s_1, W_\mathrm{b}, \zeta]^\mathrm{T}$. The bar parameters are all functions of time. The temporal derivatives of the reduced moments can

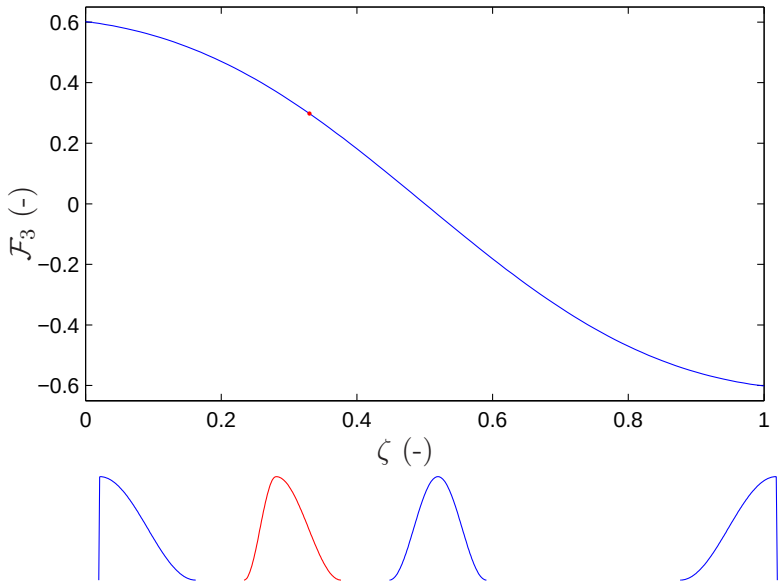

Figure C.4: *Variation of the dimensionless component of the third order moment with the skewness parameter.*

therefore be calculated by successive use of various chain rules.

$$\left(\frac{\partial \mathcal{M}_0}{\partial t}\right)_\psi = M_0^* \frac{\partial V}{\partial t}$$

$$\left(\frac{\partial \mathcal{M}_1}{\partial t}\right)_\psi = \frac{\partial s_1}{\partial t} + \frac{\mathrm{d}}{\mathrm{d}t}\left(\mathcal{F}_1 W_\mathrm{b}\right)$$

$$\left(\frac{\partial \mathcal{M}_2}{\partial t}\right)_\psi = \mathcal{F}_2 \frac{\partial W_\mathrm{b}}{\partial t} + W_\mathrm{b} \frac{\partial \mathcal{F}_2}{\partial \zeta}\frac{\partial \zeta}{\partial t}$$

$$\left(\frac{\partial \mathcal{M}_3}{\partial t}\right)_\psi = \frac{\partial \mathcal{F}_3}{\partial \zeta}\frac{\partial \zeta}{\partial t}$$

where $\frac{\partial \mathcal{F}_2}{\partial \zeta}$ and $\frac{\partial \mathcal{F}_3}{\partial \zeta}$ are a known non-linear functions of ζ. They are however not shown here due to their extent. The strong form of the derivative of $\mathcal{F}_1 W_\mathrm{b}$ in the second equation is maintained to improve accuracy.

The system of equations may be rearranged, to the form:

$$\frac{\partial \psi}{\partial t} = f(t, \psi)$$

The order of the equations is however changed, so that they may be solved sequentially, leading to:

$$\frac{\partial \zeta}{\partial t} = \left(\frac{\partial \mathcal{F}_1}{\partial \zeta}\right)^{-1} \left(\frac{\partial \mathcal{M}_3}{\partial t}\right)_\psi$$

$$\frac{\partial W_\mathrm{b}}{\partial t} = \mathcal{F}_2^{-1}\left(\left(\frac{\partial \mathcal{M}_2}{\partial t}\right)_\psi - W_\mathrm{b}\frac{\partial \mathcal{F}_2}{\partial \zeta}\frac{\partial \zeta}{\partial t}\right) \tag{C.12}$$

$$\frac{\partial s_1}{\partial t} = \left(\frac{\partial \mathcal{M}_1}{\partial t}\right)_\psi - \frac{\mathrm{d}}{\mathrm{d}t}\left(\mathcal{F}_1 W_\mathrm{b}\right)$$
$$\frac{\partial V}{\partial t} = M_0^{*-1}\left(\frac{\partial \mathcal{M}_0}{\partial t}\right)_\psi$$

The strong form of the derivative of $\mathcal{F}_1 W_\mathrm{b}$ may be evaluated because changes to both the skewness and the bar width have been calculated. The total derivative is therefore evaluated as:

$$\frac{\mathrm{d}}{\mathrm{d}t}\left(\mathcal{F}_1 W_\mathrm{b}\right) = \mathcal{F}_1\!\left(\zeta + \frac{\partial \zeta}{\partial t}\right) \cdot \left(W_\mathrm{b} + \frac{\partial W_\mathrm{b}}{\partial t}\right) - \mathcal{F}_1\!(\zeta)\, W_\mathrm{b}$$

The system defines thus how the bar parameters will change in time for a given change in the reduced moments. A change to the reduced moments may either be determined from a 2D model and/or it may be due to a forcing towards equilibrium conditions. The change in bar moments may therefore be defined as:

$$\left(\frac{\partial \mathcal{M}_i}{\partial t}\right)_\psi = \left(\frac{\partial \mathcal{M}_i}{\partial t}\right)_\mathrm{2D} + \left(\frac{\partial \mathcal{M}_i}{\partial t}\right)_\mathrm{eq} \tag{C.13}$$

Specification of the last term has however not been tested and is therefore in all applications set to zero.

The right hand sides of equations C.12 are implemented in the Matlab function `rhsBarMom2.m`. The syntax to the function is:

```
f = rhsBarMom2(psi,dM2D,dMeq);
```

C.2.2 Derivatives in terms of erosion/deposition distribution

The temporal derivatives of the reduced moments in terms of the output from a 2D model are evaluated in their conservative form i.e.:

$$\left(\frac{\partial \mathcal{M}_0}{\partial t}\right)_\mathrm{2D} = \frac{M_0^{k+1} - M_0^k}{\Delta t}$$
$$\left(\frac{\partial \mathcal{M}_1}{\partial t}\right)_\mathrm{2D} = \frac{\left(\frac{M_1}{M_0}\right)^{k+1} - \left(\frac{M_1}{M_0}\right)^k}{\Delta t}$$
$$\left(\frac{\partial \mathcal{M}_2}{\partial t}\right)_\mathrm{2D} = \frac{\sqrt{\frac{M_2}{M_0}}^{k+1} - \sqrt{\frac{M_2}{M_0}}^{k}}{\Delta t}$$
$$\left(\frac{\partial \mathcal{M}_3}{\partial t}\right)_\mathrm{2D} = \frac{\sqrt{\frac{M_3^2 M_0}{M_2^3}}^{k+1} - \sqrt{\frac{M_3^2 M_0}{M_2^3}}^{k}}{\Delta t}$$

k as a superscript indicates the kth time step, while i as a superscript in the following equations indicates the ith power. The moments at the present time step are calculated as:

$$M_i^k = \frac{1}{\Delta L}\sum_j s_j^i\, z_\mathrm{b}(s_j, \psi^k) A_j\,, \quad i = 0, 1$$

$$M_i^k = \frac{1}{\Delta L}\sum_j \left(s_j - \frac{M_1^k}{M_0^k}\right)^i z_\mathrm{b}(s_j,\psi^k)A_j\,, \quad i=2,3$$

while the moments at the next time step are calculated by:

$$M_i^{k+1} = \frac{1}{\Delta L}\sum_j s_j^i \left(z_\mathrm{b}(s_j,\psi^k) + \frac{\partial z_j}{\partial t}\Delta t\right) A_j\,, \quad i=0,1$$

$$M_i^{k+1} = \frac{1}{\Delta L}\sum_j \left(s_j - \frac{M_1^{k+1}}{M_0^{k+1}}\right)^i \left(z_\mathrm{b}(s_j,\psi^k) + \frac{\partial z_j}{\partial t}\Delta t\right) A_j\,, \quad i=2,3$$

The moment integrals are evaluated as discrete summations over all the computational elements located inside a control volume of a bar. The index j indicates thus an operation on the jth element within the control volume. ΔL is the alongshore length of the control volume and is introduced because the original form of the moment integrals are based on an alongshore uniform profile of unit length.

The model complex shown in this section makes it thus possible to take a 2D output from a model and calculate the expected change in bar moments. This is obviously done under the assumption that the $\partial z/\partial t$ signal from the 2D model may be due to changes to the bar alone. Note that it is also possible to allow one or more of the higher order moment derivatives to be zero, thus reducing the degree of freedom of the bar. The change to the reduced bar moments may be calculated using the Matlab function: `ddt2DMoments_v2.m` which has the syntax:

```
dM2D = ddt2DMoments_v2(svec,dzdtvec,Areavec,psi,flag);
```

`svec` and `dzdtvec` hold the cross-shore coordinate and the rate of bed level change signal predicted by the 2D coastal model. `Areavec` is a vector of the corresponding area of the computational elements within the control volume divided by the alongshore length of the control volume. `psi` holds the bar parameters and `flag` is used to specify whether the change in skewness should be calculated.